

Lipids and mitochondria in diabetic muscle

Citation for published version (APA):

Feyter, de, H. M. M. L. (2007). *Lipids and mitochondria in diabetic muscle*. [Phd Thesis 1 (Research TU/e / Graduation TU/e), Biomedical Engineering]. Technische Universiteit Eindhoven.
<https://doi.org/10.6100/IR627571>

DOI:

[10.6100/IR627571](https://doi.org/10.6100/IR627571)

Document status and date:

Published: 01/01/2007

Document Version:

Publisher's PDF, also known as Version of Record (includes final page, issue and volume numbers)

Please check the document version of this publication:

- A submitted manuscript is the version of the article upon submission and before peer-review. There can be important differences between the submitted version and the official published version of record. People interested in the research are advised to contact the author for the final version of the publication, or visit the DOI to the publisher's website.
- The final author version and the galley proof are versions of the publication after peer review.
- The final published version features the final layout of the paper including the volume, issue and page numbers.

[Link to publication](#)

General rights

Copyright and moral rights for the publications made accessible in the public portal are retained by the authors and/or other copyright owners and it is a condition of accessing publications that users recognise and abide by the legal requirements associated with these rights.

- Users may download and print one copy of any publication from the public portal for the purpose of private study or research.
- You may not further distribute the material or use it for any profit-making activity or commercial gain
- You may freely distribute the URL identifying the publication in the public portal.

If the publication is distributed under the terms of Article 25fa of the Dutch Copyright Act, indicated by the "Taverne" license above, please follow below link for the End User Agreement:

www.tue.nl/taverne

Take down policy

If you believe that this document breaches copyright please contact us at:

openaccess@tue.nl

providing details and we will investigate your claim.

Lipids & Mitochondria in Diabetic Muscle

A catalogue record is available from the Eindhoven University of Technology Library

ISBN: 978-90-386-1056-6

Cover design: **Dirk & Dirk** illustratie en grafisch ontwerp, Henk De Feyter

Lipids and mitochondria in diabetic muscle

PROEFSCHRIFT

ter verkrijging van de graad van doctor aan de
Technische Universiteit Eindhoven, op gezag van de
Rector Magnificus, prof.dr.ir. C.J. van Duijn, voor een
commissie aangewezen door het College voor
Promoties in het openbaar te verdedigen
op donderdag 5 juli 2007 om 16.00 uur

door

Henk Marie Maurits Luc De Feyter

geboren te Ninove, België

Dit proefschrift is goedgekeurd door de promotor:

prof.dr. K. Nicolay

Copromotor:

dr. J.J. Prompers

Table of Contents

Chapter 1	General introduction	9
Chapter 2	Regional variations in intramyocellular lipid concentration correlate with muscle fiber type distribution in rat tibialis anterior muscle	29
Chapter 3	An NMR-compatible, minimally invasive electrical stimulation method to study rat skeletal muscle <i>in vivo</i>	43
Chapter 4	³¹ P MR spectroscopy and <i>in vitro</i> markers of oxidative capacity in type 2 diabetes patients	53
Chapter 5	Intersubject differences in the effect of acidosis on phosphocreatine recovery kinetics in muscle after exercise are due to differences in proton efflux rates	71
Chapter 6	Early or advanced stage type 2 diabetes is not accompanied by <i>in vivo</i> skeletal muscle mitochondrial dysfunction	91
Chapter 7	Increased intramyocellular lipid content but normal skeletal muscle mitochondrial function throughout the pathogenesis of type 2 diabetes in the ZDF rat	107
Chapter 8	Exercise training improves glycemic control in long-standing, insulin-treated type 2 diabetes patients	127
Chapter 9	General discussion	141
	Summary Samenvatting List of publications Dankwoord	149

Chapter 1

General introduction

The prevalence of diabetes, in particular type 2 diabetes, has nowadays reached proportions of a worldwide epidemic. According to data published in the latest Diabetes Atlas (2006) of the International Diabetes Federation (IDF), the disease now affects 246 million people worldwide¹. The number of people living with diabetes will increase to ~380 million within 20 or 30 years if nothing is undertaken¹⁻³. The explosive increase in type 2 diabetes prevalence is believed to be driven by a complex interplay of genetic, social and environmental factors. One of the earliest characteristics in the pathogenesis of type 2 diabetes is the presence of skeletal muscle insulin resistance eventually leading to a disturbed glucose homeostasis. Insulin resistance has been associated with increased lipid deposits in skeletal muscle and has recently also been linked to a functional impairment of mitochondria, the cellular “powerhouses” generating energy.

The present chapter will discuss glucose housekeeping, insulin action, intramyocellular lipid storage and mitochondrial function. Aberrations in these processes will be viewed from the perspective of the pathogenesis of type 2 diabetes. Different methods used to measure intramyocellular lipid levels and skeletal muscle mitochondrial function will be described, highlighting the techniques predominantly used in the present thesis.

Glucose homeostasis

In the healthy human body the blood glucose concentration is very well controlled. After ingesting an average meal, which normally contains a substantial amount of carbohydrates, the blood glucose level will rise quickly. As the glucose is subsequently taken up by the peripheral tissue, the blood glucose level is gradually returning to its base level. The tissue predominantly responsible for the uptake of blood glucose is skeletal muscle as this constitutes ~80 % of the total glucose deposition capacity^{4, 5}. A family of facilitative glucose transport proteins (GLUTs) is responsible for the clearance of glucose from the bloodstream⁶. In skeletal muscle, GLUT4 is the most important GLUT isoform and is regulated by insulin, a hormone secreted by the pancreas, or by contractile activity^{6, 7}. GLUT4 is sequestered in specialized storage vesicles that under basal conditions are localized in the cell’s interior. Separate storage vesicles have been distinguished containing GLUT4 responsive to the insulin and exercise signaling, respectively^{8, 9}.

In response to the rise of the blood glucose concentration, insulin is instantly secreted by the β -cells of the pancreas to regulate the blood glucose level. After binding of insulin to its receptor at the muscle cell membrane, the insulin signaling cascade induces a translocation of the GLUT4 storage compartments to the sarcolemma and T-tubuli^{6, 10}. Thereupon, the GLUT4 containing vesicles dock to and fuse with the sarcolemma and T-tubuli, which increases the rate of glucose transport through facilitated diffusion^{6, 10}. The insulin signaling involves the binding to the insulin receptor, the phosphorylation of insulin receptor substrates (IRS) on tyrosine residues and the activation of phosphatidylinositol 3-kinase (PI3-kinase) (Figure 1). Downstream of PI3-kinase, the insulin signaling cascade includes several serine/threonine kinases such as Akt (protein kinase B) (reviewed in¹¹). Insulin exerts its function as a blood glucose regulator not only by stimulating the glucose uptake by the peripheral tissue but also

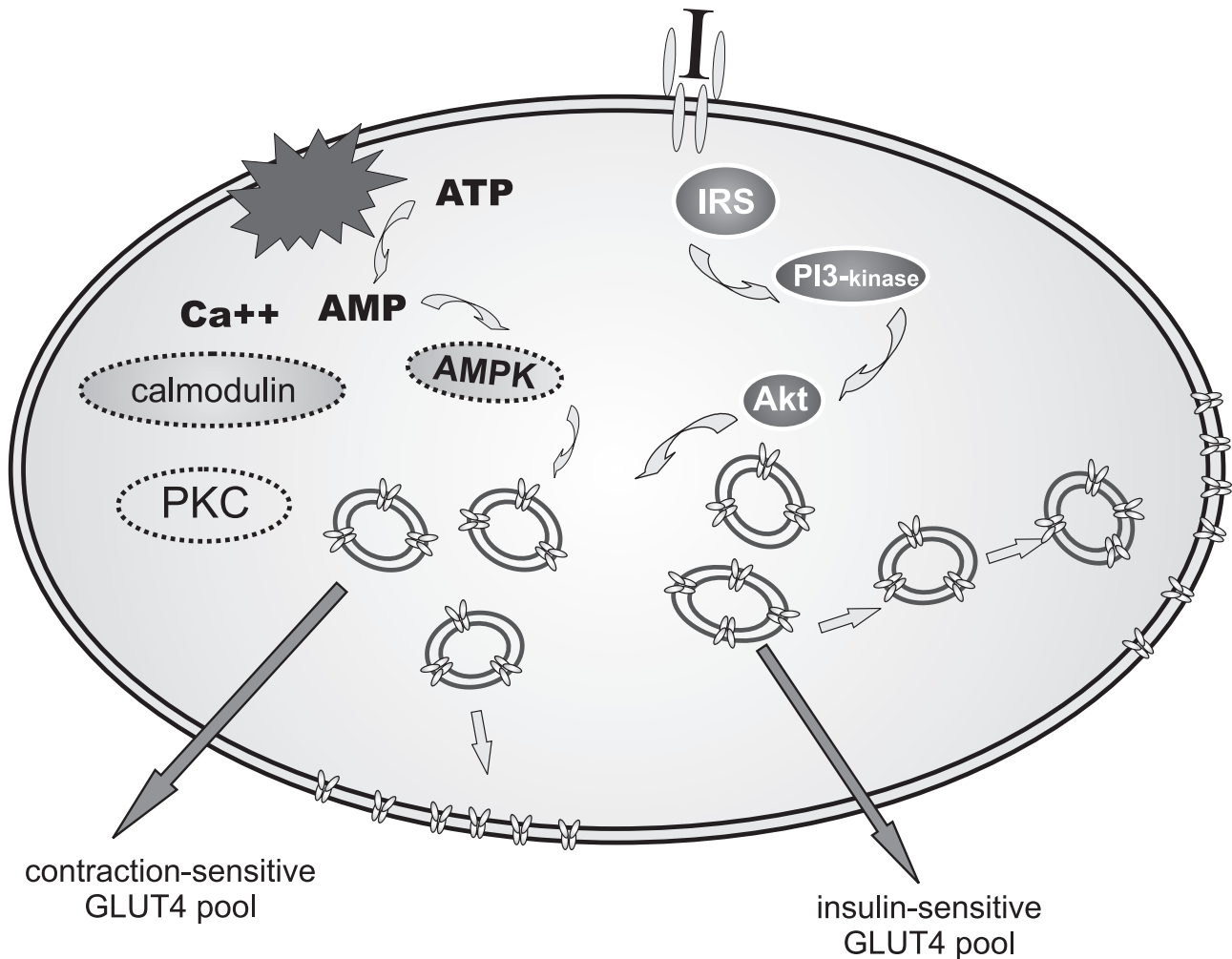


Figure 1 Cartoon representing a muscle cell. A summary of the insulin signaling pathway is depicted on the right. Upon binding of insulin to the insulin receptor, the pathway involves phosphorylation of the IRS and activation of PI3-kinase eventually inducing translocation, docking and fusion of the insulin-responsive GLUT4 vesicles with the plasma membrane upon which the GLUT4 proteins can function as a glucose transporter. On the left side of the cartoon, a summary of the hypothesized mechanisms of contraction-induced GLUT4 recruitment is shown. Increased concentration of AMP during contractions triggers the “fuel gauge” AMPK, which is suggested to be a critical signaling molecule in this pathway. Other potential proteins with a role in the contraction-induced GLUT4 translocation are calmodulin and PKC. I: insulin, IRS: insulin receptor substrate, PI3-kinase: phosphatidylinositol 3-kinase, Akt: protein kinase B, ATP: adenosine tri-phosphate, AMP: adenosine mono-phosphate, AMPK: AMP-activated protein kinase, PKC: protein kinase C.

by inhibiting the endogenous glucose production by the liver ¹². Although both insulin and contraction/exercise induce increased glucose uptake via GLUT4 recruitment, the exercise-induced upregulation of glucose transport does not involve phosphorylation of IRSs, indicating that the signaling occurs along a different pathway ¹³⁻¹⁶. The contraction-induced glucose transport pathway is far from elucidated, however data point towards AMP-activated protein kinase (AMPK) as a critical signaling molecule ¹⁷. AMPK has been proposed as an important “fuel gauge” in mammalian cells ^{18, 19}. On the other hand, the increased intracellular calcium concentrations during contractions have also been suggested to be a signal for contraction-induced GLUT4 translocation and enhanced glucose transport. Potential proteins involved in this pathway are calmodulin and protein kinase C (reviewed in ²⁰) (Figure 1).

Insulin resistance and type 2 diabetes

Insulin resistance is the situation in which the target tissue becomes less sensitive to the action of insulin. Insulin resistant skeletal muscle exposes less GLUT4 under insulin-stimulated conditions and therefore takes up less glucose than insulin sensitive muscle tissue⁷. The liver, another major target tissue of insulin, experiences inhibition of the endogenous glucose production under insulin-stimulated conditions²¹. Thus, in case of insulin resistance in the liver, the inhibiting action of insulin becomes less effective which leads to higher production rates of endogenous glucose by the liver^{12, 22}. Both insulin resistant muscle tissue and an insulin resistant liver contribute to increased levels of blood glucose. This situation is initially counteracted by an increased production of insulin by the pancreas, guaranteeing normal blood glucose levels (hyperinsulinemia)²². The insulin resistance generally deteriorates, reaching a point at which the increased blood glucose levels can no longer be compensated by an increased insulin production due to β -cell failure²³. At this point, subjects are being classified as type 2 diabetes patients. In an attempt to better define the gradual transition of insulin resistance towards overt type 2 diabetes, the World Health Organization introduced classifications for several disease stages²⁴. Subjects can be classified to have normal glucose tolerance (NGT), impaired glucose tolerance (IGT), impaired fasting glucose (IFG) or type 2 diabetes based on the relatively simple and practical oral glucose tolerance test²⁴. It should be noted that this classification originated from a practical point of view and that the disease itself is an ongoing process, mostly gradually deteriorating if interventions involving lifestyle changes are absent. An obvious lifestyle alteration is to increase the daily activity with exercise²⁵, because in contrast to the disturbed insulin signaling, the contraction/exercise-induced glucose transport is not impaired in type 2 diabetes patients²⁶. Therefore, exercise represents a powerful tool to improve glucose homeostasis in type 2 diabetes patients.

Intramyocellular lipids

In the human body lipids are not only stored in the adipose tissue, but also in skeletal muscle lipid deposits are present²⁷. Skeletal muscle lipids can be stored in extracellular adipocytes (extramyocellular lipids; EMCL) or in intramyocellular deposits. The intramyocellular lipids (IMCL) form droplet-like structures, mostly situated in the close neighborhood of mitochondria²⁷, the organelles producing the majority of the cell's energy necessary for normal function and muscle contraction. In accordance with its location close to mitochondria, IMCL has been shown to be a metabolically active lipid pool²⁸⁻³⁰ (reviewed in³¹). IMCL is used as a substrate during endurance exercise and the increased IMCL levels found in endurance-trained athletes compared to controls are believed to be one of the many adaptations of the muscle tissue to endurance exercise training³²⁻³⁴. However, also in obese subjects and type 2 diabetes patients IMCL concentrations were increased compared to healthy, lean control subjects³⁵. In these obese and type 2 diabetes patients, the IMCL content was inversely related to the whole-body insulin sensitivity. This association did not hold in the insulin-sensitive endurance-trained athletes, a phenomenon described as a metabolic paradox³⁵. Compared to other fat related measures such as body mass index and plasma free fatty acid levels, IMCL appeared to be the best predictor of insulin resistance³⁶. The strong relation between insulin sensitivity and IMCL was not only seen in humans, but was also shown to hold in rat models of insulin resistance

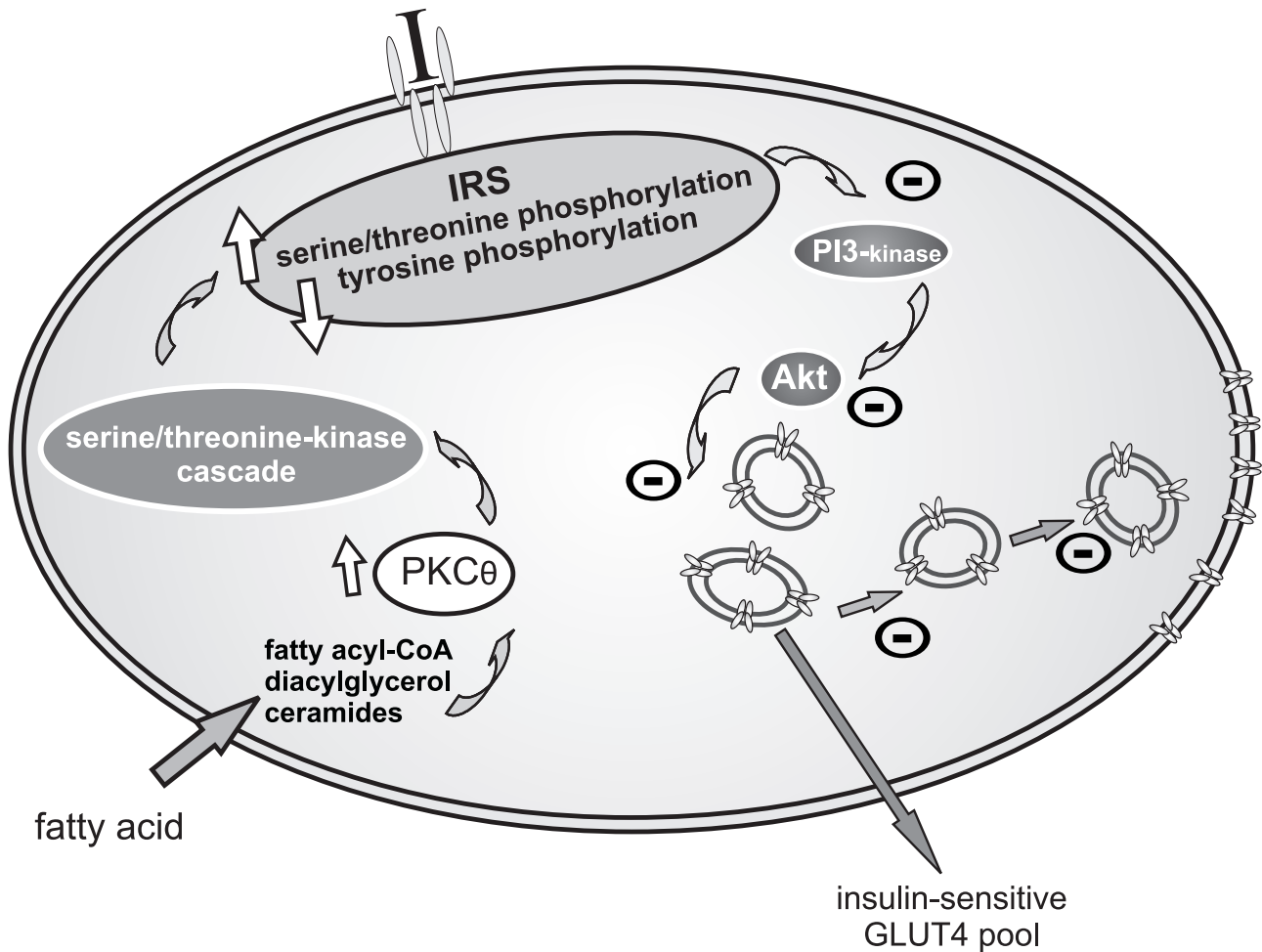


Figure 2 Cartoon representing a muscle cell. A summary of the insulin signaling pathway is depicted on the right (abbreviations as in Figure 1). On the left, the hypothesized mechanism of fatty-acid induced insulin resistance: increased delivery of fatty acids to the muscle or a decreased intracellular fatty acid metabolism leads to increase of intracellular fatty acid metabolites such as long-chain fatty acyl-CoA, diacylglycerol and ceramides. These activate a serine/threonine-kinase cascade, presumably initiated by PKC θ (protein kinase C θ), leading to phosphorylation of serine/threonine sites on the IRS and inhibiting phosphorylation of tyrosine sites. As a consequence, a decreased ability of IRS to activate PI3-kinase leads to impaired insulin signaling and decreased GLUT4 translocation and glucose transport. (Adapted from Shulman⁴⁵).

and type 2 diabetes^{37, 38}. However, it became clear that IMCL itself is not interfering with the insulin signaling pathway, but rather represents a surrogate marker of a systemic lipid oversupply³⁹.

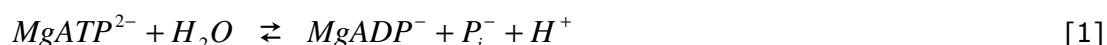
How do intracellular lipids impair glucose metabolism? The traditional view is that fatty acids compete with glucose for substrate oxidation by a series of events described by Randle *et al.* as the glucose-fatty acid cycle⁴⁰. An increase in fatty acids causes an increase in the intramitochondrial acetyl-CoA/CoA and NADH/NAD⁺ ratios, subsequently inhibiting pyruvate dehydrogenase (PDH). This, in turn, would inhibit phosphofructokinase, a key rate-controlling enzyme of glycolysis through a feedback mechanism of increased citrate concentrations. Eventually this should lead to increased levels of glucose-6-phosphate (G-6-P), inhibiting hexokinase II activity and resulting in accumulation of intracellular glucose and decreased glucose uptake⁴¹. However, a series of studies by the group of Shulman have challenged this concept. Using non-invasive ³¹P and ¹³C magnetic resonance spectroscopy (MRS) to measure

skeletal muscle G-6-P and glycogen synthesis, respectively, they were unable to detect an increase in skeletal muscle G-6-P in type 2 diabetes patients⁴² and during fatty acid-induced insulin resistance in skeletal muscle⁴³. They even observed a decrease in G-6-P, preceding a decrement in glycogen synthesis⁴³.

A following study pointed towards a defect in the glucose transport induced by free fatty acids, a few steps earlier in the glucose pathway than proposed by Randle *et al.*⁴⁴. As an alternative for the glucose-fatty acid cycle, Shulman proposed a mechanism explaining fatty acid-induced hampering of glucose transport, in which intracellular lipids interfere with the insulin signaling pathway⁴⁵. The proposed alternative mechanism involves the increase in intracellular lipid metabolites such as diacylglycerol, long chain fatty-acyl-CoA and ceramides due to increased delivery of lipids to muscle or decreased intracellular fatty acid oxidation. These metabolites activate a protein kinase leading to the phosphorylation of serine/threonine sites on the insulin receptor substrate 1, which in turn hampers the activation of phosphatidylinositol 3-kinase, eventually resulting in a diminished glucose transport activity (Figure 2)⁴⁵. Studies in animals, humans and *in vitro* systems have since then confirmed several steps of the proposed mechanism⁴⁶. However, data are still not conclusive about which fatty acid intermediates most strongly interfere with the intracellular insulin cascade^{44, 46-49}.

Mitochondrial dysfunction and insulin resistance

In biological systems, ATP is the universal currency of free energy. Upon the hydrolysis of ATP [1], free energy is released which can be used to drive the active transport of molecules and ions, the synthesis of macromolecules and the performance of mechanical work in muscle contractions and other cellular movements.



Normally the energy needed for ATP synthesis is predominantly derived from the metabolic conversion of carbohydrates and fat, which are directly derived from an ingested meal, or liberated from glycogen or triglyceride depots, respectively. In mammalian muscle cells there are two major pathways for ATP formation: glycolysis, producing ATP anaerobically in the cytosol and oxidative phosphorylation, which takes place in the mitochondria and generates ATP aerobically. Irrespective of whether carbohydrates or lipids are used as a substrate, the oxidative ATP production almost completely occurs in the mitochondrion, a highly organized organelle.

Mitochondrion

Mitochondria are double-membrane cell organelles which play a pivotal role in many aspects of cellular metabolism (Figure 3). Their primary function, however, is to deliver energy in the

form of adenosinetriphosphate (ATP) via aerobic respiration for intracellular energy-consuming processes ⁵⁰. In line with the function as energy powerhouse, the density of mitochondria varies from one tissue to another, related to the dependency of the tissue on oxidative energy production ⁵¹. Thus, neurons and cardiac and skeletal muscle cells have a high density of mitochondria. Given their fundamental role in the human body, defects in mitochondrial function generally have severe consequences and are associated with a wide range of human diseases (reviewed in ⁵¹).

Because mitochondria are enclosed by a double membrane they are made up of two aqueous compartments: the intermembrane space and the matrix. In contrast to the outer membrane, the inner membrane surface area is greatly increased by a large number of folds (cristae), protruding into the matrix ^{50, 52}. The outer membrane is fairly permeable because it contains a large number of transmembrane proteins with a large pore, i.e. porins. The inner membrane is semi-permeable and has a very high content of proteins, among which the multi-subunit complexes which constitute the ATP-generating oxidative phosphorylation system ^{50, 52}.

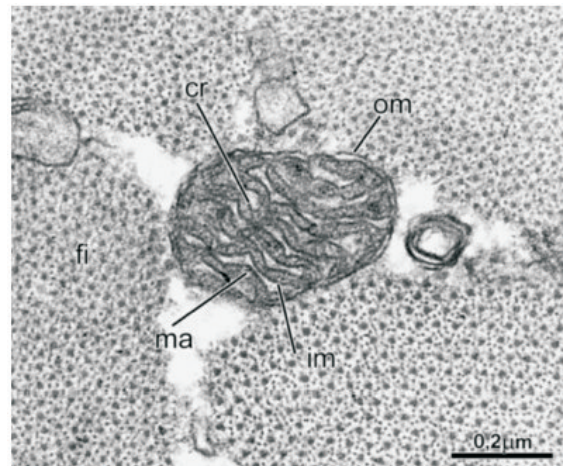


Figure 3 Electron microscopy image of a mitochondrion in a cross-section of human skeletal muscle sample. om: outer membrane; im: inner membrane; ma: matrix; cr: cristae; fi: myofibrils. Courtesy of Hoppeler: Med sci Sports Exerc 2003; 35:95-104. Copyright: LWW; Reproduced with permission

The oxidative phosphorylation (OXPHOS) system can be broken up into two closely linked components: the electron transport chain (ETC) responsible for oxidation on one hand and the F_1F_0 ATP-ase complex governing the phosphorylation on the other hand (Figure 4). The ETC consists of four specialized transmembrane complexes, of which complex I, III and IV act as proton pumps. Complex II is, in addition to complex I, an acceptor of reducing equivalents. The F_1F_0 ATP-ase complex (complex V) is a highly specialized molecular machine built out of several sub-units, which also crosses the inner mitochondrial membrane.

Under normal conditions, fatty acids and carbohydrates fuel the mitochondrial ATP production. Carbohydrates are converted to pyruvate through glycolysis, which takes place in the cytosol. Pyruvate is subsequently transported to the mitochondria and converted to acetyl-CoA by the pyruvate dehydrogenase multi-enzyme complex. Fatty acids are transported into the mitochondria through the carnitine shuttle and further degraded to acetyl-CoA in the β -oxidation pathway. So, both carbohydrate and fatty acid metabolism result in acetyl-CoA as an intermediate metabolite. Acetyl-CoA is next fed into the tricarboxylic acid cycle (TCA) releasing carbon dioxide (CO_2) and reducing the special electron carriers: nicotinamide adenine dinucleotide (NADH) and flavin adenine dinucleotide ($FADH_2$). NADH and $FADH_2$ transfer their electrons to oxygen (O_2) via the ETC. During this process electrons flow between the different transmembrane complexes leading to the pumping of protons across the inner mitochondrial membrane, this way converting electron-motive force into proton-motive force. NADH delivers

its electrons to complex I, whereas the electrons of FADH_2 are fed into the ETC via complex II. Eventually this sequential process results in the donation of the electrons (mediated by complex IV) to O_2 , the final electron acceptor and the formation of water (H_2O) (Figure 4). The proton-motive force created across the inner membrane is ultimately the driving force for the generation of ATP through the $\text{F}_1\text{F}_0\text{ATP-ase}$ complex (complex V). This latter mechanism was first postulated by Sir Peter Mitchell in 1961⁵³, formulating how the proton-motive force is redirected into a phosphoryl potential. ATP is formed as protons travel from the intermembrane compartment towards the matrix, passing through the $\text{F}_1\text{F}_0\text{ATP-ase}$ complex. In doing so, energy derived from this proton flow is used to generate ATP by combining adenosinediphosphate (ADP) and inorganic phosphate (Pi).

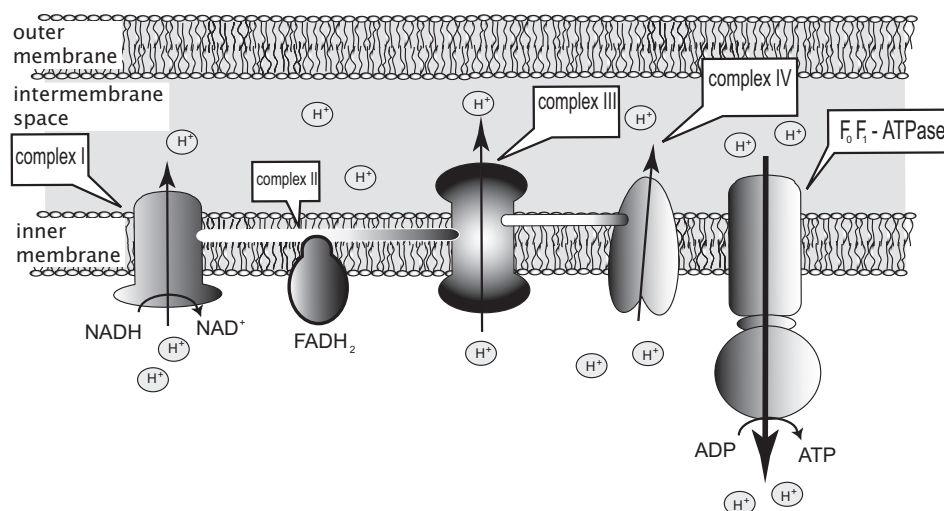


Figure 4 Cartoon depicting the different components of the electron transport chain and the ATP-synthase in the inner membrane of the mitochondrion. Upon transferring the electrons of NADH and FADH to complex I and complex II, respectively, the electrons travel along the different complexes accompanied by the pumping of protons from the matrix to the intermembrane space. The protons in the intermembrane space subsequently travel back to the matrix passing through the ATP-synthase, which goes along with the formation of ATP.

Mitochondria and insulin resistance

Recently, insulin resistance has been associated with skeletal muscle mitochondrial dysfunction (reviewed in⁵⁴). Data originating from *in vivo* measurements⁵⁵⁻⁵⁷, *in vitro* enzyme assays⁵⁸⁻⁶¹ and measurements of expression of genes involved in oxidative metabolism^{62, 63} all point towards a role for skeletal muscle mitochondrial dysfunction in insulin resistance and type 2 diabetes. Current hypotheses link inherited or acquired mitochondrial dysfunction to a dysregulated fatty acid metabolism which subsequently results in increased levels of IMCL and fatty acid intermediates inducing insulin resistance^{55, 56, 64}. However, solid evidence of functional impairment of mitochondria in type 2 diabetes is lacking. Most reported impairments in oxidative capacity could alternatively be explained by decreases in mitochondrial content which could be the result of a sedentary lifestyle⁵⁴. After all, exercise or chronic contractile activity are known to induce remarkable phenotypic alterations in mitochondria (reviewed in⁶⁵ and²⁷)

IMCL, how to measure?

Overall, techniques applied over the years to measure IMCL can be divided into two categories: invasive methods and non-invasive methods. Besides the major disadvantage and advantage of the different methods already defined by this classification, there are more pros and cons to be discussed.

Invasive methods

In humans, these methods mostly involve the application of the percutaneous muscle biopsy technique²⁸, yielding a small sample of muscle tissue (~100 mg). This immediately identifies another drawback of the invasive methods: only a very small part in relation to the entire muscle is studied. In animal studies, in general the animal is sacrificed and the complete muscle can be studied. The muscle sample can be used for biochemical triglyceride extraction or microscopic analyses. The biochemical analysis involves freeze-drying and chloroform-methanol extraction to isolate lipids. Critical to the application of this method is the removal of all visible fat deposits from the sample, since these can easily cause a high variability of the lipid content^{66, 67}.

Traditional light microscopy, fluorescence microscopy and electron microscopy (EM) techniques are all being used to measure IMCL. When stained with Oil Red O, lipid droplets appear reddish under light microscopy⁶⁸. When combining Oil Red O staining with immunofluorescent staining, IMCL can be studied in relation to e.g. muscle fiber type⁶⁸.

Due to the much higher resolution, EM allows to investigate IMCL in an ultra-structural way²⁷. However, the sample size examined applying EM is dramatically small compared to the entire muscle volume. Therefore, in practice, EM analysis of IMCL is poorly representative for whole muscle.

Non-invasive methods

Computed tomography and magnetic resonance imaging

Both computed tomography (CT) and magnetic resonance imaging (MRI) are non-invasive imaging techniques. While CT is an X-ray based method, MRI uses the magnetic properties of protons to discriminate fat from other tissue. Although both methods allow to measure the fat content of a whole muscle or even different muscles of a limb in one shot, they cannot discriminate between IMCL and EMCL^{69, 70}.

Magnetic resonance spectroscopy

The discovery that IMCL and EMCL resonate at different frequencies in the ¹H MR spectrum of human skeletal muscle measured at clinical magnetic field strengths was an important methodological advance for the study of skeletal muscle lipid metabolism⁷¹. The resonance at 1.28 ppm is independent of the angle between the muscle fibers and the static magnetic field

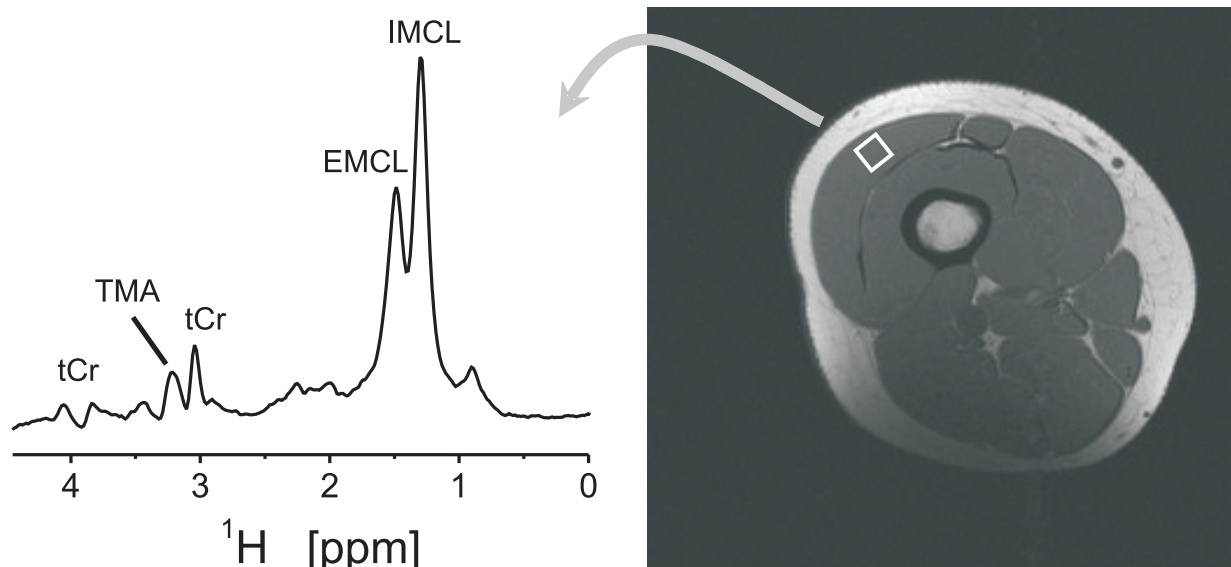


Figure 5 Right: MR image with voxel positioned in the *M. vastus lateralis*. Left: ^1H MR spectrum with peaks of creatine (tCr), tri-methylammonium groups (TMA), extramyocellular lipids (EMCL) and intramyocellular lipids (IMCL).

and was therefore attributed to the CH_2 groups of IMCL, because IMCL is dispersed as spherical droplets within the muscle cells. The other lipid CH_2 peak shifts with the angle between the muscle fibers and the field and was therefore attributed to EMCL, which supposedly is arranged in a sheet-like manner along the muscle fibers. The largest chemical shift difference between the two peaks is 0.2 ppm, which is obtained when the muscle fibers are aligned parallel with the magnetic field ⁷². Since ^1H MRS is a non-invasive method, it allows repetitive analysis of IMCL in the same area. Thus, ^1H MRS based IMCL measures are especially useful for the determination of IMCL levels in human studies, as well as for animal intervention and longitudinal studies (Figure 5).

To measure IMCL, ^1H MRS is mostly applied using a single voxel-based approach. Typical voxel sizes are $12 \times 11 \times 18 \text{ mm}^3$ for single-voxel applications in humans ⁷² and $2 \times 2 \times 2 \text{ mm}^3$ in animals ^{73, 74}. The processing of ^1H MRS data requires sophisticated analyses to discriminate between IMCL and EMCL peaks, as these peaks mostly partially overlap. Overlap of IMCL and EMCL is especially an issue in obese subjects and at lower field strengths (1.5 T) ⁷⁵.

As an alternative to single-voxel ^1H MRS, spectroscopic imaging (SI) can be applied, in which a matrix of voxels can be scanned across e.g. a whole cross-section of a lower leg ^{74, 76}. In combination with the increasing availability of higher clinical field strengths, SI is most likely the method of choice in future studies. In analogy with MRI, SI allows to measure IMCL in different muscles of a limb in one exam ⁷⁶, at a higher spatial resolution ⁷⁶ and provides the possibility of post-acquisition voxel re-positioning in order to avoid EMCL signals that complicate IMCL quantification (reviewed in ⁷⁵). However, ^1H SI will not achieve the resolution enabling muscle fiber type-specific IMCL measurements in humans, which is a limitation compared to the histological techniques.

Mitochondrial function, how to measure?

Similar to techniques used to measure IMCL, the methods applied to measure mitochondrial function can be divided into invasive and non-invasive methods. Again, the former involves sampling of human muscle via a biopsy method or, in case of animal studies, sacrificing the animal and harvesting complete muscles. The typical drawbacks of invasive methods are limited sample size in case of studies in humans and the limited feasibility, or impossibility in case of small animal studies, to repetitively sample muscle. On the other hand, sampling muscle tissue offers the opportunity to measure directly in mitochondria, whereas the non-invasive methods only allow indirect assessment of the function of mitochondria.

Invasive methods (in vitro)

As described above, the OXPHOS system is built out of enzymes and transport proteins forming the ETC and F_1F_0 ATP-ase complex, residing in the inner mitochondrial membrane. *In vitro* analyses of mitochondrial function range from measurements on gene expression^{62, 63, 77, 78} and protein content of enzymes involved in OXPHOS⁷⁸⁻⁸⁰, to measurements of enzyme activity^{59, 60, 81} and n respirometry measurements in permeabilized muscle fibers⁸²⁻⁸⁴.

Gene and protein expression studies on mitochondrial function often focus on peroxisome proliferator-activated receptor (PPAR) gamma coactivator (PGC) 1alpha (PGC-1 α), a transcriptional co-activator that can be considered as a master regulator of mitochondrial gene expression^{62, 63, 77, 78}. A decreased PGC-1 α expression is suggested to be responsible for decreased expression of proteins playing a role in OXPHOS.

Another *in vitro* approach is to measure the activity of individual enzymes that are part of the OXPHOS system. This method requires a homogenized muscle sample or intact, isolated mitochondria and the rationale of this assay is to measure the enzyme's maximal activity when catalyzing the reaction of interest under ideal conditions (i.e., pH and temperature) in order to detect a possible impairment⁵⁸⁻⁶¹.

High resolution respirometry of isolated, intact mitochondria makes it possible to measure the OXPHOS system as an entity while keeping the inner mitochondrial membrane of the mitochondria intact. This technique requires the isolation of mitochondria out of the muscle cell's dense myofibrillar network, via several ultracentrifugation steps. The isolated mitochondria are then re-suspended in a buffer solution and subsequently the respiration is measured using an oxygen sensitive electrode. Classically, the mitochondrial respiration is measured with different substrates and under stimulated (high ADP concentration, a condition termed "state 3") and non-stimulated conditions (no ADP, "state 4"). By varying the substrates and using enzyme-specific inhibitors, the activity of certain segments of the respiratory chain can be measured selectively, while residing in their normal environment. The ratio of state 3 over state 4 can be calculated, known as the respiratory control ratio (RCR), reflecting the degree of coupling between electron transfer and oxidative phosphorylation⁸⁵. Adding an artificial uncoupler allows protons to travel back from the intermembrane space towards the

cytosol via another route than through the F_1F_0 ATP-ase complex and thus without generating ATP. Uncoupling agents can be used to study the capacity of the ETC isolated from the phosphorylation step.

An alternative approach for the high resolution respirometry of isolated mitochondria is to carry out these measurements in permeabilized skeletal muscle fibers^{86, 87}. The permeabilized muscle fiber methodology can be performed in smaller muscle samples and is characterized by a relatively high amount of mitochondria present in the sample (>90%) compared to the isolated mitochondria (10-40%)⁸⁶. Permeabilized fibers have also the advantage that the mitochondria remain in a more physiological surrounding. Whereas isolated mitochondria appear swollen in generally used incubation media⁸⁸, there are indications that this is not the case in permeabilized fibers⁸⁷. On the other hand, using the permeabilized fiber method makes it difficult to compare different samples since weight-related mitochondrial content may differ across samples resulting in different respiratory rates⁸⁶.

Non-invasive methods (in vivo)

In the next section, a description of different *in vivo* MRS methods will be given, with the emphasis on the post-exercise recovery kinetics of phosphorous metabolites, the dynamic ^{31}P MRS application used to measure oxidative capacity in the studies presented in this thesis.

Figure 6 shows an *in vivo* ^{31}P MR spectrum measured in human skeletal muscle at rest. The spectrum shows several peaks from different ^{31}P -containing metabolites. The most prominent peak is from phosphocreatine (PCr) and there are three peaks originating from the α -, β - and γ -phosphates in ATP and one from inorganic phosphate (Pi). A smaller peak can also be recognized, which belongs to phosphodiester (PDE).

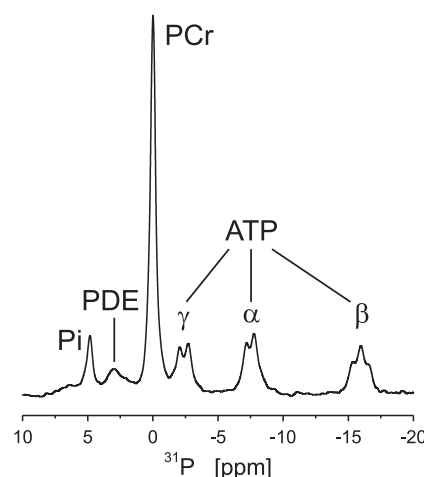


Figure 6 ^{31}P MR spectrum from human *m. vastus lateralis* at rest. Pi indicates inorganic phosphate; PDE, phosphodiester; PCr, phosphocreatine; and α , β and γ indicate the 3 phosphate groups of ATP.

The spectrum also allows to measure the intracellular pH, based on the difference in resonance frequency between PCr and Pi^{89, 90}. The PCr peak position remains constant within the physiological pH range, whereas the Pi peaks shifts depending on the intracellular pH. The NMR signal of the Pi peak originates from the phosphorous atoms of both H_2PO_4^- and HPO_4^{2-} . However, as these compounds are in rapid chemical exchange, a single peak is observed. The chemical shift of Pi is therefore a function of the ratio of the H_2PO_4^- and HPO_4^{2-} concentrations and in this way serves as an indicator of intracellular pH^{89, 90}.

Intracellular ADP concentrations are too low to directly detect in a ^{31}P MR spectrum. However, using the equilibrium constant (K_{eq}) of the creatine kinase (CK) reaction it is possible to calculate the ADP concentration, knowing the concentration of ATP and total creatine from biochemistry measurements and determining the pH and PCr concentration from the ^{31}P MR

spectrum⁹¹. Two different *in vivo* ³¹P MRS methodologies have thus far been applied to study mitochondrial function in relation to insulin resistance and type 2 diabetes: 1) saturation transfer to measure the ATP synthesis flux at rest^{55, 56}, and 2) post-exercise recovery of PCr^{57, 92, 93} and/or ADP⁹⁴.

Saturation transfer

Under certain conditions, MRS allows the *in vivo* measurement of steady-state fluxes of NMR-visible metabolites. The principle of these measurements is to disturb the magnetic equilibrium of the system of interest and consequently monitor the response to this disturbance. In case of a saturation transfer (ST) experiment, the disturbance is actually the saturation (canceling) of the magnetization of one of the reactants. Due to the chemical exchange of the reactants, this results in a decrease of magnetization of the exchange partner. A prerequisite for the determination of the flux is that the system of interest (reaction) is in a metabolic steady state. This is obviously easiest to accomplish at rest. However, ST experiments have also been applied in animals during steady state exercise conditions⁹⁵.

ST has extensively been applied to study the CK reaction. Due to the relatively fast exchange of the reactants of the CK reaction, saturation of the γ -ATP peak results in large differences in the magnetization of PCr. Applying the described ST technique, the CK reaction has been studied in skeletal muscle^{96, 97}, heart⁹⁸⁻¹⁰⁰ and brain tissue^{101, 102}.

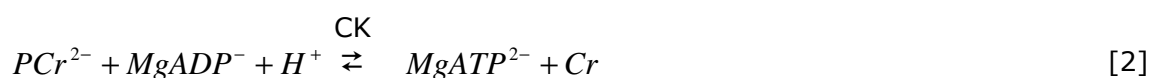
³¹P saturation transfer can also be performed to measure the unidirectional flux from P_i towards ATP^{95, 103-105}. The measured P_i → ATP flux originates from reactions catalyzed by both the mitochondrial F₁F₀-ATP-ase and by the glycolytic enzymes glyceraldehyde-3-phosphate dehydrogenase and phosphoglycerate kinase^{104, 106}. Therefore the calculated flux comprises both oxidative and glycolytic ATP production. Unfortunately, ST experiments cannot discriminate between the different reactions catalyzing the formation of ATP. However, the glycolytic ATP production is assumed to have only a small contribution to the total ATP synthesis flux at rest and therefore the ST method has often been applied taking for granted that the measured P_i → ATP flux predominantly represented the flux through the F₁F₀-ATP-ase^{56, 107, 108}.

ST has been applied in human skeletal muscle to evaluate mitochondrial function at rest in elderly people⁵⁵, insulin-resistant offspring from type 2 diabetes subjects under normal⁵⁶ and under insulin-stimulated conditions¹⁰⁸. Both the elderly population and the type 2 diabetes offspring showed decreased P_i → ATP fluxes at rest compared to controls, which was suggested to originate from a dysfunction of the skeletal muscle mitochondria^{55, 56}. Under insulin-stimulated conditions, this lower P_i → ATP flux became even more prominent, as control subjects witnessed a ~90% increase in ATP synthesis rate, whereas the insulin resistant offspring hardly displayed any change¹⁰⁸. The authors explained these data as "...further evidence of mitochondrial dysfunction in skeletal muscle..."¹⁰⁸. The use of the term "mitochondrial dysfunction" by Petersen *et al.* suggests that the decreased P_i → ATP fluxes measured in their insulin resistant and type 2 diabetes subjects are reduced because of a defect in the mitochondria.

Although research on the control of OXPHOS is still ongoing, it has become clear over the years that OXPHOS is controlled by extramitochondrial factors, from which ADP has been identified as the principal one, reflecting the intracellular energy status ¹⁰⁹⁻¹¹¹. High ADP levels, e.g. during exercise, can induce ATP synthesis rates more than 10 times higher compared to the rest situation when ADP levels are low ¹¹². OXPHOS is predominantly controlled by the energy demand in the cell and can easily cope with an energy demand that is several times the resting metabolic rate. Therefore, it is equally plausible that a lower ATP synthesis rate at rest and under insulin-stimulated conditions in insulin resistant or diabetic subjects is reflecting a lower energy demand, rather than a mitochondrial defect. The reduced energy demand could in this case be related to the insulin resistant status of the muscle and could be the result of reductions in the rates of GLUT4 trafficking, glucose phosphorylation, glycogen synthesis and protein synthesis due to an impairment in the insulin signaling pathway. Data in support of this concept arise from ST measurements in young, healthy, insulin sensitive subjects ¹⁰⁷. In these subjects the insulin-stimulated ATP synthesis rate was measured in a control situation and after inducing insulin resistance by 3 hours of intravenous lipid infusion. After becoming insulin resistant, the ATP synthesis rate did not change upon insulin stimulation and was 24% lower compared to the control situation (saline infusion). Moreover, grouping the data from both experimental conditions, the change in ATP synthesis rate was positively correlated with the change in G-6-P ¹⁰⁷. This is in agreement with the concept that the energy demand resulting from cellular glucose uptake is matched by the ATP synthesis flux ¹⁰⁷, and is probably not related to an intrinsic defect of the mitochondria.

Post-exercise PCr recovery

The energy needed for muscle cells to contract is provided by the hydrolysis of ATP. However, in order to guarantee cellular integrity, the ATP level in a cell has to be constant within a narrow range. For muscle contractions to sustain and muscle cells to survive, the ATP pool has to be replenished continuously. As glycolysis and oxidative ATP-producing pathways cannot cope with an immediate ATP demand, a rapidly available source of ATP is necessary. This is provided by the creatine kinase (CK) system that catalyzes the reversible reaction:



PCr acts as a temporal energy buffer keeping the intracellular ATP concentration at an almost constant level during contractions. The temporal buffering capacity of the CK system can be observed in a sequential acquisition of ³¹P spectra during exercise (Figure 7). At the start of the exercise, the PCr signal drops, while the ATP level is maintained despite a continuous use of ATP during the muscle contractions. The moment the exercise ceases, the PCr pool is restored. The PCr resynthesis is almost completely fueled by ATP originating from oxidative phosphorylation, since there is no restoration of PCr during ischemic recovery ^{90, 113}. As the CK reaction is much faster than the oxidative ATP production, the PCr recovery reports on the mitochondrial oxidative ATP production. Analysis of the PCr recovery kinetics therefore provides information about mitochondrial respiratory function. The most straightforward

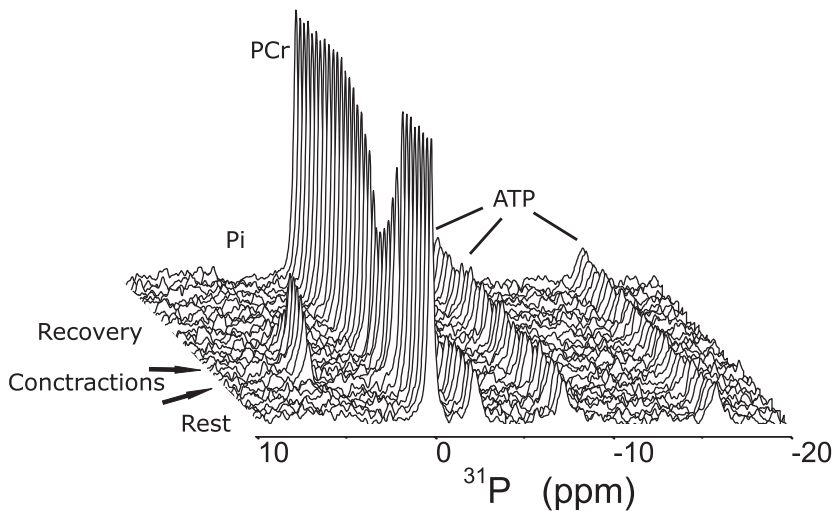


Figure 7 Stack plot of ^{31}P MR spectra from a time series measured during a rest-exercise-recovery protocol in a rat tibialis anterior muscle. Contractions were induced by electrical stimulation. Time resolution = 20 s. Peaks are from inorganic phosphate (Pi), phosphocreatine (PCr) and ATP. PPM = parts per million.

approach of post-exercise PCr analysis is determining the time constant or half-time of the recovery of the PCr signal. This can be done by fitting the recovery data with a mono-exponential function.

Measurement of post-exercise PCr recovery kinetics with ^{31}P MRS has been used over years to evaluate mitochondrial function ¹¹⁴⁻¹¹⁶. The PCr recovery reflects mitochondrial activity in a highly stimulated condition, since at the start of the post-exercise recovery ADP levels are high. In a simplified concept, PCr recovery kinetics could be considered as the *in vivo* equivalent of the *in vitro* state 3 respiration. Therefore post-exercise PCr-recovery analysis seems a more suitable ^{31}P MRS technique to detect defects in mitochondrial function than ATP synthesis rate measurements at rest, resembling more closely the *in vitro* state 4 respiration. However, measuring post-exercise PCr recovery kinetics can be laborious and/or difficult to carry out. After all, it requires exercise to be carried out in the MR-scanner and the exercise intensity has to be sufficiently high to result in a significant PCr depletion. This might require relatively strenuous exercise protocols, not always tolerable for patients. Furthermore, a significant decrease in PCr is usually associated with a decrease in intracellular pH due to anaerobic glycolysis and concomitant lactate production. The end-exercise pH is known to affect the PCr recovery kinetics, in that it slows down the resynthesis of PCr ¹¹⁷. Therefore it has been recommended to avoid low end-exercise pH values, which is obviously difficult to achieve in combination with a significant PCr depletion.

There are several strategies to deal with the end-exercise pH issue. First of all, when comparing PCr recovery kinetics of different groups of patients or when measuring before and after an intervention, one could attempt to reproduce the end-exercise pH as much as possible. As an alternative to the PCr recovery, also the ADP recovery can be measured. The ADP recovery kinetics has been suggested to be even a more suitable parameter to evaluate mitochondrial oxidative capacity ¹¹⁸. Also Q_{\max} , the maximum aerobic capacity can be calculated from the PCr recovery data. Both the ADP recovery ^{114, 119-121} and Q_{\max} ^{120, 122, 123} have been shown to be pH-independent. However, both parameters are indirect measures, since they are derived from the PCr recovery data. The calculation of the ADP concentration relies on the calculated pH and on assumptions made about the CK equilibrium constant and

the total creatine concentration ⁹¹. Q_{\max} on the other hand is based on the ADP control model, assuming that OXPHOS is regulated by the ADP concentration according Michaelis-Menten kinetics ¹²⁴. A more extensive description of different ³¹P MRS markers of oxidative capacity is presented in Chapter 4.

Outline of the thesis

The aim of the present thesis is to study IMCL and mitochondrial function in relation to insulin resistance and type 2 diabetes, in humans as well as in animals. Both ³¹P and ¹H MRS play a crucial role in being the methodologies that were predominantly applied in the presented studies. The chapters which focus on the implementation of the different *in vivo* MRS methods are compiled in a first methodological section of the thesis, whereas the second section comprises the studies which address the role of mitochondrial function and IMCL in insulin resistance and type 2 diabetes.

The application of localized ¹H MRS to measure IMCL in rat tibialis anterior muscle is described in **Chapter 2**. The muscle fiber type is an important determinant of IMCL. Oxidative type I fibers can contain up to three times more IMCL than the glycolytic type II muscle fibers. Since the different muscle fiber types are inhomogeneously distributed in rodent muscle, we investigated the distribution of IMCL *in vivo* within the rat tibialis anterior muscle along with the *ex vivo* determined muscle fiber type distribution. Also the effect of interventions inducing changes in IMCL concentration, such as high-fat diet and fasting, was studied. In **Chapter 3** a technical aspect related to dynamic *in vivo* MRS in rodents is covered. To allow the measurement of PCr recovery in rat skeletal muscle, muscle contractions need to be induced through electrical stimulation. A minimally invasive, subcutaneous electrical stimulation procedure for rat lower hind limb is presented that induces isolated contractions of the dorsal flexor muscles. The specificity of the set-up for the tibialis anterior and the extensor digitorum muscles was tested by analyzing the contraction-induced signal enhancement in ¹H MR images. **Chapters 4 and 5** both discuss the implementation of ³¹P MRS to study *in vivo* skeletal muscle mitochondrial function in humans. In **Chapter 4** the relationship between ³¹P MRS-derived parameters describing mitochondrial function, an *in vitro* marker of muscle oxidative capacity and muscle fiber type composition was evaluated in a group of long-term, insulin-treated type 2 diabetes patients. **Chapter 5** deals with the effect of the end-exercise pH on the recovery kinetics of PCr, as studied in healthy control subjects. Measurements were performed in the same muscle group and applied a similar exercise protocol as used in the studies with type 2 diabetes patients.

The second section of this thesis starts with a cross-sectional study with the aim to gain insight in the proposed role of mitochondrial dysfunction in the etiology of insulin resistance and/or type 2 diabetes (**Chapter 6**). Three groups of subjects were compared: long-standing, insulin-treated type 2 diabetes patients, subjects with early stage type 2 diabetes and subjects with normal glucose tolerance, which were all matched for age, body composition and had similar habitual physical activity levels. *In vivo* skeletal muscle mitochondrial function was determined from post-exercise PCr recovery kinetics using ³¹P MRS and IMCL content was measured using

single-voxel ^1H MRS. In order to gain insight in the sequence of events during the development of type 2 diabetes, a longitudinal study in animals was performed in an established rodent model of type 2 diabetes: the Zucker Diabetic Fatty (ZDF) rat (**Chapter 7**). The homozygous animals (fa/fa) are characterized by a progressive loss of insulin sensitivity during maturation that results in overt type 2 diabetes in adulthood, while the heterozygous animals (fa/+) remain normoglycemic and served as a control group. Similar to the human studies, IMCL was measured using localized ^1H MRS and *in vivo* skeletal muscle mitochondrial function was evaluated by means of PCr post-exercise kinetics. The latter required the implementation of the minimally invasive electrical stimulation method described in Chapter 3, in order to measure the same animals during the development of type 2 diabetes in a longitudinal manner. Both IMCL and *in vivo* skeletal muscle oxidative capacity were measured at 6, 12 and 18 weeks of age, characteristic time points in the development of type 2 diabetes in this rat model. Parallel to the *in vivo* experiments, animals were sacrificed at the same ages at which their congeners underwent the MRS examinations. The muscles of the sacrificed animals were excised and mitochondria were isolated for *in vitro* analyses of mitochondrial respiration. State 3, state 4 and uncoupled respiration were measured on different substrates.

The group of long-standing, insulin-treated type 2 diabetes patients described in Chapter 6 did also participate in an exercise intervention study. In that study, described in **Chapter 8**, we aimed to investigate the feasibility and the benefits of a specifically designed low-impact exercise intervention program. The exercise training program combined both endurance and resistance type exercise. The impact of 5 months of exercise training on glycemic control, body composition, whole-body and skeletal muscle oxidative capacity and cardiovascular risk profile was assessed. **Chapter 9** provides an overview of the results and presents the main outcomes of the described studies. The results are discussed from the perspective of current hypotheses and contemporary paradigms.

References

1. International Diabetes Federation. (2006).
2. Wild, S. et al. *Diabetes Care* **27**, 1047-1053 (2004).
3. Zimmet, P., Alberti, K.G. & Shaw, J. *Nature* **414**, 782-787 (2001).
4. DeFronzo, R.A. et al. *J Clin Invest* **76**, 149-155 (1985).
5. DeFronzo, R.A. et al. *Diabetes* **30**, 1000-1007 (1981).
6. Watson, R.T. & Pessin, J.E. *Recent Progress in Hormone Research* **56**, 175-194 (2001).
7. Tremblay, F., Dubois, M.J. & Marette, A. *Front Biosci* **8**, d1072-1084 (2003).
8. Coderre, L. et al. *J Biol Chem* **270**, 27584-27588 (1995).
9. Douen, A.G. et al. *J Biol Chem* **265**, 13427-13430 (1990).
10. Zorzano, A., Fandos, C. & Palacin, M. *Biochem J* **349 Pt 3**, 667-688 (2000).
11. Bjornholm, M. & Zierath, J.R. *Biochem Soc Trans* **33**, 354-357 (2005).
12. Weickert, M.O. & Pfeiffer, A.F.H. *Diabetologia* **V49**, 1732-1741 (2006).
13. Goodyear, L.J. et al. *Am J Physiol* **268**, E987-995 (1995).
14. Treadway, J.L. et al. *Am J Physiol* **256**, E138-144 (1989).
15. Ivy, J.L. & Holloszy, J.O. *Am J Physiol* **241**, C200-203 (1981).
16. Klip, A. et al. *FEBS Lett* **224**, 224-230 (1987).
17. Hayashi, T. et al. *Diabetes* **47**, 1369-1373 (1998).
18. Hardie, D.G., Carling, D. & Carlson, M. *Annu Rev Biochem* **67**, 821-855 (1998).
19. Winder, W.W. *Diabetes Technol Ther* **2**, 441-448 (2000).
20. Jessen, N. & Goodyear, L.J. *J Appl Physiol* **99**, 330-337 (2005).
21. Guyton, A.C.H., J. E. Textbook of Medical Physiology, Edn. 9. (W.B. Saunders Company, Philadelphia; 1996).
22. Eckel, R.H., Grundy, S.M. & Zimmet, P.Z. *Lancet* **365**, 1415-1428 (2005).
23. Kahn, S.E. *J Clin Endocrinol Metab* **86**, 4047-4058 (2001).
24. Alberti, K.G. & Zimmet, P.Z. *Diabet Med* **15**, 539-553 (1998).
25. Tuomilehto, J. et al. *N Engl J Med* **344**, 1343-1350 (2001).
26. Kennedy, J.W. et al. *Diabetes* **48**, 1192-1197 (1999).
27. Hoppeler, H. et al. *Pflugers Arch* **344**, 217-232 (1973).
28. Bergstrom, J., Hultman, E. & Saltin, B. *Int Z Angew Physiol* **31**, 71-75 (1973).
29. Carlson, L.A., Ekelund, L.G. & Froberg, S.O. *Eur J Clin Invest* **1**, 248-254 (1971).
30. Froberg, S.O. & Mossfeldt, F. *Acta Physiol Scand* **82**, 167-171 (1971).
31. van Loon, L.J. *J Appl Physiol* **97**, 1170-1187 (2004).
32. van Loon, L.J. & Goodpaster, B.H. *Pflugers Arch* **451**, 606-616 (2006).
33. Schrauwen-Hinderling, V.B. et al. *J Clin Endocrinol Metab* **88**, 1610-1616 (2003).
34. Hurley, B.F. et al. *J Appl Physiol* **60**, 562-567 (1986).
35. Goodpaster, B.H. et al. *J Clin Endocrinol Metab* **86**, 5755-5761 (2001).
36. Krssak, M. et al. *Diabetologia* **42**, 113-116 (1999).
37. Dobbins, R.L. et al. *Diabetes* **50**, 123-130 (2001).
38. Kuhlmann, J. et al. *Diabetes* **52**, 138-144 (2003).
39. Hulver, M.W. et al. *Am J Physiol Endocrinol Metab* **284**, E741-747 (2003).
40. Randle, P.J. et al. *Lancet* **1**, 785-789 (1963).
41. Randle, P.J. et al. *Ann N Y Acad Sci* **131**, 324-333 (1965).
42. Rothman, D.L., Shulman, R.G. & Shulman, G.I. *J Clin Invest* **89**, 1069-1075 (1992).
43. Roden, M. et al. *J Clin Invest* **97**, 2859-2865 (1996).
44. Dresner, A. et al. *J Clin Invest* **103**, 253-259 (1999).
45. Shulman, G.I. *J Clin Invest* **106**, 171-176 (2000).
46. Yu, C. et al. *J Biol Chem* **277**, 50230-50236 (2002).
47. Aerts, J.M. et al. *Diabetes* (2007).
48. Kruszynska, Y.T. et al. *J Clin Endocrinol Metab* **87**, 226-234 (2002).
49. Powell, D.J. et al. *Biochem J* **382**, 619-629 (2004).
50. Bruce Alberts, D.B., Julian Lewis, Martin Raff, Keith Roberts, James D. Watson Molecular Biology of THE CELL, Edn. third. (Garland Publishing, New York; 1994).
51. Schapira, A.H. *Lancet* **368**, 70-82 (2006).
52. Stryer, L. Biochemistry, Edn. fourth. (W.H. Freeman and Company, New York; 1995).
53. Mitchell, P. *Nature* **191**, 144-148 (1961).
54. Rabol, R., Boushel, R. & Dela, F. *Appl Physiol Nutr Metab* **31**, 675-683 (2006).
55. Petersen, K.F. et al. *Science* **300**, 1140-1142 (2003).
56. Petersen, K.F. et al. *N Engl J Med* **350**, 664-671 (2004).
57. Schrauwen-Hinderling, V.B. et al. *Diabetologia* **50**, 113-120 (2007).
58. He, J., Watkins, S. & Kelley, D.E. *Diabetes* **50**, 817-823 (2001).
59. Kelley, D.E. et al. *Diabetes* **51**, 2944-2950 (2002).
60. Ritov, V.B. et al. *Diabetes* **54**, 8-14 (2005).
61. Simoneau, J.A. & Kelley, D.E. *J Appl Physiol* **83**, 166-171 (1997).
62. Mootha, V.K. et al. *Nat Genet* **34**, 267-273 (2003).
63. Patti, M.E. et al. *Proc Natl Acad Sci U S A* **100**, 8466-8471 (2003).
64. Roden, M. *Int J Obes (Lond)* **29 Suppl 2**, S111-115 (2005).
65. Hood, D.A. *J Appl Physiol* **90**, 1137-1157 (2001).
66. Guo, Z., Mishra, P. & Macura, S. *J Lipid Res* **42**, 1041-1048 (2001).
67. Wendling, P.S. et al. *J Appl Physiol* **81**, 1150-1155 (1996).
68. Koopman, R., Schaart, G. & Hesselink, M.K. *Histochem Cell Biol* **116**, 63-68 (2001).
69. Goodpaster, B.H. et al. *J Appl Physiol* **89**, 104-110 (2000).

70. Schick, F. et al. *Magn Reson Med* **47**, 720-727 (2002).
71. Schick, F. et al. *Magn Reson. Med.* **29**, 158-167 (1993).
72. Boesch, C. et al. *Magn Reson. Med.* **37**, 484-493 (1997).
73. Neumann-Haefelin, C. et al. *Magn Reson Med* **50**, 242-248 (2003).
74. De Feyter, H.M. et al. *Magn Reson Med* **56**, 19-25 (2006).
75. Boesch, C. et al. *NMR Biomed* **19**, 968-988 (2006).
76. Vermathen, P., Kreis, R. & Boesch, C. *Magn Reson Med* **51**, 253-262 (2004).
77. Timmons, J.A. et al. *Genomics* **87**, 165-172 (2006).
78. Morino, K. et al. *J Clin Invest* **115**, 3587-3593 (2005).
79. Hojlund, K. et al. *J Biol Chem* **278**, 10436-10442 (2003).
80. Asmann, Y.W. et al. *Diabetes* **55**, 3309-3319 (2006).
81. Short, K.R. et al. *Proc Natl Acad Sci U S A* **102**, 5618-5623 (2005).
82. Chansemaume, E. et al. *J Nutr* **136**, 2194-2200 (2006).
83. Chansemaume, E. et al. *Obesity (Silver Spring)* **15**, 50-59 (2007).
84. Boushel, R. et al. *Diabetologia* **50**, 790-796 (2007).
85. Devlin, T.M. Textbook of BIOCHEMISTRY with clinical correlations, Edn. fourth. (Wiley-Liss, Inc., New York; 1997).
86. Wolfgang, S. et al. *Molecular and Cellular Biochemistry* **V174**, 71-78 (1997).
87. Letellier, T. et al. *Pediatr Res* **32**, 17-22 (1992).
88. Bakeeva, L.E. et al. *Biochim Biophys Acta* **275**, 319-332 (1972).
89. Moon, R.B. & Richards, J.H. *J. Biol. Chem.* **248**, 7276-7278 (1973).
90. Taylor, D.J. et al. *Mol Biol Med* **1**, 77-94 (1983).
91. Lawson, J.W. & Veech, R.L. *J Biol Chem* **254**, 6528-6537 (1979).
92. Scheuermann-Freestone, M. et al. *Circulation* **107**, 3040-3046 (2003).
93. Challiss, R.A., Vranic, M. & Radda, G.K. *Am J Physiol* **256**, E129-137 (1989).
94. Sirikul, B. et al. *Am J Physiol Endocrinol Metab* **291**, E724-728 (2006).
95. Brindle, K.M. et al. *Biochemistry* **28**, 4887-4893 (1989).
96. Gadian, D.G. et al. *Biochem J* **194**, 215-228 (1981).
97. Meyer, R.A., Kuchmerick, M.J. & Brown, T.R. *Am J Physiol Cell Physiol* **242**, C1-11 (1982).
98. Nunnally, R.L. & Hollis, D.P. *Biochemistry* **18**, 3642-3646 (1979).
99. Matthews, P.M. et al. *Biochim Biophys Acta* **721**, 312-320 (1982).
100. Blackledge, M.J. et al. *Proc Natl Acad Sci U S A* **84**, 4283-4287 (1987).
101. Degani, H. et al. *Magn Reson Med* **5**, 1-12 (1987).
102. Cadoux-Hudson, T.A., Blackledge, M.J. & Radda, G.K. *Faseb J* **3**, 2660-2666 (1989).
103. Robitaille, P.M. et al. *Magn Reson Med* **15**, 8-24 (1990).
104. Kingsley-Hickman, P.B. et al. *Biochemistry* **26**, 7501-7510 (1987).
105. Matthews, P.M. et al. *Biochemical and Biophysical Research Communications* **103**, 1052-1059 (1981).
106. Brindle, K.M. & Radda, G.K. *Biochim Biophys Acta* **928**, 45-55 (1987).
107. Brehm, A. et al. *Diabetes* **55**, 136-140 (2006).
108. Petersen, K.F., Dufour, S. & Shulman, G.I. *PLoS Med* **2**, e233 (2005).
109. Chance, B. & Williams, G.R. *J. Biol. Chem.* **217**, 383-394 (1955).
110. Balaban, R.S. *Am J Physiol* **258**, C377-389 (1990).
111. Kunz, W.S. *Biochim Biophys Acta* **1504**, 12-19 (2001).
112. Wilson, D.F. *Med Sci Sports Exerc* **26**, 37-43 (1994).
113. Quistorff, B., Johansen, L. & Sahlin, K. *Biochem J* **291 (Pt 3)**, 681-686 (1993).
114. Arnold, D.L., Matthews, P.M. & Radda, G.K. *Magn Reson Med* **1**, 307-315 (1984).
115. Chance, B. et al. *Proc Natl Acad Sci U S A* **78**, 6714-6718 (1981).
116. Taylor, D.J. et al. *Gerontology* **30**, 2-7 (1984).
117. Iotti, S. et al. *Biochem Biophys Res Commun* **178**, 871-877 (1991).
118. Kemp, G.J. & Radda, G.K. *Magn Reson Q* **10**, 43-63 (1994).
119. Argov, Z., De Stefano, N. & Arnold, D.L. *NMR Biomed* **9**, 165-172 (1996).
120. Lodi, R. et al. *Magma* **5**, 165-171 (1997).
121. Boska, M.D. et al. *Magn Reson Med* **41**, 1145-1151 (1999).
122. Roussel, M. et al. *Biochim Biophys Acta* **1457**, 18-26 (2000).
123. Walter, G. et al. *Am J Physiol* **272**, C525-534 (1997).
124. Chance, B. et al. *Proc Natl Acad Sci U S A* **82**, 8384-8388 (1985).

Chapter 2

Regional variations in
intramyocellular lipid concentration
correlate with muscle fiber type
distribution in rat tibialis anterior
muscle

Adapted from:

De Feyter H.M., Schaart G., Hesselink M. K., Schrauwen P., Nicolay K., Prompers J.J.
Regional variations in intramyocellular lipid concentration correlate with muscle fiber
type distribution in rat tibialis anterior muscle.
Magn Reson Med 2006; 56:19-25

Abstract

^1H MR spectroscopy (MRS) has proven to be a valuable non-invasive tool to measure intramyocellular lipids (IMCL) in research focused on insulin resistance and type 2 diabetes, both in humans as well as in rodents. An important determinant of IMCL is the muscle fiber type, since oxidative type I fibers can contain up to three times more IMCL than glycolytic type 2 muscle fibers. Because these different muscle fiber types are heterogeneously distributed in rodent muscle, the present study investigated the distribution of IMCL within the rat tibialis anterior muscle (TA) *in vivo* using single-voxel ^1H MRS along with the muscle fiber distribution in the TA *ex vivo* determined from immunohistological assays.

IMCL levels in the TA differed by up to a factor of three, depending on the position of the voxel. The distribution of IMCL over the TA cross-section was not random, but emerged in a pattern similar to the distribution of the predominantly oxidative muscle fiber types. Dietary interventions like high-fat feeding and 15 hours of fasting did not significantly change this typical fiber type dependent pattern of IMCL content. These results stress the importance of the voxel positioning, when using single-voxel ^1H MRS to study IMCL in rodent muscle.

Introduction

Skeletal muscle insulin resistance is one of the earliest detectable aberrations in and a predisposing factor for the development of type 2 diabetes. Increased content of intramyocellular lipids (IMCL) has been closely associated with decreased whole body and skeletal muscle insulin sensitivity in both healthy and diabetic humans, as well as in animals (reviewed in ¹). IMCL itself probably does not interfere with the insulin signaling pathway directly, but is considered a surrogate marker of lipid metabolites, such as long chain acyl-CoA, diacylglycerol and ceramides, which are likely to induce defects in the insulin signaling cascade ². The good correlation of IMCL with insulin resistance even led to the suggestion of using IMCL as a biomarker for insulin resistance in rat models ³.

Skeletal muscle not only stores lipids intracellularly, but also extracellularly within interstitial adipocytes. Lipid extraction analysis of muscle biopsy samples therefore cannot differentiate between IMCL and extramyocellular lipids (EMCL) and hence may overestimate the actual IMCL content ¹. The discovery that IMCL and EMCL resonate at different frequencies in the ¹H MR spectrum of human skeletal muscle was an important methodological advance for the study of skeletal muscle lipid metabolism ⁴. The resonance at 1.28 ppm is independent of the angle between the muscle fibers and the static magnetic field and was therefore attributed to the CH₂ groups of IMCL, because IMCL is dispersed as spherical droplets within the muscle cells. The other lipid CH₂ peak shifts with the angle between the muscle fibers and the field and could therefore be attributed to EMCL, which supposedly is arranged in a sheet-like manner along the muscle fibers. The largest chemical shift difference between the two peaks is 0.2 ppm, which is obtained when the muscle fibers are aligned parallel with the magnetic field ⁵. Since ¹H MRS is a non-invasive method, it allows repetitive analysis of IMCL in the same area. Thus, ¹H MRS based IMCL measures are especially useful for the determination of IMCL levels in human studies, as well as for animal intervention and longitudinal studies.

Using ¹H MRS, Neumann-Haefelin et al. showed that the IMCL content in rat depends on age, strain and gender, complicating comparisons between different rat groups and different studies ⁶. They also showed that the IMCL content in the rather oxidative soleus muscle (SOL) is higher than in the predominantly glycolytic tibialis anterior (TA) ^{6, 7}. Similar differences have been observed in human calf skeletal muscles: the SOL contained about three times more IMCL than the TA ^{8, 9}. This can be attributed to differences in muscle fiber type composition in the different muscles, since it is well documented that the oxidative type I muscle fibers can contain up to three times more IMCL than the glycolytic type 2 muscle fibers ^{10, 11}.

Variations in fiber type composition can explain differences in IMCL levels found between different muscles studied as a whole. However, rodent muscle can also show a marked regionalization of the different muscle fiber types *within* a specific muscle itself, both in the cross-sectional plane as well as in the longitudinal direction ¹². Wang et al. showed a pronounced regionalization of type I muscle fibers in cross-sections of the TA of the rat. These type I fibers were clustered in the medial-posterior part of the muscle, close to the tibia bone ¹². The pronounced regionalization of type I muscle fibers in the rat TA and the higher capacity

of type I fibers to store IMCL compared to type II fibers suggest that IMCL levels could vary significantly within the cross-section of the rat TA. This may imply that differences in the voxel positioning within the rat TA can cause a large variability in the IMCL signal measured by single-voxel ¹H MRS, which could result in a misjudgment of changes in IMCL content during longitudinal and/or interventional studies in rats. Therefore the aim of the present study was to examine the IMCL content at different positions in TA of Wistar rat and relate it to muscle fiber type composition assessed by immunohistological analysis.

Furthermore, we determined the IMCL content at different positions within the TA after starvation and high-fat feeding. Neumann-Haefelin et al. showed that the increase in plasma free fatty acids (FFA) during starvation was paralleled by muscle-type dependent changes in IMCL content in the rat, when studying muscles as a whole. To examine if interventions with predicted increases in blood FFA (fasting and a high-fat diet) affected IMCL within the TA in a

fiber type specific manner, IMCL content was examined after 15 hours of fasting and after consumption of a high-fat diet and its relation with muscle fiber typology was assessed.

Materials and Methods

Animals and study design

Experiments were performed on 14 male Wistar rats, ~16 weeks old (mean body weight \pm standard error of the mean (SEM): 0.375 \pm 0.007 kg). Animals were housed in pairs at 20 C and 50% humidity, on a 12-h light-dark cycle with *ad libitum* access to normal chow and water during the time preceding the experiments. All experimental procedures were approved by the Animal Ethical Committee of the Maastricht University.

Twelve animals were subjected to two single-voxel ^1H MRS measurements, separated by 7 days. All animals were in the fed state unless stated otherwise. Six animals were put on a high-fat diet (~16% fat, ~50% carbohydrate, ~18% protein, diet W402106, Arie Blok Diervoeding, Woerden, The Netherlands) *ad libitum*, during the 7 days after the first measurement. The remaining 6 animals stayed on normal chow but fasted for 15 hours preceding the second measurement. Both MRS sessions were performed at identical time points starting at 8 a.m. and lasted approximately 4.5 hours. The animals were randomly assigned to the dietary intervention groups.

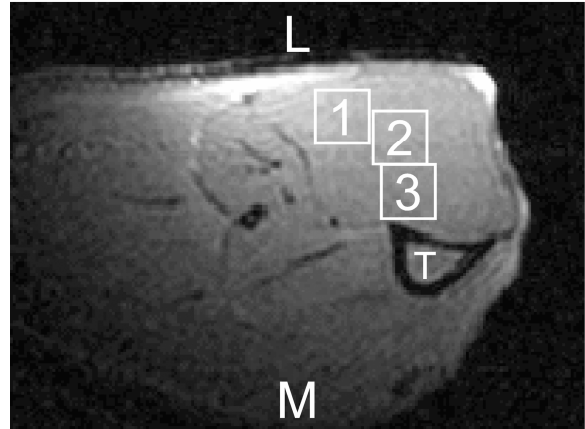


Figure 1 Transversal adiabatic spin echo image of the midbelly region of a rat lower hindleg with voxel positioning within the TA muscle for single-voxel ^1H MRS. M: medial, L: lateral, T: tibia bone. Acquisition parameters: TR: 2 s, TE: 24 ms.

During the MR experiments animals were anaesthetized using isoflurane (Forene®) (1 – 2%) in a mixture of O_2 and N_2O (0.15:0.30 L/min) and body temperature was maintained at 37 ± 1 C using a heating pad. Respiration was monitored using a pressure sensor registering the movement of the thorax (ECG trigger unit, Rapid Biomedical, Wurzburg, Germany), whereas blood oxygenation and heart rate were measured with a pulse oximeter (Nonin 8600V, Nonin Medical, Inc., Plymouth, Minnesota, USA).

At the end of the second MRS measurement, the anaesthetized animals were killed by cervical dislocation. TA from the hindleg measured during the MRS experiment was rapidly excised, the midbelly region was frozen in melting isopentane and stored at -80 C until used for immunohistological analysis. Two animals were used to study the reproducibility of the ^1H MRS measurement (see below).

MR experiments

Single-voxel ^1H MRS

All MR experiments were performed on a 6.3 Tesla horizontal bore Varian MR system using an ellipsoid ^1H surface coil (18/22 mm). In all rats the SOL and the TA were measured, always starting with the SOL and repositioning the animal in between. The animal was positioned laterally on the heating pad with the lateral side of the lower hindleg on the ^1H surface coil. The leg was positioned in such a way that the largest cross-section of the SOL or the TA, respectively, was in the isocenter of the magnet and that the muscle fibers were aligned with the static magnetic field. Transversal images of the midbelly region of the muscles were

acquired using an adiabatic spin echo sequence (pulse repetition time (TR) = 2 s, echo time (TE) = 24 ms) to achieve proper placement of the spectroscopic regions of interest.

Single-voxel localized ^1H MR spectra were acquired using the LASER sequence¹³ with additional outer volume suppression (TR = 1 s, TE = 28 ms, spectral width = 4000 Hz, number of data points = 2048, SWAMP water suppression¹⁴, 2048 averages for SOL, 1024 averages for TA). The voxel size used was $1.3 \times 1.3 \times 2 \text{ mm}^3$ for the SOL and $2 \times 2 \times 2 \text{ mm}^3$ for the TA. In the SOL one voxel was measured, whereas for the TA voxels were placed at three different positions within the muscle cross-section: (TA1) lateral, (TA2) in the center, and (TA3) medial, close to the tibia bone (Figure 1). Unsuppressed water spectra (128 averages for SOL, 64 averages for TA) were recorded from the same voxels and used as internal reference. Furthermore, a series of 8 unsuppressed water spectra was recorded with varying echo times (32 averages) to determine the T_2 of muscle water. The reproducibility of the IMCL quantification in the TA cross-section was determined in one rat, measured at three different days within one week. In one other animal, the IMCL content at the described voxel positions was studied in 4 different cross-sectional planes of the TA, going from the knee towards the ankle, to analyse IMCL variations in the longitudinal direction of the muscle.

Spectroscopic imaging

Spectroscopic imaging (SI) was performed on one rat only. Because in control rats the IMCL content in the rat TA is low, the SI data were collected from a rat that had been on the high-fat diet for 7 days. A 2D SI sequence with LASER volume preselection was used. The slice (3 mm thick) was selected in the transverse orientation. The position and size of the LASER box was adjusted to exclude subcutaneous fat and bone marrow as much as possible, while covering most of the TA muscle. The spectra were acquired with TR = 1 s, TE = 29 ms, SWAMP water suppression and 48 averages. A matrix of 8×8 was used over a field of view of $5 \times 5 \text{ mm}^2$, resulting in a scan time of 51 min. Unsuppressed water spectra were recorded with identical settings, except that 4 scans were averaged.

Data analysis

For the single-voxel spectra no further post-processing was applied, except for manual phasing. For the SI data, a Hanning filter was applied in both spatial dimensions and spatial zero-filling was applied to 16×16 points, resulting in a nominal voxel size of $0.29 \mu\text{l}$. All spectra were fitted in the time domain by using a nonlinear least squares algorithm (AMARES) in the jMRUI software package¹⁵. The unsuppressed water spectrum was phased and fitted to a Lorentzian line shape. The zero-order phase correction from the water spectrum was applied to the corresponding water suppressed ^1H spectrum and the total creatine (tCr) CH_3 peak was referenced to 3.02 ppm. In the water suppressed spectrum, the central line of the tCr CH_3 peak and the IMCL CH_2 peak (1.28 ppm) were fitted to Gaussian line shapes. The tCr linewidth (LW_{tCr}) and IMCL linewidth (LW_{IMCL}) were constrained with respect to the linewidth of the water peak (LW_{water}) according to

$$LW_{\text{tCr}} = -0.71 + 0.49 \cdot LW_{\text{water}} \quad [1]$$

and

$$LW_{\text{IMCL}} = 4.06 + 1.04 \cdot LW_{\text{water}} \quad [2]$$

The constraint for the tCr linewidth was derived from previously measured and present data sets featuring a well-resolved triplet for the tCr CH_3 resonance at 3.02 ppm (number of data sets = 74, R = 0.735, $p < 0.0001$, not shown). The constraint for the IMCL linewidth was

derived from data sets uncontaminated with EMCL (number of data sets = 91, $R = 0.537$, $p < 0.0001$, not shown).

The IMCL and tCr levels were expressed as a percentage of the water signal measured in the same voxel. For the SI data set, the water and IMCL signals in the voxels from the two left most columns and the two upper most rows do not originate from the same location, due to the water-fat shift. Therefore these voxels have been discarded, resulting in 14×14 useable voxels.

Immunohistology

The TA muscles of 5 animals participating in the dietary intervention study were used for immunohistological staining. Cryostat sections ($5 \mu\text{m}$ thick) of midbelly muscle were thaw-mounted on uncoated glass slides. Air-dried cryosections were treated with 0.5% Triton X-100 (Merck) in phosphate buffered saline (PBS) for 5 min, washed with three exchanges of PBS for 5 min and processed for triple-immunofluorescence staining. In brief, sections were incubated for 45 min at room temperature with a mixture of primary antibodies: a rabbit polyclonal antiserum against the basement membrane protein laminin (L-9393, Sigma, Zwijndrecht, The Netherlands); a monoclonal antibody against myosin heavy chain 1 (A4.840); and a monoclonal IgG₁ antibody against myosin heavy chain 2A (N2.261). The latter two antibodies developed by Dr. Helen Blau, were obtained from the Developmental Studies Hybridoma Bank under the auspices of the NICHD and maintained by the University of Iowa, Dept. of Biological Sciences, Iowa City, IA, USA. Antibodies were diluted in 0.05% Tween20 (Sigma) in PBS. Thereafter sections were washed three times with PBS for 5 min and incubated for 30 min at room temperature with the appropriate secondary antibody mixture diluted in 0.05% Tween20/PBS. Next, sections were washed again three times for 5 min with PBS and mounted in Mowiol.

Sections were examined using a Nikon E800 fluorescence microscope coupled to a Basler A101C progressive scan color charge-coupled device camera. Images were captured for every single color (red, green and blue) from all section, processed and analyzed using Lucia GF 4.80 software (Lucia, Czech Republic). Special care was taken to use the same camera settings (gain and exposure time) while grabbing images.

Statistics

Results are presented as mean \pm SEM. Normality of the data was examined with the Shapiro-Wilk test. One-way ANOVA with Bonferroni post-hoc test was used to compare the IMCL and tCr values from the different voxel positions. The effect of the different dietary interventions was evaluated using a paired Student's T-test. $p < 0.05$ was considered statistically significant.

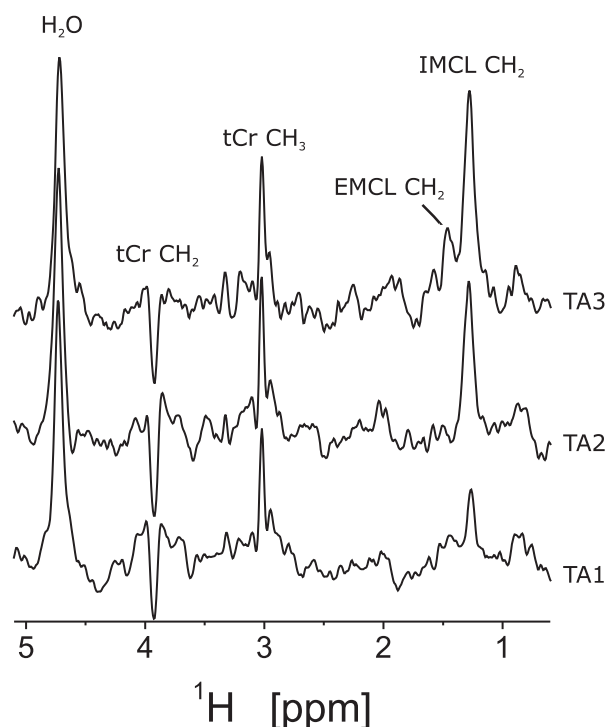


Figure 2 Typical examples of single-voxel localized ^1H MR spectra using LASER and SWAMP water suppression from voxel positions 1-3 in rat TA muscle. Acquisition parameters: TR: 1 s, TE: 28ms, 1024 averages, voxel size: $2 \times 2 \times 2 \text{ mm}^3$.

Results

Single-voxel ^1H MRS

Typical linewidths of the water peak after localized shimming were 14 Hz or 0.052 ppm at 6.3 Tesla. The SWAMP water suppression performed very well making post-processing techniques to remove residual water signal unnecessary. Figure 2 shows typical single-voxel water suppressed ^1H spectra from the TA. The orientation-dependent dipolar splitting of the tCr CH_2 resonance at 3.92 ppm (doublet) and tCr CH_3 resonance at 3.02 ppm (triplet) confirm the proper positioning of the rat hindleg. The majority of the spectra did not contain an observable EMCL peak. For the spectra that did contain an EMCL signal, the IMCL and EMCL peaks were well separated (~ 0.15 ppm).

Figure 3 shows the IMCL content for the different voxel positions in the TA and the SOL measured in 12 rats during the first MRS session. IMCL was remarkably heterogeneously distributed within the cross-section of the TA. The IMCL levels displayed a typical pattern related to the voxel position from which the signal originates: IMCL values were lowest in the lateral region (voxel position 1) and highest in voxel position 3, close to the tibia bone while the IMCL level at voxel position 2, in the center of the TA cross-section, lies in between the values from voxel positions 1 and 3. The IMCL contents at the different TA voxel positions all differed significantly from each other ($n = 12$; TA1 vs. TA2, $p = 0.022$; TA1 vs. TA3, $p < 0.001$; TA2 vs. TA3, $p = 0.007$). The IMCL content of the SOL was significantly different from the IMCL content of the TA at voxel position 1 ($n = 12$; $p = 0.003$) and 3 ($n = 12$; $p = 0.047$), but similar to the IMCL content of the TA at voxel position 2.

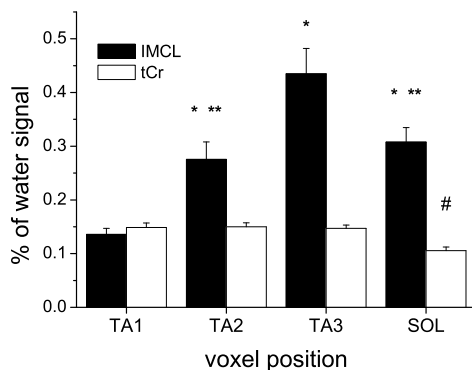


Figure 3 IMCL and tCr content relative to the water signal as a function of voxel position. Data are presented as mean ($n = 12$) \pm SEM. * $p < 0.05$ relative to voxel position TA1, ** $p < 0.05$ relative to voxel position TA3, # $p < 0.05$ relative to voxel position TA1, TA2 and TA3.

The tCr content of the TA, also shown in figure 3, did not change as a function of voxel position and, for each voxel position, showed a smaller variation (SEM) compared to IMCL ($n = 12$). The tCr content at any voxel position in the TA was higher than that in the SOL ($n = 12$, all $p \leq 0.001$).

The reproducibility of the IMCL determination at the different voxel positions within the TA was measured in one rat, which was not included in the dietary interventions study. The three typical voxel positions used in the TA were analyzed on three different days within one week. The coefficient of variance of the IMCL measurement was 16.7% for TA1, 16.7% for TA2 and 14.5% for TA3. The reproducibility of the tCr quantification varied from 7.6% for TA1, 10.3% for TA2 to 14.3% for TA3. The analysis of variations in IMCL content in the longitudinal direction of the TA, measured in a second rat not participating in the dietary

interventions study, revealed that the pattern shown in figure 3 was constant in the midbelly region (middle part) of the muscle (data not shown).

Spectroscopic Imaging

SI was performed to visualize the spatial IMCL distribution within the TA cross-section at a higher resolution. Figure 4 shows the IMCL levels for the 14×14 voxels from the SI data set ($n = 1$). The color-coded IMCL image was overlaid on a co-registered MR image for anatomical guidance. The SI region was covering most of the TA cross-section and confirmed the inhomogeneous distribution of IMCL. A clear gradient is observed in the IMCL levels, with the

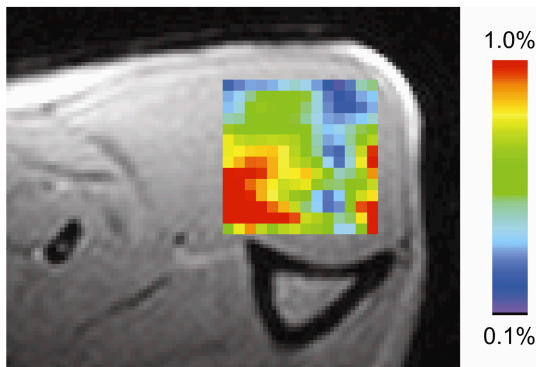


Figure 4 IMCL levels in the 14×14 voxels of the SI data set on top of a co-registered MR image. Color-coding represents the IMCL as percentage of the water signal. Acquisition parameters: TR = 1 s, TE = 29 ms, 48 averages, voxel size = $0.31 \times 0.31 \times 3$ mm³.

highest values in the medial-posterior part, close to the tibia bone and the lowest values in the peripheral anterior region.

Immunohistology

To clarify the origin of the spatial differences in IMCL concentration immunohistological analyses were performed on muscle cross-section regions corresponding to the voxel positions used for the single-voxel ¹H MRS. Examples of the immunohistological images are depicted in figure 5. The immunohistological staining shows basal lamina in blue, type I muscle fibers in red and type IIa fibers in green. Fibers without any staining represent the I Ib muscle fiber type. The

tissue displayed in the left panel of figure 5 (TA1) did not contain a single type I fiber and only a few type IIa fibers. This part of the TA muscle was mainly composed of the non-oxidative type IIb fibers. The tissue in the middle panel (TA2) contained a few type I fibers and some more type IIa fibers, but was still dominated by non-oxidative fibers. The tissue shown in the right panel (TA3) was dominated by the oxidative type I and type IIa fibers. In figure 6a-c the average IMCL content from different voxel positions is displayed as a function of the average percentage of type I, IIa and IIb muscle fibers within these similar voxel positions, respectively. The muscle fiber type quantification was performed in the histological regions corresponding to the three MRS voxel positions. The IMCL data and the immunohistological data are from the same animals ($n = 5$). A larger amount of oxidative type I and type IIa fibers was paralleled by a higher IMCL level, and the relative amount of glycolytic IIb fibers showed a negative relationship with IMCL.

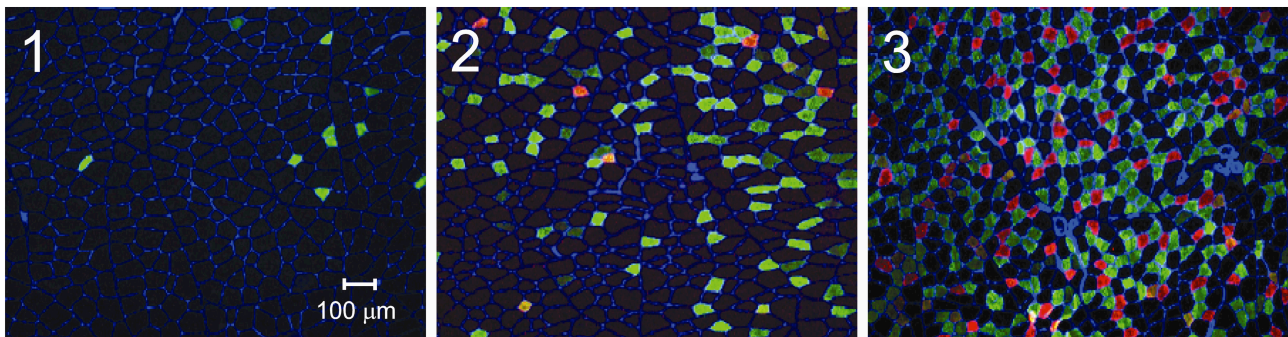


Figure 5 Triple-immunofluorescence assay in representative areas (1.36×1.07 mm²) of the TA corresponding to voxel positions 1-3. Blue: basal lamina, red: type I muscle fibers (slow oxidative), green: type IIa muscle fibers (fast oxidative).

Dietary interventions

IMCL can change during and after interventions inducing increased plasma FFA, such as high-fat diet and fasting. We examined the influence of both dietary interventions on the IMCL content in TA and SOL and the IMCL distribution within the TA. The high-fat diet resulted in a substantial increase in IMCL in all voxels of the TA ($n = 6$; post-DIET vs. pre-DIET; TA1: +115%, $p = 0.008$; TA2: +120%, $p = 0.001$; TA3: +111%, $p = 0.002$) as well as in the SOL (post-DIET vs. pre-DIET; SOL: +67%, $p = 0.036$) (Figure 7a). In contrast, the 15 hour fasting procedure did not induce any significant changes in IMCL for the voxels in the TA ($n = 5$; 1 dropout due to failing heating pad) (Figure 7b). The fasting procedure did result in a decrease of IMCL in the SOL (post-DIET vs. pre-DIET; SOL: -40%, $p = 0.004$). Neither dietary intervention affected the tCr content in the TA or the SOL (data not shown).

The dietary interventions had no effect on the T_2 of muscle water measured in the different voxels (data not shown), which justifies the use of the water signal to quantify the IMCL and tCr content.

Discussion

Using non-invasive MR techniques combined with invasive examination of spatial heterogeneity of rat muscle fiber typology, we here conclusively show that spatial differences in IMCL content are accounted for by muscle fiber type distribution. Strikingly, the increase in IMCL content upon consumption of a high-fat diet was similar across all fiber types, preserving the pronounced pattern of IMCL distribution. This study therefore underscores the importance of anatomical positioning of the voxel of interest in rat muscle, both in cross-sectional as well as in longitudinal studies.

^1H MRS is a well-established non-invasive method to measure IMCL, frequently used to study lipid storage in human skeletal muscle in relation to exercise, insulin resistance and type 2 diabetes. Also in rat studies, ^1H MRS has become an important tool for research on insulin resistance and type 2 diabetes. In these rat studies, ^1H MRS is often applied to the TA, among other aspects, because of its characteristic muscle fiber architecture that maximizes the separation of IMCL and EMCL peaks. The typical volume used in single-voxel ^1H MRS in rat TA is about 8 l , which is small relative to the total volume of the TA ($\pm 500 \text{ }\mu\text{l}$) and can therefore only be representative for the whole muscle if the muscle itself displays a homogeneous IMCL distribution. As it is known that muscle fiber type is an important determinant for IMCL content and that muscle fiber types can be strongly regionalized in rat muscle, we examined the spatial distribution of IMCL and correlated this with immunohistological analyses of muscle fiber typology within the rat TA cross-section.

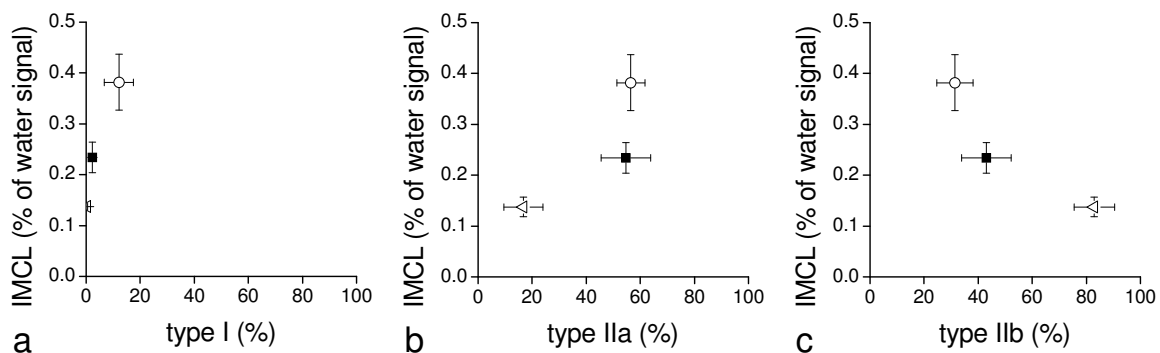


Figure 6 IMCL content in the TA plotted as a function of the muscle fiber type. Each data point represents the average IMCL content from the different voxel positions (\triangle : TA1, \blacksquare : TA2, \circ : TA3) and the corresponding percentage of type I (a), type IIa (b) and type IIb (c) fibers ($n = 5$). Error bars represent SEM.

When studying fat storage in rat skeletal muscle, IMCL is usually normalized to the tCr signal^{3, 6, 7, 16, 17}. In human studies, however, IMCL is often expressed as a percentage of the water signal originating from the same voxel, since the tCr signal is small compared to the IMCL signal and not that easy to quantify at the commonly used clinical field strengths¹⁸. The present study focuses on muscle fiber-type related effects on the IMCL content. Since the tCr concentration is also dependent on the muscle fiber type¹⁹, we choose to express both IMCL and tCr as a percentage of the water signal from the same voxel.

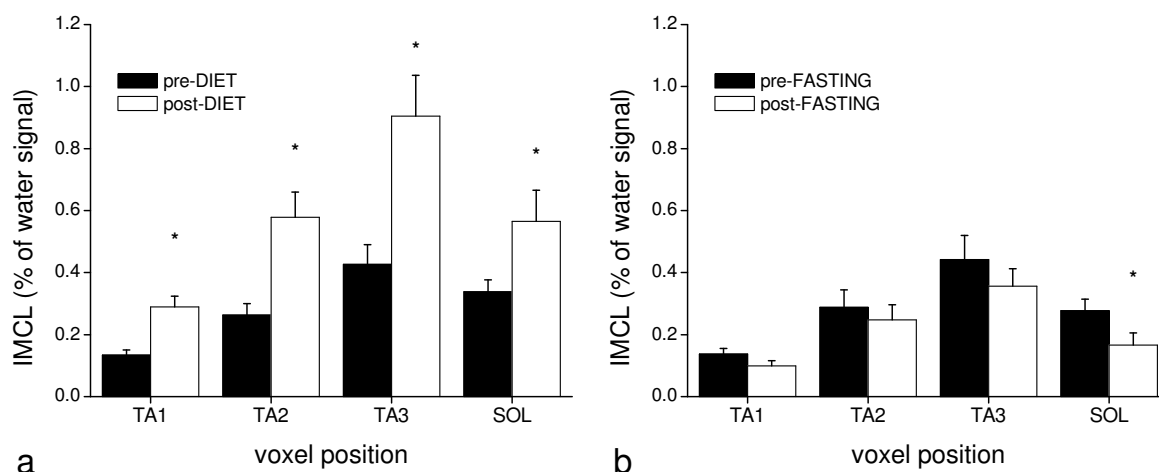


Figure 7 IMCL content of the different voxel positions in the TA and the SOL (a) before and after 7 days of high-fat diet ($n = 6$) and (b) before and after 15 hours overnight fasting ($n = 5$). * $p < 0.05$ relative to IMCL content before dietary intervention. Error bars represent SEM.

Both the single-voxel experiments at the different voxel positions and the SI experiment showed that IMCL is inhomogeneously distributed within the TA. The distribution of IMCL over the TA cross-section was not random, but emerged in a pattern very similar to the distribution of the type I, type IIa and type IIb muscle fibers. This was corroborated by the relations between the different muscle fiber types and the IMCL content (Figure 6a-c). It has been shown before that oxidative muscle fibers can contain up to three times more IMCL than glycolytic type IIb fibers^{10, 11} and therefore it is most likely that the typical muscle fiber type distribution in the TA accounts for the pronounced IMCL distribution. Thus far, rat muscles were mostly studied as a whole, classified to be predominantly oxidative (e.g. SOL), glycolytic (e.g. TA) or intermediate (e.g. extensor digitorum longus). Our results confirm the muscle fiber type regionalization of the rat TA described by Wang *et al.*¹². Despite being classified as a “glycolytic” muscle, the rat TA muscle contains a small amount of oxidative type I and fast oxidative type IIa muscle fibers, which are clustered close to the tibia bone¹². Although the amount of oxidative muscle fibers is modest relative to the total number of fibers, the pronounced regionalization of oxidative fibers within the TA profoundly affects the IMCL content measured.

Several issues complicate the comparison of these results with previous IMCL studies in Wistar rats. Besides the different methods used to measure and quantify the IMCL content, also the positioning of the voxels is not the same for different studies. The voxel position within the rat TA in the studies of Neumann-Haefelin *et al.* is not identical to any of the voxel positions used in our study. However, the voxel position used by these researchers is in a region close to the skin that contains barely any type I and only a few type IIa muscle fibers (personal observation during histological analyses) and can therefore best be compared to our voxel position 1. When the IMCL content reported in our study is normalized to the tCr signal instead of expressing it as a percentage of the water signal, then voxel position 1 contains ~30% of the IMCL signal of the SOL (data not shown), which is in good agreement with the results of Neumann-Haefelin *et al.*^{6, 7}.

Neumann-Haefelin *et al.* described various determinants of IMCL concentrations in rat hindleg muscles, including age, strain, gender and muscle type, emphasizing the need to take these factors into account when studying diseases such as insulin resistance and diabetes⁶. Our results point to the voxel position when applying localized single-voxel ¹H MRS as another determinant of the IMCL content in rodent muscle. In practice, the positioning of the voxel is done manually, with the guidance of anatomical landmarks such as the shape of the TA cross-section and the tibia bone. This raises the question how reproducible the voxel positioning and

thereby the IMCL measurement actually is. We have shown that the coefficient of variance of the IMCL content is ~16% for each voxel position in the TA, covering both day-by-day variations of the animal as well as the variation introduced by the positioning of the voxels. The typical pattern of IMCL distribution was constant in the midbelly region of the TA (data not shown), making the positioning of the voxel in the longitudinal direction far less critical than that in the cross-section of the muscle.

The described inhomogeneous distribution of different muscle fiber types is a key feature of rodent TA muscle. Besides the TA also other rodent muscles are known to display a pronounced regionalization of their different fiber types. Rat gastrocnemius muscle is for example often analyzed by separating the "white" (glycolytic) part from the "red" (mixed or oxidative) part²⁰. To our knowledge, ¹H MRS has not been used to study IMCL content in rat gastrocnemius muscle. The complex muscle fiber alignment of the gastrocnemius muscle is not ideal for IMCL determination. However, when single-voxel ¹H MRS would be applied to rodent gastrocnemius muscle one can expect a similar pronounced regionalization of the IMCL content as described in the present study for TA, due to its inhomogeneous fiber type distribution.

We investigated whether a dietary intervention could change the IMCL distribution within the TA, because it has been shown that e.g. starvation affects IMCL levels in a muscle-specific manner⁷. Seven days of high-fat feeding increased the IMCL content in the TA by more than 100% and the SOL by approximately 70%. However, IMCL was homogeneously increased within the TA and therefore the distribution of IMCL was not changed. Fifteen hours of fasting decreased the IMCL content in the SOL by 40%, but did not cause a significant change in the IMCL levels in the TA. These results seem to contrast with previous reports indicating an increase of IMCL in glycolytic muscles (TA and extensor digitorum longus) and a constant level of IMCL in oxidative muscle (SOL), measured at 12, 24, 48, and 72 hours of starvation⁷. Our group size was rather small (n = 5) and in contrast to the high-fat diet, the results of the fasting intervention were not consistent for all animals. Some animals showed an increase in IMCL in the TA, whereas others showed a decrease in IMCL following the fasting period. On average this resulted in unchanged IMCL levels in the TA muscle. It is tempting to speculate that the fasting procedure did not induce the expected increase in plasma FFA in all animals, however we do not have data on the plasma FFA levels.

In conclusion, the variation of the IMCL content within the TA was strongly related to the muscle fiber type distribution and differed by up to a factor of three for different voxel positions. Despite changes in the IMCL content due to high-fat feeding and fasting, the typical pattern of IMCL distribution within the rat TA persisted. Therefore, positioning the voxel of interest is a crucial factor when using single-voxel ¹H MRS to study IMCL in rodents.

Acknowledgement

The authors thank Dr. Gustav J. Strijkers for assistance with the processing of the SI data.

References

1. Machann, J. et al. *Diabetes, Obesity and Metabolism* 6, 239-248 (2004).
2. Yu, C. et al. *J Biol Chem* 277, 50230-50236 (2002).
3. Kuhlmann, J. et al. *Magn Reson.Med.* 53, 1275-1282 (2005).
4. Schick, F. et al. *Magn Reson.Med.* 29, 158-167 (1993).
5. Boesch, C. et al. *Magn Reson.Med.* 37, 484-493 (1997).
6. Neumann-Haefelin, C. et al. *Magn Reson Med* 50, 242-248 (2003).
7. Neumann-Haefelin, C. et al. *Diabetes* 53, 528-534 (2004).
8. Hwang, J.H. et al. *J Appl Physiol* 90, 1267-1274 (2001).
9. Vermathen, P., Kreis, R. & Boesch, C. *Magn Reson Med* 51, 253-262 (2004).
10. Malenfant, P. et al. *Int J Obes Relat Metab Disord* 25, 1316-1321 (2001).
11. van Loon, L.J. et al. *J Physiol* 553, 611-625 (2003).
12. Wang, L.C. & Kernell, D. *J Muscle Res Cell Motil* 21, 587-598 (2000).
13. Garwood, M. & DelaBarre, L. *J Magn Reson* 153, 155-177 (2001).
14. de Graaf, R.A. & Nicolay, K. *Magn Reson Med* 40, 690-696 (1998).
15. Vanhamme, L., van den Boogaart, A. & Van Huffel, S. *J Magn Reson* 129, 35-43 (1997).
16. Korach-Andre, M. et al. *Metabolism* 54, 522-528 (2005).
17. Kuhlmann, J. et al. *Diabetes* 52, 138-144 (2003).
18. Schrauwen-Hinderling, V.B. et al. *J Appl Physiol* 95, 2328-2332 (2003).
19. Brault, J.J. & Terjung, R.L. *Am J Physiol Cell Physiol* 284, C1481-1489 (2003).
20. Ferreira, L.D. et al. *Metabolism* 54, 1420-1427 (2005).

Chapter 3

An NMR-compatible, minimally invasive electrical stimulation method to study rat skeletal muscle *in vivo*

Abstract

When the dynamics of energy metabolism in skeletal muscle of anaesthetized animals is studied, muscle contractions are induced by electrical stimulation. Traditionally, muscle contractions are induced via direct nerve stimulation, thereby undermining the non-invasive nature of MRI and MRS. In this paper a minimally invasive, subcutaneous electrical stimulation procedure for rat lower hind limb is presented that induces isolated contractions of the dorsal flexor muscles. The specificity of the set-up for the Tibialis Anterior and the Extensor Digitorum muscles was shown by the signal enhancement in ^1H MR images due to contraction-induced T_2 increase and its applicability for longitudinal studies was demonstrated by a ^{31}P MRS study in ZDF rats. It was also shown that this method can be applied to the plantar flexor muscles. The NMR-compatible, minimally invasive electrical stimulation procedure was well tolerated by the animals, induced highly specific muscle contractions and proved to be applicable in longitudinal study designs.

Introduction

MR imaging (MRI) and MR spectroscopy (MRS) have proven to be valuable tools for the non-invasive study of skeletal muscle, in humans as well as in animals ¹. ³¹P MRS is widely used to monitor the dynamics of energy metabolism during and after muscle contractions. When *in vivo* ³¹P MRS is applied to skeletal muscle in anaesthetized animals, muscle contractions have to be induced by electrical stimulation. Traditionally, muscle contractions are induced via direct nerve stimulation in which the nerve of interest is surgically exposed ²⁻⁶, consequently undermining the non-invasive nature of MRI and MRS and hampering longitudinal studies. As an alternative, a chronically implanted nerve cuff has been used for muscle stimulation in mice and suggested to be applicable in other species ⁷. In this method, the leads of the nerve cuff are tunnelled towards the dorsal cervical region of the animal. Therefore, chronically implanted nerve cuffs might not be applicable to animals that are not yet fully grown, as the leads will probably experience strain during maturation.

Recently a completely noninvasive setup was presented for rat, allowing both ¹H MRI and ³¹P MRS of the contracting gastrocnemius muscle and simultaneous force measurement ⁶. This setup performed both qualitatively and quantitatively similar when compared with the traditional invasive method for electrical stimulation and force measurement. The specificity for the gastrocnemius muscle was evaluated by the well known exercise-induced T₂ increase ⁴ and it was shown that predominantly the gastrocnemius muscle was activated. However, also other muscles of the plantar flexors and even muscles from the antagonistic dorsal flexors revealed increased T₂ values (Figure 4 in ⁶). This indicates that the stimulation method did not exclusively induce muscle contractions in the plantar flexor muscles, or even more specific, in the gastrocnemius muscle.

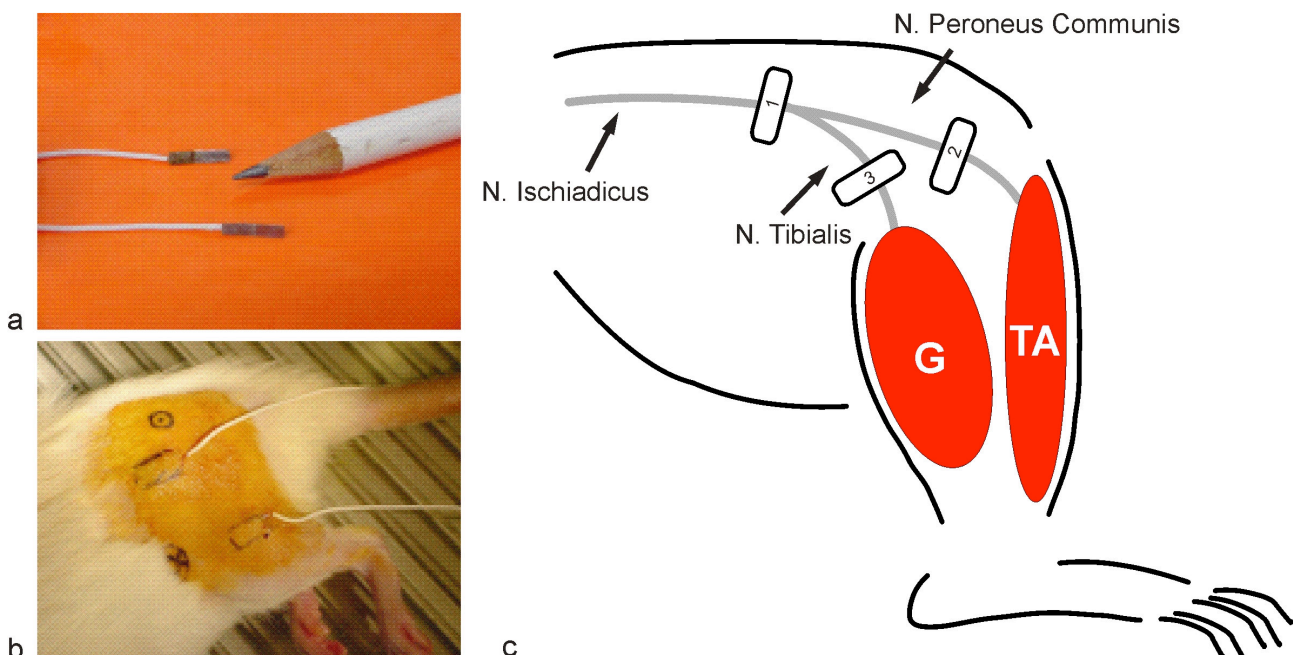


Figure 1 a) Platinum electrodes, b) subcutaneous implantation of the electrodes in the anaesthetized rat, c) cartoon of lateral view of rat hind limb showing the position of electrodes for stimulation of TA (1 & 2) and G (gastrocnemius) (1 & 3).

Chapter 3

We present a similar NMR-compatible electrical stimulation method as described by Giannesini *et al.* ⁶ for the dorsal flexor muscles: the Tibialis Anterior (TA) and the Extensor Digitorum Longus (EDL) muscles. The TA is a superficial muscle that is frequently being studied in rat, not only with ³¹P MRS, but also with ¹H MRS to measure intramyocellular lipids ⁸⁻¹². The present method can easily be applied several times in the same animal, allowing longitudinal studies. The specificity of the set-up for the TA and EDL was confirmed by the contraction-induced T₂ increase of muscle water with ¹H MRI and its applicability for longitudinal studies was demonstrated by a longitudinal ³¹P MRS study in Zucker Diabetic Fatty (ZDF) rats.

Methods

Contraction-induced T₂ increase was measured in Wistar rats (~ one year of age; n = 3). Dynamic ³¹P MRS before, during and after muscle contractions was applied in ZDF fa/fa (n = 10) and ZDF fa/+ (n = 11) rats at different ages (6, 12 and 18 weeks of age). During the subcutaneous insertion of the electrodes and the following NMR experiments animals were anaesthetized using isoflurane (Forene ®) (1–2%) and medical air (0.4 L/min)) and body temperature was maintained at 37 ± 1 °C using a heating pad. Respiration was monitored in the MR scanner using a pressure sensor registering the movement of the thorax (ECG/respiratory trigger unit, Rapid Biomedical, Rimpar, Germany).

The in-house built stimulation electrodes were made of 2 platinum strips (1.2 × 8 mm²) that were soldered to flexible multi-stranded copper wire (Cooner Wire, AS 999-30, Chatsworth, Ca, USA) (Figure 1a). The rats were anaesthetized and positioned supine in a cradle. This cradle had a support for one lower hind limb and a footplate. The hind limb support and footplate were constructed in such a way that the angle of the hip, the knee and the ankle was ~90°. Two small incisions in the skin were made (~1.5 mm wide) along the nerve trajectory of the *N. Peroneus Communis* (Figure 1b and 1c) to induce muscle contractions in the TA and EDL muscles. Two skin pockets were made by blunt preparation, both electrodes were inserted and the wounds were closed with a single stitch (6.0, Prolene, Ethicon, Inc. NJ, USA) (Figure 1b). After finishing the MR experiments, the electrodes were removed and the incisions were closed with a single stitch. As a proof of principle that the method can also be applied for other muscle complexes, in one animal the electrodes were also positioned along the *N. Tibialis* to stimulate the plantar flexor muscles: the gastrocnemius, soleus, plantaris, tibialis posterior and flexor digitorum longus muscles (Figure 1c).

All NMR experiments were performed on a 6.3 Tesla horizontal Bruker MR system. A set-up with a combination of a circular ¹H surface coil and an ellipsoid ³¹P surface coil was used. Shimming was performed on the water signal using FASTMAP ¹³ (shim volume 12 × 12 × 12 mm³) and subsequently the acquisition of T₂ weighted images or ³¹P MR spectra was started. T₂ weighted images were acquired using a multi-echo spin-echo sequence with 6 echo times (TR/TE = 2 s/11, 21, 32, 43, 53 and 64 ms, averages = 2, matrix = 256 × 192, FOV = 30 × 30 mm², in plane resolution = 117 × 156 μm², slice thickness = 2 mm). Imaging was performed before electrical stimulation and 12 minutes after the onset of electrical stimulation. To prevent a decrease in T₂ prolongation during the acquisition of the image, the stimulation protocol was continued during the delays in the imaging sequence. The stimulation protocol consisted of

NMR-compatible electrostimulation of rat skeletal muscle

block pulses with a length of 10 ms, applied every 400 ms, with a voltage of 2 - 4 V and was carried out until the end of the image acquisition. Two T_2 weighted images (TE = 32 ms) were subtracted to highlight the region that had the most signal increase due to prolongation of T_2 . ROIs were drawn by hand on a pre-stimulation T_2 weighted image (TE = 11 ms) representing different muscles of the lower hind limb and T_2 was calculated based on the signals acquired with the 6 different TEs.

^{31}P MR spectra (spectral width = 5000 Hz, number of points = 2048, TR = 5 s, 4 averages) were acquired applying an adiabatic pulse with a flip angle of 90 degrees. A time series of spectra was acquired before (9 spectra), during (6 spectra) and after (30 spectra) the muscle contractions. The muscle exercise consisted of a series of stimulation pulses, applied every second, for a duration of 2 min. The stimulation pulse length was 100 ms, the stimulation frequency was 80 Hz and the voltage varied between 2 and 4 V. The stimulation voltage was optimized during a first time series, aiming at a decrease of the phosphocreatine (PCr) peak amplitude of $\sim 50\%$. The optimized stimulation voltage was then applied in a second time series, which was recorded at least 13 minutes after the end of the previous electrical stimulation period. ^{31}P spectra were fitted in the time domain by using a nonlinear least squares algorithm (AMARES) in the jMRUI software package ¹⁴. PCr, inorganic phosphate (P_i) and adenosine triphosphate (ATP) signals were fitted to Lorentzian line shapes. Absolute concentrations of the phosphorylated metabolites were calculated after correction for partial saturation and assuming that [ATP] is 8.2 mM at rest ¹⁵. Intracellular pH was calculated from the chemical shift difference between the P_i and PCr resonances ¹⁶.

Table 1 average T_2 values

	T_2 Pre	\pm	SD	T_2 Post	\pm	SD
TA	19.9	\pm	0.8	23.9	\pm	1.4
EDL	19.9	\pm	1.9	22.5	\pm	1.6
SOL	20.7	\pm	0.2	20.9	\pm	0.6
TP & FDI	20.8	\pm	1.8	20.9	\pm	1.9
GL	22.1	\pm	0.3	22.0	\pm	0.6

Average T_2 values (ms) (n = 3) calculated from the corresponding ROIs depicted in Figure 2d. T_2 pre and post: average T_2 value before and after stimulation via the *N. Peroneus Communis*, respectively.

Results

Stimulation via *N. Peroneus Communis*

The T_2 weighted images showed an area of increased signal intensity during electrical stimulation (Figure 2a-b). The subtraction image clearly revealed that this area corresponds to the anatomical location of the TA and EDL muscles (Figure 2c). The calculation of the T_2 values in the different regions of the hind limb (Table 1) confirmed that the T_2 was increased in both the TA and the EDL, whereas no change in T_2 was observed in other muscles of the hind limb (Figure 3).

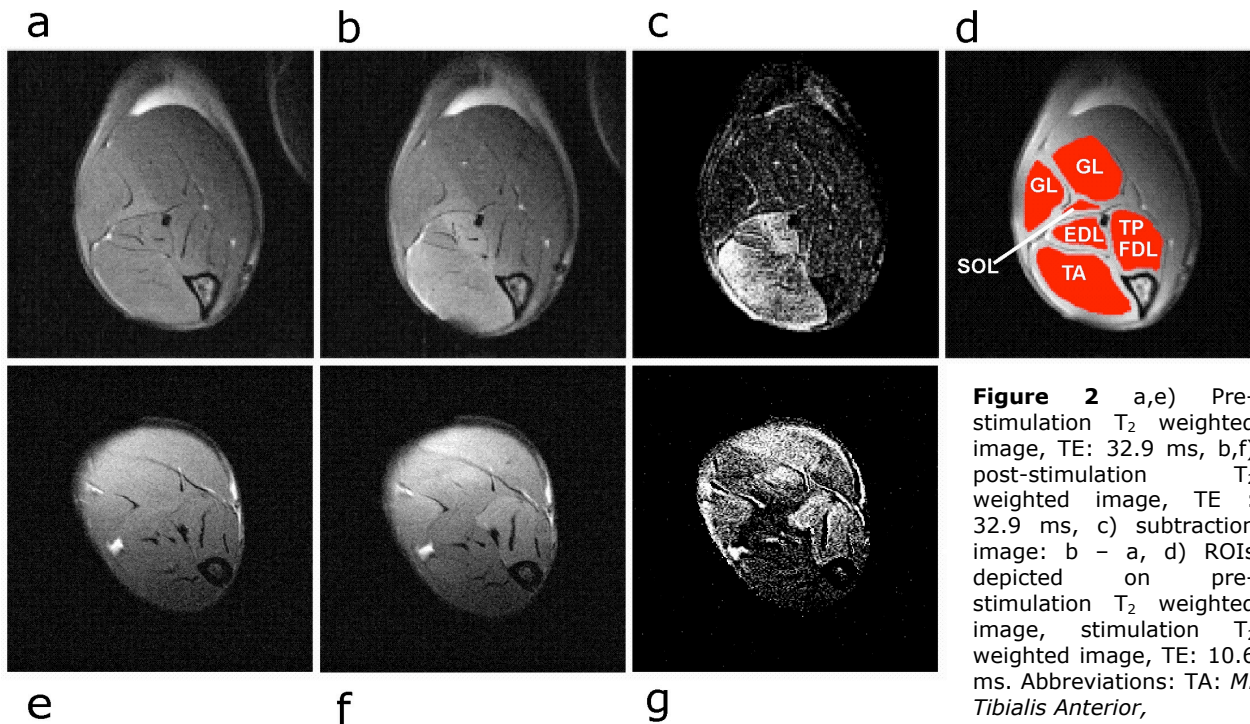


Figure 4 shows a typical example of a time series of ³¹P MRS spectra measured in the dorsal flexor muscle complex. The time series consisted of a rest period of 3 min followed by an electrical stimulation protocol of 2 min and 10 min of recovery. The line width of the PCr peak was typically ~15 Hz. Table 2 shows rest and end-exercise concentrations of PCr and the end-exercise pH from the longitudinal study in ZDF rats, measured at 6, 12 and 18 weeks of age. The data show that it was possible to create a similar end-exercise status in both lean and fatty animals at different ages.

Stimulation via *N. Tibialis*

In one animal the electrodes were positioned along the trajectory of the *N. Tibialis* to stimulate the plantar flexor muscles (Figure 1c). The T₂ weighted images showed an area of increased signal intensity during electrical stimulation (Figure 2e-f). The subtraction image clearly revealed that this area corresponds with the anatomical location of the plantar flexor muscles (Figure 2g).

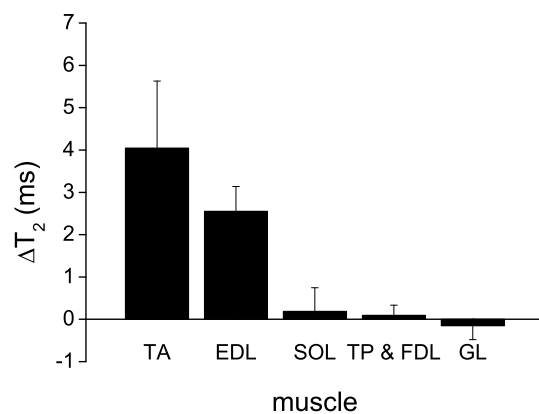


Figure 3 Average changes in T₂ for the different muscles of the lower hind limb during electrical stimulation of the dorsal flexor muscles, TA and EDL (n = 3), error bars: SD, abbreviations as defined in legend of Figure 2.

Discussion

We presented an NMR-compatible electrical stimulation method for inducing muscle contractions *in vivo* in rat skeletal muscle. The procedure was extensively verified for the dorsal flexor muscles of the lower hind limb, the TA and EDL and was shown to be also applicable for the plantar flexor muscles. The stimulation method requires some surgery, but this is minimally invasive which makes that the stimulation method can be easily repeated within the same animal.

We aimed to induce electrical stimulation through the *N. Peroneus Communis*, the nerve that innervates the TA and EDL muscles. The specificity of the stimulation procedure for the dorsal flexor muscles was confirmed by the analysis of T₂ weighted images. An increase in T₂ was only detected in the TA and EDL muscles, whereas the other muscles of the lower hind limb did not show any change in T₂. Previous studies of exercise-induced changes in rat muscle report T₂ values at rest of ~ 30 ms and changes after contractions ranging from 4 to 12 ms^{4, 6}. The T₂ values measured in the present study were ~ 1.5 times shorter. This inconsistency is most likely due to the use of a surface coil for RF transmission in the multi-echo imaging sequence, in contrast to both Giannesini *et al.* and Prior *et al.* who used a Helmholtz imaging coil^{4, 6}.

The traditional methods to induce muscle contractions in the lower hind limb of the rat mostly employ of a bipolar electrode that is positioned around the exposed *N. Ischiadicus* (Figure 1)^{2-4, 6}. Since this procedure can obviously not induce muscle contractions in the dorsal or plantar flexors separately, the nerve branch innervating the muscle group that should not contract is often cut⁴. Even in that situation contraction-induced T₂ prolongation of muscle water in muscles innervated by the cut nerve branch has occasionally been reported, which was explained as induced by field stimulation⁴. Similarly, the completely non-invasive method presented by Giannesini *et al.* presumably induces some activation of antagonist muscles, as the T₂ in dorsal flexor muscles was also increased, while the method aimed to stimulate selectively the plantar flexors. The present method did not involve cutting of adjacent nerve branches, nevertheless did not reveal any T₂ prolongation in other muscles than innervated by the *N. Peroneus Communis*. As the present stimulation method induces selective muscle contractions it is an ideal technique to combine with a setup as described by Giannesini *et al.*, combining ¹H MRI and ³¹P MRS with noninvasive force measurements⁶.

Table 2 PCr concentrations and pH of a longitudinal study in ZDF rats

	6 weeks		12 weeks		18 weeks	
	fa/+	fa/fa	fa/+	fa/fa	fa/+	fa/fa
[PCr] rest (mM)	32.5 ± 1.5	31.7 ± 1.2	38.5 ± 1.0	40.2 ± 1.2	39.4 ± 1.6	39.1 ± 2.0
[PCr] end (mM)	17.0 ± 2.3	16.7 ± 2.3	19.9 ± 2.0	21.4 ± 2.3	21.8 ± 1.6	19.5 ± 1.7
pH end	6.91 ± 0.06	6.86 ± 0.10	7.02 ± 0.10	6.98 ± 0.08	6.96 ± 0.06	6.93 ± 0.06

Values represent mean ± SD. [PCr] rest: phosphocreatine concentration at rest, [PCr] end: phosphocreatine concentration at the end of the 2 min stimulation protocol. pH end: pH at the end of the 2 min stimulation protocol. fa/+ and fa/fa, heterozygous and homozygous ZDF rats, respectively.

In order to minimize the distortions of the main magnetic field due to magnetic material, we used platinum electrodes and copper wire leads. Since the positioning of the electrodes was along the nerve trajectory of the *N. Peroneus Communis* or *N. Tibialis*, the electrodes were proximal of the muscle of interest and therefore not in the direct proximity of the RF-coil. The electrodes did not significantly degrade the homogeneity of the magnetic field, indicated by the line width of the PCr peak, which was similar to measurements without electrodes (data not shown).

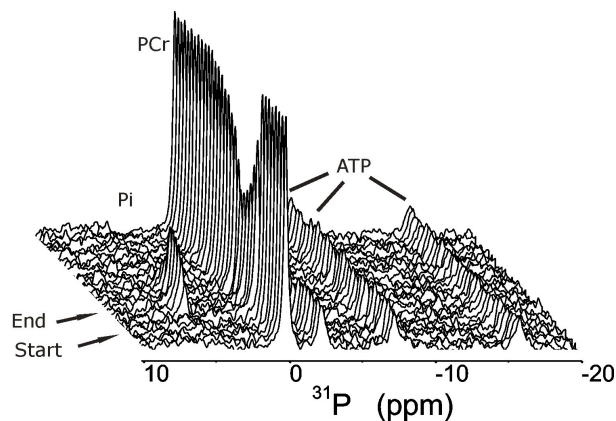


Figure 4 Example of a time series of ^{31}P spectra measured in a rat TA, time resolution: 20 s, stimulation duration: 2 min, arrows indicating start and end of electrical stimulation period.

The described electrical stimulation method was applied in a longitudinal study of fa/fa and fa/+ ZDF rats at different ages. The setup allowed for creating a reproducible end-exercise status, as confirmed by the overall similar end-exercise PCr concentration and pH. The subcutaneous electrical stimulation procedure was also well tolerated by the animals, as they quickly restored their normal food intake after the measurements. The small incisions through the skin healed fast, allowing repetitive measurements within ~ 5 days when making a new incision or even the next day when the old incision was re-opened. This longitudinal study proved that the presented stimulation method is suitable for longitudinal studies in rats and offers an alternative for chronically implanted electrodes.

Conclusions

We presented an NMR-compatible, minimally invasive electrical stimulation procedure for the muscles of the lower hind limb of the rat that 1) was well tolerated by the animals 2) induced highly specific muscle contractions and 3) proved to be applicable in longitudinal study designs. The present electrical stimulation method provides an appropriate alternative for the traditional invasive, direct stimulation method. Further research is recommended to investigate the feasibility of this method in other rodent species.

References

1. Prompers, J.J. et al. *NMR Biomed* **19**, 927-953 (2006).
2. Cole, B.G. & Gardiner, P.F. *Exp Neurol* **85**, 52-62 (1984).
3. Meyer, R.A. et al. *Am J Physiol* **250**, C264-274 (1986).
4. Prior, B.M. et al. *J Appl Physiol* **90**, 615-623 (2001).
5. Giannesini, B. et al. *Biochim Biophys Acta* **1553**, 223-231 (2002).
6. Giannesini, B. et al. *Magn Reson Med* **54**, 1058-1064 (2005).
7. Warren, G.L., Ingalls, C.P. & Armstrong, R.B. *J Appl Physiol* **84**, 2171-2176 (1998).
8. Kuhlmann, J. et al. *Diabetes* **52**, 138-144 (2003).
9. Kuhlmann, J. et al. *Magn Reson.Med.* **53**, 1275-1282 (2005).
10. Neumann-Haefelin, C. et al. *Diabetes* **53**, 528-534 (2004).
11. Neumann-Haefelin, C. et al. *Magn Reson.Med.* **50**, 242-248 (2003).
12. De Feyter, H.M. et al. *Magn Reson Med* **56**, 19-25 (2006).
13. Gruetter, R. *Magn Reson Med* **29**, 804-811 (1993).
14. Vanhamme, L., van den Boogaart, A. & Van Huffel, S. *J Magn Reson* **129**, 35-43 (1997).
15. Taylor, D.J. et al. *Magn Reson Med* **3**, 44-54 (1986).
16. Taylor, D.J. et al. *Mol Biol Med* **1**, 77-94 (1983).

Chapter 4

³¹P MR spectroscopy and *in vitro* markers of oxidative capacity in type 2 diabetes patients

Adapted from:

Praet S.F.E., De Feyter H.M., Jonkers R.A.M., Nicolay K., van Pul C., Kuipers H.,
van Loon L.J.C., Prompers J.J.

³¹P MR spectroscopy and *in vitro* markers of oxidative capacity in type 2 diabetes patients.
Magn Reson Mater Phy (MAGMA) 2006; 19:321-331

Abstract

BACKGROUND: Skeletal muscle mitochondrial function in type 2 diabetes is currently being studied intensively. *In vivo* ^{31}P magnetic resonance spectroscopy (^{31}P MRS) is a non-invasive tool used to measure mitochondrial respiratory function in skeletal muscle tissue. However, microvascular co-morbidity in long-standing type 2 diabetes can interfere with the ^{31}P MRS methodology.

AIM: To compare ^{31}P MRS-derived parameters describing *in vivo* mitochondrial respiratory function with an *in vitro* assessment of muscle respiratory capacity and muscle fiber-type composition in type 2 diabetes patients.

METHODS: ^{31}P MRS was applied in long-standing, insulin-treated type 2 diabetes patients. ^{31}P MRS markers of mitochondrial respiratory function were measured in the *M. vastus lateralis*. Muscle biopsy samples were collected from the same muscle and analyzed for succinate dehydrogenase activity (SDH) and fiber-type distribution.

RESULTS: Several ^{31}P MRS parameters of mitochondrial respiratory function showed moderate to good correlations with the percentage of type-I fibers and type-I fiber-specific SDH-activity (Pearson's R between 0.70 - 0.75). *In vivo* and *in vitro* parameters of local mitochondrial respiration also correlated well with whole body fitness levels ($\text{VO}_{2\text{peak}}$) in these patients (Pearson's R between 0.65 - 0.90).

CONCLUSION: Good correlations exist between *in vivo* and *in vitro* measurements of mitochondrial respiratory function in long-standing, insulin-treated type 2 diabetes subjects, which are qualitatively and quantitatively consistent with previous results measured in healthy subjects. This justifies the use of ^{31}P MRS to measure mitochondrial respiratory function in relation to type 2 diabetes.

Introduction

The presence of skeletal muscle mitochondrial dysfunction in ageing, insulin resistance and/or type 2 diabetes is currently a topic of intense debate¹⁻⁶. Even though recent studies seem to support the concept that mitochondrial dysfunction plays a key role in the pathogenesis of skeletal muscle insulin resistance^{1, 4, 6}, it remains to be established whether mitochondrial dysfunction represents either cause or consequence⁷. In this context, skeletal muscle mitochondrial function is now frequently being studied in type 2 diabetes patients using various experimental paradigms, each having its own specific advantages and disadvantages.

³¹P MR spectroscopy (³¹P MRS) is a commonly applied method allowing *in vivo* measurement of mitochondrial function in exercising muscle⁸⁻¹⁴. Previous studies in healthy subjects showed ³¹P MRS to be an effective non-invasive method to measure mitochondrial oxidative capacity based on moderate to good correlations between ³¹P MRS derived parameters and *in vitro* measurements of oxidative capacity^{15, 16}. ³¹P MRS can be used to measure the time constant of phosphocreatine (PCr) recovery after exercise. During recovery from exercise, PCr is resynthesized purely as a consequence of oxidative ATP synthesis and, therefore, analysis of PCr recovery provides information about mitochondrial respiratory function. Alternative measures as the recovery of adenosine diphosphate (ADP), the initial PCr recovery rate and the maximal mitochondrial aerobic capacity can all be inferred from the PCr recovery data. ³¹P MRS studies have shown that mitochondrial function is impaired in mitochondrial myopathy^{17, 18} and in chronic disease such as cardiac failure¹⁹ peripheral arterial occlusive disease²⁰. However, tissue pH^{8, 21-24}, local muscle blood flow²⁵ and concomitant tissue oxygenation²⁶ might affect the ³¹P MRS measurement of mitochondrial respiration. Both impaired vascular function^{27, 28}, and low capillary density²⁹ have been associated with type 2 diabetes. However, recently it has been postulated that a wide intersubject variability exists in the level of diabetes-related complications³⁰. Given the potential confounding influence of an impaired microcirculation and tissue oxygenation^{25, 26} on PCr-recovery kinetics, we questioned whether PCr recovery kinetics can be reliably used as an index of mitochondrial function in long-standing type 2 diabetes patients on exogenous insulin therapy. It was hypothesised that the earlier described correlations between ³¹P MRS and *in vitro* markers of mitochondrial function^{15, 16} are weaker or even entirely absent in a population of long-term diagnosed type 2 diabetes patients on exogenous insulin treatment.

In the present study, we evaluate the relationship between ³¹P MRS-derived parameters describing mitochondrial function, maximal succinate dehydrogenase activity (SDH) as an *in vitro* marker of muscle oxidative capacity and muscle fiber type composition in a group of long-term insulin-treated type 2 diabetes patients. As such, this study provides additional insight in the applicability of ³¹P MRS to investigate *in vivo* skeletal muscle mitochondrial respiratory function in type 2 diabetes.

Materials and methods

Subjects

Eleven male type 2 diabetes patients were selected to participate in this study. Subjects had been diagnosed with type 2 diabetes for over 5 years, established by a fasting blood glucose larger than or equal to 6.1 mmol/l at the time of diagnosis as defined by the World Health Organisation ³¹. All subjects were on exogenous insulin treatment for at least 24 months and had been on a stable regimen of diabetes medication over the last 3 months before being recruited. Patients using thiazolidinediones and/or β -blockers less than 6 months, and subjects with impaired liver function, renal failure, severe retinopathy or a history of severe cardiovascular problems, were excluded from participation. The nature and the risks of the experimental procedures were explained to the subjects and all gave their written informed consent to participate in the study, which was approved by the local Medical Ethical Committee of the Máxima Medical Center, Veldhoven, The Netherlands.

Body composition

Body mass index and waist circumference were measured using an analog weight scale and standard measuring tape. Segmental and whole-body bone mass and fat free mass (FFM) were determined using whole-body dual energy X-ray absorptiometry (DXA) (Hologic QDR-4500 Discovery A, software version 12.3:3, Hologic Inc. Bedford, MA, USA).

Whole-body oxygen uptake capacity

Two weeks before the muscle biopsy and MRS measurements, maximal whole-body oxygen uptake capacity (VO_{2peak}) and maximal workload capacity (W_{max}) were measured during an incremental exhaustive exercise test until exhaustion, performed on a cycle ergometer (Medifit Ergometer, Medifit systems, Maarn, The Netherlands) using a ramp protocol ³². After 4 min of unloaded cycling the load was increased linearly until exhaustion. The aim was to apply a load rate that would cause exhaustion within 8 - 12 min as recommended by Zhang *et al.* ³². Subjects were requested to abstain from exercise and caffeinated beverages on the day of the test and were tested more than 2 h after a light meal. Gas exchange measurements were performed continuously by using a computerized metabolic cart (Ergostar II, PMS Professional Medical Systems, Basel, Switzerland) that was calibrated before each study. Maximal whole-body oxygen uptake capacity was defined in the present study as VO_2 remaining unchanged or increasing less than 1 ml/min/kg for 30 s or more despite an increment in work load ³³. Cardiac function was monitored using a 12-lead electrocardiogram with heart rate (HR) being recorded continuously (Polar Electro, Kempele, Finland) and sampled at 1 kHz through a data log device (Co2ntrol™, Tildesign, Zeewolde, The Netherlands).

³¹P Magnetic resonance spectroscopy

³¹P MRS of the *M. vastus lateralis* was performed by using a 1.5-Tesla whole-body magnet (Gyrosan S15/ACS, Philips Medical Systems, Best, The Netherlands). Subjects were measured in a supine position. After collecting transversal and sagittal scout images, the magnetic field homogeneity was optimized by localized shimming on the proton signal using the body coil. The ³¹P signals were collected using a 6-cm diameter surface coil placed over the *M. vastus lateralis*. Data were acquired following a 90° adiabatic excitation pulse with a sweep width of 2 kHz and 1024 data points. A fully relaxed spectrum was measured at rest with a repetition time of 30 s and 24 scans. Then, spectra were acquired using a repetition time of 3 s at rest (60 scans/spectrum) and during a rest-exercise-recovery protocol (2 scans/spectrum yielding a time resolution of 6 s, total of 150 spectra/15 min). For the latter time series, the first 20 spectra (2 min) were measured at rest, after which the subjects started the exercise (see below). The duration of the exercise varied per subject, but never exceeded 8 min, so that at least 5 min of recovery were recorded. From the dimension of the coil and the size and geometry of a typical upper leg, it was estimated that the majority of the signal in the unlocalized ³¹P MRS measurements originates from the *M. vastus lateralis*, with minimal contaminations from the adjacent *M. rectus femoris* and underlying *M. vastus intermedius*.

Exercise protocol inside magnet

All subjects performed a single leg extension exercise in the supine position inside the magnet, which has been shown to be limited to the four muscles of the quadriceps³⁴. The exercise was conducted by rhythmically lifting a lever (resting on the lower leg, proximal of the foot) connected to an ergometer. The upper leg was supported with the hip joint in a 30 degrees ante flexed position and immobilised with two 3 cm wide Velcro straps. One contraction was performed every 1.5 s acoustically guided by a digital metronome. The workload was set at 2.5 W for the first min and then increased by 2.5 W each min (except for one subject, whose work load was increased by 5 W each min). To get subjects acquainted to the in-magnet exercise protocol subjects visited the laboratory twice within a 7 day period. During the first visit, subjects performed a test run and exercised their left leg until fatigued. The data were then used to estimate the duration of the exercise for the second visit. During the second visit, subjects exercised their right leg until phosphocreatine depletion was sufficient (~50%) to measure the recovery, aiming to avoid intracellular pH to drop below 6.8.

Analysis of ³¹P MR spectra

Zero and first order phase corrections were determined from the rest spectra and then also applied to the time series. Spectra were fitted in the time domain by using a nonlinear least squares algorithm (AMARES) in the jMRUI software package³⁵. PCr, inorganic phosphate (Pi), adenosine triphosphate (ATP) and phosphodiester (PDE) signals were fitted to Lorentzian line shapes. The three ATP peaks were fitted as two doublets and one triplet, with equal amplitudes and line widths and prior knowledge for the J-coupling constant (17 Hz). For the time series,

the PCr line width during recovery was constrained to the average PCr line width during recovery (excluding the first 10 data points), obtained from a prior, unconstrained fit.

Absolute concentrations of the phosphorylated metabolites were calculated after correction for partial saturation and assuming that [ATP] is 8.2 mM at rest ³⁶. Saturation correction factors determined from the fully relaxed spectra were 1.93 ± 0.05 , 1.60 ± 0.05 , 1.54 ± 0.06 and 2.14 ± 0.06 (mean \pm SD), respectively, for PCr, P_i, ATP and PDE. Intracellular pH was calculated from the chemical shift difference between the P_i and PCr resonances (δ ; measured in parts per million) using the following formula ³⁷:

$$\text{pH} = 6.75 + \log\left(\frac{\delta - 3.27}{5.63 - \delta}\right) \quad [1]$$

Free cytosolic [ADP] was calculated from pH and [PCr] using a creatine kinase equilibrium constant (K_{eq}) of $1.66 \times 10^9 \text{ M}^{-1}$ ³⁸ and assuming that 15% of the total creatine is unphosphorylated at rest ³⁹, using the equation:

$$[\text{ADP}] = \frac{[\text{ATP}][\text{Cr}]}{[\text{PCr}][\text{H}^+]K_{eq}} \quad [2]$$

During recovery from exercise, PCr is resynthesized purely as a consequence of oxidative ATP synthesis and therefore analysis of PCr recovery provides information about mitochondrial respiratory function. Recoveries of PCr and ADP were fitted to mono-exponential functions using Matlab (version 6.1, Mathworks, Natick, Massachusetts, USA). Results are expressed as the metabolite's time constant of recovery, i.e. τ_{PCr} and τ_{ADP} .

Calculation of the initial rate of PCr recovery (V_{PCr}) was based on the PCr recovery rate ($1/\tau_{\text{PCr}}$) and the difference between the resting and the end-exercise PCr concentrations (ΔPCr) ⁴⁰:

$$V_{\text{PCr}} = \frac{1}{\tau_{\text{PCr}}} \cdot \Delta\text{PCr} \quad [3]$$

Calculation of the maximum aerobic capacity (Q_{max}) was based on V_{PCr} , the end-exercise ADP concentration ($[\text{ADP}]_{\text{end}}$), and the assumption that oxidative ATP synthesis is regulated by the ADP concentration according to Michaelis-Menten kinetics with a K_m of 30 μM ⁴⁰:

$$Q_{\text{max}} = V_{\text{PCr}} \cdot \left(1 + \frac{K_m}{[\text{ADP}]_{\text{end}}}\right) \quad [4]$$

Table 1 Subject's characteristics

n = 11	Mean	±	SEM	Range	
Age (yrs)	59.0	±	2.5	49	- 69
Body mass index (kg/m ²)	32.2	±	1.2	25.5	- 38.7
Body weight (kg)	97.6	±	4.9	78.0	- 123.0
FFM (kg)	68.9	±	2.9	56.3	- 85.2
Waist circumference (cm)	110.6	±	3.7	94.5	- 131.5
HbA _{1c} (%)	7.6	±	0.3	6.3	- 9.5
Fasting Glucose (mmol/l)	10.4	±	0.9	4.0	- 16.4
Years of type 2 diabetes	12.1	±	2.1	6	- 29
Years of insulin therapy	7.0	±	2.4	2	- 29
Daily insulin requirement (IU)	92.5	±	11.1	16	- 150
VO _{2peak} per kg BW (ml/min/kg)	24.3	±	1.4	15.0	- 29.6
VO _{2peak} per kg FFM (ml/min/kg)	34.2	±	1.9	21.7	- 40.5

FFM: fat free mass, HbA_{1c}: glycolysated haemoglobin, IU: international units, VO_{2peak}: maximal oxygen uptake BW: body weight.

Blood and muscle biopsy samples

On the evening before the blood sample and muscle biopsy collection, subjects received a standardized meal (35.2 ± 1.8 kJ/per kg BW, containing 53 energy% (En%) fat, 10 En% protein, and 37 En% carbohydrate) after which subjects remained fasted and were allowed to drink water only. Subjects reported at the laboratory at 8.00 a.m. After 5 - 10 min of supine rest, a venous blood sample was collected from an antecubital vein. Blood plasma samples were collected into EDTA containing tubes and centrifuged for 10 min at 4°C. Aliquots of plasma were frozen immediately in liquid nitrogen and stored at -80°C until further analyses. Plasma glucose and HbA_{1c} measurements were performed on a Modular P analyzer (Roche Diagnostics, Basel, Switzerland) using the Hexokinase and Tina-quant assays, respectively.

After blood collection and local anesthesia, a percutaneous muscle biopsy was collected from the middle region of the *M. vastus lateralis*, using a modified Bergström needle to increase sample size (Maastricht Instruments, Maastricht, The Netherlands). Muscle samples were dissected carefully, freed from any visible non-muscle material, embedded in Tissue-Tek (Sakura Finetek, Zoeterwoude, The Netherlands) and rapidly frozen in liquid nitrogen-cooled isopentane to its melting point.

Multiple serial sections (5 µm) from each biopsy sample were thaw-mounted together on uncoated, pre-cleaned glass slides. The proportion of type-I, IIa, and IIx muscle fibers was determined using antibodies raised against human myosin heavy chain (MHC) type-I (A4.840) and type-IIa (N2.261), developed by Dr Blau *et al.*⁴¹. Muscle fiber-type specific oxidative capacity was estimated by measuring SDH-activity in the muscle cross-sections using

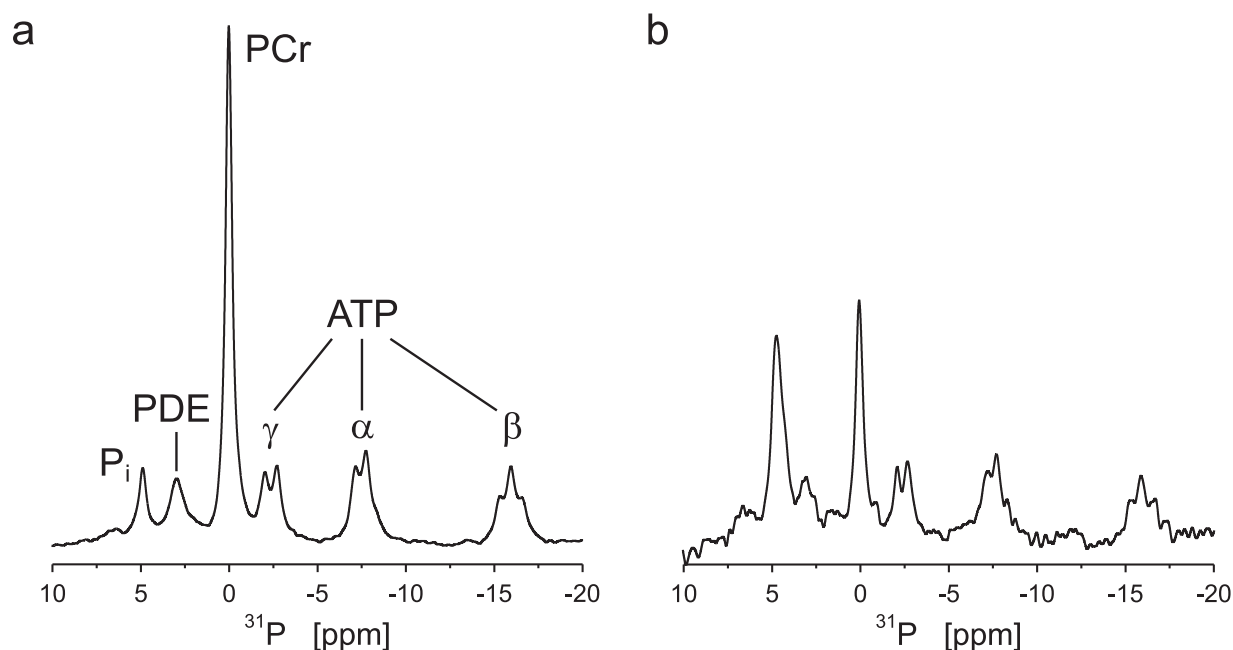


Figure 1 Typical *M. vastus lateralis* ^{31}P spectra for one subject at rest (panel a, number of scans = 60) and at the end of exercise (panel b, number of scans = 2). Pi: inorganic phosphate, PDE: phosphodiester, PCr: phosphocreatine, and α , γ , β indicate the three phosphate groups of ATP. For this subject the PCr depletion at the end of exercise was 47.6% and the corresponding pH was 6.95.

histochemical analyses ⁴². After 24 h, glass slides were examined using a Nikon E800 fluorescence microscope (Uvikon, Bunnik, The Netherlands) coupled to a Basler A113 C progressive scan color CCD camera, with a Bayer color filter. Epifluorescence signal was recorded using a fluorescein isothiocyanate (FITC) excitation filter (465 - 495 nm) for muscle fiber-type, and a 4',6-diamidino-2-phenylindole (DAPI) UV excitation filter (340 - 380 nm) for laminin.

Digitally captured images (240 × magnification) with a minimum of six fields-of-view per muscle cross-section, were processed and analyzed using Lucia 4.8 software (Nikon, Düsseldorf, Germany). SDH stained sections were captured in full color using bright field light microscopy. Digitally captured images (120 × magnification), were processed and analyzed using the Lucia 4.8 software package. The bright-field images of the SDH stains were converted *post hoc* to 8-bit grayscale values. The mean optical density of the SDH-raised signal per individual fiber was quantified by averaging the optical density measured in every pixel in the cell, corrected for the mean optical density of the background stain measured in a field-of-view containing no muscle fibers.

Statistics

All data are expressed as means \pm SEM. Student's t-test as well as simple and multiple stepwise regression analyses were applied on the data on whole-body oxygen uptake capacity, ^{31}P MRS, and muscle biopsy measurements using the SPSS 12.0.1 software package (SPSS Inc, Chicago, IL, USA). Level of statistical significance was set at $p < 0.05$.

Results

Subjects' characteristics

The characteristics of our 11 male subjects are shown in Table 1. Mean duration of type 2 diabetes was 12.1 ± 2.1 years since diagnosis. Subjects had been on exogenous insulin therapy for 7.0 ± 2.4 years, and seven patients combined this with oral blood glucose lowering medication. All subjects were using blood pressure lowering medication, and 8 patients were receiving cholesterol-lowering therapy. Whole body maximal oxygen uptake (VO_{2peak}) was 24.3 ± 1.4 ml per min per kg body weight.

MRS measurements

Figure 1a and b show typical examples of ^{31}P MR spectra from a subject's *vastus lateralis* muscle at rest and at the end of exercise, respectively. Table 2 summarizes the baseline and end-exercise ^{31}P MRS results for the 11 subjects. At the end of exercise, the average PCr depletion was $45.5 \pm 2.3\%$ and the pH was 6.90 ± 0.04 , which was significantly different from the resting condition (t-test, $p < 0.01$). Among all subjects, the end-exercise pH ranged between 6.75 - 7.05.

Table 2 ^{31}P MRS parameters

n = 11	Rest		End-exercise	
[PCr] (mM)	36.9	± 1.2	20.2	± 1.3
[Pi] (mM)	4.7	± 0.2	19.8	± 1.2
[ADP] (μ M)	10.3	± 0.1	46.8	± 2.8
pH	7.07	± 0.004	6.90	± 0.04
MRS markers of mitochondrial respiratory function	Mean	\pm SEM	Range	
τ_{PCr} (s)	49.4	± 5.5	27.2	- 86.6
τ_{ADP} (s)	22.5	± 2.9	14.9	- 45.3
V_{PCr} (mM/s)	0.37	± 0.03	0.20	- 0.54
Q_{max} (mM/s)	0.61	± 0.05	0.31	- 0.82

Data presented are means \pm SEM. PCr: phosphocreatine, Pi: inorganic phosphate, ADP: adenosine diphosphate; τ_{PCr} : PCr recovery time constant, τ_{ADP} : time constant, pH: intracellular muscle pH, V_{PCr} : initial rate of PCr recovery based on the PCr recovery rate ($1/\tau_{PCr}$) and the difference between the resting and the end-exercise PCr concentrations, Q_{max} : maximum rate of oxidative ATP synthesis calculated from V_{PCr} in relation to end-exercise ADP concentration and an assumed K_m of 30 μ M

Figure 2 illustrates both the raw data and mono-exponential fits of the PCr and ADP recoveries of one subject. Table 2 summarizes the PCr and ADP recovery time constants and the other estimates of mitochondrial respiratory function, V_{PCr} and Q_{max} . All ^{31}P MRS estimates of mitochondrial respiratory function displayed a wide range of values. For instance τ_{PCr} ranged from 27.2 to 86.6 s. All ^{31}P MRS variables correlated significantly with each other (Pearson's R between 0.77 and 0.92, $p < 0.05$).

Histochemical analyses

Table 3 summarizes muscle fiber-type distribution and both mixed and fiber-type specific SDH-activity. No significant differences in SDH-activity between type-I and type-IIa fibers were observed (t-test, NS). Type-IIx muscle fiber SDH-activity was significantly lower compared to the type-I and IIa muscle fibers (t-test, $p < 0.05$).

Correlations

Correlations between *in vivo* and *in vitro* estimates are presented in Table 4 and Figures 3 and 4. All ^{31}P MRS markers of mitochondrial respiratory function revealed a strong and significant correlation with $\text{VO}_{2\text{peak}}$ (Figure 3 and Table 4) and became somewhat stronger when $\text{VO}_{2\text{peak}}$ was expressed per kg fat free mass. A comparison between whole-body $\text{VO}_{2\text{peak}}$ and *in vitro* estimates of mitochondrial respiratory function showed strong positive correlations for both SDH-activity in the type-I muscle fibers (Figure 4 a, Pearson's R: 0.77, $p < 0.01$) and SDH-activity in the type-IIa muscle fibers (Figure 4 b, Pearson's R: 0.62, $p < 0.05$).

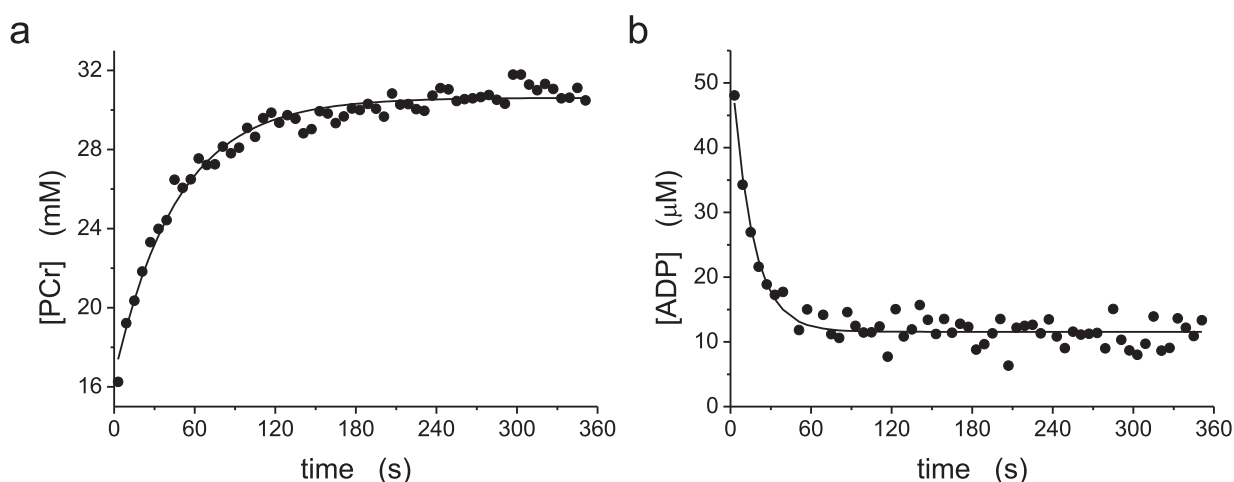


Figure 2 PCr (panel a) and ADP (panel b) recovery curves for an individual subject (the same subject as in Fig. 1). Mono-exponential functions (dark lines) were fit to the actual data (filled circles) obtained every 6 s. The time constants for PCr and ADP recovery were 46.9 and 15.6 s, respectively.

Significant relationships were observed for most of the ^{31}P MRS markers of mitochondrial function when compared with *in vitro* estimates such as type-I SDH-activity (Figure 4 c), total muscle SDH-activity (Figure 4 d) and percentage of type-I muscle fibers (Figure 4 e). An inverse correlation was observed between ^{31}P MRS parameters and the percentage of type-IIa fibers (Figure 4 f). The type-I SDH-activity was co-linear with the type-I fiber content. Type-I fiber content was the best predictor in linear stepwise regression models with ^{31}P MRS estimates set as a dependent variable in the model (Pearson's R: 0.76, $p < 0.01$).

Table 3 Skeletal muscle tissue histochemistry analyses

Characteristic	Mean	±	SEM	Range	
Type-I fiber distribution (%)	35.9	±	3.4	13.9	- 50.8
Type-IIa fiber distribution (%)	43.6	±	3.6	28.7	- 69.4
Type-IIx fiber distribution (%)	20.5	±	2.6	14.5	- 43.8
Total muscle SDH activity (AU)	53.7	±	8.5	24.5	- 114.4
SDH activity type-I fibers (AU)	29.0	±	5.2	5.5	- 68.7
SDH activity type-IIa fibers (AU)	20.0	±	3.9	4.8	- 40.4
SDH activity type-IIx fibers (AU)	4.8	±	1.3	0.4	- 13.1

SDH: succinate dehydrogenase activity in arbitrary units as measured by immunohistochemistry

Discussion

The present study shows that in a group of long-standing, insulin-treated, type 2 diabetes patients commonly used ^{31}P MRS markers of *in vivo* mitochondrial respiratory function are strongly correlated with muscle fiber type-specific SDH-activity and type-I muscle fiber content. These data imply that ^{31}P MRS represents an appropriate methodology to study *in vivo* skeletal muscle mitochondrial respiratory function in long-standing type 2 diabetes patients.

The non-invasive quantification of the post-exercise PCr recovery time constant using ^{31}P MRS provides us with an approach that can be used to measure *in vivo* mitochondrial respiration. However, several studies have shown that cytosolic pH has a strong influence on PCr recovery kinetics^{8, 21-24}. The exercise protocol in the MR scanner resulted in a small, but significant drop in intracellular pH from 7.07 ± 0.004 at rest to 6.90 ± 0.04 at the end of the exercise ($p < 0.01$). However, the variation within this end-exercise pH was relatively small, ruling out end-exercise pH as a major source of variation within τ_{PCr} . Moreover, τ_{PCr} showed good correlations with the type-I fiber specific SDH activity as well as with the type I muscle fiber content (Table 4, Figure 4e). As opposed to the PCr recovery time constant, the ADP recovery time constant has been proposed to be a pH-independent marker of mitochondrial respiratory

Table 4 Pearson's correlation matrix among ^{31}P MRS markers of mitochondrial respiratory function, whole body oxygen uptake and histochemical muscle fiber analysis

Variable	$\text{VO}_{2\text{peak}}$ per kg BW	SDH Type I	SDH Type IIa	Total SDH	%Type I	%Type IIa
τ_{PCr} (s)	-0.70*	-0.70*	-0.03	-0.48	-0.75**	0.83**
τ_{ADP} (s)	-0.90**	-0.76**	-0.38	-0.70*	-0.46	0.57
V_{PCr} (mM/s)	0.74*	0.59	0.18	0.47	0.61*	-0.58
Q_{max} (mM/s)	0.66*	0.51	0.07	0.38	0.64*	-0.67*
$\text{VO}_{2\text{peak}}$ per kg BW (ml/min/kg)	-	0.77**	0.62*	0.84**	0.22	-0.42

Muscle fiber type composition (%type I, IIa and IIx) based on number of fibers. * $p < 0.05$, ** $p < 0.01$, all correlations are based on $n = 11$.

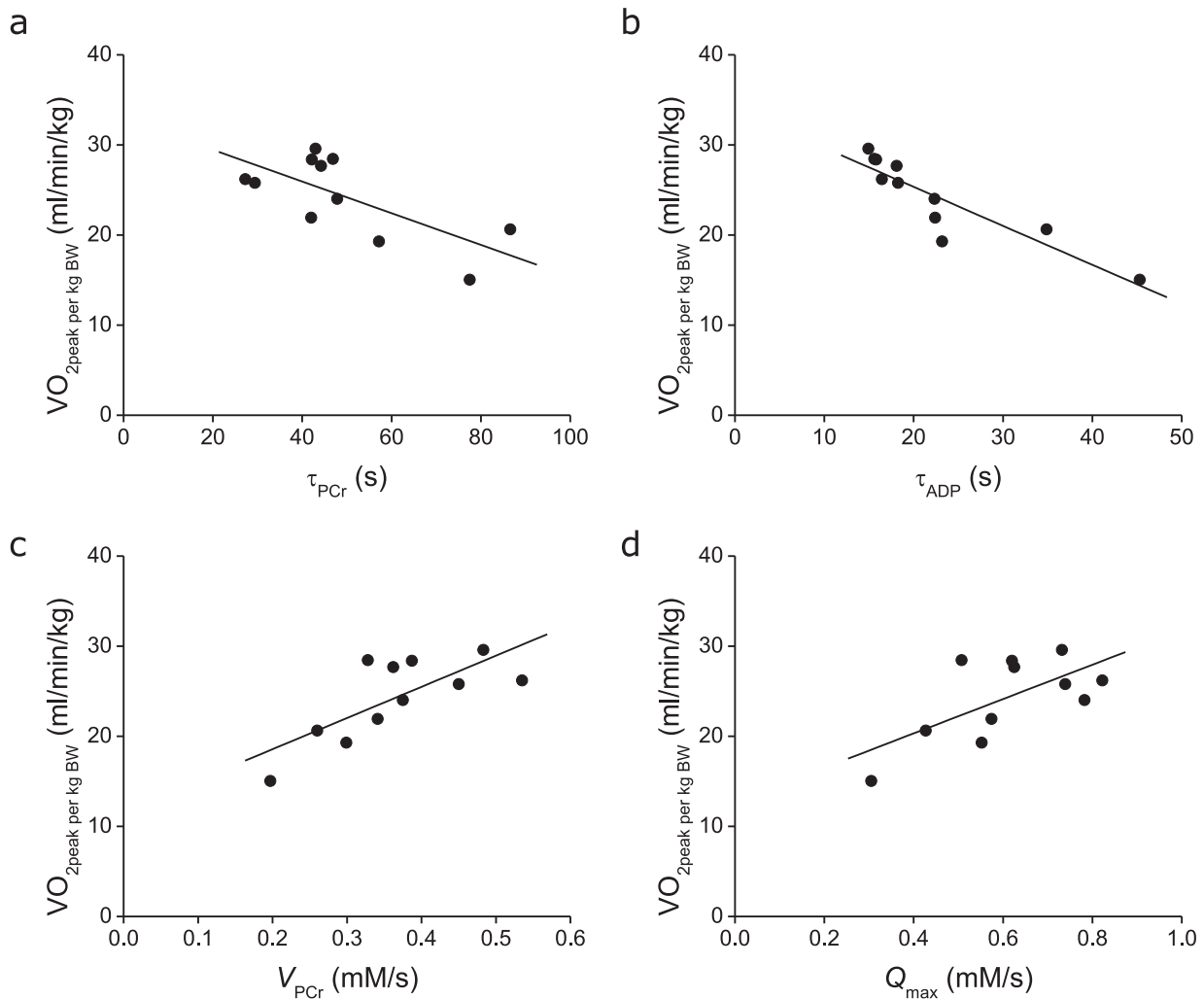


Figure 3 Relationships between maximal whole-body oxygen uptake (VO_{2peak} per kg BW) and the ^{31}P MRS parameters of mitochondrial respiratory function (panel a: τ_{PCr} ($R: -0.70, p < 0.05$), panel b: τ_{ADP} , ($R: -0.90, p < 0.01$), panel c: V_{PCr} ($R: 0.74, p < 0.05$) and panel d: Q_{max} ($R: 0.66, p < 0.05$).

function^{23, 43}. Correlations between τ_{ADP} and type-I fiber specific and total SDH activity were indeed stronger than for τ_{PCr} (Table 4, Figures 4c and 4d). The initial PCr recovery rate (V_{PCr}) and maximal aerobic capacity (Q_{max}) have also been shown to be independent of end-exercise pH^{23, 24}. However, both V_{PCr} and Q_{max} were not significantly correlated with SDH activity. All ^{31}P MRS derived parameters showed good correlations with whole-body oxygen uptake (Table 4, Figure 3). V_{PCr} is a measure of the actual mitochondrial ATP synthesis rate and therefore does not represent an absolute measure of mitochondrial function. According to the kinetic control model, V_{PCr} has a hyperbolic dependence on the end-exercise ADP concentration (Equation 4). As such, the correlation of V_{PCr} with VO_{2peak} can be explained by the small variation in end-exercise [ADP] (46.8 ± 2.8 M).

Local muscle blood flow²⁵ and tissue oxygenation²⁶ can influence local skeletal muscle metabolism and, as such modulate the ^{31}P MRS parameters. Since only a relatively small amount of muscle tissue is recruited in the single leg extension exercise and the exercise intensity is rather low, cardiac output does not reach maximal rates. Therefore, this exercise paradigm allows us to study maximal *in vivo* respiration within the *vastus lateralis* muscle in

the absence of any limits set by the potential oxygen supply dictated by a finite cardiac output⁴⁴. However, in long-standing, insulin-treated type 2 diabetes patients it has been reported that microvascular flow in the *vastus lateralis* muscle is likely impaired during dynamic exercise^{28, 45}. As such, even in our human dynamic single leg-extensor model, impaired PCr recovery caused by impaired vascular blood flow and oxygen supply or intramuscular oxygen diffusion would represent a potential confounding factor. Since there might be a rather wide intersubject variability of vascular impairments in long-term type 2 diabetes patients, we hypothesized that the correlations between ³¹P MRS and *in vitro* markers of mitochondrial function, as described in healthy populations^{15, 16}, might be weaker or even entirely absent in this population. Instead, the quality of the correlations between *in vivo* and *in vitro* parameters is strikingly similar to that found in healthy subjects. The pathological implications of these findings suggest that impairments of vascular oxygen supply or intramuscular oxygen diffusion were either not present or not severe enough to alter the relationship between *in vivo* and *in vitro* markers of mitochondrial function in these type 2 diabetes patients. Therefore, PCr recovery kinetics can be used to assess mitochondrial function in long-standing type 2 diabetes patients on exogenous insulin therapy.

It could be argued that the correlations measured between *in vivo* and *in vitro* markers of mitochondrial respiration can only explain $\sim 50\%$ of the variance (R^2 ranged from 0.38 to 0.59) of these relationships. This could point towards other mechanisms contributing to the variance of the measurements. As discussed by Larson-Meyer *et al.*¹⁵, maximal enzyme activities under ideal conditions are significantly higher than *in vivo* maximal metabolic flux rates. However, the comparison between *in vivo* and *ex vivo* conditions can be rather complex and e.g. depends on temperature factors that adjust for the *in vitro* respiratory rates of intact mitochondria⁴⁶. In addition, substrate availability and, as such, allosteric regulation of all enzymes involved is generally different as well. Therefore select marker enzyme activity may not completely reflect metabolic capacity of intact muscle. Besides the conceptual differences between *in vitro* and *in vivo* conditions, the difference in the muscle volume sampled has been suggested as an important factor that explains a large part of the variance^{15, 16}.

We compared the ³¹P MRS quantitative results with previous studies in healthy, elderly subjects published in the literature. For this purpose, PCr recovery time constants from the literature were recalculated at an end-exercise pH of 6.90 by using a correction factor of -45 s per pH unit²²⁻²⁴. For studies in *M. gastrocnemius*⁴⁷, *M. tibialis anterior*⁴⁸, *M. vastus lateralis*⁴⁹ and *M. rectus femoris*⁵⁰, τ_{PCr} ranged between 43 and 53 s, which is well in line with the average τ_{PCr} of 49.4 ± 5.5 s in our long-term type 2 diabetes patients. Scheuermann-Freestone *et al.*⁴⁷ investigated the calf muscle of type 2 diabetes patients and age-, sex- and body mass index-matched control subjects using dynamic ³¹P MRS. The end-exercise energy and pH status was similar to that in our study. However, τ_{PCr} was longer (75 s) and V_{PCr} was lower (0.25 mM/s) in their type 2 diabetes patients than in the present study. In fact, the results in our type 2 diabetes patients resemble more closely their findings in healthy controls. Scheuermann-Freestone *et al.*⁴⁷ ascribe the slower PCr recovery in their type 2 diabetes patients to microvascular disease. We speculated (see above) that in our group of type 2 diabetes patients microvascular blood flow is probably not significantly impaired, which could explain the 'normal' PCr recovery in our patients. However, a direct comparison is not

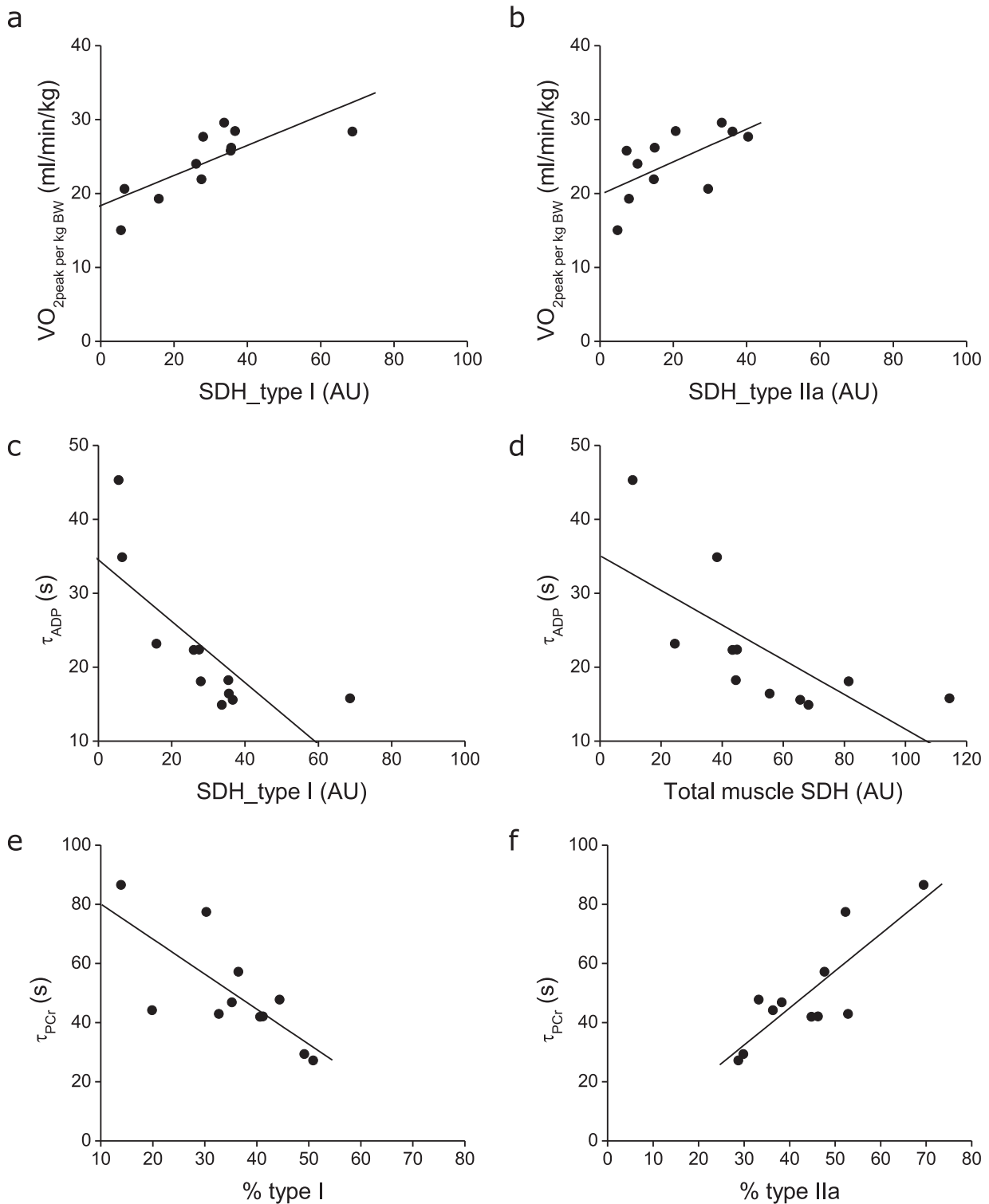


Figure 4 Relationships between maximal whole-body oxygen uptake (VO_{2peak}) and fiber-type specific mitochondrial enzyme activity (panel a: VO_{2peak} vs. SDH type-I, (R: 0.77, $p < 0.01$); panel b: VO_{2peak} vs. SDH type-IIa, (R: 0.62, $p < 0.05$)), between ^{31}P MRS recovery kinetics and fiber-type specific mitochondrial enzyme activity: τ_{ADP} vs. SDH_type I (panel c: R: -0.76, $p < 0.01$) and τ_{ADP} vs. total muscle SDH (panel d, R: -0.70 $p < 0.01$). The lower two panels show τ_{PCr} versus percentage of type-I fibers (panel e, R: -0.75, $p < 0.05$) and τ_{PCr} versus percentage of type-IIa fibers (panel f, R: 0.83, $p < 0.01$).

warranted as the two studies are performed in different muscle groups. It should be noted that even in our homogeneous group of patients large inter-individual differences exist (Table 2). Nevertheless, it is striking to note that most of our long-term diagnosed type 2 diabetes

patients show a rather normal PCr recovery time constant and as such appear to have a rather normal mitochondrial respiratory function. However, since no carefully matched control group was available for the present experimental set-up, further studies are needed to provide a more definitive answer to this question.

In conclusion, the present study shows moderate to good correlations between *in vivo* and *in vitro* measurements of oxidative capacity in a population of long-standing, insulin-treated type 2 diabetes patients. Overall, the results are both qualitatively as quantitatively consistent with previous results measured in healthy subjects. As such, the results of the present study suggest that ^{31}P MRS is an appropriate means to assess *in vivo* mitochondrial respiratory capacity in type 2 diabetes.

Acknowledgements

This study was made possible with a grant from the Ministry of Health, Welfare and Sport. The help from the nurses and staff at the Department of Internal Medicine at Máxima Medical Center in finding potential study candidates is gratefully acknowledged. The assistance of our students was greatly appreciated. The monoclonal antibodies A4.840 and N2.261 developed by Dr. Blau *et al.* were obtained from the Developmental Studies Hybridoma Bank developed under the auspices of the NICHD and maintained by the university of Iowa, Department of Biological Science, Iowa City, IA 52242, USA.

References

1. Kelley, D.E. et al. *Diabetes* **51**, 2944-2950 (2002).
2. Lowell, B.B. & Shulman, G.I. *Science* **307**, 384-387 (2005).
3. Petersen, K.F. et al. *Science* **300**, 1140-1142 (2003).
4. Petersen, K.F. et al. *N.Engl.J Med.* **350**, 664-671 (2004).
5. Short, K.R., Nair, K.S. & Stump, C.S. *N.Engl.J Med.* **350**, 2419-2421 (2004).
6. Simoneau, J.A. & Kelley, D.E. *J Appl Physiol* **83**, 166-171 (1997).
7. van Loon, L.J. & Goodpaster, B.H. *Pflugers Arch* **451**, 606-616 (2006).
8. Arnold, D.L., Matthews, P.M. & Radda, G.K. *Magn Reson Med* **1**, 307-315 (1984).
9. Arnold, D.L., Taylor, D.J. & Radda, G.K. *Ann Neurol* **18**, 189-196 (1985).
10. Kemp, G.J. & Radda, G.K. *Magn Reson Q* **10**, 43-63 (1994).
11. Kemp, G.J. et al. *NMR Biomed* **6**, 302-310 (1993).
12. Mattei, J.P., Bendahan, D. & Cozzzone, P. *Reumatismo* **56**, 9-14 (2004).
13. Radda, G.K. et al. *Biochem Soc Trans* **21 (Pt 3)**, 762-764 (1993).
14. Radda, G.K. et al. *Biochim Biophys Acta* **1271**, 15-19 (1995).
15. Larson-Meyer, D.E. et al. *Muscle Nerve* **24**, 1665-1676 (2001).
16. McCully, K.K. et al. *J Appl Physiol* **75**, 813-819 (1993).
17. Argov, Z. et al. *Neuromuscul Disord* **7**, 99-104 (1997).
18. Bendahan, D. et al. *Neurology* **42**, 1203-1208 (1992).
19. Massie, B.M. et al. *Am J Cardiol* **60**, 309-315 (1987).
20. Pipinos, II et al. *J Vasc Surg* **31**, 944-952 (2000).
21. Bendahan, D. et al. *FEBS Lett* **272**, 155-158 (1990).
22. Iotti, S. et al. *NMR Biomed* **6**, 248-253 (1993).
23. Lodi, R. et al. *MAGMA* **5**, 165-171 (1997).
24. Roussel, M. et al. *Biochim.Biophys.Acta* **1457**, 18-26 (2000).
25. Quistorff, B., Johansen, L. & Sahlin, K. *Biochem.J.* **291 (Pt 3)**, 681-686 (1993).
26. Haseler, L.J., Lin, A.P. & Richardson, R.S. *J Appl Physiol* **97**, 1077-1081 (2004).
27. Home, P. *Curr Med Res Opin* **21**, 989-998 (2005).
28. Young, J.L., Pendergast, D.R. & Steinbach, J. *Proc Soc Exp Biol Med* **196**, 61-68 (1991).
29. Marin, P. et al. *Diabetes Care* **17**, 382-386 (1994).
30. Girach, A. & Vignati, L. *J Diabetes Complications* **20**, 228-237 (2006).
31. Alberti, K.G. & Zimmet, P.Z. *Diabet Med* **15**, 539-553 (1998).
32. Zhang, Y.Y. et al. *Med Sci Sports Exerc* **23**, 625-630 (1991).
33. Weber, K.T., Janicki, J.S. & McElroy, P.A. *Herz* **11**, 88-96 (1986).
34. Richardson, R.S., Frank, L.R. & Haseler, L.J. *Int J Sports Med* **19**, 182-187 (1998).
35. Vanhamme, L., van den Boogaart, A. & Van Huffel, S. *J Magn Reson* **129**, 35-43 (1997).
36. Taylor, D.J. et al. *Magn Reson Med* **3**, 44-54 (1986).
37. Taylor, D.J. et al. *Mol Biol Med* **1**, 77-94 (1983).
38. Lawson, J.W. & Veech, R.L. *J Biol Chem* **254**, 6528-6537 (1979).
39. Boska, M. *Magn Reson Med* **32**, 1-10 (1994).
40. Kemp, G.J. et al. *Magn Reson Med* **31**, 248-258 (1994).
41. Cho, M., Webster, S.G. & Blau, H.M. *J Cell Biol* **121**, 795-810 (1993).
42. Gosker, H.R. et al. *Eur Respir J* **19**, 617-625 (2002).
43. Argov, Z., De Stefano, N. & Arnold, D.L. *NMR Biomed.* **9**, 165-172 (1996).
44. Richardson, R.S. *Med Sci Sports Exerc* **30**, 53-59 (1998).
45. Kingwell, B.A. et al. *Diabetes Care* **26**, 899-904 (2003).
46. Rasmussen, U.F. et al. *Am J Physiol Endocrinol Metab* **280**, E301-307 (2001).
47. Scheuermann-Freestone, M. et al. *Circulation* **107**, 3040-3046 (2003).
48. Kent-Braun, J.A. & Ng, A.V. *J Appl Physiol* **89**, 1072-1078 (2000).
49. Conley, K.E., Jubrias, S.A. & Esselman, P.C. *J Physiol* **526 Pt 1**, 203-210 (2000).
50. Schunk, K. et al. *Invest Radiol* **34**, 116-125 (1999).

Chapter 5

Intersubject differences in the effect of acidosis on phosphocreatine recovery kinetics in muscle after exercise are due to differences in proton efflux rates

Adapted from:

**Van den Broek N.M., De Feyter H.M., de Graaf L., Nicolay K., Prompers J.J.
Intersubject differences in the effect of acidosis on phosphocreatine recovery kinetics in muscle after exercise are due to differences in proton efflux rates.
Am J Physiol Cell Physiol; 2007**

Abstract

³¹P magnetic resonance spectroscopy provides the possibility to obtain bio-energetic data during skeletal muscle exercise and recovery. The time constant of phosphocreatine (PCr) recovery (τ_{PCr}) has been used as a measure of mitochondrial function. However, cytosolic pH has a strong influence on the kinetics of PCr recovery and it has been suggested that τ_{PCr} should be normalized for end-exercise pH. A general correction can only be applied if there are no intersubject differences in the pH dependence of τ_{PCr} . We investigated the pH dependence of τ_{PCr} on a subject-by-subject basis. Furthermore, we determined the kinetics of proton efflux at the start of recovery. Intracellular acidosis slowed PCr recovery and the pH dependence of τ_{PCr} differed among subjects, ranging from -33.0 to -75.3 s per pH unit. The slope of the relation between τ_{PCr} and end-exercise pH was positively correlated with both the proton efflux rate and the apparent proton efflux rate constant, indicating that subjects with a smaller pH dependence of τ_{PCr} have a higher proton efflux rate. Our study implies that simply correcting τ_{PCr} for end-exercise pH is not adequate, in particular when comparing patients and controls, as certain disorders are characterized by altered proton efflux from muscle fibers.

Introduction

^{31}P magnetic resonance spectroscopy (MRS) provides the possibility to obtain bio-energetic data during skeletal muscle exercise and recovery in a non-invasive manner and with a time resolution of a few seconds. This has made a major contribution to our understanding of energy metabolism, its control and the way in which it can be affected in disease ¹⁻⁷. During recovery from exercise, phosphocreatine (PCr) is resynthesized purely as a consequence of oxidative ATP synthesis ⁸⁻¹⁰ and therefore measurement of the time constant of PCr recovery (τ_{PCr}) provides information about mitochondrial function. This technology was very recently applied to study *in vivo* mitochondrial function in patients with type 2 diabetes ¹¹.

Several studies have shown that cytosolic pH has a strong influence on the kinetics of PCr recovery ^{1, 12-21}. The slower PCr recovery in the presence of intracellular acidosis could reflect a decreased mitochondrial respiration at low pH. However, there are conflicting data about the effects of low pH on respiratory rates, ranging from inhibition ²²⁻²⁴, a very small or no significant effect ^{19, 25-29} to even an increased effectiveness ^{30, 31}. PCr recovery in the presence of intracellular acidosis could also be slowed down due to factors downstream of oxidative phosphorylation, i.e. increased ATP consumption by cellular ion pumps ^{21, 32-34} and/or a pH-dependent shift in the creatine kinase equilibrium ^{35, 36}.

As an alternative to τ_{PCr} , the time constant of ADP recovery (τ_{ADP}) can be used to assess oxidative capacity. The concentration of ADP is the principal error signal in the feedback loop controlling mitochondrial oxidation and therefore ADP recovery is one of the most sensitive MRS indices of mitochondrial function ³⁷. Finally, the maximum aerobic capacity (Q_{max}), which can be calculated from the ^{31}P MRS recovery data, provides a parameter for mitochondrial function. Both τ_{ADP} ^{1, 2, 17, 18, 20} and Q_{max} ^{18, 19, 21} have been shown to be independent of end-exercise pH. A drawback of the use of these parameters compared to τ_{PCr} is that they are indirectly derived from the PCr recovery data, using a number of assumptions.

It has been suggested that τ_{PCr} can be normalized for end-exercise pH ^{13, 18, 21}. However, a general correction for pH can only be applied if there are no intersubject differences in the pH dependence of PCr recovery kinetics. In previous studies, data of different subjects have been grouped to investigate the effect of pH on PCr recovery ^{1, 12-21}. We investigated the effect of acidosis on τ_{PCr} in the *M. vastus lateralis* on a subject-by-subject basis. To this end, each subject performed 10-13 exercise protocols of different intensity to reach different levels of acidification. Furthermore, we studied the pH dependence of τ_{ADP} and Q_{max} and we determined the kinetics of proton efflux at the start of recovery to obtain a measure of the rate of pH recovery.

Materials and Methods

Subjects

Four male and two female healthy subjects participated in this study. The nature and the risks of the experimental procedures were explained to the subjects and all gave their written informed consent to participate in the study, which was approved by the local Medical Ethical Committee of the Máxima Medical Center, Veldhoven, The Netherlands. Subjects varied in age (mean age: 31 ± 12 years; five subjects in the range of 20-33 years and one subject of 53 years), body mass index (BMI) (mean BMI: 21.1 ± 1.8 kg/cm²; range: 17.9-22.6) and daily activity level, i.e. level of activities during daily living, work and leisure time (e.g. sports). However, none of the subjects was highly trained.

³¹P Magnetic resonance spectroscopy

³¹P MRS of the *M. vastus lateralis* was performed by using a 1.5-Tesla whole-body scanner (Gyrosan S15/ACS, Philips Medical Systems, Best, The Netherlands). Subjects were measured in a supine position. After collecting transversal and sagittal scout images, the magnetic field homogeneity was optimized by localized shimming on the proton signal using the body coil. The ³¹P signals were collected using a 6-cm diameter surface coil placed over the *M. vastus lateralis*. From the dimension of the coil and the size and geometry of a typical upper leg, it was estimated that the majority of the signal in the unlocalized ³¹P MRS measurements originated from the *M. vastus lateralis*, with minimal contaminations from the adjacent *M. rectus femoris* and underlying *M. vastus intermedius*. Data were acquired following a 90° adiabatic excitation pulse with a sweep width of 2 kHz and 1024 data points. Spectra were acquired using a repetition time of 3 s during a rest-exercise-recovery protocol (2 scans/spectrum yielding a time resolution of 6 s, total of 150 spectra/15 min). The first 20 spectra (2 min) were measured at rest, after which the subjects started the exercise (see below). The duration of the exercise varied per subject, but never exceeded 9 min, so that at least 4 min of recovery were recorded.

Exercise protocol inside magnet

All subjects performed a single leg extension exercise in the supine position inside the magnet, which has been shown to be limited to the four muscles of the quadriceps³⁸. The exercise was conducted by rhythmically lifting a lever (resting on the lower leg, proximal of the foot) connected to an ergometer. The upper leg was supported with the hip joint in a 30 degrees ante flexed position and immobilized with two 3 cm wide Velcro® straps. One contraction was performed every 1.5 s acoustically guided by a digital metronome. The initial workload varied per subject and ranged between 7.5 and 12.5 W. This level was maintained for the first min and the workload was then increased by 5 W each min. To achieve different levels of metabolic activation, and hence different degrees of cytosolic acidification, subjects performed exercises of different durations. Each subject performed 10-13 different protocols during 4-9 different sessions in a randomized order, with at least 15 min rest between different protocols within

one session. The position of the ^{31}P surface coil was marked on the leg during the first session and the coil was placed at the same location during the next sessions.

The reproducibility of the ^{31}P MRS measurements was determined in one subject. This subject performed 10 times the same protocol during 5 different sessions. In one other subject, it was tested whether the position of the ^{31}P surface coil on the *M. vastus lateralis*, when varied in the proximal and distal direction, influenced the ^{31}P MRS measurements. For this purpose, the subject performed 5 times the same protocol, with a maximal difference of 15 cm of the position of the ^{31}P surface coil in the proximo-distal direction.

Data analysis

Spectra were fitted in the time domain by using a nonlinear least squares algorithm (AMARES) in the jMRUI software package ³⁹. PCr, P_i and ATP signals were fitted to Lorentzian line shapes. The three ATP peaks were fitted as two doublets and one triplet, with equal amplitudes and line widths and prior knowledge for the J-coupling constant (17 Hz). For the time series, the PCr line width during recovery was constrained to the average PCr line width during recovery (excluding the first 10 data points), obtained from a prior, unconstrained fit.

Absolute concentrations of the phosphorylated metabolites were calculated after correction for partial saturation and assuming that [ATP] is 8.2 mM at rest ¹². Intracellular pH was calculated from the chemical shift difference between the P_i and PCr resonances (δ ; measured in parts per million) using the following formula ⁹:

$$\text{pH} = 6.75 + \log\left(\frac{\delta - 3.27}{5.63 - \delta}\right) \quad [1]$$

The free cytosolic ADP concentration ([ADP]) was calculated from pH and [PCr] using a creatine kinase equilibrium constant (K_{eq}) of $1.66 \times 10^9 \text{ M}^{-1}$ ³⁵ and assuming that 15% of the total creatine is unphosphorylated at rest ³³, using the equation:

$$[\text{ADP}] = \frac{[\text{ATP}][\text{Cr}]}{[\text{PCr}][\text{H}^+]K_{\text{eq}}} \quad [2]$$

Recoveries of PCr and ADP were fitted to mono-exponential functions using Matlab (version 6.1, Mathworks, Natick, Massachusetts, USA). Results are expressed as the metabolite's time constant of recovery, i.e. τ_{PCr} and τ_{ADP} .

Calculation of the initial rate of PCr recovery (V_{PCr}) was based on the PCr recovery rate ($1/\tau_{\text{PCr}}$) and the difference between the resting and end-exercise PCr concentrations (ΔPCr) ⁴⁰:

$$V_{\text{PCr}} = \frac{1}{\tau_{\text{PCr}}} \cdot \Delta\text{PCr} \quad [3]$$

The calculation of the maximum aerobic capacity (Q_{max}) was either based on the ADP-control model ⁴¹, in which V_{PCr} has a hyperbolic dependence on the end-exercise ADP concentration ($[\text{ADP}]_{\text{end}}$) according to Michaelis-Menten kinetics with a K_m of 30 M ⁴⁰:

$$Q_{\text{max-ADP}} = V_{\text{PCr}} \cdot \left(1 + \frac{K_m}{[\text{ADP}]_{\text{end}}} \right) \quad [4]$$

or on a linear approximation of the ADP-control model:

$$Q_{\text{max-lin}} = \frac{1}{\tau_{\text{PCr}}} \cdot [\text{PCr}]_{\text{rest}} \quad [5]$$

which is equivalent to the non-equilibrium thermodynamic control model ^{37, 42}. However, this approximation is only valid when pH changes are small.

The proton efflux rate at the start of recovery was calculated as described by Kemp *et al.* ^{43, 44} from the changes in the PCr concentration and pH during the first 12 s of recovery according to

$$E = (\varphi + m) \frac{\delta[\text{PCr}]}{\delta t} + \beta \frac{\delta\text{pH}}{\delta t} \quad [6]$$

where φ is the amount of protons consumed per mole of PCr hydrolysis ($\varphi = 1/[1 + 10^{(\text{pH}-6.75)}]$ ⁴⁵), m is the amount of protons produced per mole of oxidative ATP synthesis ($m = 0.16/[1 + 10^{(6.1-\text{pH})}]$ ⁴⁶) and β is the cytosolic buffering capacity (20 slykes (i.e. $\text{mmol} \cdot \text{l}^{-1} \cdot \text{pH}^{-1}$) plus the calculated contribution of P_i , which is given by $2.3 \cdot [\text{P}_i] \cdot \varphi(1-\varphi)$ ⁴⁷). The apparent proton efflux rate constant was calculated as $\lambda = E/(-\Delta\text{pH})$, where ΔpH is defined as $\text{pH} - \text{pH}_{\text{rest}}$ ³⁷. Both the proton efflux rate E and the apparent proton efflux rate constant λ at the start of recovery depend on the end-exercise pH (pH_{end}) ⁴⁴ and therefore only the data sets with a pH_{end} between 6.6 and 6.8 were used to calculate an average value for E

and λ for each subject. These data sets with rather low pH_{end} values were chosen for two reasons: (1) they had a greater PCr depletion and therefore a larger PCr resynthesis rate and proton production rate at the start of recovery and (2) they had a greater increase in P_i and therefore a better visible P_i peak at the start of recovery, which is important for an accurate and precise pH determination.

Statistics

All data are expressed as means \pm standard deviation (SD). Reproducibility is reported as the coefficient of variation ($\text{CV} = (\text{SD}/\text{mean}) \times 100$). Linear regression analyses were performed using the SPSS 14.0 software package (SPSS Inc, Chicago, IL, USA). Level of statistical significance was set at $p < 0.05$.

Table 1. Reproducibility of ^{31}P MRS recovery parameters.

		τ_{PCr} (s)	τ_{ADP} (s)	V_{PCr} (mM/s)	$Q_{\text{max-ADP}}$ (mM/s)	$Q_{\text{max-lin}}$ (mM/s)
all (n = 10)	mean	29.4	11.8	0.86	1.17	1.38
	SD	3.3	0.8	0.09	0.10	0.14
	CV (%)	11.3	6.7	10.7	8.4	10.4
$\text{pH}_{\text{end}} > 6.9$ (n = 7)	mean	27.9	12.2	0.88	1.18	1.43
	SD	1.9	0.5	0.09	0.09	0.12
	CV (%)	6.9	4.0	9.8	7.9	8.4

τ_{PCr} , phosphocreatine (PCr) recovery time constant; τ_{ADP} , adenosine diphosphate (ADP) recovery time constant; V_{PCr} , initial rate of PCr recovery based on the PCr recovery rate ($1/\tau_{\text{PCr}}$) and the difference between the resting and end-exercise PCr concentrations; $Q_{\text{max-ADP}}$, maximum rate of oxidative ATP synthesis calculated according to the ADP-control model, i.e. based on V_{PCr} related to end-exercise ADP concentration and an assumed K_m of $30 \mu\text{M}$; $Q_{\text{max-lin}}$, maximum rate of oxidative ATP synthesis calculated by a linear approximation of the ADP-control model. Coefficient of variation (CV) was calculated as $(\text{SD}/\text{mean}) \times 100$. The upper 3 rows are the results from all 10 data sets. The lower 3 rows are the results from the 7 data sets with an end-exercise pH (pH_{end}) higher than 6.9.

Results

Reproducibility

Figure 1 shows typical examples of ^{31}P MR spectra from a subject's *vastus lateralis* muscle at rest, at the end of exercise and at two time points during recovery. For the same data set, PCr and ADP concentrations are plotted as a function of time in Figure 2. At the end of recovery, both PCr and ADP concentrations are identical to the resting condition. Figure 2 also illustrates the mono-exponential fits of the PCr and ADP recoveries. The reproducibility of the

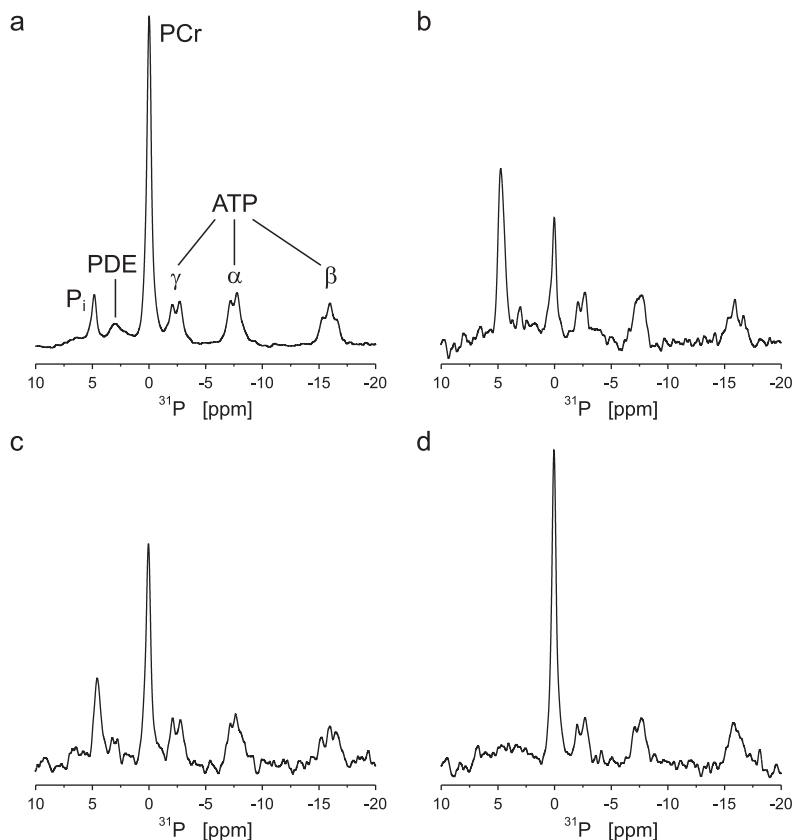


Figure 1 Typical *M. vastus lateralis* ^{31}P MR spectra for one subject at rest (panel a, number of scans = 60), at the end of exercise (panel b, number of scans = 2) and at 15 and 93 s of recovery (panels c and d, respectively, number of scans = 2). Spectra were processed with 5 Hz line broadening. Pi: inorganic phosphate, PDE: phosphodiester, PCr: phosphocreatine, and α , β and γ indicate the three phosphate groups of ATP. For this subject the PCr depletion at the end of exercise (panel b) was 65% and the corresponding pH_{end} was 6.93. Note that the Pi signal is not discernible in the spectrum in panel d.

determination of ^{31}P MRS parameters for mitochondrial function, i.e. τ_{PCr} , τ_{ADP} , V_{PCr} , $Q_{\text{max-ADP}}$ and $Q_{\text{max-lin}}$, was determined in one subject and the results are shown in Table 1. When including all 10 measurements, the CV ranged from 6.7% for τ_{ADP} to 11.3% for τ_{PCr} . However, even though the exercise protocol was identical for all 10 measurements, there was still some variation in pH_{end} . For 7 of the 10 data sets pH_{end} ranged between 6.91 and 6.96 (mean pH_{end} : 6.93 ± 0.02), while for 3 data sets pH_{end} was lower than 6.9, i.e. 6.87, 6.84 and 6.81, respectively. When only the 7 data sets with pH_{end} above 6.9 were considered, the CV for τ_{PCr} became 6.9%, which is comparable to other studies^{19, 34}. No systematic differences were observed for the two measurements performed during one session.

In one other subject, it was tested whether the position of the ^{31}P surface coil on the *M. vastus lateralis*, when varied in the proximal and distal direction, influenced the ^{31}P MRS measurements. For the 5 measurements, with a maximal difference of 15 cm of the position of the ^{31}P surface coil in the proximo-distal direction, the CVs for τ_{PCr} and τ_{ADP} were 4.5 and 3.0%, respectively. Therefore, it can be concluded that within a certain range the exact positioning of

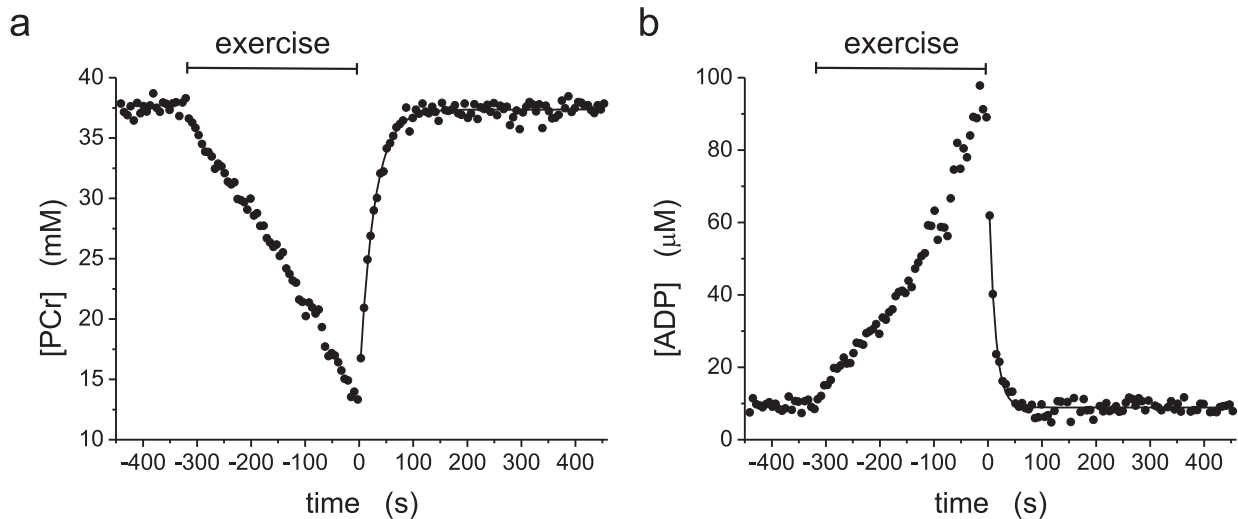


Figure 2 PCr (panel a) and ADP (panel b) concentrations during rest, exercise and recovery obtained from the data set that was also used in Figure 1 with a time resolution of 6 s. The recoveries of PCr and ADP (starting at $t = 0$) were fitted to mono-exponential functions (solid lines). The time constants for PCr and ADP recovery were 26.9 and 11.8 s, respectively.

the ^{31}P surface coil does not affect the parameters for mitochondrial function and that regional variations in fiber type composition in the proximo-distal direction of the *M. vastus lateralis* are probably small.

End-exercise status

To achieve different levels of metabolic activation, and hence different degrees of cytosolic acidification, subjects performed 10-13 exercises of different durations. For all measurements, homeostasis of ATP was maintained throughout the exercise protocol. None of the subjects showed a split P_i peak during exercise or recovery and therefore acidosis was not extremely heterogeneous in the measured muscle tissue. The ranges of pH_{end} , ΔPCr and $[\text{ADP}]_{\text{end}}$ reached for each subject are summarized in Table 2. The smallest range in pH_{end} values was obtained for subject 4 and covered 0.3 pH units, while the largest range was obtained for subject 2 and covered 0.6 pH units. For subject 5, one protocol resulted in a rather low $[\text{ADP}]_{\text{end}}$ of 25 μM . For all other measurements, $[\text{ADP}]_{\text{end}}$ was well above the accepted K_m value of 30 μM for oxidative ATP synthesis. In the two top rows of Figure 3, ΔPCr and $[\text{ADP}]_{\text{end}}$ are plotted as a function of pH_{end} , from which it can be seen that ΔPCr was negatively correlated with pH_{end} for all three subjects, whereas $[\text{ADP}]_{\text{end}}$ was not significantly correlated with pH_{end} .

Recovery

Recoveries of PCr and ADP could be satisfactorily described by mono-exponential functions, also at low pH_{end} values (average R^2 values for the mono-exponential fits were 0.971 ± 0.025 and 0.915 ± 0.063 for PCr and ADP recovery data, respectively). Table 3 lists the average values for τ_{PCr} , τ_{ADP} , V_{PCr} , $Q_{\text{max-ADP}}$ and $Q_{\text{max-lin}}$ for all subjects. For each subject, there was a strong negative linear relationship between τ_{PCr} and pH_{end} . The third row of Figure 3 shows the correlation between τ_{PCr} and pH_{end} for three of the subjects. Around $\text{pH}_{\text{end}} 7$, τ_{PCr} was very similar for these three subjects, but at lower pH_{end} values τ_{PCr} differed. Therefore, the pH

dependence of τ_{PCr} differed, with subject 1 showing the weakest pH dependence and subject 3 showing the strongest pH dependence. The results of the linear regression analyses for all subjects are shown in Table 4. The slope of the relation between τ_{PCr} and pH_{end} ranged from -33.0 to -75.3 s per pH unit. For five of the six subjects, τ_{PCr} at pH_{end} 7 calculated from the linear relation between τ_{PCr} at pH_{end} was very similar. Only the older subject, subject 6, had a longer τ_{PCr} at pH_{end} 7.

The post-exercise ADP recovery was faster than the PCr recovery (Table 3). For subjects 1 - 5, τ_{ADP} was again very similar, while subject 6 had a longer τ_{ADP} (Table 3). In the fourth row of Figure 3, τ_{ADP} is plotted against pH_{end} for three of the subjects. For subjects 2, 3 and 5, τ_{ADP} did not depend on pH_{end} (Table 4). However, for subjects 1, 4 and 6, τ_{ADP} was significantly positively correlated with pH_{end} (Table 4).

V_{PCr} is a measure of the actual mitochondrial ATP synthesis rate and according to the ADP-control model ⁴¹, V_{PCr} has a hyperbolic dependence on $[\text{ADP}]_{\text{end}}$ (Eq. [4]). For all but one measurement, $[\text{ADP}]_{\text{end}}$ was well above the accepted K_m value of 30 μM for oxidative ATP synthesis and therefore differences in $[\text{ADP}]_{\text{end}}$ will not have a large effect on V_{PCr} . From Figure 3, it can be seen that ΔPCr and τ_{PCr} vary in the same direction as a function of pH_{end} . As a consequence, for five of the subjects, V_{PCr} was independent of pH_{end} (Table 4). Only for subject 2, a significant positive correlation between V_{PCr} and pH_{end} was found (Figure 3, Table 4).

Table 2 Ranges of pH_{end} , ΔPCr and $[\text{ADP}]_{\text{end}}$ reached at the end of exercise.

subject	pH_{end}	ΔPCr (mM)	$[\text{ADP}]_{\text{end}}$ (μM)
1	6.56 - 7.02	13.6 - 28.1	48.2 - 143.4
2	6.41 - 6.99	17.2 - 33.2	55.3 - 123.2
3	6.53 - 7.02	17.3 - 34.5	39.5 - 174.2
4	6.65 - 6.96	17.4 - 33.7	45.9 - 128.3
5	6.50 - 6.95	9.8 - 29.9	25.1 - 149.1
6	6.63 - 7.01	21.1 - 39.1	59.6 - 192.3

pH_{end} : intracellular muscle pH at the end of exercise, ΔPCr : difference between the resting and end-exercise PCr concentrations, $[\text{ADP}]_{\text{end}}$: ADP concentration at the end of exercise.

The average values of $Q_{\text{max-ADP}}$ were smaller than the average values of $Q_{\text{max-lin}}$ (Table 3). In accordance with the longer τ_{PCr} (at pH 7) and τ_{ADP} , subject 6 also showed smaller values for $Q_{\text{max-ADP}}$ and $Q_{\text{max-lin}}$ compared to the other subjects (Table 3). $Q_{\text{max-ADP}}$ showed significant positive correlations with pH_{end} for three of the six subjects (Figure 3, Table 4). These are the subjects with the largest correlation coefficients for V_{PCr} versus pH_{end} . For each subject, there was a strong positive linear relationship between $Q_{\text{max-lin}}$ and pH_{end} (Figure 3, Table 4).

For subject 5, the proton efflux rate E and the apparent proton efflux rate constant λ could not be determined. For the other five subjects, the mean total cytosolic buffering capacity β at the start of recovery amounted 35 ± 1 slykes, the mean proton efflux rate E was 16 ± 3 mM/min and the mean apparent proton efflux rate constant λ was 38 ± 6 mM/(min \cdot pH unit). In Figures 4a and 4b, the slope of the relation between τ_{PCr} and pH_{end} is plotted against E and λ ,

respectively. The slope of the relation between τ_{PCr} and pH_{end} was positively correlated with both E ($R = 0.91$, $p = 0.03$) and λ ($R = 0.96$, $p = 0.01$).

Table 3 Averages of ^{31}P MRS recovery parameters for the different exercise protocols.

subject	τ_{PCr} (s)	τ_{ADP} (s)	V_{PCr} (mM/s)	$Q_{\text{max-ADP}}$ (mM/s)	$Q_{\text{max-lin}}$ (mM/s)
1	32.7 ± 6.3	11.1 ± 2.5	0.71 ± 0.12	0.96 ± 0.08	1.10 ± 0.22
2	38.4 ± 10.8	10.4 ± 1.3	0.70 ± 0.09	0.97 ± 0.14	1.06 ± 0.29
3	44.4 ± 12.0	12.3 ± 1.4	0.60 ± 0.11	0.83 ± 0.16	0.94 ± 0.31
4	37.9 ± 6.0	12.6 ± 1.7	0.66 ± 0.07	0.90 ± 0.07	1.00 ± 0.15
5	35.0 ± 4.9	13.0 ± 2.1	0.68 ± 0.15	0.97 ± 0.13	1.12 ± 0.18
6	51.1 ± 9.6	16.1 ± 2.5	0.56 ± 0.05	0.76 ± 0.07	0.86 ± 0.18

Data are presented as mean ± SD

Discussion

Several studies have shown that cytosolic pH has a strong influence on the kinetics of PCr recovery^{1, 12-21}. In order to establish a relationship between e.g. τ_{PCr} and pH_{end} , one or a few data points of different subjects have generally been grouped. However, this procedure will not reveal intersubject differences in the pH dependence of τ_{PCr} and, moreover, the effect of pH on PCr recovery might be exaggerated by a systematic bias. We investigated the effect of acidosis on PCr recovery on a subject-by-subject basis by collecting 10-13 data sets per subject, using protocols of different intensity and duration resulting in different degrees of cytosolic acidification. We showed that for each subject there is a strong negative linear relationship between τ_{PCr} and pH_{end} , but that the slopes are different for different subjects, ranging from -33.0 to -75.3 s per pH unit. This implies that no general formula can be applied to correct τ_{PCr} for differences in pH_{end} . Qualitatively and quantitatively, the results obtained when the data of the different subjects are grouped (Table 4; last column) are in good agreement with data from the literature on the pH dependence of PCr recovery kinetics measured in different muscle types, revealing linear relationships between τ_{PCr} and pH_{end} (or the minimum pH reached during recovery; pH_{min}) with slopes ranging from roughly -20 to -90 s per pH unit^{14, 16-21}.

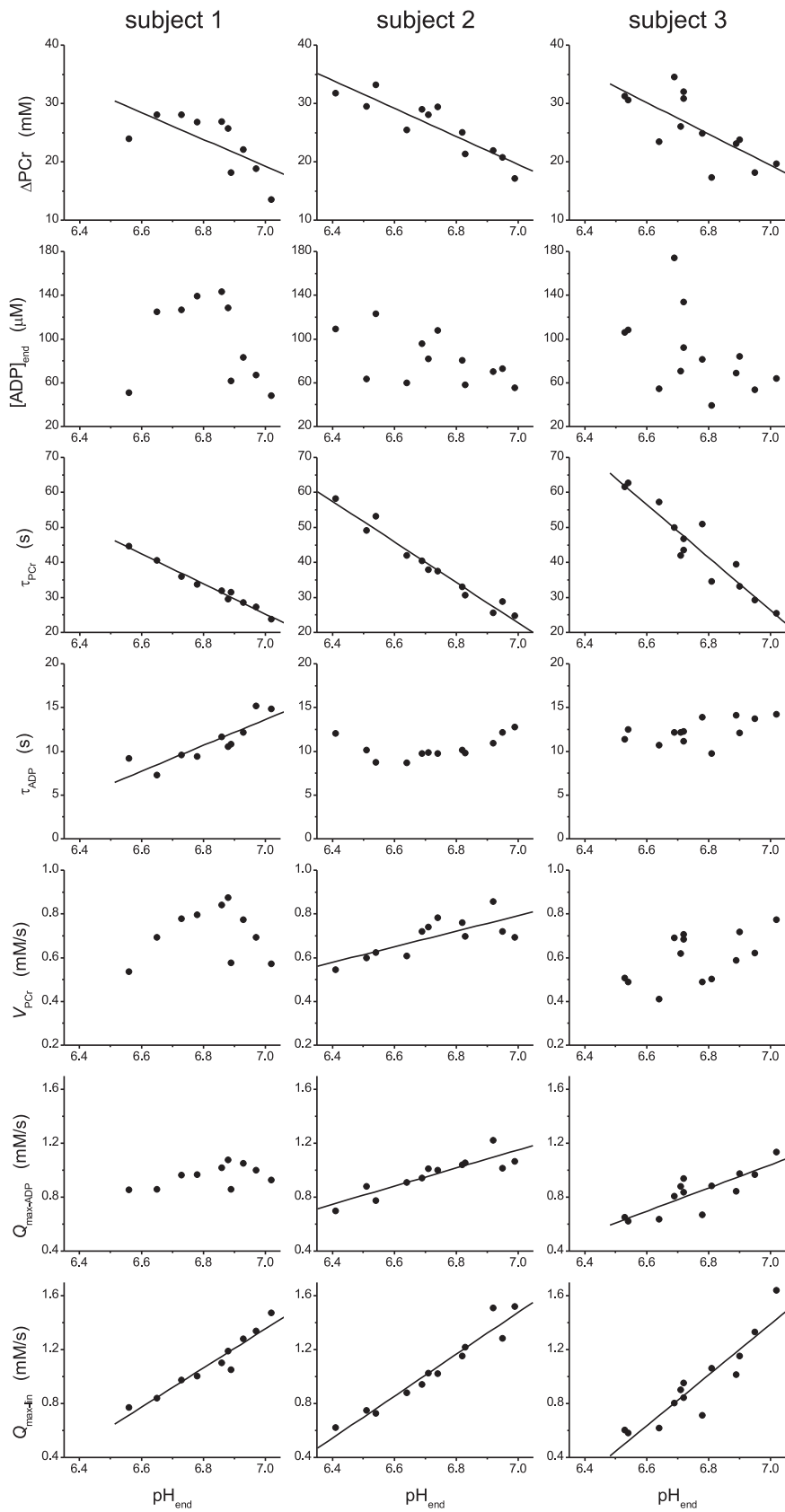


Figure 3 ΔPCr , $[\text{ADP}]_{\text{end}}$, τ_{PCr} , τ_{ADP} , V_{PCr} , $Q_{\text{max-ADP}}$ and $Q_{\text{max-lin}}$ plotted as a function of pH_{end} for three subjects. Results of the linear regression analysis (solid lines) are shown for significant correlations ($p < 0.05$).

Table 4 Correlation of ^{31}P MRS recovery parameters with end-exercise pH.

		subject 1 (n = 10)	subject 2 (n = 12)	subject 3 (n = 13)	subject 4 (n = 12)	subject 5 (n = 13)	subject 6 (n = 11)	grouped data (n = 71)
τ_{PCr}	R	-0.99*	-0.98*	-0.94*	-0.87*	-0.85*	-0.94*	-0.74*
	slope (s/U)	-42.9	-57.9	-75.3	-56.2	-33.0	-62.9	-54.1
	SE	2.1	3.5	8.1	9.9	6.3	7.7	6.0
	τ_{PCr} at pH 7 (s)	25.3	22.8	26.4	26.8	28.7	39.6	28.6
τ_{ADP}	R	0.86*	0.40	0.53	0.78*	0.13	0.89*	0.41*
	slope (s/U)	14.8	2.9	4.9	14.2	2.3	15.8	8.0
	SE	3.1	2.1	2.4	3.6	5.4	2.6	2.1
V_{PCr}	R	0.13	0.74*	0.55	-0.26	0.06	0.47	0.24*
	slope (mM/s/U)	0.11	0.36	0.41	-0.20	0.07	0.16	0.20
	SE	0.29	0.10	0.19	0.24	0.37	0.10	0.10
$Q_{\text{max-ADP}}$	R	0.52	0.88*	0.83*	0.40	0.14	0.79*	0.47*
	slope (mM/s/U)	0.30	0.67	0.86	0.31	0.14	0.37	0.46
	SE	0.17	0.12	0.18	0.23	0.31	0.10	0.10
$Q_{\text{max-lin}}$	R	0.96*	0.97*	0.92*	0.85*	0.85*	0.95*	0.83*
	slope (mM/s/U)	1.45	1.56	1.88	1.41	1.24	1.18	1.41
	SE	0.16	0.13	0.25	0.27	0.23	0.13	0.12

R: correlation coefficient determined from a linear regression analysis, * $p < 0.01$, slope values (\pm standard error, SE) representing the steepness of the correlation, U: pH unit, τ_{PCr} at pH 7 was obtained from the linear relation between τ_{PCr} and end-exercise pH.

The slower PCr recovery in the presence of intracellular acidosis could reflect a decreased mitochondrial respiration at low pH. The mechanisms by which protons affect oxidative phosphorylation include (1) a direct effect on the mitochondria, i.e. a decreased oxidative capacity at low pH, or (2) an indirect effect, because a low pH decreases the ADP concentration through the constraints set by the creatine kinase (CK) equilibrium resulting in a lower signal for mitochondrial ATP supply. There are conflicting data about the effects of low pH on respiratory rates. Hypercapnic acidosis has been found to reduce the aerobic capacity of perfused cat soleus muscle by a factor of three²². However, it is not clear whether this change was caused by acidosis per se or by some other effect of hypercapnic perfusion. Moreover, it has been shown that in skinned fibers from rat soleus muscle the rate of respiration is

impaired by lactic acidosis and elevated concentrations of P_i ²³. Jubrias *et al.* showed that intracellular acidosis inhibits oxidative phosphorylation *in vivo* in hand and lower limb muscle and their results suggest that pH has a direct effect on mitochondrial function, because oxidative flux did not increase during exercise that generated acidosis despite a significant rise in [ADP] ²⁴. In contrast, *in vitro* studies on isolated mitochondria suggest that the effect of acidosis on oxidative phosphorylation is very small ^{25-27, 29} and not significant in the range pH 6.5-7.5 ²⁵. Likewise, an *in vivo* study of electrically stimulated rabbit muscle showed that CO₂-induced acidosis (to pH 6.7) did not decrease the maximum aerobic capacity ²⁸. Moreover, in human medial gastrocnemius muscle aerobic ATP synthesis rates were not lowered by acidosis ¹⁹. Other reports have suggested that mitochondrial respiration is even more effective at low pH ^{30, 31}.

PCr recovery in the presence of intracellular acidosis could also be slowed down due to factors downstream of oxidative phosphorylation, consistent with the observation that the recovery of oxyhemoglobin saturation measured by near-infrared spectroscopy is not affected by acidosis ¹⁵. Ion pumping reactions also require ATP and therefore not all the ATP that is synthesized oxidatively during recovery is available for the CK reaction. At low pH the amount of ATP that is shuttled to cellular ion pumps might be increased ^{21, 34} in order to reestablish pH homeostasis. It has been reported that ion pumping reactions can consume about 43% of the total ATP produced ^{32, 33}. The slow PCr recovery at low pH has also been attributed to a pH-dependent shift in the CK equilibrium. The CK equilibrium constant (K_{eq}) depends on proton and metal ion concentrations ³⁵. Iotti *et al.* showed that at the end of muscular exercise, K_{eq} can increase even more than threefold compared to rest, due to a decrease in pH and an increase in the free Mg^{2+} concentration ³⁶. Therefore, net PCr resynthesis throughout recovery behaves as a function of both intracellular pH and net ATP flux ^{1, 19}. This was confirmed by a model for ATP production (according to the ADP-control model; see Eq. [4]) and pH recovery, which reproduced the main features of recovery from exercise, including the feature that PCr recovery is slowed when the pH is low ⁴⁸. Finally, with the incremental exercise protocol that we used, part of the pH dependence of PCr recovery could originate from selective fiber type recruitment, i.e. recruitment of mainly oxidative type I fibers (with short τ_{PCr}) during the low exercise intensities with a high pH_{end} and recruitment of relatively more type II fibers (with long τ_{PCr}) during the higher exercise intensities with a low pH_{end} .

The observed intersubject differences in the pH dependence of τ_{PCr} are likely to reflect differences in the rate of pH recovery. Unfortunately, the recovery of pH could not be investigated, because the P_i peak consistently disappeared within the noise after about 1 min of recovery (Figure 1d) and for the exercises at higher intensities was not fully recovered by the end of the time series. This phenomenon has been reported before in the literature ^{9, 14, 17, 20, 34, 49} and has been attributed to sequestering of P_i inside the mitochondria where it becomes "NMR-invisible" ^{1, 50}, or trapping of P_i into the glycogenolytic pathway during exercise leading to phosphomonoester (PME) production ⁵¹. The recovery of pH is much slower than PCr recovery ^{1, 17, 19, 52} and therefore it was attempted to increase the signal-to-noise ratio of the P_i peak by the summation of spectra during the recovery phase. However, even when 4 spectra were added, yielding a time resolution of 24 s, the position of the P_i peak could not be accurately determined.

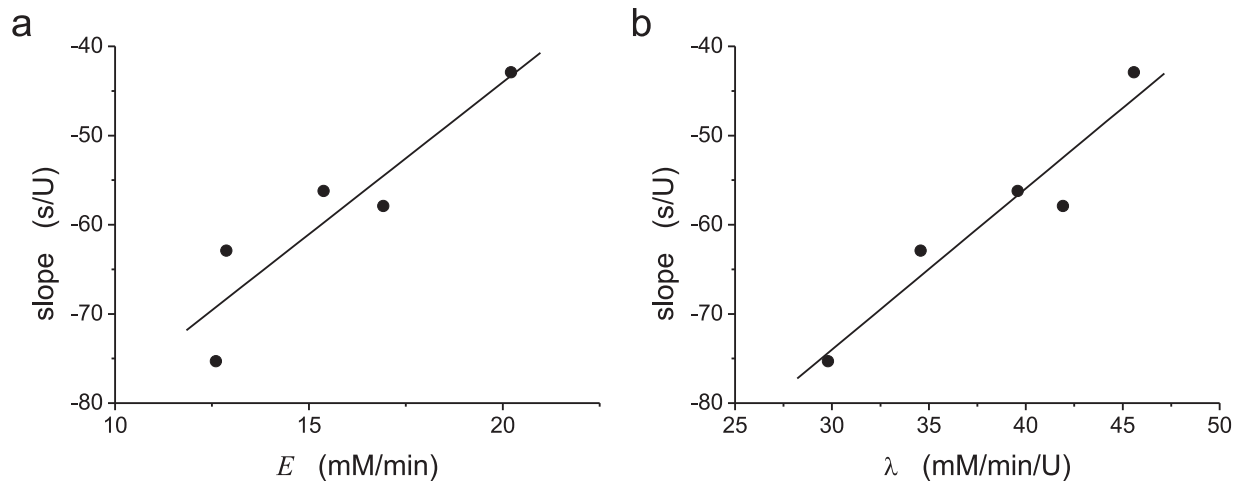


Figure 4 Correlations between the slope of the relation between τ_{PCr} and pH_{end} and (panel a) the proton efflux rate E ($R = 0.91$, $p = 0.03$) and (panel b) the apparent proton efflux rate constant λ ($R = 0.96$, $p = 0.01$) for five of the six subjects.

The recovery of cytosolic pH to the resting value is a function of net proton efflux⁹. Several mechanisms are responsible for proton efflux, such as sodium/proton exchange, sodium-dependent chloride/bicarbonate exchange, efflux of undissociated lactic acid, and outward proton/lactate co-transport. The change in proton concentration in the cell can be calculated from the change in pH multiplied by the cytosolic buffer capacity and equals the proton efflux rate minus the rate of proton generation by PCr resynthesis and aerobic ATP production⁴³. We calculated proton efflux rates E and apparent proton efflux rate constants λ at the start of recovery. Both E and λ are pH dependent⁴⁴ and therefore only the data sets with a pH_{end} between 6.6 and 6.8 were used to calculate an average value for E and λ for each subject. The mean values that we found for the total cytosolic buffering capacity β , E and λ correspond with values reported by Kemp *et al.*, calculated for a similar pH_{end} range with exactly the same formulas⁴⁴. The slope of the relation between τ_{PCr} and pH_{end} was positively correlated with both E ($R = 0.91$, $p = 0.03$) and λ ($R = 0.96$, $p = 0.01$), indicating that subjects with a smaller pH dependence of τ_{PCr} have a higher proton efflux rate, most likely as a result of a better blood flow due to e.g. an increased capillary density possibly related to the subject's fiber type composition. Higher proton efflux rates will lead to faster pH recovery and therefore the observed correlations support our hypothesis that the intersubject differences in the pH dependence of τ_{PCr} are caused by differences in the rate of pH recovery.

To overcome the problems of pH determination during recovery associated with the transient loss of P_i signal, Chen *et al.* modeled the pH recovery based on the CK equilibrium by considering the transition from exercise to recovery as a step function input⁵³. The entire pH recovery was characterized by calculating the time required for pH recovery (t_{pHrec}) and a strong linear correlation was observed between t_{pHrec} and the half-time of PCr recovery in normal subjects (average $pH_{end} \sim 6.7$). This strong correlation corroborates the link between the PCr recovery rate and the overall pH recovery rate. Moreover, the large variation in t_{pHrec} within normal subjects (t_{pHrec} ranged from about 2 - 18 min) implies that differences in the pH dependence of τ_{PCr} can be significant, as we demonstrated in the present study. Certain

disorders, e.g. hypertension and mitochondrial myopathy⁴³ and dermatomyositis and polymyositis⁵⁴, are associated with altered proton efflux from muscle fibers, which will affect the rate of pH recovery. Therefore, when comparing PCr recovery measurements between patients and controls, differences in proton efflux rates or rates of pH recovery should be considered, as these might lead to systematic changes of τ_{PCr} , in particular when pH_{end} is low.

As an alternative to τ_{PCr} , the kinetics of ADP recovery can be used to assess oxidative capacity. As [ADP] is the principal error signal in the feedback loop controlling mitochondrial oxidation, ADP recovery is one of the most sensitive MRS indices of mitochondrial function³⁷. It has been shown that in contrast to τ_{PCr} , τ_{ADP} is independent of end-exercise pH^{1, 2, 17, 18, 20}, which was confirmed by a theoretical model⁴⁸. We investigated the pH dependence of τ_{ADP} for each subject. For 3 subjects τ_{ADP} was not significantly correlated with pH_{end} , while for the 3 other subjects τ_{ADP} was positively correlated with pH_{end} , i.e. ADP recovery became faster at low pH. This phenomenon was also observed by Larson-Meyer *et al.*³⁴, but we doubt that it has any physiological meaning. It has been reported that the recovery of ADP is not always mono-exponential and that [ADP] can decrease below the resting concentration during the second min of recovery¹⁷. The size and duration of this so-called ADP undershoot was found to correlate with pH_{min} ¹⁷. We also observed an ADP undershoot in some of our data sets. However, it was difficult to quantify this effect, as the undershoot occurs in the period during which the P_i peak becomes invisible, resulting in a less reliable pH estimation. When the ADP recovery data with an undershoot are fitted with a mono-exponential function, the time constant will be underestimated⁵⁵ and this could explain the positive correlation between τ_{ADP} and pH_{end} . Furthermore, it was assumed that the CK equilibrium constant was not affected by the different metabolic conditions present after exercise and therefore changes in pH and the free Mg^{2+} concentration⁵⁶, in particular for the exercises at higher intensities, are sources of error for the [ADP] calculation which might lead to deviations in τ_{ADP} .

V_{PCr} is a measure of the actual mitochondrial ATP synthesis rate and therefore does not represent an absolute measure of oxidative capacity. Still, a number of studies have reported that V_{PCr} is independent of pH^{18, 19, 21}. This is a consequence of $[\text{ADP}]_{\text{end}}$ being either similar for different degrees of acidification²¹ or well above the accepted K_m value of 30 μM for oxidative ATP synthesis^{18, 19}. The latter was also the case for most of our measurements and for five of the subjects V_{PCr} was independent of pH_{end} . V_{PCr} can be calculated from the product of $1/\tau_{\text{PCr}}$ and ΔPCr (Eq. [3])^{18, 21, 40}, like in our study, or V_{PCr} can be measured directly from the first data points (typically 10-14 s)^{19, 20, 34}. Boska *et al.* applied both methods and found good correlations between calculated and measured V_{PCr} in controls ($R = 0.753$) and patients with peripheral vascular occlusive disease ($R = 0.646$)²⁰. However, Walter *et al.* observed that at low pH ($\text{pH}_{\text{end}} 6.45$) the calculated V_{PCr} was about two times smaller than the measured V_{PCr} ¹⁹. Under conditions in which intracellular pH is decreased, any model that relies on τ_{PCr} is no longer valid and V_{PCr} should be measured directly from the initial phase of recovery. However, this method is extremely sensitive to sampling rate and signal-to-noise values¹⁹. Moreover, it has been shown that V_{PCr} measured from the first 10 s of recovery is underestimated by up to 56% and that a 1-2 s time window is needed for the determination of V_{PCr} , requiring very high time-resolution ³¹P MRS data⁵⁷. The fact that V_{PCr} calculated from τ_{PCr} was still independent of pH_{end} in five of our subjects results from the fact that $1/\tau_{\text{PCr}}$ and ΔPCr vary in opposite

directions as a function of pH_{end} (Figure 3). For the sixth subject changes in these two quantities apparently did not compensate each other completely.

In the literature, $Q_{\text{max-ADP}}$ has been found to be independent of pH^{18, 21}, although in the study of Walter *et al.* only $Q_{\text{max-ADP}}$ based on the measured V_{PCr} was pH independent¹⁹. In our study, $Q_{\text{max-ADP}}$ was based on the calculated V_{PCr} and $[\text{ADP}]_{\text{end}}$ (Eq. [4]). Although V_{PCr} and $[\text{ADP}]_{\text{end}}$ were not significantly correlated with pH_{end} (except for one subject), these parameters tend to vary in opposite directions as a function of pH_{end} (Figure 3), resulting in significant positive correlations between $Q_{\text{max-ADP}}$ and pH_{end} for three of the six subjects. For each subject, there was a strong positive linear relationship between $Q_{\text{max-lin}}$ and pH_{end} . $Q_{\text{max-lin}}$ was calculated as the inverse of τ_{PCr} multiplied by $[\text{PCr}]_{\text{rest}}$ (Eq. [5]). Within one subject, $[\text{PCr}]_{\text{rest}}$ was more or less constant within the time span of the study and therefore $Q_{\text{max-lin}}$ was equivalent to the inverse of τ_{PCr} , showing an equally strong relationship with pH_{end} . The slopes of the relation between $Q_{\text{max-ADP}}$ and pH_{end} were much smaller than for $Q_{\text{max-lin}}$ and thus at low pH the error is smaller for $Q_{\text{max-ADP}}$. However, in accordance with Walter *et al.*¹⁹, our data show that none of the models that rely on τ_{PCr} are reliable to predict Q_{max} in the presence of intracellular acidosis¹⁹.

In conclusion, intracellular acidosis slowed PCr recovery and the pH dependence of τ_{PCr} differed among subjects, ranging from -33.0 to -75.3 s per pH unit. The effect of acidosis on PCr recovery kinetics after exercise correlated with the kinetics of proton efflux at the start of recovery, strongly indicating that the intersubject differences in the pH dependence of τ_{PCr} reflect differences in the rate of pH recovery. Our study implies that simply correcting τ_{PCr} for end-exercise pH using a general formula is not adequate, in particular when comparing patients and controls, as certain disorders are characterized by altered proton efflux from muscle fibers. Also, matching for end-exercise pH is not sufficient when subject groups systematically differ in proton efflux kinetics. Therefore, τ_{PCr} can only be used as a measure of mitochondrial function when end-exercise pH is close to resting values. Avoiding a decrease in intracellular pH along with a sufficient drop in PCr to model PCr recovery may however be difficult in untrained subjects or patients¹⁹. An exercise protocol that progressively increases work, like we used in this study, has been reported to be successful in decreasing PCr without severe acidification as opposed to sustained-load exercise^{19, 24}. Indeed, we obtained data sets with pH_{end} close to 7 with a drop in PCr of roughly 50%. Alternatively, one could use an exercise protocol of short duration (9 s) with very rapid contractions, which has the advantage that it is believed to simultaneously recruit all fibers¹⁹, or a gated protocol in which the acquisition is gated to contractions of short duration without significant muscle acidification that are repeated in a steady state for as many times as necessary to obtain the desired signal-to-noise ratio⁵⁸. The kinetics of ADP recovery is independent of end-exercise pH. Disadvantages of using τ_{ADP} as a measure of mitochondrial function are the complex time-dependent undershoot of ADP during recovery and the assumptions that have to be made to calculate $[\text{ADP}]$ ¹⁷. Q_{max} can only be used when based on V_{PCr} directly measured from the initial recovery data points. However, the reproducibility of the latter parameter is much lower than for τ_{PCr} and τ_{ADP} ¹⁹.

Acknowledgement

We are very grateful to Jan van Ooyen and Peter Coolen for their continuing support in maintaining the MR scanner. We also like to express our appreciation to the research volunteers who participated in this study.

References

1. Arnold, D.L., Matthews, P.M. & Radda, G.K. *Magn Reson Med* **1**, 307-315 (1984).
2. Arnold, D.L., Taylor, D.J. & Radda, G.K. *Ann Neurol* **18**, 189-196 (1985).
3. Kemp, G.J. et al. *NMR Biomed* **6**, 302-310 (1993).
4. Kent-Braun, J.A., Miller, R.G. & Weiner, M.W. *Radiol Clin North Am* **32**, 313-335 (1994).
5. Radda, G.K. et al. *Biochim Biophys Acta* **1271**, 15-19 (1995).
6. Mattei, J.P., Bendahan, D. & Cozzzone, P. *Reumatismo* **56**, 9-14 (2004).
7. Chance, B. et al. *NMR Biomed* **19**, 904-926 (2006).
8. Sahlin, K. *Acta Physiol Scand Suppl* **455**, 1-56 (1978).
9. Taylor, D.J. et al. *Mol Biol Med* **1**, 77-94 (1983).
10. Quistorff, B., Johansen, L. & Sahlin, K. *Biochem J* **291 (Pt 3)**, 681-686 (1993).
11. Schrauwen-Hinderling, V.B. et al. *Diabetologia* **50**, 113-120 (2007).
12. Taylor, D.J. et al. *Magn Reson Med* **3**, 44-54 (1986).
13. Bendahan, D. et al. *FEBS Lett* **272**, 155-158 (1990).
14. Iotti, S. et al. *NMR Biomed* **6**, 248-253 (1993).
15. McCully, K.K. et al. *J Appl Physiol* **77**, 5-10 (1994).
16. Takahashi, H. et al. *Eur J Appl Physiol Occup Physiol* **71**, 396-404 (1995).
17. Argov, Z., De Stefano, N. & Arnold, D.L. *NMR Biomed* **9**, 165-172 (1996).
18. Lodi, R. et al. *Magma* **5**, 165-171 (1997).
19. Walter, G. et al. *Am J Physiol* **272**, C525-534 (1997).
20. Boska, M.D. et al. *Magn Reson Med* **41**, 1145-1151 (1999).
21. Roussel, M. et al. *Biochim Biophys Acta* **1457**, 18-26 (2000).
22. Harkema, S.J. & Meyer, R.A. *Am J Physiol* **272**, C491-500 (1997).
23. Walsh, B. et al. *J Appl Physiol* **92**, 2273-2276 (2002).
24. Jubrias, S.A. et al. *J Physiol* **553**, 589-599 (2003).
25. Chance, B. & Conrad, H. *J Biol Chem* **234**, 1568-1570 (1959).
26. Tobin, R.B., Mackerer, C.R. & Mehlman, M.A. *Am J Physiol* **223**, 83-88 (1972).
27. Mitchelson, K.R. & Hird, F.J. *Am J Physiol* **225**, 1393-1398 (1973).
28. Nioka, S. et al. *J Appl Physiol* **72**, 521-528 (1992).
29. Willis, W.T. & Jackman, M.R. *Med Sci Sports Exerc* **26**, 1347-1353 (1994).
30. Connett, R.J. *Am J Physiol* **254**, R949-959 (1988).
31. Funk, C.I., Clark, A., Jr. & Connett, R.J. *Am J Physiol* **258**, C995-1005 (1990).
32. Baker, A.J. et al. *Am J Physiol* **266**, C825-831 (1994).
33. Boska, M. *Magn Reson Med* **32**, 1-10 (1994).
34. Larson-Meyer, D.E. et al. *NMR Biomed* **13**, 14-27 (2000).
35. Lawson, J.W. & Veech, R.L. *J Biol Chem* **254**, 6528-6537 (1979).
36. Iotti, S. et al. *Biochim Biophys Acta* **1708**, 164-177 (2005).
37. Kemp, G.J. & Radda, G.K. *Magn Reson Q* **10**, 43-63 (1994).
38. Richardson, R.S., Frank, L.R. & Haseler, L.J. *Int J Sports Med* **19**, 182-187 (1998).
39. Vanhamme, L., van den Boogaart, A. & Van Huffel, S. *J Magn Reson* **129**, 35-43 (1997).
40. Kemp, G.J. et al. *Magn Reson Med* **31**, 248-258 (1994).
41. Chance, B. et al. *Proc Natl Acad Sci U S A* **82**, 8384-8388 (1985).
42. Meyer, R.A. *Am J Physiol* **254**, C548-553 (1988).
43. Kemp, G.J. et al. *NMR Biomed* **6**, 73-83 (1993).
44. Kemp, G.J. et al. *Eur J Appl Physiol Occup Physiol* **76**, 462-471 (1997).
45. Wolfe, C.L. et al. *Biochim Biophys Acta* **971**, 9-20 (1988).
46. Mainwood, G.W. & Renaud, J.M. *Can J Physiol Pharmacol* **63**, 403-416 (1985).
47. Roos, A. & Boron, W.F. *Physiol Rev* **61**, 296-434 (1981).
48. Styles, P., Kemp, G.J. & Radda, G.K. *Proceedings of the 11th Annual Meeting of the Society of Magnetic Resonance in Medicine, Berlin, Germany, , p. 2702 (1992).*
49. Rossiter, H.B. et al. *J Appl Physiol* **93**, 2059-2069 (2002).
50. Iotti, S. et al. *Biochem Biophys Res Commun* **176**, 1204-1209 (1991).
51. Bendahan, D. et al. *FEBS Lett* **269**, 402-405 (1990).
52. Walter, G. et al. *J Physiol* **519 Pt 3**, 901-910 (1999).
53. Chen, J.T. et al. *Magn Reson Med* **46**, 870-878 (2001).
54. Cea, G. et al. *Brain* **125**, 1635-1645 (2002).
55. Chen, J.T. et al. *Magn Reson Med* **41**, 926-932 (1999).
56. Iotti, S. et al. *Magn Reson Imaging* **18**, 607-614 (2000).
57. Newcomer, B.R., Boska, M.D. & Hetherington, H.P. *NMR Biomed* **12**, 545-551 (1999).
58. Slade, J.M. et al. *NMR Biomed* **19**, 573-580 (2006).

Chapter 6

Early or advanced stage type 2 diabetes is not accompanied by *in vivo* skeletal muscle mitochondrial dysfunction

Adapted from:

De Feyter H.M., van den broek N.M., Praet S.F.E., Nicolay K., van Loon L.J.C., Prompers J.J.
Early or advanced stage type 2 diabetes is not accompanied by *in vivo* skeletal muscle mitochondrial dysfunction.

Submitted

Abstract

Aims/hypothesis: Several lines of evidence support a potential role of skeletal muscle mitochondrial dysfunction in the pathogenesis of insulin resistance and/or type 2 diabetes. However, it remains to be established whether mitochondrial dysfunction represents either cause or consequence of the disease. We examined *in vivo* skeletal muscle mitochondrial function in early and advanced stages of type 2 diabetes, with the aim to gain insight in the proposed role of mitochondrial dysfunction in the development of insulin resistance and/or type 2 diabetes.

Methods: 11 long-standing, insulin-treated type 2 diabetes patients, 11 subjects with impaired fasting glucose, impaired glucose tolerance and/or recently diagnosed diabetes, and 12 healthy, normoglycaemic controls, matched for age, body composition and similar habitual physical activity levels were studied. *In vivo* mitochondrial function of the vastus lateralis muscle was evaluated from post-exercise phosphocreatine (PCr) recovery kinetics using ^{31}P magnetic resonance spectroscopy (MRS). Intramyocellular lipid (IMCL) content was assessed in the same muscle using single-voxel ^1H MRS.

Results: ^{31}P MRS parameters for mitochondrial function, i.e. PCr and ADP recovery time constants and the maximum aerobic capacity, and IMCL content did not differ between groups.

Conclusions/interpretation: The finding that *in vivo* skeletal muscle oxidative capacity does not differ between long-standing, insulin-treated type 2 diabetes patients, subjects with impaired fasting glucose, impaired glucose tolerance and/or recently diagnosed diabetes, and healthy, normoglycaemic controls suggests that mitochondrial dysfunction does not necessarily represent either cause or consequence of insulin resistance and/or type 2 diabetes.

Introduction

Insulin resistance is an early event in the pathogenesis of type 2 diabetes. However, the exact processes leading to insulin resistance remain unresolved. Excessive lipid storage inside muscle cells has been linked to the development of insulin resistance, as intramyocellular lipid (IMCL) content has been shown to be negatively correlated with whole-body insulin sensitivity^{1, 2}. Several lines of evidence indicate that mitochondrial dysfunction, presumably associated with a reduced capacity to oxidize fatty acids, might lead to IMCL accretion and subsequent development of skeletal muscle insulin resistance³. Data to support the proposed role of skeletal muscle mitochondrial dysfunction in the development of insulin resistance and/or type 2 diabetes have been obtained with various *in vitro* methods, including measurements of oxidative enzyme activities⁴⁻⁷, mRNA and/or protein expression of OXPHOS (oxidative phosphorylation) genes⁸⁻¹¹ as well as mitochondrial content, morphology and respiration^{6, 7, 11, 12}. Furthermore, *in vivo* magnetic resonance spectroscopy (MRS) measurements of basal mitochondrial adenosine triphosphate (ATP) synthesis rates^{13, 14} and post-exercise phosphocreatine (PCr)¹⁵ and adenosine diphosphate (ADP)¹⁶ recovery kinetics also point towards a potential role for mitochondrial dysfunction in the etiology of insulin resistance and/or type 2 diabetes.

Despite the wealth of data suggesting that mitochondrial dysfunction plays a key role in the development and progression of the type 2 diabetes state, Rabøl *et al.*¹⁷ recently concluded that the evidence for an intrinsic functional impairment in mitochondria from type 2 diabetes patients is far from convincing. Environmental factors play an important role in regulating skeletal muscle oxidative capacity, and impairments in oxidative metabolism in type 2 diabetes patients might simply be the result of a sedentary lifestyle^{18, 19}. Furthermore, mitochondrial dysfunction in type 2 diabetes might be secondary to impaired insulin signalling²⁰⁻²² and/or abnormal blood glucose, insulin^{23, 24} and non-esterified fatty acid (NEFA)²² levels. Therefore, the debate continues as to whether mitochondrial dysfunction represents either cause or consequence of insulin resistance and/or type 2 diabetes.

The aim of this study was to assess whether *in vivo* mitochondrial function is impaired in the early and/or overt diabetes state. Therefore, we examined *in vivo* muscle mitochondrial function in 3 groups of subjects representative for different stages in the development of type 2 diabetes: long-standing, insulin-treated type 2 diabetes patients, subjects with impaired fasting glucose, impaired glucose tolerance and/or recently diagnosed diabetes, and healthy, normoglycemic controls, all matched for age and body composition and with low habitual physical activity levels. *In vivo* mitochondrial function was determined from post-exercise PCr recovery kinetics measured with ³¹P MRS, which has been used as an index of mitochondrial function since the early days of *in vivo* MRS²⁵⁻²⁷.

Materials and methods

Subjects

Eleven long-standing, insulin-treated type 2 diabetes patients (T2D), 11 subjects with impaired fasting glucose, impaired glucose tolerance and/or recently diagnosed diabetes (early stage diabetes; ESD) and 12 healthy, normoglycemic controls (normal glucose tolerance; NGT) volunteered to participate in this study. All subjects were male. The T2D patients had been diagnosed with type 2 diabetes for over 5 years, established by a fasting plasma glucose concentration larger than or equal to 7.0 mmol/l at the time of diagnosis as defined by the World Health Organization (WHO) ²⁸. All T2D patients were on exogenous insulin treatment for at least 2 years and had been on a stable regimen of diabetes medication over the last 3 months before being recruited. Patients using thiazolidinediones for less than 6 months were excluded from participation. Except for the T2D patients, all other subjects had no family history of diabetes and underwent a standard oral glucose tolerance test (OGTT) according to WHO criteria ²⁸. Based on the OGTT, glucose tolerance was classified as normal for 12 subjects (NGT group), whereas glycemic control was impaired for 11 subjects (ESD group). Within the ESD group, 5 subjects showed elevated fasting plasma glucose concentrations (fasting glucose ≥ 6.1 and < 7.0 mmol/l, and 2 h glucose < 7.8 mmol/l), 2 subjects had impaired glucose tolerance (fasting glucose < 7.0 mmol/l, and 2 h glucose ≥ 7.8 and < 11.1 mmol/l) and 4 subjects were diagnosed with type 2 diabetes (< 1 month; fasting glucose ≥ 7.0 mmol/l or 2 h glucose ≥ 11.1 mmol/l). None of the subjects in the ESD group used blood glucose lowering medication and all showed glycosylated hemoglobin (HbA_{1c}) contents below 6%.

Subjects using β -blockers for less than 6 months and subjects with impaired liver function, renal failure, severe retinopathy or a history of severe cardiovascular problems were excluded from participation. The nature and the risks of the experimental procedures were explained to the subjects and all gave their written informed consent to participate in the study, which was approved by the local Medical Ethical Committee of the Máxima Medical Center, Veldhoven, The Netherlands. This study is part of a larger project that studies mitochondrial function in chronic metabolic disease ²⁹.

Body composition

Body mass index (BMI) and waist circumference were measured using an analogue weight scale and standard measuring tape. Whole-body fat free mass (FFM) and truncal fat mass were determined using whole-body dual energy X-ray absorptiometry (DXA) (Hologic QDR-4500 Discovery A, software version 12.3:3, Hologic Inc. Bedford, MA, USA).

Habitual physical activity level

Habitual physical activity level was assessed with the Tecumseh and Minnesota Occupational and Leisure Time Activity Questionnaire ³⁰. The activity level was expressed in metabolic equivalents (MET), which is a scale of the energy cost of various physical activities in multiples of the resting metabolic rate.

Whole-body oxygen uptake capacity

Maximal whole-body oxygen uptake capacity (VO_{2peak}) and maximal workload capacity (W_{max}) were measured during an incremental exercise test until exhaustion, performed on a cycle ergometer (Medifit Ergometer, Medifit systems, Maarn, The Netherlands) using a ramp protocol³¹. Gas exchange measurements were performed continuously (Ergostar II, PMS Professional Medical Systems, Basel, Switzerland). Maximal whole-body oxygen uptake capacity was defined as the VO_2 value remaining unchanged or increasing less than $1 \text{ ml}\cdot\text{min}^{-1}\cdot\text{kg}^{-1}$ for 30 s or more despite an increment in workload³². Cardiac function was monitored using a 12-lead electrocardiogram with heart rate being recorded continuously (Polar Electro, Kempele, Finland).

Blood sampling and analyses

Subjects reported at the laboratory at 8.00 a.m. after an overnight fast. After 5-10 min of supine rest, fasting samples of venous blood were collected from an antecubital vein. Subsequently, a standard OGTT was performed for all subjects, except for the T2D patients, and blood samples were collected 2 h after ingestion of the glucose load. Blood plasma samples were collected into EDTA containing tubes and centrifuged for 10 min at 4°C. Aliquots of plasma were frozen immediately in liquid nitrogen and stored at -80°C until further analyses. Plasma concentrations of glucose (Roche, Basel, Switzerland) and NEFA (Wako Chemicals, Neuss, Germany) were analyzed with a COBAS semi-automatic analyzer (Roche). Plasma insulin was determined in duplicate by radioimmunoassay (Linco, St. Charles, MO, USA) for NGT and ESD subjects. Cross sensitivity of exogenously administered insulin with this radioimmunoassay prohibited the detection of endogenously produced insulin in the insulin-treated T2D subjects. Blood HbA_{1c} content was analyzed by high-performance liquid chromatography (Bio-Rad Diamat, Munich, Germany). For the NGT and ESD subjects, the homeostasis model assessment (HOMA) index³³ was calculated.

MRS measurements

MRS measurements were performed with a 1.5-Tesla whole-body scanner (Gyrosan S15/ACS, Philips Medical Systems, Best, The Netherlands) during 2 sessions. On the evening before the first MRS session, subjects received a standardized meal ($40.6 \pm 2.6 \text{ kJ}$ per kg body weight, containing 41 energy% (En%) fat, 15 En% protein, and 44 En% carbohydrate) after which subjects remained fasted and were allowed to drink water only. Subjects traveled by car or public transport and reported at the laboratory at 8.30 a.m., where they received a standardized breakfast. First, ^1H MRS measurements were performed for the quantification of IMCL. After a short break, the ^{31}P MRS protocol was carried out to familiarize the subjects to the in-magnet exercise and to determine the optimal exercise intensity for the second visit. During the second MRS session, scheduled within one week, ^{31}P MRS measurements were performed to assess skeletal muscle mitochondrial function.

¹H MRS

IMCL was measured in the *M. vastus lateralis* with image-guided single-voxel ¹H MRS using the body coil for transmission and a 8-cm diameter surface coil for signal reception. For each subject, 5 voxels with a size of 10×10×15 mm³ were measured at different positions within the *M. vastus lateralis*. The voxels were carefully placed to avoid subcutaneous fat and visible interstitial fat using standard T₁-weighted images. Spectra were recorded with a point resolved spectroscopy (PRESS) sequence (repetition time, 1500 ms; echo time, 35 ms; spectral width, 2000 Hz; number of data points, 2048; 128 averages) using chemical shift selective (CHESS) saturation for water suppression. Unsuppressed water spectra (32 averages) were recorded from the same voxels and used as an internal reference.

¹H MRS data analysis

All spectra were fitted in the time domain by using a nonlinear least squares algorithm (AMARES) in the jMRUI software package³⁴ without further post-processing, except for manual phasing. The unsuppressed water spectrum was phased and fitted to a Lorentzian line shape. The zero-order phase correction from the water spectrum was applied to the corresponding water suppressed spectrum and the total creatine (tCr) CH₃ peak was referenced to 3.02 ppm. In the water suppressed spectrum, peaks from trimethylammonium (TMA) and tCr CH₃, extramyocellular lipid (EMCL) and IMCL CH₂ and EMCL and IMCL CH₃ protons (see Figure 1) were fitted to Gaussian line shapes. The positions and areas of the EMCL and IMCL CH₃ peaks were constrained with respect to the positions and areas of the EMCL and IMCL CH₂ peaks, respectively³⁵. To increase the reliability of the fit, the linewidth of the IMCL CH₂ peak (LW_{IMCL}) was constrained with respect to the linewidth of the water peak (LW_{water}) according to

$$LW_{IMCL} = -0.09 + 1.02 \cdot LW_{water} \quad [2]$$

This constraint was derived from previously recorded data sets with a well resolved IMCL peak (number of data sets = 20, R = 0.821, p<0.0001). A soft constraint, which was empirically determined from previously recorded data sets, was applied to the linewidth of the EMCL CH₂ peak (LW_{EMCL}), i.e. $LW_{EMCL} \leq LW_{IMCL} + 3.33$ Hz. When the resonance frequency (δ) of the IMCL CH₂ peak could not be accurately fitted (i.e. $\delta \leq 1.25$ ppm or $\delta \geq 1.31$ ppm), the position of the IMCL CH₂ peak was constrained with respect to the position of the tCr CH₃ peak (chemical shift difference = 3.02 – 1.28 ppm). IMCL was expressed as a percentage of the water signal

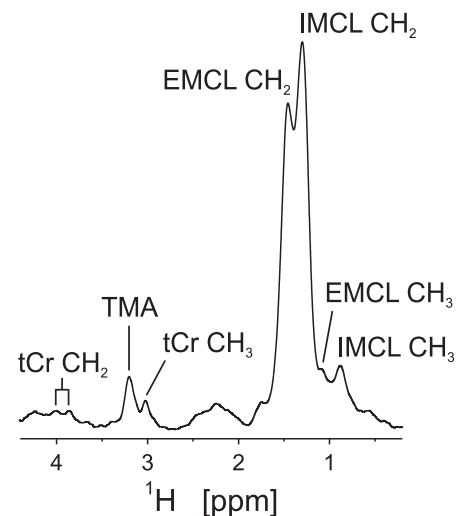


Figure 1 Typical ¹H MR spectrum from a 10×10×15 mm³ voxel in the *M. vastus lateralis* of a T2D subject. The spectrum was processed with 1 Hz line broadening. Peak annotations: tCr CH₂/CH₃: CH₂/CH₃ protons of total creatine, TMA: CH₃ protons of trimethylammonium groups, EMCL CH₂/CH₃: CH₂/CH₃ protons of extramyocellular lipid, IMCL CH₂/CH₃: CH₂/CH₃ protons of intramyocellular lipid.

measured in the same voxel without water suppression. IMCL levels determined from different voxels of one subject were averaged.

³¹P MRS

³¹P MRS was performed as described previously ²⁹. In short, ³¹P signals were collected using a 6-cm diameter surface coil placed over the *M. vastus lateralis* (spectral width, 2000 Hz; number of data points, 1024). A fully relaxed spectrum was measured at rest with a repetition time of 30 s and 24 scans. Then, spectra were acquired during a rest-exercise-recovery protocol with a repetition time of 3 s and 2 scans yielding a time resolution of 6 s. The first 20 spectra (2 min) were measured at rest, after which the subjects started the exercise. Subjects performed an incremental single-leg extension exercise in the supine position using a home-built MR compatible ergometer. The duration of the exercise varied per subject, but never exceeded 8 min, so that at least 5 min of recovery were recorded. During the first visit, subjects performed a test run and exercised until fatigued. During the second session, the duration of the exercise was chosen to deplete PCr by about 50%, while aiming to avoid the intracellular pH to drop below 6.8.

³¹P MRS data analysis

The ³¹P MRS data were analyzed as described previously ²⁹. In short, spectra were fitted in the time domain by using a nonlinear least squares algorithm (AMARES) in the jMRUI software package ³⁴. PCr, inorganic phosphate (P_i), ATP and phosphodiester (PDE) signals were fitted to Lorentzian line shapes. Absolute concentrations of the phosphorylated metabolites were calculated after correction for partial saturation and assuming that the ATP concentration is 8.2 mM at rest ³⁶. Intracellular pH was calculated from the chemical shift difference between the P_i and PCr resonances ³⁷. The free cytosolic ADP concentration was calculated from the PCr concentration and pH using a creatine kinase equilibrium constant (K_{eq}) of $1.66 \times 10^9 \text{ M}^{-1}$ ³⁸. Recoveries of PCr and ADP were fitted to mono-exponential functions using Matlab (version 7.3., Mathworks, Natick, Massachusetts, USA). Results are expressed as the metabolite's time constant of recovery, i.e. τ_{PCr} and τ_{ADP} , which are both measures of mitochondrial function. Calculation of the initial rate of PCr recovery (V_{PCr}) was based on the PCr recovery rate ($1/\tau_{PCr}$) and the difference between the resting and end-exercise PCr concentrations ³⁹. Calculation of the maximum aerobic capacity (Q_{max}) was based on the ADP-control model ⁴⁰, in which V_{PCr} has a hyperbolic dependence on the end-exercise ADP concentration according to Michaelis-Menten kinetics with a K_m of 30 M ³⁹.

Statistics

All data are expressed as means \pm SEM. To determine whether there were differences between groups, statistical analyses were performed using the SPSS 14.0 software package (SPSS Inc, Chicago, IL, USA). An ANOVA test was performed to test for overall differences between the NGT, ESD and T2D groups and a Bonferroni post-hoc test was applied for pair-wise comparisons between the 3 groups. For comparisons between 2 groups, differences were determined with an unpaired *t*-test. All tests were carried out in a 2-sided way and the level of significance was set at $p < 0.05$.

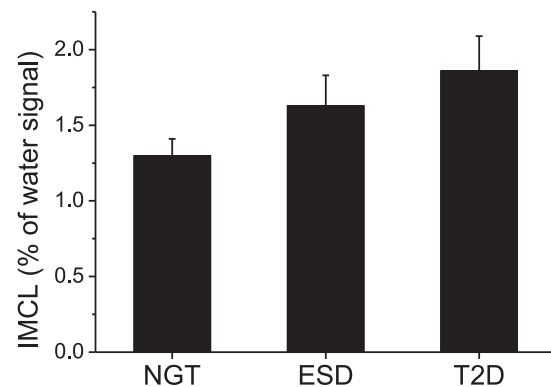


Figure 2 IMCL content in NGT, ESD and T2D groups was not significantly different.

Results

Subjects' characteristics

The subjects' characteristics are shown in Table 1. Subjects were carefully matched for age and BMI. In accordance, FFM and truncal fat mass did not differ between the NGT, ESD and T2D subjects ($p = 0.6$ and $p = 0.9$, respectively). W_{\max} and $VO_{2\text{peak}}$ were similar for the NGT and ESD subjects ($p = 1$), but significantly lower in the T2D group. The habitual physical activity level was not significantly different between groups ($p = 0.08$).

Fasting plasma glucose and insulin levels were not significantly different for the NGT and ESD subjects ($p = 0.7$ and $p = 0.14$, respectively), but the HOMA index was significantly higher for the ESD group than for the NGT group. Also the glucose and insulin concentrations measured 2 h after ingestion of the glucose load during the OGTT were significantly higher for the ESD subjects than for the NGT subjects. HbA_{1c} contents were similar for the NGT and ESD groups ($p = 1$) and all subjects had HbA_{1c} contents below 6%. Fasting glucose concentrations and HbA_{1c} content were significantly higher in the T2D subjects (glucose ≥ 8 mmol/l and $HbA_{1c} \geq 6.3\%$) compared to the NGT and ESD subjects. T2D subjects had been diagnosed with type 2 diabetes for 12.1 ± 2.1 years and had been on exogenous insulin therapy for 7.0 ± 2.4 years. Plasma NEFA concentrations did not differ between groups ($p = 0.13$).

Table 1 Subjects' characteristics.

	NGT		ESD		T2D	
n	12		11		11	
Age (yrs)	56.5	± 1.7	58.5	± 1.5	59.5	± 2.3
BMI (kg/m ²)	32.9	± 1.3	32.1	± 1.0	32.2	± 1.2
Body weight (kg)	101.0	± 4.3	103.9	± 3.0	97.5	± 4.9
FFM (kg)	70.7	± 2.1	72.4	± 2.1	68.9	± 2.9
Truncal fat mass (kg)	15.5	± 1.6	16.3	± 0.9	16.0	± 1.4
W _{max} (W)	247	± 12	244	± 9	152	± 12 ^{ab}
W _{max} per kg BW (W/kg)	2.48	± 0.14	2.39	± 0.14	1.59	± 0.12 ^{ab}
VO _{2peak} per kg BW (ml/min/kg)	32.3	± 1.6	33.8	± 1.8	24.3	± 1.4 ^{ab}
VO _{2peak} per kg FFM (ml/min/kg)	45.6	± 1.7	48.5	± 2.5	34.2	± 1.9 ^{ab}
Activity level (MET h/day)	19.3	± 2.2	19.5	± 2.6	13.3	± 1.3
Fasting glucose (mmol/l)	5.7	± 0.1	6.6	± 0.2	10.4	± 0.9 ^{ab}
Fasting insulin (µU/ml)	16.2	± 2.6	22.2	± 2.9	nd	
HOMA index	4.1	± 0.6	6.5	± 0.8 ^c	nd	
2-h glucose (mmol/l)	5.7	± 0.4	8.4	± 0.8 ^d	nd	
2-h insulin (µU/ml)	74.8	± 11.7	146.2	± 19.5 ^d	nd	
HbA _{1c} (%)	5.3	± 0.1	5.5	± 0.1	7.6	± 0.3 ^{ab}
NEFA (mmol/l)	0.31	± 0.03	0.39	± 0.04	0.46	± 0.07
Years with type 2 diabetes	na		na		12.1	± 2.1
Years of insulin therapy	na		na		7.0	± 2.4

BMI: body mass index, FFM: fat free mass, W_{max}: maximal workload capacity, W_{max} per kg BW: W_{max} per kg body weight, VO_{2peak}: maximal oxygen uptake per kg body weight or per kg FFM, MET: metabolic equivalents, HOMA: homeostasis model assessment, 2-h glucose/insulin, glucose/insulin concentration 2 h after ingestion of glucose load during the oral glucose tolerance test, HbA_{1c}: glycosylated haemoglobin, NEFA: non-esterified fatty acids, na: not applicable, nd: not determined. ^a Significantly different from NGT (ANOVA, p<0.01). ^b Significantly different from ESD (ANOVA, p<0.01). ^c Significantly different from NGT (t-test, p<0.05). ^d Significantly different from NGT (t-test, p<0.01).

IMCL content

Due to excessive EMCL contamination in the spectra, IMCL content could not be determined for 2 subjects in the NGT group and 1 subject in the T2D group. For all other subjects, spectra from at least 2 out of the 5 voxels were quantified. IMCL content did not differ significantly between groups (1.30 ± 0.11 (n = 10), 1.63 ± 0.20 (n = 11) and 1.86 ± 0.23 (n = 10) % of the water signal in NGT, ESD and T2D subjects, respectively, p = 0.13; Figure 2).

Skeletal muscle mitochondrial function

Figure 3a and 3b show typical examples of ³¹P MR spectra from a subject's *vastus lateralis* muscle at rest and at the end of exercise, respectively. Table 2 summarizes the baseline, end-exercise and recovery ³¹P MRS results for the NGT, ESD and T2D groups. At rest, PCr, P_i, ADP and PDE concentrations and intracellular pH were not significantly different for the NGT, ESD and T2D subjects (p = 0.9, p = 0.4, P=0.08, p = 0.9 and p = 0.09, respectively). The end-

exercise PCr and P_i concentrations were significantly different for the 3 groups (for both: $p = 0.04$), but the post-hoc test did not reveal significant differences for pair-wise comparisons. The end-exercise ADP concentration was lower in the T2D patients compared to both NGT and ESD subjects. The average PCr depletion was 54 ± 3 , 56 ± 2 and 46 ± 2 % for NGT, ESD and T2D subjects, respectively. For none of the subjects did the end-exercise pH drop below 6.75. The average end-exercise pH was not different for the 3 groups ($p = 0.9$), which is a prerequisite for comparing τ_{PCr} .

PCr and ADP recoveries could be satisfactorily described by mono-exponential functions (average R^2 values for the mono-exponential fits were 0.962 ± 0.003 and 0.906 ± 0.009 for PCr and ADP recovery data, respectively). Figure 4 illustrates both the raw data and mono-exponential fits of the PCr and ADP recoveries for one subject. Figure 5 shows the mean values and the distribution of τ_{PCr} for the NGT, ESD and T2D groups. The ^{31}P MRS parameters for mitochondrial function, i.e. τ_{PCr} , τ_{ADP} and Q_{max} , did not differ between the NGT, ESD and T2D groups ($p = 0.4$, $p = 0.14$ and $p = 0.11$, respectively, Table 2, Figure 5). V_{PCr} was significantly lower for the T2D group compared to the ESD group as a result of the lower end-exercise ADP concentration.

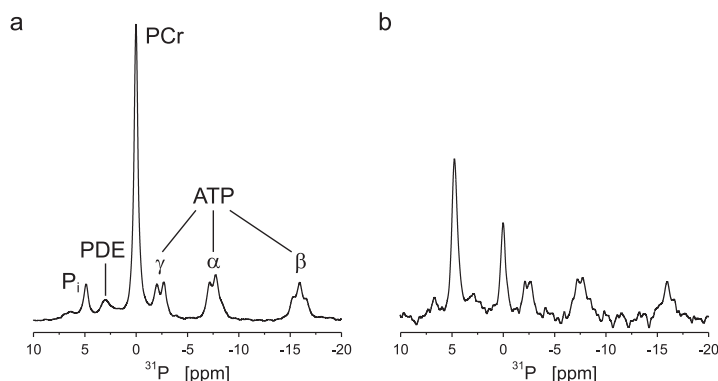


Figure 3 Typical *M. vastus lateralis* ^{31}P MR spectra for a NGT subject at rest (panel a, number of scans = 60) and at the end of exercise (panel b, number of scans = 2). Spectra were processed with 5 Hz line broadening. P_i : inorganic phosphate, PDE: phosphodiester, PCr: phosphocreatine and α , β and γ indicate the 3 phosphate groups of ATP. For this subject the PCr depletion at the end of exercise (panel b) was 61% and the corresponding end-exercise pH was 6.96.

Discussion

In this study, it was shown that *in vivo* skeletal muscle oxidative capacity, as determined from post-exercise PCr recovery kinetics using ^{31}P MRS, does not differ between long-standing, insulin-treated type 2 diabetes patients, subjects with early stage type 2 diabetes, and healthy, normoglycemic controls, all matched for age and body composition and with low habitual physical activity levels. Therefore, our results suggest that mitochondrial dysfunction represents neither cause or consequence of type 2 diabetes.

In the present study, ^{31}P MRS was applied to assess *in vivo* skeletal muscle mitochondrial function from measurements during recovery from exercise. During recovery from exercise, PCr is resynthesized purely as a consequence of oxidative ATP synthesis^{37, 41}. Therefore, τ_{PCr} provides information about mitochondrial function. Very recently, Schrauwen-Hinderling *et al.* applied the same technique to study mitochondrial function in the *M. vastus lateralis* in overweight type 2 diabetes patients and BMI-matched control subjects¹⁵. Contrary to our results, τ_{PCr} was 45% longer in the type 2 diabetes compared to their control group (i.e. 39.4 ± 5.0 vs 27.0 ± 1.3 s), suggestive of impaired *in vivo* mitochondrial function in the type 2 diabetic patients. The apparent contradictory finding can be explained by a number of

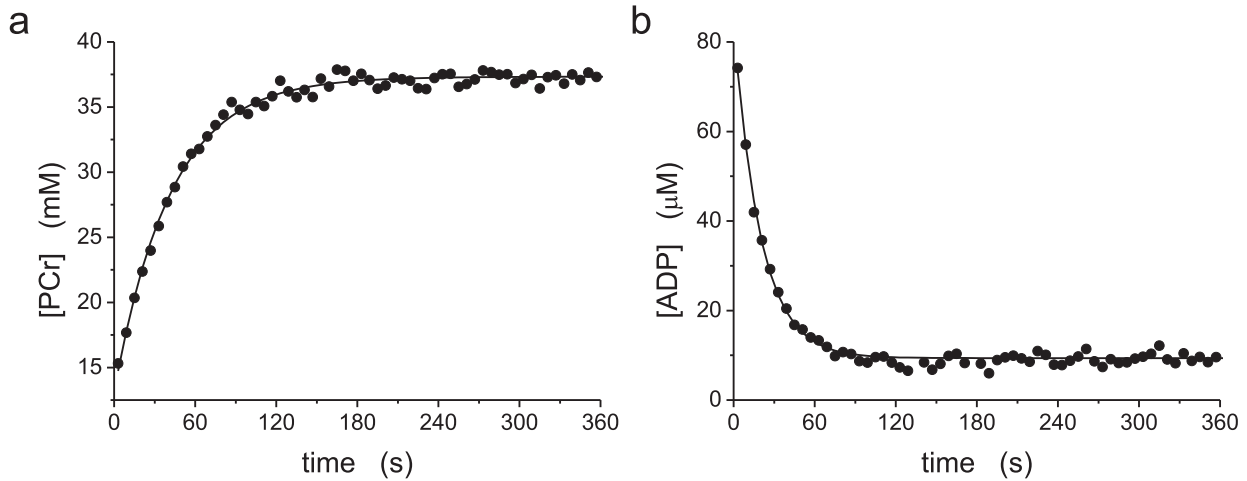


Figure 4 PCr (panel a) and ADP (panel b) recovery curves from the data set that was also used in Figure 3. Mono-exponential functions (dark lines) were fit to the actual data (filled circles) obtained every 6 s. The time constants for PCr and ADP recovery were 41.8 and 19.8 s, respectively

differences between studies. First of all, different exercise protocols were chosen for the ^{31}P MRS measurements. We used an exercise protocol that progressively increased work to deplete PCr by about 50% without severe acidification. In the previous study, exercise was performed with a single load, until a steady state was reached with an average PCr depletion of 28%. The larger PCr depletion in the current study was accompanied by a slightly larger drop in pH (change in pH was on average 0.15 in this study vs. 0.04 in ¹⁵), resulting in high quality PCr recovery curves which could be fitted reliably with a 3-parameter model. The smaller PCr depletion in the previous study necessitated the use of a 4-parameter model to estimate τ_{PCr} . Several studies have shown that PCr recovery is slowed in the presence of

Table 2 ^{31}P MRS parameters during rest, end of exercise and recovery.

		NGT	ESD	T2D
Rest	[PCr] (mM)	37.3 ± 0.7	37.7 ± 0.8	37.3 ± 1.2
	[Pi] (mM)	4.8 ± 0.2	5.0 ± 0.2	4.6 ± 0.2
	[ADP] (μM)	10.0 ± 0.1	10.4 ± 0.2	10.1 ± 0.1
	[PDE] (mM)	6.0 ± 0.2	6.0 ± 0.3	5.8 ± 0.4
	pH	7.059 ± 0.004	7.075 ± 0.007	7.063 ± 0.005
End- exercise	[PCr] (mM)	16.9 ± 1.0	16.7 ± 0.8	20.2 ± 1.3
	[Pi] (mM)	23.3 ± 1.4	24.2 ± 1.1	19.8 ± 1.2
	[ADP] (μM)	68.2 ± 5.2	70.2 ± 3.4	47.8 ± 3.1 ^{ab}
	pH	6.91 ± 0.02	6.92 ± 0.02	6.90 ± 0.04
Recovery	τ_{PCr} (s)	44.5 ± 3.0	41.7 ± 1.9	49.4 ± 5.5
	τ_{ADP} (s)	19.1 ± 1.0	16.9 ± 1.5	22.5 ± 2.9
	V_{PCr} (mM/s)	0.47 ± 0.03	0.51 ± 0.02	0.37 ± 0.03 ^b
	Q_{max} (mM/s)	0.69 ± 0.04	0.74 ± 0.03	0.62 ± 0.05

PCr: phosphocreatine, Pi: inorganic phosphate, ADP: adenosine diphosphate, PDE: phosphodiesterases, pH: intracellular muscle pH, τ_{PCr} : PCr recovery time constant, τ_{ADP} : ADP recovery time constant, V_{PCr} : initial rate of PCr recovery: Q_{max} , maximum rate of oxidative ATP synthesis. ^a Significantly different from NGT (ANOVA, $p < 0.01$). ^b Significantly different from ESD (ANOVA, $p < 0.01$).

intracellular acidosis^{26, 42}. However, we carefully matched the end-exercise pH for the NGT, ESD and T2D groups, to allow a direct comparison of τ_{PCr} between groups. As an alternative to τ_{PCr} , both τ_{ADP} and Q_{max} can also be used to assess *in vivo* mitochondrial function and these parameters have been shown to be independent of pH^{26, 43}. In accordance with the τ_{PCr} data matched for end-exercise pH, τ_{ADP} and Q_{max} also did not differ between groups.

As was suggested in the literature, τ_{PCr} can be normalized for pH using a correction factor of -46 s per pH unit⁴². Recalculating the values from Schrauwen-Hinderling *et al.* to a 0.11 lower end-exercise pH results in τ_{PCr} 's of about 44 and 32 s for the type 2 diabetes and control group, respectively. This implies that the mitochondrial function in our NGT, ESD and T2D groups is similar to that of the type 2 diabetes patients in the study of Schrauwen-Hinderling *et al.*, but that the controls in the latter study show a greater mitochondrial oxidative capacity. The healthy, normoglycemic controls in the present study were selected based on a low habitual physical activity level. Therefore, the apparent discrepancy between studies might likely be attributable to differences in physical activity levels of the control groups that were used. For other studies in healthy, elderly subjects previously reported in the literature⁴⁴⁻⁴⁶, average values for τ_{PCr} (recalculated at an end-exercise pH of 6.9 if necessary) have been shown to range between 43 and 46 s, which is well in line with the average τ_{PCr} in our NGT subjects. As such, muscle mitochondrial function in the obese NGT subjects does not seem to be impaired compared to other healthy subjects of similar age.

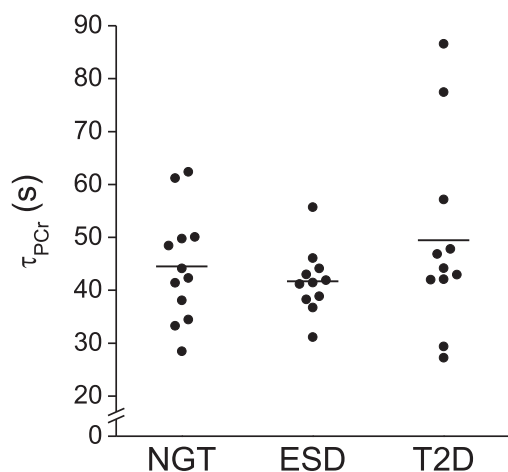


Figure 5 τ_{PCr} in NGT, ESD and T2D groups was not significantly different. Bars indicate the mean values for the 3 groups and filled circles represent individual data

As an alternative to measuring muscle oxidative capacity from dynamic ^{31}P MRS experiments after exercise, Petersen *et al.* applied ^{31}P MRS saturation transfer experiments to measure mitochondrial ATP synthesis rates in resting skeletal muscle of healthy, young, lean, insulin-resistant offspring of type 2 diabetes patients and insulin-sensitive control subjects matched for age, height, weight and physical activity¹⁴. ATP synthesis rates were approximately 30% lower in insulin-resistant subjects than in controls and it was concluded that the insulin-resistant offspring might have an inherited defect in mitochondrial phosphorylation. However, as commented by Short *et al.*²⁰ and Wagenmakers²¹, the lower ATP synthesis rates in insulin-resistant subjects could actually be caused by the impaired insulin signaling, jeopardizing insulin-dependent mitochondrial processes, rather than the reverse. This view is supported by studies that show that high-dose insulin infusions increase mRNA transcript levels of genes involved in mitochondrial function, mitochondrial protein synthesis and mitochondrial ATP production rates in healthy people, but not in type 2 diabetes patients^{24, 47, 48}. In summary, it seems likely that the decreased basal ATP synthesis rates in type 2 diabetes

patients are a result of the decreased insulin sensitivity and do not necessarily reflect any intrinsic mitochondrial defects.

Rabøl *et al.* recently reviewed the experimental data on mitochondrial dysfunction in type 2 diabetes and concluded that evidence of an intrinsic defect in mitochondria of type 2 diabetes patients is far from convincing¹⁷. Considering that patients with diabetes are generally physically inactive, the impairments in oxidative metabolism in type 2 diabetes patients might well be acquired as a result of their sedentary lifestyle. In this regard, it is important to note that in most studies physical activity has not been (strictly) controlled for. For *in vitro* studies in which physical activity was taken into account, the results suggest that the abnormalities in oxidative metabolism in type 2 diabetes patients can at least partly be attributed to physical inactivity^{11, 24, 49, 50}. In accordance with this view, very recent data from respiration measurements on permeabilized muscle fibers show that when O₂ flux was normalized for mitochondrial DNA content or citrate synthase activity, differences in mitochondrial respiration between patients with type 2 diabetes and healthy control subjects disappeared¹⁸. In other words, the type 2 diabetic subjects had normal intrinsic mitochondrial function, but an impaired oxidative capacity which can be fully accounted for by a lower mitochondrial content, most likely as a result of a reduced habitual physical activity level^{18, 19}. In accordance with those *in vitro* data, we report no differences in *in vivo* muscle mitochondrial function between long-standing type 2 diabetes patients, subjects with early stage type 2 diabetes and sedentary, normoglycemic controls.

In conclusion, subjects with early stage type 2 diabetes as well as long-standing, insulin-treated type 2 diabetes patients do not show any *in vivo* skeletal muscle mitochondrial dysfunction, when compared to sedentary, normoglycemic controls matched for age and body composition. These findings imply that mitochondrial dysfunction does not necessarily represent either cause or consequence of insulin resistance and/or type 2 diabetes. Impairments in oxidative metabolism in type 2 diabetes patients observed in previous studies are likely to be secondary to a more sedentary lifestyle and/or impaired insulin signaling.

Acknowledgements

We are very grateful to Larry de Graaf for his technical assistance with the MR scanner.

References

1. Pan, D.A. et al. *Diabetes* **46**, 983-988 (1997).
2. Krssak, M. et al. *Diabetologia* **42**, 113-116 (1999).
3. Morino, K., Petersen, K.F. & Shulman, G.I. *Diabetes* **55 Suppl 2**, S9-S15 (2006).
4. Simoneau, J.A. & Kelley, D.E. *J Appl Physiol* **83**, 166-171 (1997).
5. He, J., Watkins, S. & Kelley, D.E. *Diabetes* **50**, 817-823 (2001).
6. Kelley, D.E. et al. *Diabetes* **51**, 2944-2950 (2002).
7. Ritov, V.B. et al. *Diabetes* **54**, 8-14 (2005).
8. Mootha, V.K. et al. *Nat Genet* **34**, 267-273 (2003).
9. Patti, M.E. et al. *Proc Natl Acad Sci U S A* **100**, 8466-8471 (2003).
10. Hojlund, K. et al. *J Biol Chem* **278**, 10436-10442 (2003).
11. Morino, K. et al. *J Clin Invest* **115**, 3587-3593 (2005).
12. Mogensén, M. et al. *Diabetes* (2007).
13. Petersen, K.F. et al. *Science* **300**, 1140-1142 (2003).
14. Petersen, K.F. et al. *N Engl J Med* **350**, 664-671 (2004).
15. Schrauwen-Hinderling, V.B. et al. *Diabetologia* **50**, 113-120 (2007).
16. Sirikul, B. et al. *Am J Physiol Endocrinol Metab* **291**, E724-728 (2006).
17. Rabol, R., Boushel, R. & Dela, F. *Appl Physiol Nutr Metab* **31**, 675-683 (2006).
18. Boushel, R. et al. *Diabetologia* **50**, 790-796 (2007).
19. Hawley, J.A. & Lessard, S.J. *Diabetologia* **50**, 699-702 (2007).
20. Short, K.R., Nair, K.S. & Stump, C.S. *N Engl J Med* **350**, 2419-2421; author reply 2419-2421 (2004).
21. Wagenmakers, A.J. *PLoS Med* **2**, e289 (2005).
22. Brehm, A. et al. *Diabetes* **55**, 136-140 (2006).
23. Sreekumar, R. et al. *Diabetes* **51**, 1913-1920 (2002).
24. Asmann, Y.W. et al. *Diabetes* **55**, 3309-3319 (2006).
25. Radda, G.K. et al. *Nature* **295**, 608-609 (1982).
26. Arnold, D.L., Matthews, P.M. & Radda, G.K. *Magn Reson Med* **1**, 307-315 (1984).
27. Chance, B. et al. *NMR Biomed* **19**, 904-926 (2006).
28. World Health Organization and International Diabetes Federation Definition and diagnosis of diabetes mellitus and intermediate hyperglycaemia: report of a WHO/IDF consultation. (WHO Press, Geneva, Switzerland; 2006).
29. Praet, S.F. et al. *Magma* **19**, 321-331 (2006).
30. Montoye, H.J. et al. Measuring physical activity and energy expenditure. (Human Kinetics, Champaign, Illinois; 1996).
31. Zhang, Y.Y. et al. *Med Sci Sports Exerc* **23**, 625-630 (1991).
32. Weber, C.T., Janicki, J.S. & McElroy, P.A. Cardiopulmonary exercise testing (CPX) testing. (W. B. Saunders, Philadelphia; 1986).
33. Matthews, D.R. et al. *Diabetologia* **28**, 412-419 (1985).
34. Vanhamme, L., van den Boogaart, A. & Van Huffel, S. *J Magn Reson* **129**, 35-43 (1997).
35. Boesch, C. et al. *Magn Reson Med* **37**, 484-493 (1997).
36. Taylor, D.J. et al. *Magn Reson Med* **3**, 44-54 (1986).
37. Taylor, D.J. et al. *Mol Biol Med* **1**, 77-94 (1983).
38. Lawson, J.W. & Veech, R.L. *J Biol Chem* **254**, 6528-6537 (1979).
39. Kemp, G.J. et al. *Magn Reson Med* **31**, 248-258 (1994).
40. Chance, B. et al. *Proc Natl Acad Sci U S A* **82**, 8384-8388 (1985).
41. Quistorff, B., Johansen, L. & Sahlin, K. *Biochem J* **291 (Pt 3)**, 681-686 (1993).
42. Iotti, S. et al. *NMR Biomed* **6**, 248-253 (1993).
43. Lodi, R. et al. *Magma* **5**, 165-171 (1997).
44. Kent-Braun, J.A. & Ng, A.V. *J Appl Physiol* **89**, 1072-1078 (2000).
45. Conley, K.E., Jubrias, S.A. & Esselman, P.C. *J Physiol* **526 Pt 1**, 203-210 (2000).
46. Scheuermann-Freestone, M. et al. *Circulation* **107**, 3040-3046 (2003).
47. Stump, C.S. et al. *Proc Natl Acad Sci U S A* **100**, 7996-8001 (2003).
48. Petersen, K.F., Dufour, S. & Shulman, G.I. *PLoS Med* **2**, e233 (2005).
49. Ortenblad, N. et al. *Biochim Biophys Acta* **1741**, 206-214 (2005).
50. Timmons, J.A. et al. *Genomics* **87**, 165-172 (2006).

Chapter 7

Increased intramyocellular lipid content but normal skeletal muscle mitochondrial function throughout the pathogenesis of type 2 diabetes in the ZDF rat

Adapted from:

De Feyter H.M., Lenaers E., Schrauwen P., Hesselink M.K., Nicolay K., Prompers J.J.
Increased intramyocellular lipid content but normal skeletal muscle mitochondrial function throughout the pathogenesis of type 2 diabetes in the ZDF rat.
In preparation

Abstract

Recently skeletal muscle mitochondrial dysfunction has been related to insulin resistance and type 2 diabetes in humans. Current hypotheses link inherited or acquired mitochondrial dysfunction to a dysregulated fatty acid metabolism, which subsequently results in increased levels of IMCL and fatty acid intermediates inducing insulin resistance. To determine whether mitochondrial dysfunction is either a cause or a consequence of type 2 diabetes, we investigated both mitochondrial function and IMCL levels in a longitudinal study in the Zucker Diabetic Fatty (ZDF) rat.

The homozygous ZDF animals (fa/fa) develop type 2 diabetes during maturation whereas their heterozygous control littermates (fa/+) remain normoglycemic. In both genotypes, IMCL and skeletal muscle oxidative capacity were measured at ages corresponding to a) the pre-diabetic, state, b) the overt type 2 diabetic and c) a late type 2 diabetes stage of the fa/fa animals. Both IMCL and skeletal muscle mitochondrial oxidative capacity were measured *in vivo*, applying localized ^1H magnetic resonance spectroscopy (MRS) and dynamic ^{31}P MRS, respectively. Parallel to the *in vivo* MRS study, animals were sacrificed at the same ages and skeletal muscles were excised to isolate mitochondria and *in vitro* analyses of mitochondrial respiration using high-resolution respirometry were performed.

Blood plasma analyses confirmed the different states of type 2 diabetes at the different ages of the animals. Neither the *in vivo* oxidative capacity measured by ^{31}P MRS, nor the *in vitro* measurements of mitochondrial respiration showed compelling evidence of mitochondrial dysfunction related to the development of type 2 diabetes. However, the *in vitro* data do suggest an upregulation of mitochondrial respiratory capacity, possibly as a compensatory mechanism related to overt type 2 diabetes or increased IMCL levels in 12 weeks old fa/fa rats. In both genotypes the *in vivo* oxidative capacity was substantially affected by the age of the animals. The fa/fa rats had a higher IMCL content than the control rats throughout the duration of the study and IMCL levels increased excessively between 6 and 12 weeks of age. However, this change in IMCL levels was not related to changes in mitochondrial function.

The *in vivo* and *in vitro* data from this animal model of type 2 diabetes do not support the concept of skeletal muscle mitochondrial dysfunction, neither as a predisposing factor for IR and type 2 diabetes, nor as an acquired defect as a consequence of the disease.

Introduction

Skeletal muscle accounts for the great majority of insulin-stimulated glucose uptake^{1, 2} and insulin resistance (IR) of skeletal muscle tissue is one of the earliest detectable disturbances in and a predisposing factor for the development of type 2 diabetes (reviewed in³). Research into the pathogenesis of IR and type 2 diabetes showed that the content of intramyocellular lipids (IMCL), the triglyceride storage form within skeletal muscle cells, is negatively correlated with insulin sensitivity in sedentary humans⁴⁻⁷ as well as in rat models of IR and type 2 diabetes⁸⁻¹⁰. Yet, a causal relationship between IMCL and IR has never been proven. There are strong indications that intermediates, rather than the stored triglycerides themselves, of lipid metabolism such as long-chain acyl-CoA, diacylglycerol and/or ceramides interfere with the insulin signaling pathway¹¹⁻¹³. Therefore increased IMCL levels are nowadays valued more as a marker of ectopic lipid oversupply than as a direct cause of IR^{14, 15}.

Recently, IR has also been associated with skeletal muscle mitochondrial dysfunction (reviewed in¹⁶). Data originating from *in vivo* magnetic resonance spectroscopy (MRS) measurements¹⁷⁻¹⁹, *in vitro* enzyme activity assays²⁰⁻²³ and expression analysis of genes involved in oxidative metabolism^{24, 25} all suggest that skeletal muscle mitochondrial dysfunction might play a role in IR and type 2 diabetes. Current hypotheses link inherited or acquired mitochondrial dysfunction to a dysregulated fatty acid metabolism, which subsequently results in increased levels of IMCL and fatty acid intermediates inducing IR^{17, 18, 26}. However, evidence of dysfunctional mitochondria in type 2 diabetes is not conclusive since most reported impairments in mitochondrial function could also be explained by decreases in mitochondrial content, which is strongly linked to daily physical activity levels^{16, 27, 28}.

For various ethical and methodological reasons, studies in humans on the relationship between mitochondrial function and IR or type 2 diabetes have thus far been carried out using cross-sectional study designs. As such, they do not allow to discriminate between cause and consequence as there is no information about the time course of events. To circumvent the limitations of a cross-sectional study design, we performed a longitudinal study in an established animal model of adult-onset type 2 diabetes.

The present study aimed to unravel the order in which possible changes in IMCL and skeletal muscle mitochondrial function occurred during the development of type 2 diabetes in the Zucker Diabetic Fatty (ZDF) rat. Both IMCL and skeletal muscle mitochondrial oxidative capacity were measured *in vivo*, applying localized ¹H magnetic resonance spectroscopy (MRS) and dynamic ³¹P MRS, respectively. The minimally invasive MRS methods allowed to measure the same animals consecutively at characteristic time points throughout the pathogenesis of type 2 diabetes.

The homozygous ZDF animals (fa/fa) develop type 2 diabetes during maturation whereas their heterozygous control littermates (fa/+) remain normoglycemic. In both genotypes, IMCL and skeletal muscle oxidative capacity were measured at ages corresponding to a) the pre-diabetic, normoglycemic but insulin resistant state, b) the overt type 2 diabetic state characterized by hyperinsulinemia and hyperglycemia and c) a late type 2 diabetes stage characterized by

hyperglycemia and hypoinsulinemia due to beta-cell failure, of the fa/fa animals. Parallel to the *in vivo* MRS study, animals were sacrificed at the same characteristic time points and skeletal muscles were excised. The skeletal muscle tissue was used to isolate mitochondria and perform *in vitro* analyses of mitochondrial respiration using high-resolution respirometry.

Because IR is expected at young age in fa/fa ZDF rats we hypothesized that mitochondrial function would be impaired and levels of IMCL increased in 6 weeks old fa/fa animals compared to the control fa/+ rats. Furthermore we hypothesized that the development of severe type 2 diabetes in the fa/fa rats would lead to a more severe loss of mitochondrial function, accompanied by increases in IMCL and thus make the difference with the control fa/+ rats more pronounced.

Research design and methods

Animals

Male obese ZDF rats (ZDF/Gmi, fa/fa) and lean littermates (ZDF/Gmi, fa/+) were obtained from Charles River (Charles River Laboratories, Maastricht, The Netherlands). Animals were housed in pairs at 20 C and 50% humidity, on a 12-h light-dark cycle with *ad libitum* access to water and chow during the entire study. The animals arrived at the laboratory at 5 weeks of age and were fed normal chow for 2 weeks. From 7 weeks of age, animals received Purina 5008 diet (16.7 energy percentage (En%) fat, 56.4 En% carbohydrates and 26.8 En% protein, Altromin, Germany). In total, 26 fa/fa and 27 fa/+ rats were randomly assigned to the MRS groups or the satellite groups (see below) (figure 1). All experimental procedures were approved by the Animal Ethics Committee of Maastricht University.

MRS groups

In 10 fa/fa and 11 fa/+ animals, IMCL and skeletal muscle oxidative capacity was measured in the tibialis anterior (TA) muscle applying *in vivo* ¹H and ³¹P MRS, respectively at 6, 12 and 18 weeks of age. Animals were not fasted overnight before the MRS experiments. In the week after the last MRS experiments (19 weeks of age), these animals were all sacrificed for *in vitro* analysis of

mitochondrial respiration, according to the procedures described for the satellite groups (see below). Body weight, food intake and fasting blood glucose were monitored weekly during the entire study.

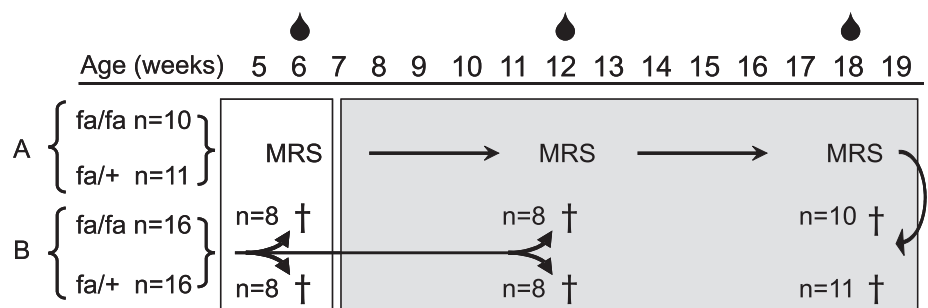


Figure 1 Schematic overview of the study design. A = MRS groups; B = satellite groups. ● represents blood sampling. MRS indicates *in vivo* IMCL and ³¹P MRS measurements; † indicates animal sacrificed and *in vitro* respiration measurements. White background = fed normal chow; light grey background = fed Purina 5008

Satellite groups

Parallel to the MRS measurements, ZDF rats were sacrificed at 6 (fa/fa, n = 8; fa/+, n = 8) and 12 (fa/fa, n = 8; fa/+, n = 8) weeks of age by cervical dislocation during mild CO₂ sedation. Of each rat, the left TA muscle was excised and plunged in ice-cold isolation buffer, typically taking less than 30 s.

MRS

All MRS experiments were performed on a 6.3 Tesla horizontal Bruker MR system. During the preparatory surgical procedures and the MRS experiments animals were anaesthetized using isoflurane (Forene®) (1–2%) with medical air (0.4 L/min) and body temperature was maintained at 37 ± 1 °C using heating pads. In the MR scanner, respiration was monitored using a pressure sensor registering the movement of the thorax (ECG trigger unit, Rapid Biomedical, Rimpfing, Germany).

Localized ¹H MRS was applied to measure IMCL levels in the TA as previously described²⁹ except that no additional outer volume suppression was applied. In short, 2 voxels of $2 \times 2 \times 2$ mm³ were placed in the white (ventral) and red (dorsal) TA using an ellipsoid ¹H surface coil (18/22 mm). Single-voxel localized ¹H MR spectra were acquired using the LASER sequence³⁰ (TR = 1 s, TE = 16 ms, SWAMP water suppression, 512 averages).

³¹P MRS was applied using a combination of a circular ¹H surface coil (40 mm diameter) and an ellipsoid ³¹P surface coil (10/18 mm) positioned over the TA muscle. Localized shimming was performed on the water signal using the ¹H surface coil. ³¹P spectra were acquired applying an adiabatic excitation pulse with a flip angle of 90 degrees. A fully relaxed spectrum (TR = 20 s, 32 averages) and a partially saturated spectrum (TR = 5 s, 128 averages) were measured at rest, followed by the acquisition of a time series of spectra (TR = 5 s, 4 averages) before, during and after electrical stimulation of the TA muscle. Electrical stimulation was applied via acutely, subcutaneously implanted platinum electrodes, which were positioned along the nerve trajectory of the *N. Peroneus Communis* to induce contractions in the TA muscle. A time series consisted out of 3 min rest, 2 min of electrical stimulation and 10 min of recovery. The electrical stimulation protocol consisted of a series of stimulation pulses, applied every second, for a duration of 2 min. Stimulation pulse length was 100 ms, frequency was 80 Hz and stimulation voltage varied between 2 and 4 V. For each rat and at each age, 3 consecutive time series were measured. The first time series was used to adjust the stimulation voltage in order to induce significant depletion of phosphocreatine (PCr) in the subsequent time series. The other two time series were used for the analysis of PCr recovery kinetics.

Both ³¹P and ¹H MR spectra were fitted in the time domain by using a nonlinear least squares algorithm (AMARES) in the jMRUI software package³¹. ¹H spectra were fitted using prior knowledge for line shapes and line widths for IMCL CH₂ and total creatine (tCr) CH₃ peaks, as described previously (Chapter 2)²⁹. In ³¹P MR spectra recorded at rest, PCr and the intra- and extracellular inorganic phosphate (Pi) peaks³² were fitted to Lorentzian line shapes. The α -

and γ -ATP peaks were fitted to Gaussian line shapes with equal peak areas. Due to the limited bandwidth of the excitation pulse, the β -ATP had a lower amplitude and was not fitted. In the ^{31}P MR spectra from the time series, peaks from intra- and extracellular P_i could not be distinguished and therefore a single P_i peak was fitted to a Gaussian line shape. Absolute concentrations of the phosphorylated metabolites were calculated after correction for partial saturation and assuming that the ATP concentration is 8.2 mM at rest ³³. Saturation correction factors determined from the fully relaxed spectra were 1.28 ± 0.02 , 1.68 ± 0.27 , 2.43 ± 0.59 and 1.13 ± 0.03 (mean \pm standard deviation, SD), respectively, for PCr, intracellular P_i , extracellular P_i and ATP. Intracellular pH was calculated from the chemical shift difference between the P_i and PCr resonances ³⁴. The free cytosolic ADP concentration was calculated from the PCr concentration and pH using a creatine kinase equilibrium constant (K_{eq}) of $1.66 \times 10^9 \text{ M}^{-1}$ ³⁵ and assuming that 15% of the total creatine is unphosphorylated at rest ³⁶. For the time series, the PCr line width during recovery was constrained to the average PCr line width during recovery (excluding the first 5 data points), obtained from a prior, unconstrained fit. The resynthesis of PCr was fit to a mono-exponential function using Matlab (version 6.5., Mathworks, Natick, Massachusetts, USA) yielding a time constant, τ_{PCr} , a measure of skeletal muscle mitochondrial oxidative capacity. Two time series with similar end-exercise pH values were analyzed. The analyses resulted in two values for τ_{PCr} which were averaged for each animal.

Mitochondrial isolations and functional assays

Mitochondrial isolation

Skeletal muscle mitochondria were isolated principally as previously described by Shabalina *et al.* ³⁷ with some modifications. Briefly, tissues were freed of white fat and connective tissue, weighed, finely minced with scissors and homogenized in a Potter homogeniser with a Teflon pestle. During mincing and homogenising, the skeletal muscle tissue fragments were treated with proteinase Nagarse (Fluka, Zwijndrecht, The Netherlands; 1 mg per g of tissue) added to the medium. Throughout the isolation process tissues were kept on ice constantly.

Mitochondria were isolated by differential centrifugation. Tissue homogenates were centrifuged at 8500 g for 10 min at 4°C using a Beckman J2-21M centrifuge. The resulting supernatants, containing floating fat and proteinase were discarded. Pellets from skeletal muscle were resuspended in cold medium containing 100 mM sucrose, 50 mM KCl, 20 mM K^+ -TES, 1 mM EDTA and 0.2 % (w/v) BSA. The resuspended tissue homogenates were centrifuged at 800 g for 10 min, and the resulting supernatants were centrifuged at 8500 g for 10 min. The resulting mitochondrial pellet from skeletal muscle was resuspended in the same buffer and centrifuged again at 8500 g for 10 min. The final mitochondrial pellets were resuspended by hand homogenisation in a small glass homogeniser in the appropriate final centrifugation medium. The concentration of mitochondrial protein was measured using fluorescamine (Floram[®], Fluka, Zwijndrecht, The Netherlands) with BSA as a standard ³⁸. Subsequently, the freshly isolated mitochondria were used immediately for oxygen consumption measurements.

Oxygen Consumption

Skeletal muscle mitochondria were incubated in a medium consisting of 100 mM sucrose, 20 mM K⁺-TES (pH 7.2), 50 mM KCl, 2 mM MgCl₂, 1 mM EDTA, 4 mM KH₂PO₄, 3 mM malate and 0.1% of (w/v) BSA. The substrates used were 5 mM pyruvate, 10 mM glutamate and 2 mM carnitine plus 50 μ M palmitoyl-CoA. State 3 respiration was initiated by addition of 450 μ M ADP. State 4 respiration was measured as the residual respiration following addition of 1 μ g/ml oligomycin. Maximal oxygen consumption rates (state uncoupled; state U) were obtained by titration of the chemical uncoupler carbonyl cyanide p-trifluoromethoxyphenylhydrazone (FCCP). All substrates were dissolved in double distilled water while FCCP and oligomycin were dissolved in 96% ethanol. Ethanol in itself did not have any effects on the parameters measured.

Mitochondrial respiratory rates were measured at 37°C by polarographic oxygen sensors in a two-chamber Oxygraph (OROBOROS[®] Instruments, Innsbruck, Austria) equipped with a Peltier thermostat and electromagnetic stirrers. The oxygen concentration was recorded at 0.5 sec intervals and using the acquisition software DatLab 4 (OROBOROS[®] Instruments, Innsbruck, Austria). The first derivative of the oxygen tension changes is displayed as oxygen flux and mean values during about 1 min were obtained from these recordings for calculation of stable oxygen consumption rates. Oxygen consumption was expressed as nmol O₂ per mg mitochondrial protein per minute. The respiratory control ratio (RCR) and the uncoupling control ratio (UCR) were calculated as state 3/state 4 and state 3/state U, respectively.

Blood plasma collection

Blood samples were collected via the retro-orbital plexus at 6, 12 and 18 weeks of age, under isoflurane anesthesia, after 4 hours of fasting. The blood samples were collected in K-EDTA coated tubes, centrifuged for 10 min at 1000 g and plasma aliquots were frozen in liquid nitrogen and stored at -80°C.

Analytical procedures of plasma

Plasma substrates were determined using the hexokinase method (Roche, Basel, Switzerland) for glucose and the Wako NEFA C test kit (Wako Chemicals, Neuss, Germany) for free fatty acids. Fasting plasma insulin concentrations were determined using an ultra-sensitive solid phase two-site enzyme linked immuno sorbent assay (ELISA) kit specific for rat insulin (Mercodia, Uppsala, Sweden).

Statistical analysis

Data are presented as mean \pm standard deviation (SD). Data of the MRS group were analyzed using an ANOVA for repeated measures with one within-subjects factor (age) and one

between-subjects factor (genotype). A one-way ANOVA was performed to examine the data from the satellite groups and Bonferroni corrected post-hoc tests were carried out in order to identify differences between time points and genotypes. All tests were performed two-sided using SPSS 14.0 (SPSS Inc, Chicago, IL, USA) and statistical significance was set at $p < 0.05$.

Results

Animal model

The plasma concentrations of glucose, insulin and FFA determined at 6, 12 and 18 weeks of age are depicted in Figures 2a-c. The glucose and insulin concentrations of the *fa/fa* animals confirm the pre-diabetic state at 6 weeks of age with normal glucose and high insulin levels, the diabetic state at 12 weeks characterized by both high insulin and high glucose levels and an advanced diabetic state at 18 weeks, with high glucose levels and decreased insulin levels compared to 12 weeks, indicating progressive failure of β -cell function. The *fa/+* animals by contrast displayed normal glucose and constant insulin levels throughout the entire study (Figure 3a, b). Both genotypes showed similar and constant plasma FFA levels in the period of the study (Figure 3c).

The body weight was higher in the *fa/fa* than in the *fa/+* rats during the entire study (Figure 2d). The *fa/fa* rats had a higher body weight at the start of the study and appeared to increase in body weight at a higher rate than the *fa/+* between week 6 and 11. *Ad libitum* food intake of the *fa/fa* rats was over the entire study duration higher than that of the *fa/+* rats (Figure 2e).

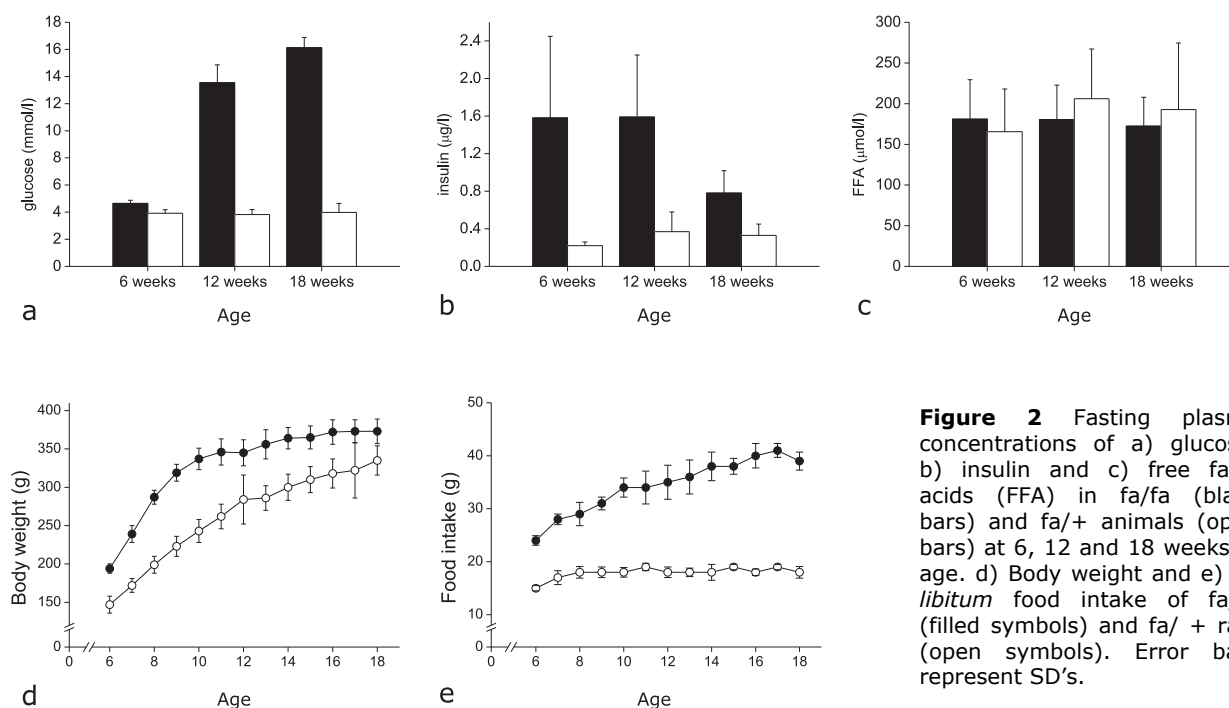


Figure 2 Fasting plasma concentrations of a) glucose, b) insulin and c) free fatty acids (FFA) in *fa/fa* (black bars) and *fa/+* animals (open bars) at 6, 12 and 18 weeks of age. d) Body weight and e) *ad libitum* food intake of *fa/fa* (filled symbols) and *fa/+* rats (open symbols). Error bars represent SD's.

IMCL

Figure 3a and 3b show two spectra measured in the red TA of a fa/fa and a fa/+ rat of 12 weeks old, respectively. The mean IMCL levels for the white and red regions of the TA muscle, at different ages are presented in Figure 3c. In both genotypes and at all different ages, the IMCL levels were 2-3 times higher in the red region of the TA compared to the white region. While the IMCL levels tended to decrease with age in the fa/+ animals, IMCL levels significantly increased in fa/fa rats between 6 and 12 weeks of age and decreased again between 12 and 18 weeks of age. However, at each time point, the IMCL levels at both voxel positions in the fa/fa animals were significantly higher compared to the fa/+ animals.

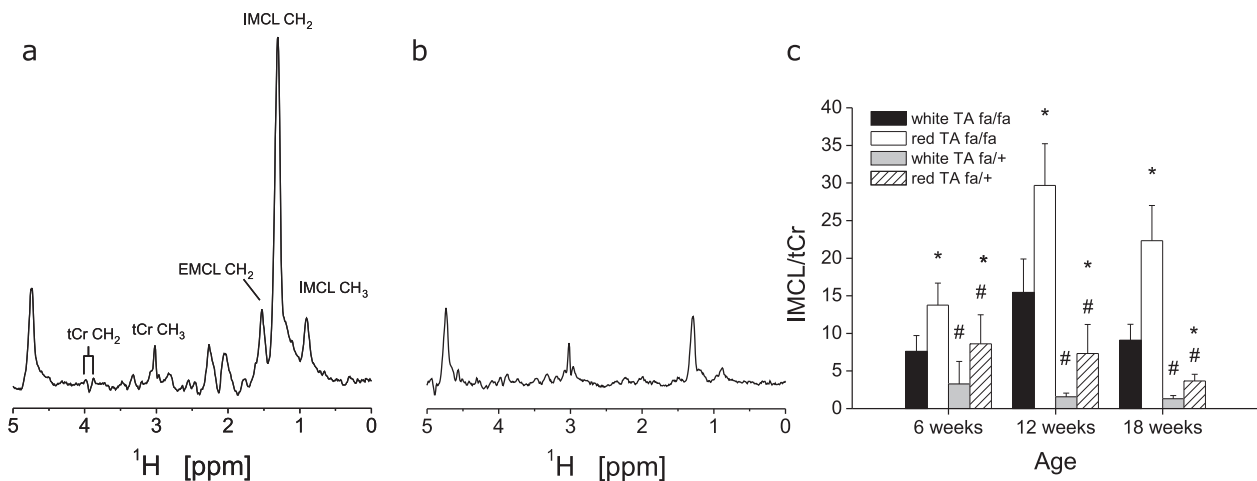


Figure 3 Examples of water-suppressed ¹H MR spectra measured in the red TA from a fa/fa (a) and a fa/+ (b) rat of 12 weeks old. Peak annotations: tCr: total creatine; EMCL: extramyocellular lipids; IMCL: intramyocellular lipids. c) IMCL content at different ages in white and red TA of fa/fa and fa/+ rats. Error bars represent SD's. * significantly different from white TA in same genotype, # significantly different from same muscle region in other genotype.

³¹P MRS

Table 1 shows the phosphorus metabolite concentrations and pH at rest. At rest, the Pi concentration and [Pi]/[PCr] ratio was higher in fa/fa rats than in fa/+ rats, at all ages. This could indicate a difference in muscle fiber type composition between fa/fa and fa/+ rats, with relatively more oxidative muscle fibers in fa/fa rat muscle. There was an effect of aging on [PCr], [ADP] and pH which all increased from 6 to 12 weeks of age, but remained constant during further maturation.

Figure 4a shows a stack plot of spectra measured during a rest-exercise-recovery protocol and displays how the PCr signal drops in the beginning of the electrical stimulation, reaches a steady state and then recovers to the rest value. End-exercise metabolite concentrations and pH are displayed in Table 2. None of the metabolite's concentrations were different between genotypes, except for [Pi] which was higher than in fa/+ animals. [PCr], [ADP] and pH were higher at 12 weeks of age compared to 6 weeks of age, which can completely be attributed to the applied electrical stimulation protocol. At 12 weeks of age, (erroneously) slightly less strenuous contractions were induced via the electrical stimulation, explaining both the

difference in PCr and end-exercise pH. At each time point however, the end-exercise pH was not different between genotypes.

In Figure 4b an example of the PCr recovery fit is depicted. The mean PCr recovery time constant of both genotypes at different ages is depicted in figure 4c. The repeated measures ANOVA revealed no significant effect of genotype on τ_{PCr} . However, in both genotypes there was a significant effect of age, i.e. τ_{PCr} was higher at 12 weeks and at 18 weeks of age compared to the respective previous time point, indicating a significant decrease in oxidative capacity of skeletal muscle during maturation.

Table 1 Concentration of ^{31}P metabolites and intracellular pH at rest

	6 weeks			12 weeks			18 weeks					
	fa/fa		fa/+	fa/fa		fa/+	fa/fa		fa/+			
[PCr]	31.7	± 1.2	32.5	± 1.5	40.2	± 1.2*	38.5	± 1.0*	39.1	± 2.0	39.5	± 1.6
[Pi] #	3.2	± 0.7	2.5	± 0.6	3.1	± 0.7	2.3	± 0.5	4.3	± 0.6 [§]	3.3	± 0.6 [§]
[Pi]/[PCr] [#]	0.1	± 0.02	0.08	± 0.02	0.08	± 0.02*	0.06	± 0.01*	0.11	± 0.02 [§]	0.08	± 0.02 [§]
[ADP]	9.6	± 1.6	9.9	± 1.6	12.0	± 0.4*	11.4	± 0.5*	11.3	± 0.5	11.7	± 0.7
pH	7.04	± 0.08	7.05	± 0.07	7.14	± 0.02*	7.12	± 0.02*	7.11	± 0.02	7.13	± 0.03

[PCr], [Pi] in mM; [ADP] in μM . Pi: intracellular inorganic phosphate. # Significantly different between genotypes; * significantly different compared to 6 weeks old animals, [§] significantly different compared to 12 weeks old animals. Differences between ages were analyzed with ANOVA for repeated measures: 12 weeks vs 6 weeks and 18 weeks vs 12 weeks.

Mitochondrial respiration

The RCR measured in the isolated mitochondria was larger than 10 for pyruvate and glutamate (Figure 5a). The RCR reflects the degree of coupling between substrate oxidation and ADP phosphorylation. The presented RCR values indicate a high degree of coupling, implicating that the mitochondria were highly intact. The RCR values did not differ between the genotypes, except for 6 weeks old fa/fa rats on palmitoyl-CoA RCR was lower than controls. At 12 weeks of age, the RCR on palmitoyl-CoA of the fa/fa animals was higher than that at 6 weeks and 19 weeks of age and similar as in fa/+ animals.

Figure 5b displays state 3 respiration of both rat genotypes, on different substrates and at different ages. There were no differences in state 3 respiration between genotypes in six weeks old rats, except for palmitoyl-CoA respiration, which was lower in fa/fa rats. At 12 weeks of age, the respiration on palmitoyl-CoA in fa/fa rats was higher than at 6 weeks and also higher than fa/+ rats of the same age. At 19 weeks, on the other hand, palmitoyl-CoA state 3 respiration in fa/fa was again lower than in 12 week old fa/fa rats, and similar as in control fa/+ rats of that age. Pyruvate and glutamate state 3 respiration was lower in 19 week old fa/fa rats compared to 12 weeks old animals, but similar to control values. State 4 respiration

with oligomycin was similar for all substrates and at all ages, except for 19 weeks old fa/fa rats which displayed lower state 4 respiration on pyruvate and glutamate than 12 weeks old fa/fa rats (data not shown). State 4 respiration represents endogenous proton leakage of the inner membrane.

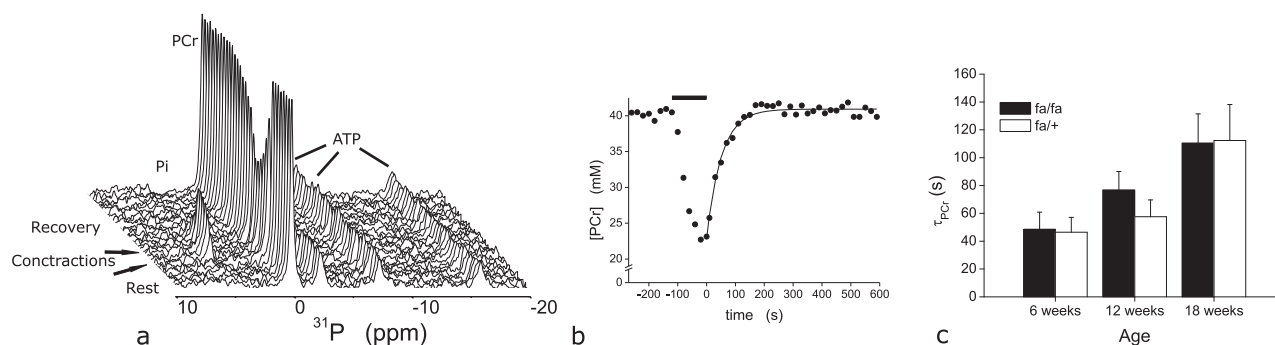


Figure 4 a) Stack plot of ^{31}P MR spectra measured in TA during a time series of a 12 weeks old fa/+ rat during a rest-exercise-recovery protocol. Contractions were induced by electrical stimulation. Time resolution = 20 s. Peaks are from inorganic phosphate (Pi), phosphocreatine (PCr) and ATP. b) [PCr] during rest-exercise-recovery protocol, bar represents period of electrical stimulation. Recovery data were fit with a mono-exponential function (black line) and T_{PCr} was 51.1 s. c) Average T_{PCr} of fa/fa (black bars) and fa/+ rats (open bars) at different weeks. Error bars represent SD's.

The measurements of uncoupled respiration (Figure 5c) in control fa/+ rats did not display changes over time, whereas uncoupled mitochondrial respiration in fa/fa rats changed in a similar way over time as state 3 respiration for the same substrates. In 12 weeks old fa/fa rats, uncoupled respiration was higher than in 6 weeks old fa/fa rats for both palmitoyl-CoA and pyruvate. State U on palmitoyl-CoA was also higher than its value in fa/+ rats of the same age. At 19 weeks of age, state U on palmitoyl-CoA and pyruvate was again lower in fa/fa rats than at 12 weeks of age and similar to the control rats. Also glutamate uncoupled respiration was lower at 19 weeks in fa/fa rats than at 12 weeks of age, however, similar as in control animals.

In Figure 5d the UCR, i.e. the ratio of state 3 over uncoupled respiration, is depicted. The UCR reflects the capacity of the electron transport chain and enzymatic reactions involved in NADH and/or FADH₂ generation relative to the capacity of the oxidative phosphorylation system. As an example, an UCR of 0.6 implies that 60% of the maximal capacity of the electron transport chain can be used during state 3 respiration. There were no differences in UCR between the fa/fa and fa/+ rats. However, in both genotypes there appeared to be an age-related decline of the UCR. At 19 weeks of age the UCR was lower than that in 6 weeks old animals for all substrates, except for glutamate, which did not change throughout the study. The age-related decline in UCR was already detectable at 12 weeks of age for pyruvate in both genotypes.

Discussion

The present study aimed to unravel the order in which possible changes in IMCL content and skeletal muscle mitochondrial function in skeletal muscle occurred during the development of type 2 diabetes in the ZDF rat. The characteristic development of the ZDF phenotype was confirmed by the plasma analyses of fasting glucose and insulin levels (Figures 2a & b) and justified the different time points/ages chosen to measure IMCL and mitochondrial function: the pre-diabetic state (6 weeks), overt diabetic (12 weeks) and late stage type 2 diabetic state (18 weeks).

Table 2 Concentration of ^{31}P metabolites and intracellular pH at the end of exercise

	6 weeks		12 weeks		18 weeks	
	fa/fa	fa/+	fa/fa	fa/+	fa/fa	fa/+
[PCr]	16.7 ± 2.3	17.0 ± 2.3	21.4 ± 2.3*	19.9 ± 2.0*	19.5 ± 1.7	21.8 ± 1.6
[Pi] #	21.1 ± 3.7	17.7 ± 1.8	20.5 ± 3.7	15.8 ± 2.4	22.5 ± 4.4	17.6 ± 2.9
[ADP]	47.3 ± 16.4	53.4 ± 19.3	57.9 ± 9.06*	67.2 ± 9.8*	59.2 ± 13.0	51.3 ± 10.9
pH	6.86 ± 0.11	6.91 ± 0.07	6.98 ± 0.08*	7.02 ± 0.10*	6.93 ± 0.02	6.96 ± 0.06

[PCr], [Pi] in mM, [ADP] in μM . Pi: intracellular inorganic phosphate. # significantly different between genotypes, * significantly different compared to 6 weeks old animals. Differences between ages were analyzed with ANOVA for repeated measures: 12 weeks vs. 6 weeks and 18 weeks vs. 12 weeks.

Neither the *in vivo* oxidative capacity measured by ^{31}P MRS, nor the *in vitro* measurements of mitochondrial respiration showed compelling evidence of mitochondrial dysfunction related to the development of type 2 diabetes. However, the *in vitro* data do suggest an upregulation of mitochondrial respiratory capacity, possibly as a compensatory mechanism related to overt type 2 diabetes or increased IMCL levels in 12 weeks old fa/fa rats. In both genotypes the *in vivo* oxidative capacity was substantially affected by the age of the animals. The fa/fa rats had a higher IMCL content than the control rats throughout the duration of the study and IMCL levels increased excessively between 6 and 12 weeks of age. However, this change in IMCL levels was not related to changes in mitochondrial function.

The *in vivo* IMCL measurements confirm previous results on the muscle fiber type-related levels of IMCL within rat TA muscle ²⁹, as in both ZDF genotypes. IMCL levels were roughly twice as high in the red region compared to the white region of the TA muscle. Relative changes in IMCL levels during the study were similar in white and red regions of the TA, in fa/fa as well as in fa/+ rats. In general, the changes in the IMCL concentration of growing ZDF rats are in good agreement with earlier reports ^{9, 39}. However, increases in IMCL content over time in the fa/fa animals were more pronounced in the present study whereas decreases over time in the fa/+ animals were less explicit. Our animals were fed Purina 5008, a diet containing a modest, yet significantly higher amount of fat than standard diets as used by others ^{9, 39}. This higher amount of fat in the diet used in the present study may explain the amplified increase and blunted decrease in IMCL over time in fa/fa and fa/+ animals, respectively.

The measurements of IMCL did confirm its role as a marker of IR and type 2 diabetes. IMCL levels were increased in the insulin resistant fa/fa rats of 6 weeks old and vastly increased in parallel with the development of type 2 diabetes. However, as glycemic control even further deteriorated, IMCL levels did not increase simultaneously. On the contrary, 18 weeks old fa/fa rats had lower IMCL levels than their 12 weeks old congeners, indicating that IMCL can only serve as a qualitative biomarker of IR and type 2 diabetes in rodents.

At 6 weeks of age, *in vivo* skeletal muscle oxidative capacity was identical in both genotypes despite an evident insulin resistant status of the fa/fa rats. This implies that mitochondrial function was not impaired in the fa/fa rats and indicates that mitochondrial dysfunction is not a prerequisite for the development of insulin resistance. During the development of severe type 2 diabetes in the fa/fa animals, τ_{PCr} gradually increased, resulting in about three times higher values at 18 weeks compared to 6 weeks of age. However, this change in mitochondrial activity was not related to type 2 diabetes, since the control fa/+ rats demonstrated the same mitochondrial oxidative capacity at 18 weeks of age. It is therefore most likely that the decrease in oxidative capacity can completely be attributed to the maturation of the animals. This was confirmed by the statistical analysis which showed no significant effect of genotype on τ_{PCr} .

The measurement of τ_{PCr} can be influenced by a number of parameters, some physiological, some related to technical aspects. First of all, in human skeletal muscle a low intracellular end-exercise pH (1) is known to slow down PCr resynthesis (see also Chapter 4) ^{40, 41}. A similar mechanism could be present in rodent skeletal muscle. Comparing τ_{PCr} values when end-exercise pH is different should therefore be treated with caution. Also a lowered tissue perfusion (2) could be responsible for slowing down PCr recovery by reducing the availability of oxygen and, to a lesser extent, substrate, both essential for a proper functioning of oxidative phosphorylation. Another factor that can possibly bias the measurement of τ_{PCr} is a mix of both biological and methodological aspects: the inhomogeneous muscle fiber type distribution in rodent muscle in combination with the use of a surface coil for the detection of the MR signal (3). The characteristics of different muscle fiber types are for a great part determined by the density and intrinsic properties of their mitochondria. Measuring τ_{PCr} with a surface coil placed on the muscle of interest will result in an average value, determined by the PCr recovery kinetics of the different muscle fiber types that contribute to the MR signal. The use of a surface coil, however, implicates that the MR signal originating from a region distant from the coil will contribute less to the MR spectrum than signal originating from a region close to the coil. When the different fiber types are homogeneously distributed within the muscle, they all will contribute relatively equal to the PCr recovery kinetics. However, rodent TA muscle is characterized by a pronounced regionalization, with the oxidative type I fibers located far from the surface, close to the tibia bone and the most glycolytic fiber type close to the surface ^{42, 43}. In case of the rat TA muscle, this implies that the signal arising from the oxidative muscle fibers would contribute less to the total ³¹P signal. We already described the inhomogeneous distribution of muscle fiber types in rat TA muscle and its consequences for *in vivo* IMCL measurements in Chapter 2, but the inhomogeneous fiber distribution could also influence the ³¹P MRS measurements.

What is the impact of these three parameters on the comparison of *in vivo* oxidative capacity between genotypes? In the present study care was taken to avoid large differences in end-exercise pH, especially between genotypes at the same age. The largest difference between end-exercise pH values was 0.05. This small difference in end-exercise pH is not hampering the interpretation of the results.

Frisbee demonstrated reduced skeletal muscle performance in fa/fa ZDF rats compared to the fa/+ rats, which was suggested to be related to impaired arteriolar reactivity and reduced microvessel density⁴⁴. A disturbed muscle perfusion could hence be present in the fa/fa rats. Apparently, this phenomenon did not significantly hamper the PCr recovery in the present study, since there was no difference in τ_{PCr} between fa/fa and fa/+ ZDF rats. The first time series of contractions, which was used to adjust the stimulation voltage, was not included in the PCr recovery analysis. Possibly this first series of contractions primed the skeletal muscle perfusion system and blunted differences between ZDF genotypes in such a way that perfusion was not noticeably affecting τ_{PCr} .

The fa/fa rats showed a higher rest [Pi] and [Pi]/[PCr] which could point towards a higher amount of type I muscle fibers in the TA. If this is the case, apparently it did not significantly influence the results on whole muscle level, as τ_{PCr} was not different between genotypes. However, it could also suggest that in the relatively higher amount of type II fibers in the fa/+ animals, the oxidative capacity is increased compared to the fa/fa animals, which overall results in a similar whole-muscle oxidative capacity.

The end-exercise pH, perfusion and muscle fiber type can also influence the comparisons of τ_{PCr} measured at different ages. The largest difference between end-exercise pH values within one genotype, between two time points was 0.12. This value is too small to account for the large differences observed in τ_{PCr} at the various time points. Moreover, the lowest end-exercise pH was witnessed in 6 weeks old animals. Thus, the τ_{PCr} may actually be overestimated at that age, which means that the effect of maturation on *in vivo* oxidative capacity may even be larger.

Growth-related decreases in capillary density and related parameters such as capillary to fiber ratio could potentially interfere with the PCr recovery kinetics via the changes in muscle perfusion. However, recent data show that heterogeneity of capillary spacing compensates for decrease in capillary density and in this way preserves adequate intramuscular oxygenation⁴⁵.

The age-related increase in τ_{PCr} could be associated with a shift in muscle fiber typology. Data of Sprague-Dawley rat soleus muscle suggest that postnatal fiber type transitions are completed by the age of 6 weeks⁴⁶. However, we cannot exclude that muscle fiber type composition shifted towards more glycolytic fibers, during maturation⁴³. Besides a change in muscle fiber type composition, also migration of specific fiber types within the muscle has been reported in growing rats⁴³. Konishi *et al.* showed in the Wistar rat TA muscle that the type I fibers gradually “move” in the direction of the tibia bone, towards the deep region⁴³. The effect of an inhomogeneous distribution of muscle fiber types in rat TA muscle on the overall ³¹P MRS signal, as described above, could therefore change with maturation. This implies that

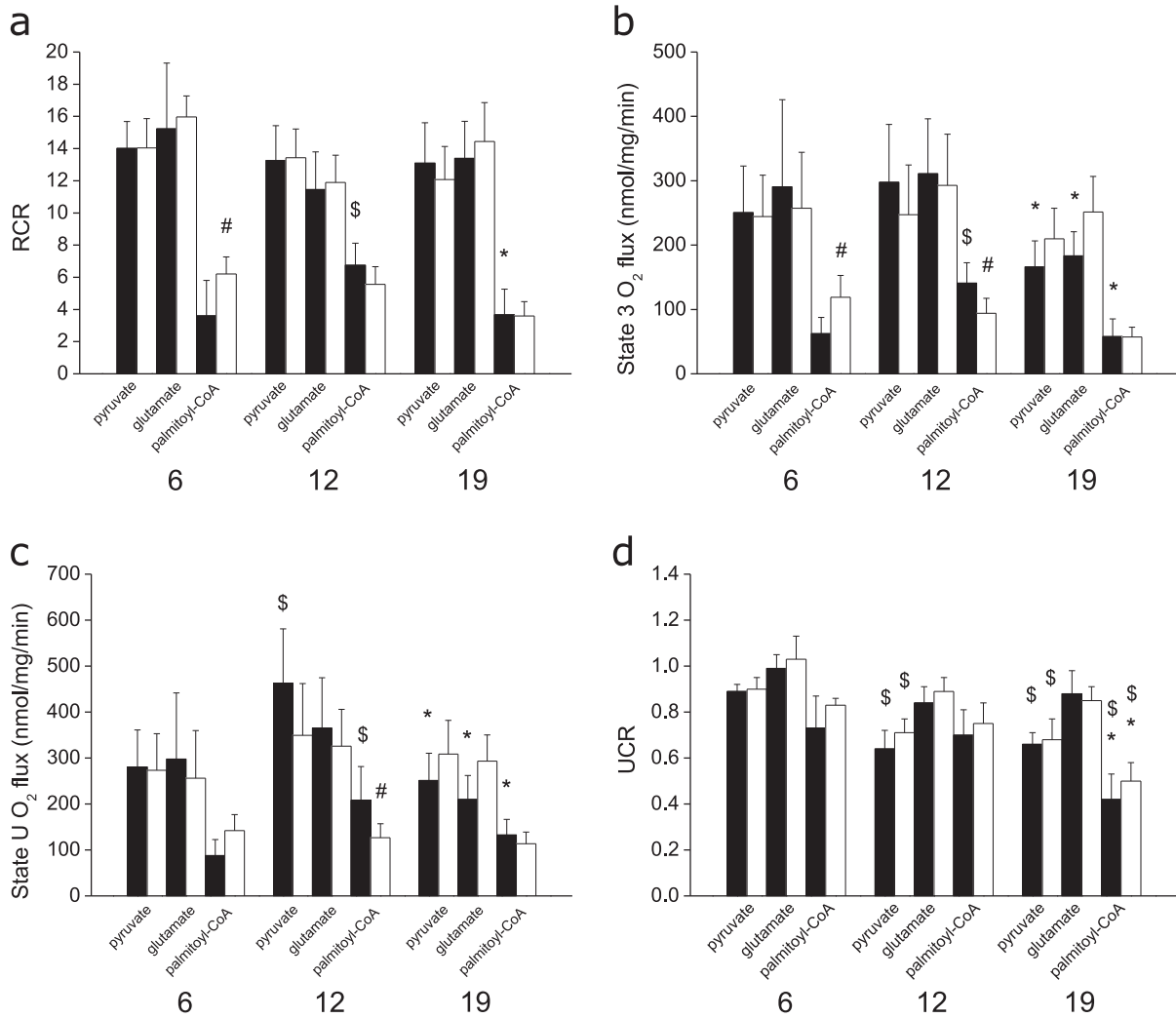


Figure 5 Respiration data measured in isolated mitochondria on different substrates. a) RCR = state 3/state 4, b) state 3 respiration, c) state U respiration, d) UCR = state 3/state U. Black bars represent fa/fa, open bars represent fa/+ rats. 6, 12 and 19 indicate the age of the animals in weeks. # significantly different from fa/fa of the same age, \$ significantly different from 6 weeks old animals with same genotype, * significantly different from 12 weeks old animals with same genotype according to one-way ANOVA. Error bars represent SD's.

the signal arising from the oxidative muscle fibers would contribute less to the total ^{31}P signal at a higher age. As different muscle fibers are suggested to display different PCr recovery kinetics ⁴⁷, the described change in fiber type distribution with maturation might affect τ_{PCr} . This effect could even be larger due to the increase of the muscle volume during maturation, which also causes the population of type I muscle fibers to be situated further away from the RF coil. The migration of type I muscle fibers and the increased muscle volume would increase the relative contribution of the glycolytic muscle fibers to the total ^{31}P signal and slow down the PCr recovery. Therefore, the described increase in τ_{PCr} with the maturation of the animals probably not only represents a decrease in oxidative capacity in the predominant glycolytic TA muscle fibers, but might also reflect a decreasing contribution of the type I muscle fibers to the measured ^{31}P MR signal. However, this latter is not paralleled by an age-related change in the $[\text{Pi}]/[\text{PCr}]$ ratio.

We are not aware of *in vivo* MRS studies measuring τ_{PCr} as function of age in growing rats. However, combining results of various studies qualitatively support the age-related decrease of τ_{PCr} witnessed in our study. Values of PCr recovery time constants vary from 25 s in control rats with body weights less than 200 g⁴⁸, to 121 s in heavier, and therefore presumably older rats⁴⁹. Also pilot-experiments in healthy Wistar rats of varying age confirmed the age-related increase in τ_{PCr} (data not shown)

Since τ_{PCr} is predominantly defined by the density and the intrinsic characteristics of mitochondria, this implies that the density and/or the functionality would become less with maturation. Age-related decline in mitochondrial DNA copy number, a measure of the density of mitochondria, has been described in old rats in several skeletal muscles⁵⁰. However, studies on aging-related changes in skeletal muscle are performed in rats that are noticeably older than the animals in the present study, which complicates generalizing previous results.

Besides *in vivo* oxidative capacity, the mitochondrial function was evaluated by *in vitro* respiration measurements on isolated mitochondria. These measurements occur in suspensions normalized for the mitochondrial protein content and are therefore determined exclusively by the intrinsic characteristics of the mitochondria. Thus, the *in vitro* respiration measurements are not a function of the mitochondrial density. State 3 *in vitro* respiration mostly resembles the *in vivo* mitochondrial state during PCr recovery. Interestingly, the state 3 respiration rate did not show a significant age-related decline, while *in vivo* oxidative capacity did. Only fa/fa rats showed changes in state 3 respiration throughout the study, however these involved both increases and decreases over time. The fa/+ animals showed no changes in state 3 respiration over time. Therefore the age-related decline of *in vivo* oxidative capacity is probably more related to the mitochondrial density and/or muscle fiber type composition, than to the functionality of the mitochondria, *per se*.

State 3 and state U are the parameters generally used to describe the overall oxidative capacity of mitochondria and the isolated capacity of the electron chain, respectively. Fa/fa rats differed from control animals in state 3 or state U respiration only in a few age/substrate combinations, in which fa/fa rats mostly performed better than controls. The *in vitro* mitochondrial respiration measurements therefore did not reveal impaired mitochondrial function in fa/fa rats compared to fa/+ rats.

State 3 respiration and RCR on palmitoyl-CoA at 6 weeks of age were lower in fa/fa rats. This could point towards a lowered capacity to metabolize fatty acids, whether or not as a result of an inborn defect. Surprisingly, in 12 weeks old fa/fa rats the respiration on palmitoyl-CoA was higher than in fa/+ rats of the same age. At 19 weeks, state 3 palmitoyl-CoA respiration was again lower than at 12 weeks and equal to control rats. Uncoupled respiration and RCR on palmitoyl-CoA changed over time in a comparable way: they were increased at 12 weeks, and again lower and similar as fa/+ rats, at 19 weeks. This could indicate an upregulation of mitochondrial function as a compensatory, protective mechanism related to type 2 diabetes or the increased IMCL levels.

This striking pattern of increased respiration at 12 weeks in fa/fa rats on palmitoyl-CoA as seen in state 3, state U and RCR was also observed in previous studies on gene expression in ZDF rats⁵¹ and in respiration of skinned muscle fibers of insulin resistant Wistar rats⁵². Suh *et al.* characterized gene expression profiles from skeletal muscle of ZDF rats at 6, 12, and 20 weeks of age⁵¹. Several genes, among which genes involved in oxidative, in particular fat metabolism, showed a differential expression profile over the different ages: many of the genes that were up- or downregulated in skeletal muscle of pre-diabetic ZDF rats became down- or upregulated reversely at 12 weeks of age and sometimes the opposite was the case at 20 weeks of age⁵¹. Chanséaume *et al.* studied mitochondrial respiration in skinned muscle fibers of high fat diet-induced insulin resistant Wistar rats⁵². The insulin resistant Wistar rats did not demonstrate any differences in mitochondrial function in the TA muscle, while after 2 weeks of high fat diet, the respiration rate was higher in the soleus muscle with glutamate/malate/succinate as substrate mix. After about 3 weeks of diet intervention, mitochondrial respiration was again similar to control animals and became worse at 6 weeks of high fat diet⁵². Also in mouse models of IR and type 2 diabetes an increased expression of proteins related to mitochondrial function was found, together with an improved capacity for fatty acid oxidation⁵³.

The *in vitro* data of 12 weeks old rats are perhaps even more intriguing when compared to the *in vivo* data. After all, when the *in vivo* ³¹P MRS data at 12 weeks of age would be treated as a separate data set (not taking into account the data from 6 and 19 weeks old animals), an unpaired T-test would reveal a significantly higher τ_{PCr} and thus lower oxidative capacity in fa/fa rats compared to control fa/+ rats. How can this mismatch between *in vivo* and *in vitro* data be explained? The apparent improvements in mitochondrial respiration were all on palmitoyl-CoA as substrate. Possibly, the contribution of fat as a substrate in the PCr recovery was not that significant. The exercise simulated via the electrical stimulation did not take more than 2 minutes, which is in general far too short of a time to fully activate fatty acid metabolism. Presumably the PCr recovery is fueled predominantly by ATP generated by carbohydrate-derived substrate metabolism, passing through pyruvate dehydrogenase. State 3 and state U respiration on pyruvate were not different between fa/fa and fa/+ rats, which would be compatible with the proposed mechanism, which points towards mitochondrial density as an explanation. If the number of mitochondria is notably lower in the fa/fa rats, this could outstrip the similar intrinsic mitochondrial function.

A key question is, whether it is justified to directly compare *in vitro* and *in vivo* data. After all, *in vitro* data report on the properties of the isolated mitochondrial system, without any information involving the regulation of oxidative metabolism. The *in vivo* ³¹P MRS data, on the other hand are defined by a combination of intrinsic characteristics of the oxidative phosphorylation system, the density of mitochondria but not in the least, also by the *in vivo* regulation of the mitochondrial function. It is not inconceivable that *in vivo* oxidative phosphorylation is influenced by intermediates from lipid or carbohydrate metabolism. Ciapaite *et al.* applied modular kinetic analysis, a systems biology approach and showed an inhibiting effect of palmitoyl-CoA on oxidative phosphorylation in isolated liver mitochondria⁵⁴. Palmitoyl-CoA inhibited the adenine nucleotide translocator without direct effects on other components of the oxidative phosphorylation system⁵⁴. A similar mechanism might also be

present in skeletal muscle and explain the discrepancy between *in vitro* and *in vivo* data of 12 weeks old rats. On the other hand, the data from 18 weeks old animals do not show a discrepancy between *in vitro* and *in vivo* data, which weakens the previous argumentation.

The results of the *in vivo* and *in vitro* assays applied in the present study do not indicate a defect in the skeletal muscle mitochondria of the *fa/fa* rat, neither in the pre-diabetic state nor in the late stage of type 2 diabetes. These results are inconsistent with current paradigms of inherited or type 2 diabetes-induced defects in mitochondrial function in humans^{18, 26}. On the other hand, Boushel *et al.* showed that type 2 diabetes patients display normal mitochondrial function, as measured by *in vitro* respiration in permeabilized muscle fibers, when the respiration data were corrected for the amount of mitochondria²⁷. They and others pointed towards the daily activity level as an important variable accounting for the apparent mismatch between studies reporting mitochondrial dysfunction related to type 2 diabetes and their own results^{27, 28}. Indeed, chronic inactivity results in a decrease in the mitochondrial density, whereas exercise training induces marked mitochondrial biogenesis⁵⁵. Spontaneous daily activity was not measured in the present study. However, a previous study reports highly similar spontaneous daily activity levels in both genotypes of ZDF rats⁵⁶.

Besides the lack of a measurement of mitochondrial content, the present study has another limitation. We chose to study a muscle which consists of predominantly glycolytic muscle fibers. Human muscle, in contrast, has a much larger fraction of oxidative type I muscle fibers, which jeopardizes the generalization of the present results of the rodent model. Despite the robust correlation between increased IMCL levels and IR in rat, also in glycolytic muscle fibers⁹, we cannot exclude that type 2 diabetes-related mitochondrial dysfunction is more related to oxidative than to glycolytic muscle fibers.

In conclusion, *in vivo* mitochondrial oxidative capacity was not different between both ZDF genotypes. The *in vitro* respiration measurements in isolated mitochondria did not provide evidence for an intrinsic mitochondrial defect. Consequently, the *in vivo* and *in vitro* data do not support the concept of skeletal muscle mitochondrial dysfunction, neither as a predisposing factor for IR and type 2 diabetes, nor as an acquired defect as a consequence of the disease. In contrast, the *in vitro* results from the diabetic animals suggest a transient upregulation of mitochondrial function, possibly as a compensatory mechanism induced by disease-related factors or by the high IMCL content. The IMCL content was noticeably high in the diabetic animals but did not display a link with mitochondrial function.

References

1. DeFronzo, R.A. et al. *J Clin Invest* **76**, 149-155 (1985).
2. DeFronzo, R.A. et al. *Diabetes* **30**, 1000-1007 (1981).
3. Petersen, K.F. & Shulman, G.I. *Am J Med* **119**, S10-16 (2006).
4. Goodpaster, B.H. et al. *J Clin Endocrinol Metab* **86**, 5755-5761 (2001).
5. Krssak, M. et al. *Diabetologia* **42**, 113-116 (1999).
6. Pan, D.A. et al. *Diabetes* **46**, 983-988 (1997).
7. Perseghin, G. et al. *Diabetes* **48**, 1600-1606 (1999).
8. Dobbins, R.L. et al. *Diabetes* **50**, 123-130 (2001).
9. Kuhlmann, J. et al. *Diabetes* **52**, 138-144 (2003).
10. Kuhlmann, J. et al. *Magn Reson. Med.* **53**, 1275-1282 (2005).
11. Hegarty, B.D. et al. *Acta Physiologica Scandinavica* **178**, 373-383 (2003).
12. Shulman, G.I. *J Clin Invest* **106**, 171-176 (2000).
13. Yu, C. et al. *J Biol Chem* **277**, 50230-50236 (2002).
14. Hulver, M.W. et al. *Am J Physiol Endocrinol Metab* **284**, E741-747 (2003).
15. Slawik, M. & Vidal-Puig, A.J. *Ageing Res Rev* **5**, 144-164 (2006).
16. Rabol, R., Boushel, R. & Dela, F. *Appl Physiol Nutr Metab* **31**, 675-683 (2006).
17. Petersen, K.F. et al. *Science* **300**, 1140-1142 (2003).
18. Petersen, K.F. et al. *N Engl J Med* **350**, 664-671 (2004).
19. Schrauwen-Hinderling, V.B. et al. *Diabetologia* **50**, 113-120 (2007).
20. He, J., Watkins, S. & Kelley, D.E. *Diabetes* **50**, 817-823 (2001).
21. Kelley, D.E. et al. *Diabetes* **51**, 2944-2950 (2002).
22. Ritov, V.B. et al. *Diabetes* **54**, 8-14 (2005).
23. Simoneau, J.A. & Kelley, D.E. *J Appl Physiol* **83**, 166-171 (1997).
24. Mootha, V.K. et al. *Nat Genet* **34**, 267-273 (2003).
25. Patti, M.E. et al. *Proc Natl Acad Sci U S A* **100**, 8466-8471 (2003).
26. Roden, M. *Int J Obes (Lond)* **29 Suppl 2**, S111-115 (2005).
27. Boushel, R. et al. *Diabetologia* **50**, 790-796 (2007).
28. Hawley, J.A. & Lessard, S.J. *Diabetologia* **50**, 699-702 (2007).
29. De Feyter, H.M. et al. *Magn Reson Med* **56**, 19-25 (2006).
30. Garwood, M. & DelaBarre, L. *J Magn Reson* **153**, 155-177 (2001).
31. Vanhamme, L., van den Boogaart, A. & Van Huffel, S. *J Magn Reson* **129**, 35-43 (1997).
32. Brindle, K.M. et al. *Biochemistry* **28**, 4887-4893 (1989).
33. Taylor, D.J. et al. *Magn Reson Med* **3**, 44-54 (1986).
34. Taylor, D.J. et al. *Mol Biol Med* **1**, 77-94 (1983).
35. Lawson, J.W. & Veech, R.L. *J Biol Chem* **254**, 6528-6537 (1979).
36. Boska, M. *Magn Reson Med* **32**, 1-10 (1994).
37. Shabalina, I.G. et al. *J Biol Chem* **281**, 13882-13893 (2006).
38. Udenfriend, S. et al. *Science* **178**, 871-872 (1972).
39. Korach-Andre, M. et al. *Metabolism* **54**, 522-528 (2005).
40. van den Broek, N.M. et al. *Am J Physiol Cell Physiol* (2007).
41. Iotti, S. et al. *Biochem Biophys Res Commun* **178**, 871-877 (1991).
42. Wang, L.C. & Kernell, D. *J Muscle Res Cell Motil* **21**, 587-598 (2000).
43. Konishi, M. et al. *Kaibogaku Zasshi* **75**, 267-273 (2000).
44. Frisbee, J.C. *Am J Physiol Regul Integr Comp Physiol* **285**, R1124-1134 (2003).
45. Degens, H. et al. *Microcirculation* **13**, 467-476 (2006).
46. Watchko, J.F., Daood, M.J. & LaBella, J.J. *Pediatr Res* **40**, 53-58 (1996).
47. Meyer, R.A. et al. in ISMRM, Vol. 5 13091997).
48. Mizobata, Y. et al. *J Surg Res* **59**, 165-173 (1995).
49. Kemp, G.J. et al. *Magn Reson Med* **31**, 103-109 (1994).
50. Barazzoni, R., Short, K.R. & Nair, K.S. *J Biol Chem* **275**, 3343-3347 (2000).
51. Suh, Y.H. et al. *J Mol Endocrinol* **34**, 299-315 (2005).
52. Chanseau, E. et al. *Obesity (Silver Spring)* **15**, 50-59 (2007).
53. Turner, N. et al. *Diabetologia* **49**, 333-333 (2006).
54. Ciapaite, J. et al. *Diabetes* **54**, 944-951 (2005).
55. Hood, D.A. et al. *J Exp Biol* **209**, 2265-2275 (2006).
56. Keeseey, R.E., Swiergiel, A.H. & Corbett, S.W. *Physiology & Behavior* **48**, 327-331 (1990).

Chapter 8

Exercise training improves glycemic control in long-standing, insulin-treated type 2 diabetes patients

Adapted from:

De Feyter H.M., Praet S.F.E., van den Broek N.M., Kuipers H., Stehouwer C.D., Nicolay K., Prompers J.J., van Loon L.J.C.

Exercise training improves glycemic control in long-standing, insulin-treated type 2 diabetes patients.

Submitted

Abstract

Objective: To determine the health benefits of exercise intervention in deconditioned, long-standing type 2 diabetes patients on exogenous insulin treatment.

Research design and methods: Eleven male, long-standing type 2 diabetes patients (12 ± 2 y) on exogenous insulin treatment (92 ± 11 IU/d) participated in an exercise intervention program combining both resistance and endurance type exercise training. Glycemic control (HbA_{1c}), body composition (DXA/MRI), intramyocellular lipid content (^1H -MRS), and skeletal muscle oxidative capacity (^3P -MRS and $\text{VO}_{2\text{max}}$) were assessed before and after 5 months of exercise intervention (3 exercise sessions/wk).

Results: All subjects completed the study and showed a high compliance ($>83\%$) to the prescribed exercise sessions. Exercise training significantly reduced blood HbA_{1c} levels (7.6 ± 0.3 to $7.2 \pm 0.2\%$; $p < 0.05$) and tended to lower fasting plasma glucose concentrations (10.4 ± 0.9 to 8.6 ± 0.7 mmol/l, $p = 0.05$). This was associated with lower exogenous insulin requirements, increased exercise performance capacity and reduced fat mass. Also the cardiovascular risk was reduced as mean arterial pressure decreased from 105.8 ± 2.3 to 98.1 ± 3.1 mmHg ($p < 0.05$).

Conclusion: Long-standing, insulin-treated type 2 diabetes patients should be stimulated to participate in specifically designed exercise intervention programs. A combination of low-impact resistance and endurance type exercise training improves glycemic control, augments exercise performance capacity, improves body composition and attenuates exogenous insulin requirements in these patients.

Introduction

Besides diet and medication, exercise training forms one of the 3 cornerstones of type 2 diabetes treatment. Over the years, it has been established that regular physical exercise represents an effective strategy to prevent and/or treat type 2 diabetes¹⁻⁴. Exercise training is now generally prescribed for newly diagnosed type 2 diabetes patients to reduce insulin resistance, improve glycemic control, and prevent cardiovascular co-morbidities^{1, 3-7}. Clinical guidelines for the practical application of exercise intervention in the prevention and treatment of type 2 diabetes prescribe that *'... at least 150 min/week of moderate-intensity aerobic physical activity is recommended and/or at least 90 min/week of vigorous aerobic exercise, ... distributed over at least 3 days/week and with no more than 2 consecutive days without physical activity.'*^{8, 9}.

The increase in type 2 diabetes prevalence can only partly be attributed to the changing population demographics, as epidemiological data show diabetes incidence to increase particularly in the young and middle-aged¹⁰. As a consequence, the population long-standing, type 2 diabetes patients on exogenous insulin treatment will expand considerably in the coming years¹¹. This type 2 diabetes subpopulation is characterized by a progressive rise in exogenous insulin requirements, the presence of co-morbidities, a high cardiovascular risk profile and substantial exercise intolerance^{12, 13}. The application of intense endurance exercise activities in this deconditioned group of type 2 diabetes patients is not always feasible and often contraindicated. Therefore, generic exercise intervention programs designed to prevent and/or treat type 2 diabetes are generally not applicable in this diabetes subpopulation. Furthermore, research studies investigating the health benefits of exercise intervention programs generally exclude long-standing, insulin-treated type 2 diabetes patients with co-morbidities for obvious methodological considerations. As such, the potential benefits of exercise intervention in this specific type 2 diabetes subpopulation with a high cardiovascular risk profile have not yet been established.

Besides endurance exercise, resistance type exercise has been recognized as a useful therapeutic tool for the treatment of type 2 diabetes^{3, 4, 14, 15}. As intense endurance exercise is often difficult to adhere to for those who have been habitually sedentary^{15, 16}, it has been suggested that progressive resistance training would be more feasible in a population of elderly, obese type 2 diabetes patients^{3, 4, 14, 15}. In the present study, we aimed to investigate the feasibility and the benefits of a specifically designed low-impact exercise intervention program, combining both endurance and resistance type exercise, in a population of long-standing, insulin-treated type 2 diabetes patients with a high cardiovascular risk profile. We assessed the impact of 5 months of exercise training on glycemic control, body composition, whole-body and skeletal muscle oxidative capacity and cardiovascular risk profile.

Research design & methods

Subjects

Eleven male, type 2 diabetes patients were selected to participate in this study. Subjects had been diagnosed with type 2 diabetes for 12 ± 2 y and had been on exogenous insulin treatment for 7.0 ± 2.4 y. All subjects were sedentary and had no history of participating in any regular exercise program for at least 10 y prior to the study. All patients had been on a stable regimen of diabetes medication for at least 3 months before being recruited. Type 2 diabetes patients using thiazolidinediones and/or beta-blockers shorter than 6 months and subjects with impaired liver function, macroalbuminuria, severe retinopathy or a history of severe cardiovascular problems were excluded from participation. Out of the 11 participating subjects, 7 patients were treated with short (Novorapid[®], n = 6) or rapid acting insulin (Humulin[®], n = 1) before each meal either in combination with NPH insulin (Insulatard[®], n = 5), premixed biphasic isophane insulin (Mixtard 30/70[®] in combination with metformin, n = 1), or a very long-acting insulin analogue (insulin glargine, n = 1), all administered before bedtime. Three subjects were treated with premixed biphasic isophane insulin twice a day (Mixtard 30/70[®]) in combination with metformin. One subject used NPH insulin (Humulin NPH[®]) once a day before breakfast in combination with metformin and a sulphonylurea (glimpiride). The nature and the risks of the experimental procedures were explained to the subjects and all gave their written informed consent to participate in the study, which was approved by the local Medical Ethical Committee of the Máxima Medical Center, Veldhoven, The Netherlands.

Study design

All 11 subjects participated in a 5 month (22 wk) exercise intervention program. Before and after the exercise program the following variables were assessed: body composition, glycemic control, blood lipid profile, blood pressure, whole-body oxygen uptake and maximal workload capacity, intramyocellular lipid content (IMCL) and whole-body and skeletal muscle oxidative capacity.

Body composition

Body mass and waist circumference were measured using an analog weight scale and standard measuring tape, respectively. Segmental and whole-body fat mass (FM) and lean mass (LM) were determined using whole-body dual X-ray absorptiometry (DXA) (Hologic QDR-4500 Discovery A, software version 12.3:3, Hologic Inc. Bedford, MA, USA). Magnetic resonance (MR) imaging was performed in the upper leg using a 1.5-Tesla whole-body MR scanner (Gyrosan S15/ACS, Philips Medical Systems, Best, The Netherlands). A stack of 42 transversal T₁-weighted spin-echo images (TR/TE = 500/12 ms) was acquired covering 48.3 cm of the upper leg. Muscle tissue was segmented from the images using EasyVision (5.1.1.2, 2001, Philips Medical Systems, Best, The Netherlands) and the total upper leg muscle and *Musculus (M.) vastus lateralis* volumes were calculated.

Blood analyses

Two weeks before the start of the exercise program and 3 days after the last exercise session blood samples were collected. On the evening before the blood sample collection, subjects received a standardized meal (35.2 ± 1.8 kJ/per kg body mass (BM), containing 53 energy% (En%) fat, 10 En% protein, and 37 En% carbohydrate) after which subjects remained fasted. The following morning at 8.00 am, subjects arrived at the laboratory by car or public transportation. After 10 min of supine rest, a venous blood sample was collected from an antecubital vein. Blood samples (4 ml) were collected in tubes containing a glycolytic inhibitor (sodium fluoride) and an anticoagulant (potassium oxalate), immediately centrifuged at $1000g$ and $4^{\circ}C$ for 5 min, after which aliquots of plasma were frozen immediately in liquid nitrogen and stored at $-80^{\circ}C$ until analyses. Plasma glucose (Glucose 125 Hexokinase kit, ABX Diagnostisc, Montpellier, France), serum cholesterol (CHOD-PAP, ABX Diagnostics), HDL-cholesterol (543004, Roche Diagnostics, Basel, Switzerland), LDL-Cholesterol (LDL-C plus 2nd generation test kit, Roche), non-esterified fatty acids (NEFA) (Wako NEFA-C test kit, Wako Chemicals, Neuss, Germany) and triacylglycerol (GPO-Tinder 337B: Sigma Diagnostics, St Louis, MO) concentrations were analyzed with the COBAS FARA semi-automatic analyzer (Roche). To determine basal fasting blood HbA_{1c} content a 3 ml blood sample was collected in EDTA containing tubes and analyzed by high-performance liquid chromatography (Bio-Rad Diamat, Munich, Germany). The serum concentration of adiponectin was quantified using a commercially available Human Adiponectin ELISA (#HADP-61K, Linco Research Inc. St. Charles, MO). TNF- α concentration was analysed using a solid-phase, chemiluminescent immunometric assay (IMMULITE TNF- α , DPC Biermann GmbH, Bad Nauheim, Germany). HsCRP was measured by means of immunoephelometry (*Cardiophase*, Dade Behring GmbH, Marburg, Germany). C-peptide was analysed by an electrochemiluminescent immunoassay (Nr 03184897, Elecsys Module, Roche GmbH, Mannheim).

Blood pressure

Before and after the 22 wk exercise program systolic and diastolic blood pressure were recorded on 2 separate occasions during 15 min of supine rest using a Dinamap 1846SX automatic blood pressure measuring device (model 8262, Critikon, Tampa Florida, USA). Arterial blood pressure measures (mean arterial blood pressure, MAP, mean systolic, MSP and diastolic blood pressure, MDP) were calculated from the last 3 stable blood pressure measurements (i.e. mean arterial pressure difference < 4 mmHg) over a 10 min period. Blood pressure lowering medication was not changed during the study.

Whole-body oxygen uptake capacity

Peak whole-body oxygen uptake capacity (VO_{2peak}) and maximal workload capacity (W_{max}) were measured during an incremental exercise test to exhaustion, performed on a cycle ergometer (Medifit Ergometer, Medifit systems, Maarn, The Netherlands) using a ramp protocol¹⁷. Gas exchange (VO_2) measurements were performed continuously (Ergostar, PMS Professional Medical Systems, Basel, Switzerland). Cardiac function was monitored using a 12-lead electrocardiogram with heart rate being recorded continuously (Polar Electro, Kempele, Finland) and sampled at 1 kHz through a data log device (Co2ntrol™, Tildesign, Zeewolde, The Netherlands).

Magnetic resonance spectroscopy

MR spectroscopy (MRS) measurements were performed using a 1.5-Tesla whole-body MR scanner (Gyrosan S15/ACS, Philips Medical Systems, Best, The Netherlands) following blood sampling. Subjects received a standardized breakfast before the start of the MRS measurements. First 1H MRS was applied to measure IMCL, which was followed by ^{31}P MRS to assess *in vivo* skeletal muscle oxidative capacity.

1H MRS

Five single-voxel measurements were performed in the *M. vastus lateralis* using the PRESS sequence (TR/TE=1500/35 ms). The voxels ($10 \times 10 \times 15 \text{ mm}^3$) were positioned in different regions of the *M. vastus lateralis*, avoiding subcutaneous and visible interstitial fat using standard T_1 -weighted images. From each voxel a spectrum with (128 acquisitions) and without (32 acquisitions) CHESS water suppression was collected. Water and IMCL CH_2 peak areas were quantified from the unsuppressed and suppressed spectra, respectively, using a nonlinear least squares algorithm (AMARES) in the jMRUI software package¹⁸. IMCL content was expressed as percentage of the water signal and IMCL levels determined from the different voxels of one subject were averaged.

^{31}P MRS

Phosphocreatine (PCr) recovery after exercise was measured as described previously¹⁹. In short, subjects performed a single-leg extension exercise in an MR compatible ergometer. ^{31}P MRS was applied during the rest-exercise-recovery protocol to measure PCr recovery kinetics. To get subjects acquainted to the in-magnet exercise protocol, subjects visited the laboratory twice within a 7 day period. During the first visit, subjects performed a test run and exercised their leg until fatigue. These data were then used to determine the exercise duration for the second visit. During the second visit, subjects exercised their leg until PCr depletion was sufficient (~50%) to measure the recovery, while avoiding intramuscular pH to fall below 6.8. Spectra were fitted in the time domain by using a nonlinear least squares algorithm (AMARES) in the jMRUI software package¹⁸. Recoveries of PCr and ADP were fitted to mono-exponential functions using Matlab (version 6.1, Mathworks, Natick, Massachusetts, USA). Results are

expressed as the metabolite's time constant of recovery, i.e. τ_{PCr} and τ_{ADP} , representing skeletal muscle oxidative function ²⁰.

Exercise training program

The exercise intervention program was designed specifically for long-standing, deconditioned type 2 diabetes patients suffering from exercise intolerance and with a high cardiovascular risk profile. The backbone of the exercise training program was progressive resistance training (PRT), with high intensity interval training (HIT) as a supplement. The modality and intensity of the different exercise routines was chosen to recruit sufficient muscle mass without causing delayed onset of muscle soreness or feelings of dyspnoea in this deconditioned group of type 2 diabetes patients.

The training sessions started with a 5 min warm-up procedure on a cycle ergometer at 50% of the individuals pre-determined W_{max} , followed by 4 bouts of resistance exercise targeting the upper-body (vertical traction, vertical row, upright row and abdominal crunches), each bout consisting of 2 sets of 10 repetitions. The intensity of these exercises was set at 50% of the previously determined 1 repetition maximum (RM) ²¹. Two sets of 20 alternate left/right lunges without additional weights concluded the warm-up. Thereafter, the resistance training was continued with horizontal leg press and leg extension, each 2 sets of 10 repetitions with ~ 2 min rest between sets. Throughout the PRT the intensity was progressively increased from 50 to 80% of the subjects' individual 1RM. The 1RM was re-evaluated every 4 wk until week 11. In each training session, the PRT was followed by multiple bouts of HIT on a cycle ergometer aimed to stress the working leg muscles without overloading the cardiovascular system ¹⁷. Both the number of bouts and work rate for the interval modes were progressively increased. The interval exercise included 4 - 8 bouts of 30/60 s at 50 - 60% of the W_{max} achieved during the previous steep ramp test (increments of 25W/10 s, described by Meyer *et al.* ¹⁷). Similar to the 1RM, the steep ramp test was performed every 4 weeks to re-evaluate W_{max} . Each exercise session required ~ 45 min to complete and was carried out 3 times a week for 22 wk. All subjects were verbally encouraged during the training sessions to complete the entire protocol.

Statistical analyses

All data are presented as mean \pm standard error of the mean (SEM). Paired samples T-tests were applied to evaluate changes in body composition, glycemic control, blood lipid profile and blood pressure, MRS parameters, whole-body oxygen uptake capacity and W_{max} following the exercise training program. The test was performed two-sided and statistical significance was set at $p < 0.05$. All statistical data processing was performed using SPSS 14.0 (SPSS Inc, Chicago, IL, USA).

Results

Subjects

Subjects (age: 59.0 ± 2.5 y; BMI: 32.2 ± 1.2 kg/m²) had been diagnosed with type 2 diabetes for 12 ± 2 y and were treated with exogenous insulin for 7.0 ± 2.4 y. At the start of the exercise intervention program daily insulin requirements averaged 92.5 ± 11.1 IU. All subjects completed the 5 months exercise training program. A total of 4 subjects reported mild and uncomplicated hypoglycemia (capillary blood glucose 2.7 - 3.8 mmol/l) following the 4th (n = 2) and 9th (n = 2) exercise session. Only 1 of these 4 subjects required multiple adjustments of exogenous insulin dosage to prevent recurrent hypoglycemia. On average 55.1 ± 2.6 (range 40 - 63) of the 66 available exercise sessions were attended, resulting in an overall compliance of $83 \pm 4\%$.

Body composition

The exercise program induced a significant change in body composition (Table 1). Truncal fat percentage declined from 30.1 ± 1.1 to $28.8 \pm 1.3\%$ ($P < 0.05$). Leg lean muscle mass increased from 20.6 ± 1.0 to 21.2 ± 0.9 kg ($p < 0.05$). MRI segmentation analyses of the upper leg showed an increase in muscle volume of the *M. vastus lateralis* from 0.50 to 0.54 L ($p < 0.05$) but no significant increase in total leg muscle volume ($p = 0.08$). Total body mass (BM) ($p = 0.87$), whole-body fat percentage ($p = 0.09$), whole-body lean mass ($p = 0.25$), waist circumference ($p = 0.78$) and IMCL content ($p = 0.22$) did not change significantly.

Glycemic control

Blood HbA_{1c} content declined from 7.6 ± 0.3 to $7.2 \pm 0.2\%$ during the exercise training program ($p < 0.05$) (Table 1). Fasting plasma glucose concentrations showed a strong tendency to decline from 10.4 ± 0.9 at the onset to 8.6 ± 0.7 mmol/L following the 22 wk intervention period ($p = 0.05$). Exogenous insulin requirements did not change significantly during the intervention period (from 92.5 ± 11.1 to 85.4 ± 12.3 IU; $p = 0.26$). As exogenous insulin requirements had increased progressively from 60.7 ± 12.7 to 92.5 ± 11.1 IU over a period of 3 y (Jan 2002 - Jan 2005) prior to this intervention, exogenous insulin requirements were attenuated during the intervention. When calculating the slope of the insulin requirements over time, it changed from on average $+ 6.69$ IU/6 months in the 3 y prior to the exercise program to -1.6 IU/6 months ($p < 0.01$) following onset of the exercise program.

Blood pressure

A significantly lower MAP (from 105.8 ± 2.3 to 98.1 ± 3.1 mmHg; $p = 0.02$) and lower MSP (from 147.4 ± 3.7 to 137.9 ± 5.1 mmHg; $p = 0.06$) was observed following the exercise training, whereas MDP did not change ($p = 0.13$).

Table 1 Body composition, muscle and whole-body oxidative capacity, functional performance and fasting plasma analyses (n = 11)

	BEFORE training	AFTER training	p
BM (kg)	97.5 ± 4.9	97.5 ± 4.8	0.95
WC (cm)	112.6 ± 3.7	113.2 ± 4.0	0.7
Total fat (%)	27.0 ± 0.8	25.9 ± 0.9	0.09
Truncal fat (%)	30.1 ± 1.1	28.8 ± 1.3	0.04
TBLM (kg)	68.9 ± 2.9	69.6 ± 2.7	0.25
LLMM (kg)	20.6 ± 1.0	21.2 ± 0.9	0.03
MRI tot. muscle (l)	3.55 ± 0.17	3.65 ± 0.15	0.08
MRI vast. lat. (l)	0.50 ± 0.03	0.54 ± 0.08	0.01
Fasting plasma glucose (mmol/l)	10.4 ± 0.9	8.6 ± 0.7	0.05
HbA_{1c} (%)	7.6 ± 0.3	7.2 ± 0.2	0.04
Daily insulin requirement (IU)	92.5 ± 11.1	85.4 ± 12.3	0.26
VO_{2peak} (ml/min/kg BM)	24.3 ± 1.4	24.2 ± 1.5	0.87
W_{max} (W/kg BM)	1.6 ± 0.1	1.9 ± 0.2	<0.01
Ave. 1RM	77 ± 4	90 ± 6	<0.01
IMCL (% of water signal)	1.9 ± 0.2	2.0 ± 0.3	0.15
τ_{PCr} (s)	49.4 ± 5.5	45.6 ± 5.6	0.09
τ_{ADP} (s)	22.5 ± 2.9	21.2 ± 2.4	0.43
MAP (mmHg)	105.8 ± 2.3	98.1 ± 3.1	0.02
SP (mmHg)	147.4 ± 3.7	137.9 ± 5.1	0.06
DP (mmHg)	82.5 ± 2.1	78.3 ± 2.4	0.13
Total cholesterol (mmol/l)	4.24 ± 0.17	4.37 ± 0.24	0.55
HDL cholesterol (mmol/l)	0.87 ± 0.07	0.91 ± 0.07	0.55
LDL cholesterol (mmol/l)	3.44 ± 0.13	3.53 ± 0.21	0.57
Triacylglycerol (mmol/l)	2.31 ± 4.26	2.26 ± 3.31	0.86
NEFA (mmol/l)	0.459 ± 0.073	0.367 ± 0.044	0.07
Adiponectin (g/l)	5.43 ± 0.78	5.47 ± 0.82	0.9
TNF-α (ng/l)	7.19 ± 0.46	7.06 ± 0.47	0.74
hsCRP (mg/l)	2.1 ± 0.6	2.08 ± 0.5	0.4
C-peptide (nmol/l)	0.94 ± 0.14	0.90 ± 0.12	0.7

BM: Body Mass, WC: Waist Circumference, TBLM: Total Body Lean Mass, LLMM: Leg Lean Muscle Mass, MRI tot. muscle and MRI vast. lat.: volume measurements based on MRI data for total upper leg muscle compartment and *M. Vastus Lateralis*, respectively, W_{max}: maximal power output on cycle ergometer, Ave. 1RM: Average weight lifted in 1 Repetition Maximum tests from 5 different resistance exercises, IMCL: intramyocellular lipids, τ_{PCr}: PCr recovery time constant, τ_{ADP}: ADP recovery time constant, MAP: Mean Arterial blood Pressure, SP: mean Systolic blood Pressure, DP: mean Diastolic blood Pressure, NEFA: Non-Esterified Fatty Acids, TNF: Tumor Necrosis Factor, hsCRP: high sensitivity C-reactive Protein.

Blood analyses

Blood analyses results are shown in Table 1. Blood lipid-related parameters did not change following the exercise training program. Plasma adiponectin, TNF- α , hsCRP and C-peptide also did not change after the exercise intervention program.

Whole-body and skeletal muscle oxidative capacity

Maximal whole-body oxygen uptake capacity was similar before and after exercise intervention (24.3 ± 1.4 and 24.2 ± 1.5 ml/min/kg BM, respectively; $p = 0.87$) (Table 1). Both ^{31}P MRS derived parameters reflecting *in vivo* muscle oxidative capacity, did not change following exercise intervention (τ_{PCR} and τ_{ADP} , $p = 0.09$ and $p = 0.43$, respectively).

Physical performance capacity

The exercise training induced a significant increase in maximal power output during the maximal exercise test on the cycle ergometer (1.6 ± 0.1 to 1.9 ± 0.2 W/kg BM; $p < 0.01$). Also muscle strength improved significantly, indicated by an increase in the 1RM values of the different strength exercises. Leg press 1RM increased from 159 ± 12 (pre-intervention), 162 ± 14 (4 wk), 172 ± 16 (8 wk) to 187 ± 18 kg (11 wk). Leg extension 1RM increased from 42 ± 15 (pre-intervention), 43 ± 5 (4 wk), 47 ± 6 (8 wk) to 51 ± 6 kg (11 wk). Vertical traction 1RM increased from 85 ± 4 (pre-intervention), 85 ± 4 (4 wk), 90 ± 4 (8 wk) to 96 ± 5 kg (11 wk). Vertical row 1RM increased from 61 ± 3 (pre-intervention), 62 ± 3 (4 wk), 66 ± 4 (8 wk) to 70 ± 4 kg (11wk). Upright row 1RM increased from 37 ± 2 (pre-intervention), 40 ± 3 (4 wk), 43 ± 3 (8 wk) to 47 ± 3 kg (11 wk). Overall, the average of the weight lifted in the 5 different exercises increased from 77 ± 4 kg at the start of the exercise program to 90 ± 6 kg in wk 11 ($p < 0.01$) (Table 1).

Conclusions

This study demonstrates that a combination of low-impact resistance and endurance type exercise training is feasible and well tolerated in deconditioned, long-standing type 2 diabetes patients on exogenous insulin treatment. Proper exercise intervention in these diabetes patients with a high cardiovascular risk profile is shown to improve glycemic control, improve body composition, decrease blood pressure and attenuate the progressive increase in exogenous insulin requirements.

It has been firmly established that regular physical exercise should form one of the main strategies for the prevention and treatment of type 2 diabetes^{3, 4}. As such, newly diagnosed type 2 diabetes patients are generally recommended to participate in exercise intervention programs²². However, the clinical relevance of exercise intervention in a vastly expanding group of long-standing, insulin-treated type 2 diabetes patients suffering from co-morbidities is less evident. These patients are generally excluded from participation in exercise intervention

studies for obvious methodological considerations. Furthermore, as these long-standing, insulin-treated type 2 diabetes patients generally suffer from muscle weakness^{12, 23-25}, cardiovascular co-morbidities²⁶⁻²⁹ and/or exercise intolerance^{12, 13, 30, 31}, it has been proven difficult or even impossible to have these patients adhere to an intense endurance type exercise intervention program^{32, 33}.

In long-standing, insulin-treated type 2 diabetes patients it would be preferred to implement a combination of low-impact endurance and resistance type exercise training, as this provides a much lower cardiovascular challenge¹⁷ and improves functional performance capacity to a similar extent^{34, 35}. In the present study, we evaluated the efficacy of such a combined endurance and resistance type exercise intervention program, which appeared to be well tolerated by these patients. All subjects completed the training program and participated in more than 83% of the supervised training sessions. The 5-month training program improved glycemic control in that both fasting blood glucose levels and blood HbA_{1c} content were lowered after 5 months of training (Table 1). The observed decline in HbA_{1c} content (-0.4%) is in line with previous studies reporting a reduction in HbA_{1c} content between 0.1 - 1.2% after combined endurance and resistance type exercise training in mild type 2 diabetes patients³⁶. The improved glycemic control in the insulin-treated type 2 diabetes patients was accompanied by an attenuation of the progressive increase in exogenous insulin requirements.

The combined exercise training program resulted in significant changes in body composition in the obese type 2 diabetes patients. Both total and truncal body fat percentage had declined with 1.1 ± 0.4 and $1.2 \pm 0.6\%$, respectively, following 5 months of intervention (Table 1). The reduction in body fat mass was accompanied by an increase in leg lean muscle mass (Table 1). In contrast to endurance training programs¹⁵, resistance type exercise training has been shown to increase lean muscle mass in type 2 diabetes patients¹⁴ as well as in the elderly³⁷. The latter is an important advantage for the inclusion of resistance type exercise in an intervention program, as total muscle mass represents a key factor in determining whole-body blood glucose disposal capacity. The observed increase in muscle mass likely contributed to the observed improvements in glycemic control³⁸. In accordance with the increase in lean muscle mass, muscle strength and workload capacity were substantially improved after the exercise training program (Table 1). This substantially enhances functional capacity, thereby contributing to a healthier, more active lifestyle. Improvements in workload capacity can be used to assess progress of the training program, and to decide on the subsequent possibility to enroll these patients in the more generic type 2 diabetes exercise intervention programs.

As insulin resistance and/or type 2 diabetes are presently being associated with mitochondrial dysfunction³⁹⁻⁴¹, we were interested in evaluating the effects of exercise training on whole-body oxygen uptake capacity and skeletal muscle mitochondrial oxidative capacity in these patients. Five months of combined endurance and resistance type exercise training did not raise whole-body oxygen uptake capacity (VO_{2peak}). In accordance, we observed no evidence of improvements in skeletal muscle oxidative capacity, τ_{PCr} and τ_{ADP} , in these patients. Next to these findings, localized single-voxel ¹H MRS did not reveal any differences in IMCL content in the *M. vastus lateralis* following exercise training (Table 1). Despite the reported correlations between insulin resistance and IMCL contents, improvements in glycemic control and/or insulin

Chapter 8

resistance are not necessarily mechanistically related to IMCL content ⁴². In accordance, previous studies have either reported no change ⁴³⁻⁴⁵, a decrease ⁴⁶, or even an increase ^{47, 48} in IMCL content after exercise training. Finally, we observed a significant decline in resting mean arterial blood pressure (MAP - 7.7 mmHg; Table 1), which is likely to have a substantial health impact. It has been estimated that a reduction of 3 mmHg in systolic blood pressure reduces cardiac morbidity by 5 to 9%, stroke by 8 to 14% and all-cause mortality by 4% in an average population ⁴⁹. Therefore, the observed decline in MAP appears to represent another health benefit of exercise intervention in these patients.

In summary, low impact endurance and resistance type exercise training is well tolerated in long-standing, insulin-treated type 2 diabetes patients with a high cardiovascular risk profile. Five months of endurance and resistance type exercise training improves glycemic control, improves body composition, reduces blood pressure, increases muscle strength and workload capacity, and attenuates the progressive increase in exogenous insulin requirements. Low impact combined endurance and resistance type exercise training should be prescribed in the vastly expanding population of long-standing, insulin-treated type 2 diabetes patients.

Acknowledgments

This study was made possible with a grant from the Ministry of Health, Welfare and Sport. The help from the nurses and staff at the Department of Internal Medicine at the Máxima Medical Center in finding potential study candidates is gratefully acknowledged. The exercise testing equipment was kindly provided free of charge by Ms. Stans van der Poel from *Energy Control b.v.* The assistance of our students and the enthusiastic support of our volunteers are greatly appreciated. The authors are very grateful to Jan van Ooyen and Peter Coolen (Philips Medical Systems) for their continuing support in maintaining the MR scanner.

References

1. Boule, N.G. et al. *Jama* **286**, 1218-1227 (2001).
2. Diabetes Prevention Program Research, G. *N Engl J Med* **346**, 393-403 (2002).
3. Sigal, R.J. et al. *Diabetes Care* **27**, 2518-2539 (2004).
4. Sigal, R.J. et al. *Diabetes Care* **29**, 1433-1438 (2006).
5. Maiorana, A. et al. *J Am Coll Cardiol* **38**, 860-866 (2001).
6. Maiorana, A. et al. *Diabetes Res Clin Pract* **56**, 115-123 (2002).
7. Stewart, K.J. *Jama* **288**, 1622-1631 (2002).
8. Albright, A. et al. *Med Sci Sports Exerc* **32**, 1345-1360 (2000).
9. American Diabetes, A. *Diabetes Care* **29**, S4-42 (2006).
10. Wild, S. et al. *Diabetes Care* **27**, 1047-1053 (2004).
11. Detournay, B. et al. *Diabetes Metab* **31**, 3-18 (2005).
12. Sayer, A.A. et al. *Diabetes Care* **28**, 2541-2542 (2005).
13. De Rekeneire, N. et al. *Diabetes Care* **26**, 3257-3263 (2003).
14. Eves, N.D. & Plotnikoff, R.C. *Diabetes Care* **29**, 1933-1941 (2006).
15. Willey, K.A. & Singh, M.A.F. *Diabetes Care* **26**, 1580-1588 (2003).
16. Plotnikoff, R.C. et al. *Med Sci Sports Exerc* **38**, 1526-1534 (2006).
17. Meyer, K. et al. *Eur Heart J* **17**, 1040-1047 (1996).
18. Vanhamme, L., van den Boogaart, A. & Van Huffel, S. *J Magn Reson* **129**, 35-43 (1997).
19. Praet, S.F. et al. *Magn Reson Mater Phy* **19**, 321-331 (2006).
20. Arnold, D.L., Matthews, P.M. & Radda, G.K. *Magn Reson Med* **1**, 307-315 (1984).
21. Reynolds, J.M., Gordon, T.J. & Robergs, R.A. *J Strength Cond Res* **20**, 584-592 (2006).
22. American, D.A. *Diabetes Care* **25**, 64S- (2002).
23. Andersen, H. et al. *Diabetes* **53**, 1543-1548 (2004).
24. Volpato, S. et al. *Diabetes Care* **25**, 678-683 (2002).
25. Petrofsky, J.S. et al. *Med Sci Monit* **11**, CR470-477 (2005).
26. Wackers, F.J. et al. *Diabetes Care* **27**, 1954-1961 (2004).
27. Zabalgoitia, M. et al. *Am J Cardiol* **87**, 320-323 (2001).
28. Gazzaruso, C. et al. *Circulation* **110**, 22-26 (2004).
29. Spijkerman, A.M. et al. *Diabetes Care* **26**, 2604-2608 (2003).
30. Boule, N.G. et al. *Diabetologia* **46**, 1071-1081 (2003).
31. Fang, Z.Y. et al. *Diabetes Care* **28**, 1643-1648 (2005).
32. Schneider, S.H. et al. *Diabetes Care* **15**, 1800-1810 (1992).
33. Dunstan, D.W. et al. *Diabetes Care* **28**, 3-9 (2005).
34. Meyer, K. et al. *Clin Cardiol* **13**, 851-861 (1990).
35. Ivy, J.L. *Sports Med* **24**, 321-336 (1997).
36. Snowling, N.J. & Hopkins, W.G. *Diabetes Care* **29**, 2518-2527 (2006).
37. Rogers, M.A. & Evans, W.J. *Exerc Sport Sci Rev* **21**, 65-102 (1993).
38. Miller, W.J., Sherman, W.M. & Ivy, J.L. *Med Sci Sports Exerc* **16**, 539-543 (1984).
39. Kelley, D.E. et al. *Diabetes* **51**, 2944-2950 (2002).
40. Morino, K. et al. *J Clin Invest* **115**, 3587-3593 (2005).
41. Morino, K., Petersen, K.F. & Shulman, G.I. *Diabetes* **55 Suppl 2**, S9-S15 (2006).
42. van Loon, L.J. & Goodpaster, B.H. *Pflugers Arch* **451**, 606-616 (2006).
43. Helge, J.W. & Dela, F. *Diabetes* **52**, 1881-1887 (2003).
44. Gan, S.K. et al. *Diabetes Care* **26**, 1706-1713 (2003).
45. Hurley, B.F. et al. *J Appl Physiol* **60**, 562-567 (1986).
46. Bergman, B.C. et al. *Am J Physiol* **276**, E106-117 (1999).
47. Pruchnic, R. et al. *Am J Physiol Endocrinol Metab* **287**, E857-862 (2004).
48. Schrauwen-Hinderling, V.B. et al. *J Clin Endocrinol Metab* **88**, 1610-1616 (2003).
49. Braith, R.W. & Stewart, K.J. *Circulation* **113**, 2642-2650 (2006).

Chapter 9

General discussion

General discussion

The prevalence of type 2 diabetes confirms that the disease has become a worldwide health problem that is expected to only get worse in the next decades¹⁻³. Despite a significant amount of research, the causes of the disease are still largely unknown. Since the life style-related development of type 2 diabetes starts with insulin resistance (IR) in skeletal muscle, this tissue has extensively been studied⁴.

Type 2 diabetes research in skeletal muscle has revealed a strikingly negative correlation between intramyocellular lipids (IMCL) levels and insulin sensitivity⁵⁻¹¹. However, this correlation does not hold when endurance trained athletes are included in the research population⁶, which suggests that the relation between IMCL and insulin sensitivity is modulated by other factors, such as the oxidative capacity of the muscle^{6, 12, 13}.

The role of oxidative capacity, which in essence is determined by the density and intrinsic properties of the mitochondria, recently gained a lot of attention. Kelley *et al.* showed that the overall activity of the electron transport chain was lower in mitochondria from type 2 diabetes patients, suggesting a functional impairment of the mitochondria¹⁴. This suggestion was supported by the overall smaller size of skeletal muscle mitochondria from the type 2 diabetes patients compared to lean and obese nondiabetic controls¹⁴. Data originating from *in vivo* magnetic resonance spectroscopy (MRS) measurements¹⁵⁻¹⁷ and expression analysis of genes involved in oxidative metabolism^{18, 19} all suggest that skeletal muscle mitochondrial dysfunction might play a role in IR and type 2 diabetes. Current paradigms link inherited or acquired mitochondrial dysfunction to a dysregulated fatty acid metabolism, which subsequently results in increased levels of IMCL and fatty acid intermediates inducing IR^{15, 16, 20}.

We measured skeletal muscle oxidative capacity and IMCL content using ³¹P and ¹H MRS respectively, in subjects with normal glucose tolerance (NGT), in subjects with early stage type 2 diabetes (ESD) and in long-standing, insulin-treated type 2 diabetes patients (T2D) which were matched for sex, age and body mass index (BMI) and had similar habitual physical activity (**Chapter 6**). ³¹P MRS-derived parameters describing skeletal muscle mitochondrial function, such as the PCr and ADP recovery time constants and maximum aerobic capacity (Q_{max}), did not differ between the various groups representative for different stages of type 2 diabetes development. Also IMCL levels were not significantly different, although the highest levels were measured in T2D and the lowest in the NGT group.

Likewise, the data from our longitudinal animal study did not reveal a difference in skeletal muscle mitochondrial function between fa/fa and fa/+ Zucker Diabetic Fatty (ZDF) rats at different stages during the pathogenesis of type 2 diabetes (**Chapter 7**). *In vivo* mitochondrial oxidative capacity did decrease as a function of age, but this was not related to IR or type 2 diabetes, nor was mitochondrial function related to IMCL content. However, an apparent upregulation of *in vitro* mitochondrial activity suggests compensatory mechanisms induced by the development of type 2 diabetes or the excessively high IMCL levels.

The results of both the cross-sectional study in humans and the longitudinal study in the ZDF rats are inconsistent with current paradigms of inherited or type 2 diabetes-induced defects in mitochondrial function in humans ^{16, 20}. Differences in methodologies used in various studies are frequently proposed to explain discrepancies between results of different studies. Also the present inconsistencies, we believe, are partly originating from different methodologies used to measure mitochondrial function.

The role of skeletal mitochondrial dysfunction in the pathogenesis of IR and type 2 diabetes became recently a topic of intense research, not in the least driven by studies published in highly valued scientific journals, in which ³¹P magnetization transfer experiments were applied to measure the ATP synthesis flux in resting skeletal muscle ^{15, 16}. The question can be raised whether this method is appropriate to measure mitochondrial function. As discussed in **Chapter 1**, oxidative phosphorylation is predominantly controlled by the energy demand in the cell and can easily cope with an energy demand that is 10-20 times the resting metabolic rate. Therefore, it is equally plausible that a lower ATP synthesis rate at rest and under insulin-stimulated conditions as found in insulin resistant or diabetic subjects is reflecting a lower energy demand, rather than an intrinsic mitochondrial defect. The reduced energy demand could in this case be related to the insulin resistant status of the muscle and could reflect reduced GLUT4 trafficking, glucose phosphorylation, glycogen synthesis and protein synthesis due to an impaired insulin signaling pathway.

Because the resting ATP synthesis flux is very low compared to e.g. the flux through the creatine kinase reaction, the ³¹P MR spectra need to be of very high quality in order to reliably measure ATP synthesis flux. None of the recent reports using magnetization transfer to study mitochondrial function in relation to IR or type 2 diabetes show examples of MR spectra. This makes it impossible to appreciate the quality of the presented data.

Measurement of post-exercise PCr recovery kinetics with ³¹P MRS has been used over years to evaluate mitochondrial function ²¹⁻²³. PCr recovery reflects mitochondrial activity in a highly stimulated condition, since at the start of the post-exercise recovery the ADP concentration is high. In a simplified concept, PCr recovery kinetics could be considered as the *in vivo* equivalent of the *in vitro* state 3 respiration. Therefore post-exercise PCr recovery analysis seems a more suitable ³¹P MRS technique to detect defects in mitochondrial function than measurements of ATP synthase flux at rest, which resembles more closely the *in vitro* state 4 respiration. However, also reliable determination of the PCr recovery kinetics depends for a great part on the quality of the MR spectra.

The use of the term "mitochondrial dysfunction" suggests an actual defect in the mitochondria in insulin resistant subjects and type 2 diabetes patients. One can argue whether this is the right nomenclature. Defects in the mitochondrial machinery in general have severe consequences and are associated with a wide range of human diseases (reviewed in ²⁴). As discussed by Boushel *et al.* and others, one should discriminate between intrinsic mitochondrial function and mitochondrial content ²⁵⁻²⁷. The oxidative capacity of muscle tissue could be simplified as the product of the intrinsic properties of the mitochondria and the mitochondrial density. Differences in oxidative function can therefore occur as a consequence of differences

in one of these two terms, or in both. Boushel *et al.* showed that differences in mitochondrial respiration between type 2 diabetes patients and healthy control subjects disappeared when data were corrected for the mitochondrial density²⁶. These data indicate that the intrinsic properties of mitochondria of their type 2 diabetes patients were in essence not different from control subjects. The authors further argue that the daily physical activity level is probably the common causal factor for both the presence of IR and/or type 2 diabetes and the lower skeletal muscle mitochondrial density. The daily activity level is a known risk factor for the development of type 2 diabetes, and also plays an important role in mitochondrial biogenesis. Indeed, chronic inactivity results in a decreased mitochondrial density, whereas exercise training induces marked mitochondrial biogenesis²⁸. In that respect, it is important to note that most studies reporting mitochondrial dysfunction in type 2 diabetes did not (strictly) control for physical activity.

Our data described in **Chapters 6** and **7** are in line with the recent findings of Boushel *et al.*²⁶. In our cross-sectional study, the habitual physical activity level of the subjects was measured by a questionnaire. Although these data displayed a large variability, the average habitual physical activity level of the three groups of subjects was not significantly different. Also in ZDF rats, highly similar spontaneous daily activity levels have been reported in fa/fa and fa/+ genotypes²⁹. Therefore, in both the human and ZDF study, similar habitual physical activity levels and the concomitant similar degree of mitochondrial biogenesis may explain the apparent discrepancy with studies reporting mitochondrial dysfunction in type 2 diabetes. Hence, the results support the concept as discussed by Boushel *et al.*²⁶ and Hawley *et al.*²⁵, that habitual contractile activity could be "... the missing link connecting mitochondrial function with metabolic disease risk factors..."²⁵.

How do our results of the exercise training study (**Chapter 8**) fit in this concept? After 5 months of exercise training, the type 2 diabetes patients had an improved glucose homeostasis. However, we did not observe a significant amelioration of skeletal muscle mitochondrial function. This could be interpreted as that insulin sensitivity and mitochondrial function are not *directly* related. However, such a conclusion would be far too opportunistic, since an improved glucose homeostasis does not necessarily imply an increased insulin sensitivity. The improvement in glucose homeostasis could be the result of the acutely improved insulin sensitivity after each exercise bout^{30, 31}. As the exercise bouts took place in relatively rapid succession (3 times a week), the post-exercise effects could accumulate and mimic an improved insulin sensitivity³².

The lack of improvement in mitochondrial function seen after the training period could be due to the relatively low exercise intensity of the training sessions. As our type 2 diabetes patients were fairly deconditioned, the first aim of the training was to get them at a physical level that would allow them to enroll in generic exercise programs. Therefore, the exercise intensities might overall have been too low to stimulate pathways involved in mitochondrial biogenesis to such an extent that it resulted in improvements detectable in the measurements of PCr recovery. Furthermore, it is not inconceivable that this specific group of long-standing type 2 diabetes patients need relatively higher exercise stimuli to reach similar effects as in healthy subjects, due to blunted responses associated with the disease status. However, the results of

the exercise training study confirmed the beneficial effects of physical activity, also in this specific population of diabetes patients. Therefore, low impact combined endurance and resistance type exercise training should be prescribed in the vastly expanding population of long-standing, insulin-treated type 2 diabetes patients.

Despite all the evidence that supports the role of exercise in the prevention and treatment of type 2 diabetes, a recent survey among more than 20 000 adults in the U.S. showed that the majority of type 2 diabetic patients or people at risk of developing type 2 diabetes do not engage in regular physical activity ³³, emphasizing the need to target interventions to increase physical activity in these individuals.

Future perspectives

Over the last years, highly valued scientific journals published several clinical studies focusing on skeletal muscle mitochondrial function in IR and type 2 diabetes that relied for a large part on ³¹P MRS methodologies ^{15, 16, 34, 35}. The robustness of the analysis and the subsequent conclusions are for a great part relying on the quality of the MR spectra. However, many studies do not show examples of ³¹P MR spectra or provide measures describing the quality of fit procedures, which makes it impossible to appreciate the quality of the data. Future studies using methodologies that are not common use in daily clinical practice, e.g. ³¹P MRS, should provide quantitative measures of the quality of the data or present raw data allowing to assess the robustness of the measurements.

Our results on the role of skeletal muscle mitochondrial function in IR and type 2 diabetes support the concept that direct and indirect evidence of mitochondrial dysfunction in IR and type 2 diabetes is for a great part reflecting the lack of physical activity of subjects with IR and type 2 diabetes patients. Studies involving reliable measurement of daily activity (e.g. using accelerometers) and mitochondrial function are necessary to validate this concept. However, it will be very difficult to quantify the activity level during the years or even decades preceding the onset of type 2 diabetes.

A strategy to answer the question whether mitochondrial dysfunction is directly related to IR would be to manipulate mitochondrial biogenesis. Exercise would be a relatively easily accessible approach to achieve this. However, as exercise interventions improve both IR and mitochondrial biogenesis, albeit through largely different pathways, it will be difficult to pinpoint isolated effects of exercise on these two aspects. Techniques allowing isolated upregulation of mitochondrial biogenesis, e.g. via electrophoresis, could be highly valuable. Also the role of increased IMCL levels in type 2 diabetes and its value as a biomarker of lipid oversupply or lipotoxicity needs more research. Information on the relation between IMCL content and the lipid intermediates that are suggested to interfere with the insulin signaling pathway (diacylglycerol, long chain-CoA, and ceramides) is scarce. High levels of these intermediates may result from an imbalance between lipid availability, storage and oxidation. This underscores the need to measure the dynamics of incorporation of endogenous fatty acids in, and the liberation of stored fatty acids from IMCL, rather than performing static measurements of IMCL content *per se*.

References

1. International, D.F. (2006).
2. Wild, S. et al. *Diabetes Care* **27**, 1047-1053 (2004).
3. Zimmet, P., Alberti, K.G. & Shaw, J. *Nature* **414**, 782-787 (2001).
4. Petersen, K.F. & Shulman, G.I. *Am J Med* **119**, S10-16 (2006).
5. Dobbins, R.L. et al. *Diabetes* **50**, 123-130 (2001).
6. Goodpaster, B.H. et al. *J Clin Endocrinol Metab* **86**, 5755-5761 (2001).
7. Krssak, M. et al. *Diabetologia* **42**, 113-116 (1999).
8. Kuhlmann, J. et al. *Diabetes* **52**, 138-144 (2003).
9. Kuhlmann, J. et al. *Magn Reson.Med.* **53**, 1275-1282 (2005).
10. Pan, D.A. et al. *Diabetes* **46**, 983-988 (1997).
11. Perseghin, G. et al. *Diabetes* **48**, 1600-1606 (1999).
12. Gan, S.K. et al. *Diabetes Care* **26**, 1706-1713 (2003).
13. Thamer, C. et al. *J Clin Endocrinol Metab* **88**, 1785-1791 (2003).
14. Kelley, D.E. et al. *Diabetes* **51**, 2944-2950 (2002).
15. Petersen, K.F. et al. *Science* **300**, 1140-1142 (2003).
16. Petersen, K.F. et al. *N Engl J Med* **350**, 664-671 (2004).
17. Schrauwen-Hinderling, V.B. et al. *Diabetologia* **50**, 113-120 (2007).
18. Mootha, V.K. et al. *Nat Genet* **34**, 267-273 (2003).
19. Patti, M.E. et al. *Proc Natl Acad Sci U S A* **100**, 8466-8471 (2003).
20. Roden, M. *Int J Obes (Lond)* **29 Suppl 2**, S111-115 (2005).
21. Arnold, D.L., Matthews, P.M. & Radda, G.K. *Magn Reson Med* **1**, 307-315 (1984).
22. Chance, B. et al. *Proc Natl Acad Sci U S A* **78**, 6714-6718 (1981).
23. Taylor, D.J. et al. *Gerontology* **30**, 2-7 (1984).
24. Schapira, A.H. *Lancet* **368**, 70-82 (2006).
25. Hawley, J.A. & Lessard, S.J. *Diabetologia* **50**, 699-702 (2007).
26. Boushel, R. et al. *Diabetologia* **50**, 790-796 (2007).
27. Rabol, R., Boushel, R. & Dela, F. *Appl Physiol Nutr Metab* **31**, 675-683 (2006).
28. Hood, D.A. et al. *J Exp Biol* **209**, 2265-2275 (2006).
29. Keeseey, R.E., Swiergiel, A.H. & Corbett, S.W. *Physiology & Behavior* **48**, 327-331 (1990).
30. Albright, A. et al. *Med Sci Sports Exerc* **32**, 1345-1360 (2000).
31. Rogers, M.A. *Med Sci Sports Exerc*, 362-368 (1989).
32. Schneider, S.H. et al. *Diabetologia* **26**, 355-360 (1984).
33. Morrato, E.H. et al. *Diabetes Care* **30**, 203-209 (2007).
34. Petersen, K.F., Dufour, S. & Shulman, G.I. *PLoS Med* **2**, e233 (2005).
35. Brehm, A. et al. *Diabetes* **55**, 136-140 (2006).

Summary
Samenvatting
List of publications
Dankwoord
Curriculum vitae

Lipids and mitochondria in diabetic muscle

The research described in this thesis focused on the role of intramyocellular lipids (IMCL) and skeletal muscle mitochondrial function in the pathogenesis of type 2 diabetes. IMCL is the metabolically active storage form of lipids in skeletal muscle and is closely related to insulin resistance in sedentary subjects. Insulin resistance is a pre-diabetic stage, which can start 1 to 2 decades before the onset of type 2 diabetes. Recently also skeletal muscle mitochondrial dysfunction has been ascribed a role in the development of type 2 diabetes. The aim of the thesis was to clarify the role of skeletal muscle mitochondrial dysfunction and IMCL in the pathogenesis of type 2 diabetes.

The research presented in this thesis covers studies in type 2 diabetes patients and control subjects as well as animal studies. MR spectroscopy (MRS) plays a central role in the present thesis as it was the methodology used for measuring both IMCL (^1H MRS) and skeletal mitochondrial function (^{31}P MRS). The noninvasive character of the MRS applications allowed us to perform longitudinal studies both in an animal model of type 2 diabetes and in type 2 diabetes patients. We looked with greater detail into the implementation of both MRS modalities. The studies on methodological aspects of the different *in vivo* MRS methods are compiled in a first section of the thesis (**Chapter 2-5**), whereas the second section (**Chapter 6-8**) comprises the studies which address the role of mitochondrial function and IMCL in insulin resistance and type 2 diabetes.

Chapter 1 provides a general introduction into the current paradigms explaining the role of IMCL and mitochondrial dysfunction of skeletal muscle in the pathogenesis of type 2 diabetes. This chapter also describes different MRS methodologies used to measure IMCL and mitochondrial function.

In **Chapter 2**, the implementation of single-voxel localized ^1H MRS in rat skeletal muscle is described to measure IMCL. The study shows that IMCL levels can vary up to a factor of 2 depending on the position of the voxel within the tibialis anterior muscle of the rat. These different levels of IMCL were shown to be related to the inhomogeneous distribution of different muscle fiber types in rat tibialis anterior muscle.

To carry out post-exercise PCr recovery measurements in rats, a method to induce muscle contractions is needed. **Chapter 3** describes a minimally invasive, NMR-compatible electrical stimulation method, which allows to induce reproducible muscle contractions of hind limb muscles of the rat, while the animal is in the MR scanner. This set-up provides the possibility to carry out repetitive dynamic ^{31}P MRS measurements in the same animal, which is essential when performing longitudinal studies.

Dynamic ^{31}P MRS is used throughout the studies described in this thesis to measure the post-exercise recovery kinetics of phosphocreatine (PCr). The PCr recovery time constant is often used as a measure of mitochondrial oxidative capacity. A hampered muscle tissue perfusion, as is often witnessed in type 2 diabetes patients can slow down the PCr recovery kinetics. In an attempt to validate the use the PCr recovery time constant as a measure of mitochondrial function in type 2 diabetes patients, we compared *in vivo* ^{31}P MRS parameters of mitochondrial function with *in vitro* markers of mitochondrial oxidative capacity determined in muscle biopsy samples of type 2 diabetes patients (**Chapter 4**).

Another aspect that can jeopardize a reliable measurement of the PCr recovery time constant is the pH at the end of exercise. In **Chapter 5** we show that PCr recovery kinetics is strongly influenced by the end-exercise pH and that this effect is different between subjects. These intersubject differences were shown to be related to the rate of proton efflux out of the muscle tissue.

Chapter 6 describes a cross-sectional study comparing long-standing, insulin-treated type 2 diabetes patients with normal glucose tolerant (NGT) and early-stage diabetic (ESD) subjects. The subjects were matched for age, sex and body composition and all had a low daily physical activity level. The results of the cross-sectional study indicate that mitochondrial dysfunction does not necessarily represent cause or consequence in type 2 diabetes as these three populations showed no difference in mitochondrial oxidative capacity measured with dynamic ^{31}P MRS.

A rat model of type 2 diabetes was studied in a longitudinal way to gain insight in the sequence of possible changes in mitochondrial oxidative capacity and IMCL during the development of type 2 diabetes (**Chapter 7**). Both IMCL and mitochondrial oxidative capacity were monitored at three different stages of the disease: the pre-diabetic stage, overt type 2 diabetes and long-term type 2 diabetes. All parameters were measured in the type 2 diabetes developing animals and in control animals that remain normoglycemic. Besides measuring the *in vivo* PCr recovery kinetics also *in vitro* respiration measurements in isolated mitochondria were performed. Large differences in IMCL levels were present in the diabetes developing animals compared to controls. However, both the *in vivo* and the *in vitro* measurements did not display differences in mitochondrial function related to type 2 diabetes.

Chapter 8 covers an exercise intervention study in the long-standing, insulin-treated type 2 diabetes patients already described in **Chapter 6**. These patients are generally excluded from exercise training programs due to obvious exercise intolerance. The dedicated exercise training program, in which resistance training was the main component, resulted in improved glycemic control and a reduced need for exogenous insulin. Also the cardiovascular risk profile was

Summary

improved after the exercise training. Both IMCL levels and muscle oxidative capacity were similar before and after the exercise training program.

In **Chapter 9** the results of the various physiologically orientated studies of the present thesis are discussed and compared to the current paradigms describing the role of IMCL content and mitochondrial function in the pathogenesis of type 2 diabetes.

Vetstapeling en mitochondria in type 2 diabetes spieren

Type 2 diabetes komt vandaag de dag in zulke mate voor dat het bijna een wereldwijde epidemie mag genoemd worden. De vooruitzichten hieromtrent zijn absoluut niet rooskleurig aangezien verwacht wordt dat in 2030 er 2 maal zoveel type 2 diabetes patiënten zullen zijn dan in het jaar 2000. De toenemende voedselconsumptie en verminderde dagelijkse lichamelijke activiteit spelen hierin een belangrijke rol.

Type 2 diabetes wordt vaak ook wel (ouderdoms)suikerziekte genoemd. Deze benaming refereert naar de sterk variërende bloedsuikerspiegels, welke typerend zijn voor diabetes. De bloedsuikerspiegel wordt hoofdzakelijk gereguleerd door insuline, een hormoon dat in de alvleesklier wordt gemaakt. Wanneer onze weefsels niet normaal reageren op de aanwezigheid van insuline, wordt er minder suiker opgenomen en schommelt de bloedsuikerspiegel. De situatie waarbij weefsels minder gevoelig zijn voor de werking van insuline wordt insulineresistentie genoemd. Insulineresistentie kan gezien worden als een voorstadium van type 2 diabetes en kan al meerdere jaren aanwezig zijn vóór type 2 diabetes duidelijk wordt.

In type 2 diabetes patiënten, mensen met overgewicht en personen met een relatief inactieve levensstijl blijkt de gevoeligheid voor insuline sterk samen te hangen met de hoeveelheid opgeslagen vet in de spiercellen (intramyocellulaire lipiden, IMCL). Hoe groter deze vetopslag, hoe lager de gevoeligheid voor insuline. Deze verhoogde IMCL niveaus kunnen een gevolg zijn van een verhoogde aanvoer van vetten, bijvoorbeeld door overgewicht. Er zijn echter ook hypothesen die wijzen op een verminderde capaciteit om deze vetten te gebruiken als brandstof, wat ook hun opslag zou bevorderen. Het belangrijkste onderdeel van een cel in het vrijmaken van energie uit brandstof is het mitochondrion. Een slechter functioneren van deze mitochondria zou kunnen leiden tot een verminderd vermogen om vetten te verbranden, wat verhoogde opslag, IMCL tot gevolg heeft en uiteindelijk resulteert in insulineresistentie.

Het doel van studies beschreven in deze thesis was om de rol van zowel verhoogde IMCL niveaus als het functioneren van mitochondria te onderzoeken tijdens de ontwikkeling van type 2 diabetes. Hiervoor werden zowel studies in patiënten als in proefdieren uitgevoerd. Een rode draad doorheen alle beschreven studies is het gebruik van magnetische resonantie spectroscopie (MRS) als belangrijkste meetmethodiek. Gelokaliseerde ^1H MRS is gebruikt om non-invasief de hoeveelheden IMCL te meten, terwijl ^{31}P MRS is toegepast om de oxidatieve capaciteit van mitochondria te evalueren. De toepassing van deze technieken op zich, vormt een belangrijk onderdeel van deze thesis en wordt behandeld in 4 hoofdstukken (Hoofdstuk 2 t/m 5).

Hoofdstuk 1 is een algemene introductie waarin de huidige heersende paradigma's over de rol van IMCL en mitochondria van skeletspier in de ontwikkeling van type 2 diabetes worden toegelicht. In dit hoofdstuk worden ook verschillende MRS methoden om IMCL en mitochondriële functie te meten beschreven.

In **Hoofdstuk 2** wordt de toepassing van gelokaliseerde ^1H MRS in skeletspier van rat om IMCL te meten behandeld. In deze studie tonen we aan dat IMCL niveaus tot meer dan een factor 2 kunnen verschillen, afhankelijk van de positie in de spier waar gemeten wordt. Uit histologische analyses bleek dat deze opmerkelijke verschillen in IMCL niveaus te wijten zijn aan de uitgesproken regionalisering van de verschillende spiervezeltypes in spieren van de rat.

Dynamische ^{31}P MRS is in de beschreven studies gebruikt om de herstelsnelheid van fosfocreatine te meten na inspanning, als maat voor de oxidatieve capaciteit van de mitochondria. Om deze werkwijze te kunnen toepassen in rat is een methode nodig om spiercontracties te induceren. In **Hoofdstuk 3** wordt een minimaal invasieve, NMR-compatibele methode beschreven voor elektrostimulatie. Deze techniek stelt ons in staat om spiercontracties te induceren terwijl het dier onder anesthesie in de MR scanner ligt. Het minimaal invasieve karakter van de methode laat toe om deze in eenzelfde dier op verschillende tijdstippen toe te passen.

Een verstoorde weefseldoorbloeding kan het meten van de fosfocreatine herstelsnelheid na inspanning verstoren. Van type 2 diabetes patiënten is bekend dat ze vaak last hebben van een slechte weefseldoorbloeding. In een poging om het gebruik van de herstelsnelheid van fosfocreatine na inspanning als maat voor mitochondriële functie te valideren, hebben we verschillende ^{31}P MRS parameters voor mitochondriële functie vergeleken met *in vitro* bepalingen van oxidatieve capaciteit, gemeten in spierweefsel van type 2 diabetes patiënten (**Hoofdstuk 4**).

De intracellulaire pH op het einde van de inspanning is een ander aspect dat een betrouwbare meting van de fosfocreatine herstelsnelheid na inspanning kan verstoren. In **Hoofdstuk 5** laten we zien dat de herstelsnelheid van fosfocreatine inderdaad sterk beïnvloed wordt door de pH op het einde van de inspanning en dat dit effect niet voor iedereen hetzelfde is. De verschillen tussen proefpersonen worden verklaard door een verschil in snelheid van de protonenflux uit de spier.

Hoofdstuk 6 beschrijft een cross-sectionele studie waarin patiënten die reeds lange tijd type 2 diabetes hebben (> 12 jaar) vergeleken worden met personen die in een vroeg stadium van type 2 diabetes verkeren en met personen die nog een normale bloedsuikerspiegel hebben. De verschillende groepen proefpersonen hebben gemiddeld dezelfde leeftijd, geslacht en lichaamssamenstelling en hebben allen een laag niveau van dagelijkse lichaamsbeweging. De resultaten van deze studie duiden niet op een belangrijke rol voor mitochondriële disfunctie, noch als oorzaak, noch als gevolg van type 2 diabetes.

Een rat model van type 2 diabetes was onderzocht in een longitudinale studie om inzicht te krijgen in welke volgorde veranderingen in mitochondriële functie en IMCL zich voordoen tijdens de ontwikkeling van type 2 diabetes (**Hoofdstuk 7**). Zowel IMCL als mitochondriële functie werd bestudeerd in drie verschillende fases van de ziekte: in het voorstadium van type 2 diabetes, tijdens volledig ontwikkelde type 2 diabetes, en in een situatie van langdurig type 2 diabetes zijn. De verschillende parameters die werden bepaald werden vergeleken met rasgenoten die een normale bloedsuikerspiegel hebben. IMCL en mitochondriële functie werden

opnieuw gemeten met respectievelijk *in vivo* ^1H en ^{31}P MRS. Parallel aan deze metingen werden ratten van dezelfde soort, op dezelfde leeftijden opgeofferd en mitochondria uit hun spieren geïsoleerd. Deze mitochondria werden gebruikt voor *in vitro* respirometingen. In de dieren die diabetes ontwikkelden werden veel hogere hoeveelheden IMCL gemeten dan in de controle dieren. Zowel de *in vivo* als de *in vitro* metingen toonden echter geen verschil in mitochondriële functie aan.

Hoofdstuk 8 behandelt een trainingsinterventie studie in patiënten die reeds lange tijd type 2 diabetes hebben. Deze klasse van patiënten wordt meestal uitgesloten van trainingsstudies omdat ze slechts een laag inspanningsniveau aan kunnen en last hebben van allerlei comorbiditeiten. Het trainingsprogramma duurde 22 weken, was grotendeels gebaseerd op krachttraining en had als resultaat dat de bloedsuikerspiegel beter gehandhaafd werd. Daarnaast leek de benodigde hoeveelheid dagelijkse insuline te verminderen en zakte de bloeddruk van de patiënten. De IMCL hoeveelheid en mitochondriële oxidatieve capaciteit was niet veranderd na het volgen van het trainingsprogramma.

In **Hoofdstuk 9** worden de resultaten van de verschillende fysiologisch georiënteerde studies beschreven in deze thesis besproken in het kader van de huidige, heersende opvattingen over de rol van IMCL en mitochondriële functie in de ontwikkeling van type 2 diabetes.

Papers

De Feyter H.M., Schaart G., Hesselink K.M., Schrauwen P., Nicolay K., Prompers J.J. *Regional variations in intramyocellular lipid concentration correlate with muscle fiber type distribution in rat tibialis anterior muscle.* Magn Reson Med 2006; 56:19-25

Praet S.F.E., **De Feyter H.M.**, Jonkers R.A.M., Nicolay K., van Pul C., Kuipers H., van Loon L.J.C., Prompers J.J. *³¹P MR spectroscopy and in vitro markers of oxidative capacity in type 2 diabetes patients.* Magn Reson Mater Phy (MAGMA) 2006; 19:321-331

van den Broek N.M., **De Feyter H.M.**, de Graaf L., Nicolay K., Prompers J.J. *Intersubject differences in the effect of acidosis on phosphocreatine recovery kinetics in muscle after exercise are due to differences in proton efflux rates.* Am J Physiol Cell Physiol; 2007 (in press)

De Feyter H.M., Praet S.F.E., van den Broek N.M., Kuipers H., Stehouwer C.D., Nicolay K., Prompers J.J., van Loon L.J.C. *Exercise training improves glycemic control in long-standing, insulin treated type 2 diabetes patients. (Submitted)*

De Feyter H.M., van den Broek N.M., Praet S.F.E., Nicolay K., van Loon L.J.C., Prompers J.J. *Early or advanced stage type 2 diabetes is not accompanied by in vivo skeletal muscle mitochondrial dysfunction. (Submitted)*

De Feyter H.M., Lenaers E., Schrauwen P., Hesselink K.M., Nicolay K., Prompers J.J. *Increased intramyocellular lipids but normal skeletal muscle mitochondrial function throughout the pathogenesis of type 2 diabetes in the ZDF rat. (In preparation)*

Proceedings and abstracts (first author only)

De Feyter H.M., Majoor S.J., de Graaf A.H.J., Nicolay K., Prompers J.J. *Skeletal muscle mitochondrial function and intramyocellular lipids in the diabetic ZDF rat: a longitudinal study using in vivo ³¹P and ¹H MRS.* Ann. Meeting ISMRM, May, 2007

De Feyter H.M., Majoor S.J., de Graaf A.H.J., Nicolay K., Prompers J.J. *An NMR-compatible, minimally invasive electrical stimulation method to study rat skeletal muscle function in vivo.* Ann. Meeting ISMRM, May, 2007

De Feyter H.M., S.J. majoor, M. K. Hesselink, P. Schrauwen, J. J. Prompers, K. Nicolay. *Skeletal muscle mitochondrial function and intramyocellular lipids in the diabetic Zucker rat: baseline data of a longitudinal study using in vivo ³¹P and ¹H MRS.* Ann. Meeting EASD, 2006

De Feyter H.M., Praet S., van Loon L., Prompers J., Nicolay K. *Response of insulin-dependent Type 2 diabetic subjects to a 5-month exercise training program.* Ann. Meeting ISMRM, 2006

De Feyter H.M., Prompers J., Nicolay K. *The typical IMCL distribution pattern in rat tibialis anterior muscle remains unchanged after high-fat diet or fasting.* Ann. Meeting ISMRM, 2006

De Feyter H.M., Praet S., van Loon L., Nicolay K., Prompers J.J. *A comparison of different methodologies to study skeletal muscle mitochondrial function.* Ann. Meeting ISMRM, 2006

De Feyter H.M., K. Nicolay, G. Schaart, M.K. Hesselink, J.J. Prompers. *Local intramyocellular lipid content within rat tibialis anterior muscle measured with in vivo ¹H MRS correlates with muscle fiber type composition.* Ann. Meeting ISMRM, 2005

Dankwoord

Vier jaar lang is het dankwoord van het proefschrift totaal irrelevant tijdens de dagelijkse bezigheden van een promovendus. Vervolgens komt het dankwoord uit het niets binnen op nummer 1 in de lijst van "meest gelezen onderdelen van het proefschrift". Of het ook zo hoog zou staan in de lijst van "meest *belangrijke* onderdelen van het proefschrift" is maar de vraag. Ik denk het niet, een top-drie notering lukt vast nog wel, maar waarschijnlijk wint "de omslag" met ruime voorsprong.

Wat maakt het dankwoord zo interessant voor de gemiddelde lezer? In de eerste plaats is het in de moedertaal geschreven en is de tekst vele malen toegankelijker dan de rest van het proefschrift. Daarnaast is het nu eenmaal zo dat niet iedereen wakker ligt van *lipids and mitochondria in diabetic muscle*. Inderdaad, onbegrijpelijk! Een deel van het lezerspubliek hoopt echter ook z'n eigen naam te zien langskomen en dan liefst nog met wat extra glans en niet in een rijtje met 15 andere namen. Zo zijn wij nu eenmaal. Anderen speuren dan weer naar subtiele boodschappen of hopen sneren richting begeleiders of andere collega's te ontdekken. Zo kan geen enkele promovendus nog oprecht de zin "bedankt voor de vrijheid die ik kreeg tijdens het uitvoeren van dit project" of soortgelijks gebruiken, omdat dit door de jaren heen publiek geheime codetaal is geworden voor "ik heb helemaal geen begeleiding gehad!".

Toch zou ik graag meteen deze beruchte zin willen gebruiken: Klaas, bedankt voor alle vrijheid die ik kreeg tijdens het uitvoeren van dit project! Echt waar! Inderdaad, dit houdt ook in dat ik niet altijd veel begeleiding heb gehad, maar dat wou ik ook niet! Als ik jouw advies nodig had kon ik het altijd krijgen. Mezelf kennende is deze aanpak heel waarschijnlijk de beste geweest. Ik ervaar dit in elk geval als veel prettiger dan wanneer me van bovenaf zou zijn opgelegd welke kant het onderzoek had moeten uitgaan. Jij weet ook de waarde van robuuste, degelijke metingen in te schatten en je wordt nog steeds enthousiast van een mooi, *in vivo* gemeten fosfor spectrum. Ik wens je nog veel succes met de groei van de Biomedical NMR groep!

Jeanine (JeeJee), als jouw eerste promovendus ooit, allebei in een gedeeltelijk nieuw vakgebied beland en in een opstartend lab was ons lot lange tijd erg verbonden. De promotietijd heb ik dan ook veel meer ervaren als een gezamenlijke strijd met jou om zoveel mogelijk resultaat te behalen, dan als een begeleider-promovendus relatie. Ik ben ervan overtuigd dat we zowel wetenschappelijk als persoonlijk een heel complementair duo zijn. Als ik "in de wetenschap" blijf, hoop ik dat we in de toekomst nog vaker samen kunnen werken. Verder wens ik je nog veel plezier en succes met je 3 mannen en ik hoop dat er toch ééntje voetballer wordt!

De studies met type 2 diabetes patiënten vormen een belangrijk deel van dit proefschrift. Dit was onmogelijk geweest zonder de samenwerking met Stephan en Luc. Luc, jij hebt steeds een zo goed als blind vertrouwen gehad in onze aanpak en ons enthousiast gemaakt om proefpersonenonderzoek op een technische universiteit uit te voeren. Jij bent altijd positief ingesteld; af en toe in zulke mate dat ik het niet meer geloofwaardig vind, maar beschouw dit laatste in elk geval als een groot compliment! Stephan, een samenwerking tussen een

Dankwoord

Nederlander die in Vlaanderen woont en een Vlaming die in Nederland woont heeft alle kans van slagen, lijkt me. En dat is ook gebleken! Ik denk dat we veel van elkaar geleerd hebben en de studies die we samen hebben uitgevoerd zijn voor ons beiden belangrijke onderdelen van ons proefschrift geworden. Succes met het voltooien van je boekje en met je arts-duizendpoot-carrière!

Ook verscheidene onderdelen van de proefdierstudies waren niet mogelijk geweest zonder de hulp van anderen. Gert, bedankt voor de "effe tussendoor", prachtige fluorescentie-kleuringen van de rattenspiertjes. Matthijs en Patrick, bedankt voor de interessante oxygraaf data. Het vermelden van deze oxygraaf data kan niet zonder Ellens naam te noemen. Ellen, bedankt voor het vele werk dat je verricht hebt en veel succes met je eigen promotieonderzoek!

Van boven de rivieren kwam er ook hulp: Ron, met je ongebreidelde enthousiasme en het ten dienste stellen van je lab en mankracht. Sander, ongelooflijk hoe snel jij even een hoop enzym essays uit je mouw schudt! De data zijn net niet meer in het proefschrift beland, maar ik ben ervan overtuigd dat ze nog erg nuttig zullen zijn. Veel succes met je toekomstplannen!

Naast de gebruikelijke en niet ontorechte bedankjes richting begeleiders en mensen waarmee intensief is samengewerkt worden vaak een hele resem mensen bedankt omdat ze er nu eenmaal toevallig waren. Het is echter moeilijk vol te houden dat het proefschrift er niet was geweest zonder deze mensen. Maar, ook ik kan niet ontkennen dat het de afgelopen jaren uitermate prettig toeven was in de ruime omgeving van de Biomedical NMR groep en niet in het minst in een gebouw als N-laag dragen *human subjects* daar wezenlijk aan bij.

Uiteraard zijn er figuren waar je toevallig net iets beter mee opschiet dan met anderen. Niet in het minst behoort Willem, a.k.a. BMF, tot deze categorie. Meer nog, Willem, van collega, huisgenoot tot goede vriend hebben we mooie tijden gehad in Eindhoven. Wie weet beleven we die op korte of lange termijn opnieuw. Als *Global Warming* z'n beloftes waarmaakt kunnen we alsnog ons idee om een strandtent uit te baten misschien zelfs in Eindhoven uitvoeren!

Verder vervullen kamergenoten vaak een aparte rol als eerste klankbord voor uitingen van verbazing, frustraties, roddels enz. Geralda (Djeraldo), wat gevoel voor humor betreft, zitten we in elk geval op dezelfde frequentie. Ik hoop dat jouw ambitieuze carrièreplannen in de worstverkoop niet verhinderen dat we contact blijven houden. Ward, stiekem heb je een groot deel van m'n promotie gered. Jij hebt immers binnen 5 minuten de noodzakelijke tweedehandse NMR scanner bij elkaar "ge-googled". Daarnaast leidt jouw gestructureerde puinhoop op je bureau de aandacht af van m'n eigen rotzooi. Met dank! In m'n promotietijd heb ik ook al een aantal collega-aio's zien vertrekken: Lourens, de eenpersoons geheime informatiedienst van de B-vleugel; Anneriet, we wachten vol spanning tot jij de revival van de cowboylaars introduceert in Nederland en Carola, ik ben minstens de tweede die jouw kwaliteiten als huizenmakelaar mag roemen in een dankwoord van een proefschrift! Edwin, als *cardiac specialist* was je net als ik, een van de weinige in onze groep die (aanvankelijk) niet met *molecular imagine-eering* bezig was, veel succes en plezier bij je nieuwe, oude collega's!

Een aantal niet-aio's waar ik veel aan gehad en vooral veel lol heb mee gehad: Larry, we konden best snel, best goed opschieten. Ik ben echter alweer de naam vergeten van ons nog op te richten 'special-projects-design-and-development' bureau, wat zonder twijfel een overdonderend succes zou zijn, zoals "the dietizer" heeft bewezen. Op het moment dat ik dit schrijf weet ik het nog niet helemaal zeker, maar de kans is heel groot dat de allerlaatste actie nodig om dit boekje bij de drukker te krijgen, door jou is uitgevoerd op je Linux-machine! Mijn dank is groot! He, Jo, bedankt voor je biotechnische bijdragen, toch jammer dat we niet samen nog effe een rondje Garda-meer hebben kunnen fietsen op de mountainbike, maar wie weet als jij je huisje in Italië hebt, komt het er vast nog eens van! Jef, de onvermoeibare morele aanvoerder van het al even onvermoeibare (nou, ja, als een wedstrijd 10 minuten zou duren) *Spin 'm erin* futsal team. Bedankt voor jouw geduld om telkens opnieuw te proberen een fysiotherapeut uit te leggen hoe hoogfrequente RF-spoelen werken. Gustav, collega Apple-adept en software leverancier. Wat werk betreft hadden we niet zoveel met elkaar te maken. Dit in tegenstelling tot activiteiten naast het werk, zeker wanneer dit gepaard ging met het nuttigen van menig biertje of cocktail. Je kunt altijd komen bivakkeren in m'n woonkamer wanneer de Nederlandse Spoorwegen weer eens een najaarsstormpje hebben onderschat!

Als er iemand absoluut niet mag ontbreken in een dankwoord, zijn het wel Ria en Hedwig. Ria, al jaren stil wakend op de achtergrond en Hedwig, jij bent er nog niet zolang maar hoort er al helemaal bij! Bedankt voor al het geregeld waar ik zelf nogal een broertje dood aan heb. Ook de mannen en vrouw van de N-laag werkplaats mag ik niet vergeten! Petje af voor wat jullie telkens opnieuw in korte tijd presteren!

Een aantal hoofdstukken is tot stand gekomen met wezenlijke hulp van afstuderende studenten en sommige latere collega-aio's: Stephan, Christine, Richard, Paul, Jaap, Noud, Luuk en Nicole, bedankt en succes met jullie eigen onderzoek of baan.

Pa en ma, ik kan me voorstellen dat het traject wat ik heb afgelegd, van kinesitherapeut in Gent, via bewegingswetenschappen in Maastricht naar deze promotie in Eindhoven niet direct was wat jullie in gedachten hadden. Ik ook niet, trouwens. Bedankt om me die kans te geven.

Het schrijven van een dankwoord brengt een groot risico met zich mee. Je zult immers maar iemand vergeten! Voor diegene die denken dat ze in dit dankwoord thuishoren en hun eigen naam toch niet konden bespeuren: geen paniek! Geïnspireerd door boeken als "Het Bernini mysterie" en "De Da Vinci code", heb ik immers allerlei boodschappen en namen verborgen in deze tekst... succes ermee!

Curriculum vitae

Henk De Feyter was born April 23, 1976, in Ninove, Belgium. He grew up in Geraardsbergen and graduated from secondary school in 1994 at the St.-Jozefsinstituut in Geraardsbergen. He started his study "Motorische revalidatie & kinesitherapie" (physiotherapy) at the Ghent University in 1994 and graduated with distinction in 1999 on EMG spectral analysis of hamstring muscles in patients with anterior cruciate ligament reconstruction. Subsequently he studied Health Sciences at the Maastricht University. He obtained his master degree in Health Sciences in 2002 on the mechanical performance and exercise-induced muscle damage in truncated M-protein mice.

Henk started as a Ph.D. student in the Biomedical NMR group headed by Professor Klaas Nicolay at the Eindhoven University of Technology in October 2002. The research carried out in this period focused on the role of lipid storage and mitochondrial function in skeletal muscle and their role in the development of type 2 diabetes. Measuring lipid deposits and skeletal muscle mitochondrial function involved the application of various in vivo ¹H and ³¹P magnetic resonance spectroscopy techniques, which were applied in human subjects as well as in rat models of type 2 diabetes.

